VOLTAMMETRIC INVESTIGATION OF MICROBIOLOGICAL GROWTH MEDIA AND CARBON NANOTUBE MODIFIED ELECTRODES: A CASE STUDY OF OXYTETRACYCLINE

A thesis submitted in fulfilment of the requirements for the degree of

MASTERS IN SCIENCE

of

RHODES UNIVERSITY

in the discipline of

BIOTECHNOLOGY

by

JAN KRUID

June 2012

ABSTRACT

Oxytetracycline (OTC) is a broad spectrum antibiotic used extensively in the agricultural and human-health sector, and is effective against various gram positive and –negative bacteria as well as large viruses and certain pathogenic Rickettsiae. This study addresses the lack of voltammetric knowledge regarding the electroanalytical characterisation of OTC and its analysis in complex matrices.

Cyclic voltammetry (CV) revealed several irreversible anodic peaks for OTC at a bare glassy carbon electrode (GCE). These current responses were improved through the selection of a diluent for OTC stock preparation, electrolyte solution and electrolyte pH, stir time and applied preconditioning potential. Under enhanced adsorptive conditions and using square wave voltammetry (SWV), a detection limit of 24.3 nM was achieved. The electrode surface could be renewed *in vitro* for 10 successive scans. OTC oxidation was characterised as a one electron:one proton EC_iE mechanisms.

Next, investigating the viability of voltammetry in various complex microbiological growth media revealed that selected growth media contained interfering redox active components, which, while simultaneously coating the electrode surface, effectively reduced GCE performance and lowered the active electrode surface area, as ascertained through CV and electrochemical impedance spectroscopy (EIS) studies. This interference lowered OTC current response in the presence of growth media which was partially recovered by appropriate growth media selection and sample dilution.

In testing the use of acid functionalised multi-walled carbon nanotubes (MWCNTs) to improve anodic OTC response, charge-based attraction was observed between the MWCNT dispersal agent Nafion® and OTC, while increased surface area associated with prolonged acid functionalisation time aided in improving OTC current response.

ACKNOWLEDGEMENTS

I hereby wish to thank and acknowledge the following people and institutions who have played an instrumental role in the completion of this thesis:

- Professor Janice Limson for your continuous help and support throughout my studies. Thank you for offering me the opportunity to pursue my scientific career.

- The Nanotechnology Innovation Centre for funding my research and making the work presented in this thesis possible. The NIC has taken me further in science than I ever thought I would go, for which I am very thankful.

- My parents, who encouraged me to be inquisitive which send me on my way to study science, and the rest of my family for their constant support.

- To Louise De Almeida, thank you for your love, your belief in me and for being my driving force. Eu te amo mais do que waffles.

- All the members of the Bio-SENs research group. Thank you for all the support and the banter. In particular Michael Niland and Shane Flanagan for offering priceless insight into my research. To Wade Stanton, KTHXBY. Thank you to Lance Ho for help with the proofreading of this thesis. A special thanks to Dr. Ronen Fogel for your invaluable input into my work.

- Dr Edith Antunes for help with Raman spectroscopy.

TABLE OF CONTENT

Title **Page number**

LIST OF ABBREVIATIONS AND SYMBOLS

α	Charge transfer coefficient
°C	Degrees Celsius
ΔE_p	Peak separation
A	Amperes
AA	Ascorbic acid
AdSV	Adsorptive stripping voltammetry
A_{exp}	Experimentally observed electrode surface area
Ag/AgCl	Silver/silver chloride reference electrode
A_{geo}	Geometric electrode surface
Au-SPE	Gold screen printed electrode
AZ	Abou-Zeid media
b	Tafel slope
BAS	BioAnalytical Systems
BR	Britton-Robinson buffer
c	Analyte concentration
C_{dl}	Double layer capacitance
CE	Counter electrode
CNM	Clostridium nutrient media
CNT	Carbon nanotube
CNTPE	Carbon nanotube paste electrode
CPE	Constant phase element
CTC	Chlortetracycline
C_v	Coefficient of Variation
CV	Cyclic Voltammetry
D	Diffusion coefficient
DBB	Boron-doped diamond
DC	Direct current
dO_2	Dissolved oxygen
DPPG	Basal-plane pyrolytic graphite
DPSV	Differential Pulse Stripping Voltammetry
DPV	Differential Pulse Voltammetry
DSMZ	Deutsche Sammlung von Mikroorganismen und Zellkulturen
E	Potential
EC	Redox step followed by chemical step
ECE	Redox step followed by chemical step, followed by redox step
ECP	Electrochemical pre-treatment
E_f	Final energy state
E_i	Initial energy state
EIS	Electrochemical impedance spectroscopy
$E_{p/2}$	Half peak height
E_{pa}	Anodic peak potential
E_{pc}	Cathodic peak potential
EP-GCE	Electrochemically pretreated GCE
EPPG	Edge-plane pyrolytic graphtite
E_{sw}	Square wave amplitude
F	Faraday constant (9.65 x 104 C)
FI	Flow injection
FTIR	Fourier-transform infrared spectroscopy
g/l	Gram per liter
GCE	Glassy carbon electrode
GDP	Gross Domestic Product
GPES	General purpose electrochemical system
HBM	Hybrid bilayer lipid membrane
HMDE	Hanging mercury drop electrode
HPLC	High Performance Liquid Chromatography
HSA	Human serum albumin
I	Current
I	Predicted current by Langmuir isotherm
I_{for}	Forward current component of SWV
IgG	Immunoglobulin G
IL	Ionic liquid
I_m	Maximum achievable current according to Langmuir isotherm
I_{max}	Maximum current response
I_{net}	Net current component of SWV
I_{pa}	Anodic peak current
I_{pc}	Cathodic peak current
I_{rev}	Reverse current component of SWV
K	Adsorption coefficient for Langmuir isotherm
LB	Luria Bertani broth

LCEC	Liquid chromatography with electrochemical detection
LOD	Limit of detection
LOQ	Limit of quantification
LSV	Linear sweep voltammetry
M	Molar concentration
MDR-TB	Multidrug-resistant tuberculosis
MEM	Malt extract media
MRL	Maximum residue levels
MS	Mass spectrometry
MSM	Minimal salts media
MWCNT	Multi-walled carbon nanotube
n	Number of electrons
n_a	Number of electrons in rate-limiting step
NB	Nutrient broth
n_t	Total number of electrons transferred
OCP	Open-circuit potential
OTC	Oxytetracycline
pa	Anodic peak
pc	Cathodic peak
PP	Potassium dihydrogen phosphate buffer
Q	Constant phase element
Q_f	Film capacitance
R	Standard molar gas constant (8.31447 $J.mol^{-1}.K^{-1}$)
R^2	Correlation coefficient
R_{ct}	Charge transfer resistance
RE	Reference electrode
R_f	Roughness factor
R_f	Film resistance
RIfS	Reflectometric interference spectroscopy
RP	Reverse Phase
RPM	Revolutions per minute
R_s	Solution resistance
R_{tot}	Total resistance
SWASV	Square wave anodic stripping voltammetry
SWCNT	Single-walled carbon nanotube
SWV	Square Wave Voltammetry
T	Temperature in Kelvin (298 K at room temperature)
TC	Tetracycline
UA	Uric acid
UPLC	Ultra-high-performance liquid chromatography
V	Volt
v	Scan rate
$^v/_v$	Volume per volume
v_{aS}	Anti-Stokes frequency
v_m	Transferred energy
v_o	Raman incident light
v_R	Rayleigh scattering
v_S	Stokes frequency
W	Warburg impedance
WE	Working electrode
XPS	X-ray photoelectron spectroscopy

LIST OF FIGURES

LIST OF TABLES

LIST OF EQUATIONS

CHAPTER 1

General Introduction

1.1 ANTIBIOTICS

Antibiotics, produced by fungal and bacterial species, are described as naturally occurring, synthetic or semi-synthetic molecules that possess properties capable of mitigating the growth of susceptible microbes, and are hence categorised as antimicrobials (Kemper, 2008; Clardy *et al*., 2009). The diverse origin of antibiotics is matched by their wide range of applications in both the agricultural and human health sector. Antibiotic classes of importance for human and veterinary use include aminoglycosides, β-lactams (penicillins), cephalosporins, fenicoles, macrolides, sulphonamides and tetracyclines (Kemper, 2008). Before discussing the need for sensitive antibiotic detection systems, the implications of more than half a century of antibiotic use must be highlighted.

1.1.1 Use of antibiotics in agriculture and the human health sector

According to the data published in the 2010 World Development Indicators (World Bank, 2010), agriculture (including forestry and fishing) was accountable for 3 % of the South African Gross Domestic Product (GDP) in 2008. This represents US$ 8.2 billion or R 76 billion (at exchange rate of R 9.34/US$ at the end of 2008).

Agriculture can be subdivided into animal husbandry and crop growing. Each of these subdivisions faces a range of biological and non-biological environmental stressors, which impact substantially on the profitability thereof. For animal husbandry (commonly referred to as livestock farming which includes fish farming), these environmental conditions include ectoparasites, endoparasites, environmental toxins and weather conditions. To mitigate the effect of parasites, pesticides and antimicrobial agents are frequently used to reduce their numbers to manageable and less harmful levels (Phillips *et al*., 2004). Similarly, crop farming and forestry frequently utilise chemical and antibiotics to prevent losses due to parasites, ensuring better quality and higher quantity products coupled with less waste (Teuber, 2001).

The use of antibiotics as growth promoters was discovered by coincidence in the 1940s, when tetracycline fermentation by-products were fed to chickens, which showed a subsequent increase in growth rates (Phillips *et al*., 2004). As a feed or water additive, antibiotics have since been used to improve the rate of weight gain of animals, a practise financially justified by higher profit margins due to lower feed:weight gain ratios as shown for swine (Dewey *et al*., 1997) and poultry (Gustafson and Bowen, 1997). Improved animal health was also observed, often accredited to prophylactic actions of the antibiotics (Dewey *et al*., 1997), resulting in reducing animal fatality and higher production output.

The human health sector has utilised antibiotics since the discovery of penicillin by Alexander Fleming in 1928 (Fleming, 1929), the use of which increased dramatically during World War 2, leading to the large-scale production of antimicrobials and the beginning of the antibiotic era (Gustafson and Bowen, 1997). Antibiotics have subsequently been used to treat a number of diseases and conditions, including tuberculosis (Mukherjee *et al*., 2004), influenza (Low, 2008), Rickettsia related diseases (Finlay *et al*., 1950; Low, 2008), Lyme disease (Wormser *et al*., 2000), acne (Ross *et al*., 2003), salmonella and *E.coli* infections and as a prophylactic when microbial infections are expected (Kemper, 2008).

1.1.2 Environmental impact of antibiotic residues

With the increasing use of organic and chemically based additives used to improve livestock and crop health in the agricultural sector as well as the human health sector, their potential side-effects must be taken into consideration (Martínez, 2008; Watanabe *et al*., 2010). Compounds ranging from steroidal hormones and antibiotics to endo- and ectoparasiticides, heavy metals and dioxins have been identified in feedlot waste due to incorrect dosing and/or application, addition to animal feed, excretion and resistance of the compound to degradation under environmental conditions (Khan *et al*., 2008; Watanabe *et al*., 2010).

Many antibiotic compounds (including oxytetracycline) are excreted and secreted (in the case of milk) mostly unmetabolised, leading to feedlot waste and effluent containing these compounds in increasing concentrations which can promote

antibiotic resistance in exposed pathogenic bacteria species (Khan *et al*., 2008) as well as cause allergic reaction in hypersensitive people (Masawat and Slater, 2007). Through the process of feedlot-waste leaching and manure distribution, excreted unmetabolised antibiotics have also been identified in forage fields, ground water and river systems (Watanabe *et al*., 2010).

The presence of antibiotics in the environment has been extensively reported on (Halling-Sørensen *et al*., 2002; Khan *et al*., 2008; Watanabe *et al*., 2010). One of the primary concerns regarding the build-up of antibiotics and their degradation and metabolised by-products, is resistance to these compounds by pathogenic microorganisms of veterinary and human importance (Graham *et al*., 2011). For farmers, correct dosing of antibiotics is of importance not only to ensure successful antimicrobial effects, but also to minimise resistance by these susceptible microbes to the applied agents, while maintaining animal health without build-up of the agent in the environment where it or its degradation products can affect other members of the ecosystem. Resistance build-up reduces antibiotic efficacy, with detrimental economic and environmental consequences (Anadon and Martinez-Larranga, 1999).

1.1.3 Human health risks associated with antibiotic residues and resistance

In the wake of a report by the European Union (EC, 2003), the use of antibiotics as growth promoters in feedstock was banned in 2006 (Phillips *et al*., 2004). This aimed to prevent antibacterial resistance, believed to be associated with antibiotics used as growth promoters, from affecting humans (Kemper, 2008). The presence of antibiotic residues in food products is of concern in terms of ingestion by hyper-allergic individuals, a well-known example being penicillin allergy (De Ruyck and De Ridder, 2007; Kemper, 2008). These foodstuffs include milk, eggs, fish, honey, meat and other animal tissues (EC, 1996; Oka *et al*., 2000; De Ruyck, and De Ridder, 2007).

While opinions on the contribution of this farming practice towards antibiotic resistance are divided, and involvement of antibiotic use in the human health sector has been proposed, the decreased susceptibility of various microbes to antimicrobial agents is not contested (Phillips *et al*., 2004). As pointed out by Nwosu (2001), a correlation can be found between a rising occurrence of resistant bacterial strains

and increased quantities of antibiotics used. This author also notes transference of resistance genes between bacteria through mobile genetic elements (transposons, plasmids and bacteriophages), thus increasing the percentage population resistance.

It is clear increased resistance hinders fast and effective treatment of microbial infections. The continual re-emergence of multidrug-resistant tuberculosis (MDR-TB) is a good example of this (Mukherjee *et al*., 2004). Hospital-acquired (nosocomial) infection, such as multi-drug resistant *Staphylococcus aureus* and *Enterococcus* species are of equal concern, particularly for immune-compromised patients (Muto *et al*., 2003).

1.1.4 Production evaluation of antibiotics

A factor outside the control of the end user of store-bought antibiotics is that of quality assurance during the manufacturing process. An under-concentrated formulation applied over a prolonged period has been proposed to lead to increased microbial tolerance and resistance, due to sub-inhibitory antibiotic levels (Cloete, 2003; Martínez, 2008). Store-bought antibiotic products, on average, contained ~ 98 % of the concentration stated on the packaging and several authors have noted negligible inconsistency between analytically determined yield and product label suggested yield of commercial antibiotics (Gallinganio *et al*., 1993; Krishna Priya *et al*., 2007; Karasali and Ioannou, 2009). However, Kazemifard and Moore (1997) found a formulation of oxytetracycline antibiotic containing only 52 % of the stated active ingredient concentration.

Product evaluation, in terms of monitoring the quantity and quality of a product of interest, is also of importance during the production of antibiotics from both a quality-control and profitability perspective. Antibiotics such as oxytetracycline are produced in large-scale bacterial fermentation bioprocesses (Perlman, 1979). Measuring the antibiotic production yield for fermentation processes enables production efficiency to be evaluated. Bioprocessing parameters can be optimised to improve substrate-to-product conversion rates and improve antibiotic output. In order to achieve that, methods for quantifying the antibiotics produced, within the complex growth media of fermenters, is required.

1.2 OXYTETRACYCLINE

Oxytetracycline (OTC) (4-(Dimethylamino)-1,4,4α,5,5α,6,11,12α-octa-hydro-3,5,6,10, 12,12α-hexahydroxy-6-methyl-1,11-dioxo-2-naphtacenecarboxamide) (Forgács and Csethati, 1997) as shown in Figure 1.1, is a broad spectrum antibiotic of the tetracycline class, which includes tetracycline, chlortetracycline, doxycycline, demeclocycline, meclocycline (Masawat and Slater, 2007), roletetracycline, minocycline, methacycline and lymecycline (Chatten *et al*., 1979). All are part of a crystalline antibiotic group containing a shared hydro-naphthacene framework (Perlman, 1979). OTC was first reported on by Finlay *et* al. (1950) who had named this antibiotic Terramycin.

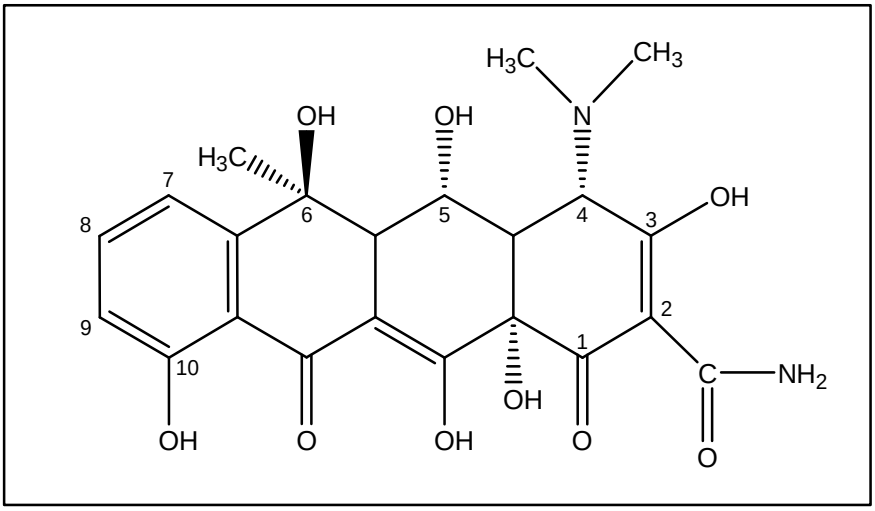

Figure 1.1 Oxytetracycline ($C_{22}H_{24}O_9N_2$).
Adapted from Kurzawa and Kowalcyk-Marzec (2004).

Tetracycline antibiotics are effective against various gram positive and -negative bacteria including some anaerobes (Castellari *et al*., 2009) as well as large viruses and certain pathogenic Rickettsiae (Perlman, 1979).

As a human and veterinary drug, tetracyclines are used to treat and prevent a range of diseases (Vega *et al*., 2007). These include pneumonia (caused by *Streptococcus pyogenes*), genital infections and meningitis (due to *Neisseria gonorrhoeae*), tetanus (due to *Clostridium tetani*), urinary tract infections (due to *Escherichia coli*, *Enterobacter aerogenes* and *Proteus mirabilis*), gastroenteritis (due to *Shigella*

species), cholera (due to *Vibrio cholerae*), and to treat diseases caused by Rickettsia species such as typhus fever, rocky mountain spotted fever and Q-fever (Perlman, 1979). Tetracyclines are also used as preserving agents for harvested vegetables, as well as pesticides for crop-borne disease prevention (Maia *et al*., 2008).

OTC, together with chlortetracycline, were the first members in the tetracycline group to be described in the late 1940s (Chorpa and Roberts, 2001). OTC production occurs by aerobic fermentation of *Streptomyces rimosus*, *S. platensis* or *S. aureofaciens* among other *Streptomyces* species (Perlman, 1979). The mode of action of OTC is bacteriostatic in nature, as the production of proteins by susceptible microorganisms in inhibited (Maia *et al*., 2008). Though not encompassing of all OTC susceptible microbes, one mode of action is described as the attachment of OTC to bacterial 30s ribosomal subunits, preventing tRNA binding which results in translation inhibition (Chorpa and Roberts, 2001). This leads to reduced growth and, when applied in sufficiently high doses, cell death (Perlman, 1979).

1.2.1 Benefits and detriments of oxytetracycline use

In terms of the general properties, uses and concerns associated with antibiotic use as highlighted in Section 1.1, OTC is a model antibiotic for study based on its wide spread use and residual build-up in the environment. However, the economic benefits of OTC use must not be ignored.

An example of OTC used as a veterinary drug, is the treatment of Rickettsial diseases commonly transmitted by ticks and biting flies (Andrew and Norval, 1989; De Waal, 2000). In particular, the effective treatments of two Rickettsial diseases are of economic relevance in the agricultural and tourism sector. Heartwater is caused by *Ehrlichia ruminantium,* which infects sheep, cattle and African buffalo (Andrew and Norval, 1989). Bovine anaplasmosis is caused by *Anaplasmosis marginale*, which infects African buffalo, a range of Southern African antelope, and cattle in which it has been shown to cause premature termination of the foetus and is transplacentally transmitted to surviving calves (Fowler and Swift, 1975).

The value of OTC use is not only limited to animal wellbeing, but also improved product output in this sector. A study revealed that even for small scale farming practices, the use of OTC for the treatment of mastitis could improve dairy farm profit margins by up to 22 % (Wickramasuriya, 1985). A study performed at a piggery revealed average body weight and average daily weight gain improved significantly for piglets whose diet was supplemented with long acting OTC (Chantaraprateep *et al*., 1987). This use of OTC as a low-dose/long term growth promoter for livestock was also shown for shrimp aquaculture, though up to 70 % of the antibiotic remains un-metabolised in the water (Vega *et al*., 2007). This non-veterinary use, coupled with its widespread application, has led to environmental build-up of OTC due to its maintained activity in the environment, which is proposed to be a major contributing factor of antibiotic resistance (Halling-Sørensen *et al*., 2002).

To prevent low-dose/long-term human ingestion of OTC through consumption of tainted animal products, which can lead to microbial resistance and allergic reactions in hypersensitive individuals, maximum residue levels (MRL) have been determined in various countries. The European Union established MRLs for OTC in various products including animal kidneys (600 µg/kg), liver (300 µg/kg), muscle tissue (100 µg/kg), milk (100 µg/kg) and eggs (200 µg/kg) (EC, 1996).

1.3 DETECTION AND QUANTIFICATION OF OXYTETRACYCLINE

With the abundance of antibiotic residues in the environment, and the health implications of tainted food products, the need for fast, accurate and reliable detection mechanisms for these compounds becomes evident. A range of detection methods for OTC have been developed.

Spectrophotometric quantification of OTC was performed by Emara *et al*. (1991) using a stable free radical as colourimetric indicator. An abstracted hydrogen atom from the phenol group of OTC reacts with the free radical causing an OTC-concentration dependent decline in colour. This method was capable of detecting the antibiotic at concentrations as low as 2.5 µg/ml. High-performance liquid chromatography (HPLC) with fluorescent detection was used by Maia *et al*. (2008),

while Castellari *et al*. (2009) used ultra-high-performance liquid chromatography tandem mass spectrometry (UPLC-MS) with great success. The latter authors found OTC to be detectable up to two months after application and achieved a limit of detection (LOD) of 10 ng/g in hair of calves, with average detectable levels of 1660.1 ng/g measured in hair of recently treated animals.

1.3.1 OTC detection in complex fermentation media

Industrial bioprocess control occurs in the form of on-line and off-line sample analysis. As detailed by Ratledge and Kristiansen (2001), on-line analysis occurs within the fermentation vessel as the production process occurs. This is commonly performed to determine essential growth parameters, e.g. pH, temperature, feedstock levels and dissolved oxygen concentration of the growth media. These measurements allow reactive measures to take place. Due to the lack of appropriate on-line sensors for product yield determination directly in complex growth media, these analyses are often performed on samples taken from the reaction vessel, and termed off-line measurements. This incurs a time-delay and prevents the measurements from being used effectively for feedback process control.

Streptomyces species are known to produce a wide spectrum of antimicrobial compounds, including OTC. Whether produced by liquid batch fermentation (Zygmunt, 1961; Baghlaf *et al*., 1979), or through an immobilised cell system (Yang and Yueh, 2001; Jetty *et al*., 2009), the determination of OTC fermentation yield is measured primarily through variations of the disk-diffusion method (Abou-Zeid *et al*., 1980; Lunestad and Goksøyr, 1990). This method involves placing paper disks, infused with the antibiotic, on agar plates inoculated with an OTC-susceptible bacterial species. A zone of clearance forms around the disk as a result of inhibited bacterial growth, and is proportional to the antibiotic concentration.

A major drawback to the disk-diffusion method for antibiotic monitoring is the time in which results are obtained, which can vary from 18 hours (Riaz, 1986) to more than 24 hours (Yang and Lee, 2001). Though accurate, considering the fermentative production of OTC only lasts for 5 – 10 days (Zygmunt, 1961; Yang and Lee, 2001), this is not a practical method to ascertain production yield on a regular basis.

In the case of tetracycline (TC), chromatographic methods such as HPLC have been used for yield determination (Yang and Ling, 1989; Doi and Stoskopf, 2000), though this is less common. HPLC, unlike disk-diffusion, can be performed within half an hour, but requires sample preparation, depending on the purity of the sample (Tsuji and Goetz, 1978; Doi and Stoskopf, 2000).

The need for a rapid, i.e. more or less real-time, monitoring system for metabolites produced in fermentation reactions becomes evident. This would allow improved process monitoring while enabling the effect of changes made to the production process to be evaluated (Schügerl, 2001). Such a monitoring system would be useful for fast OTC yield determination and fermentation reaction optimisation.

1.3.2 Electrochemical detection of OTC

Electrochemistry, as a technique to both detect and quantify analytes in complex media, offers several advantages over conventional spectroscopic and chromatographic methods. An optimised system can be made both inexpensive and portable through the use of screen printed electrodes and a hand-held potentiostat (Liu and Lin, 2005). Decreased sample pre-treatment and shorter analysis times are also achievable (Gupta *et al*., 2011). Good examples of these are glucose sensors employed as a diagnostic tool for diabetes patients (Wang, 1994).

Early electrochemical studies into the redox behaviour of tetracyclines were performed with a focus on its electro-reduction, while the first anodic oxidation was investigated by Chatten *et al*. (1979). Though OTC was not included in that study, it was found that the majority of the tetracyclines exhibit comparable anodic electrochemical properties, including similar anodic peak potentials at both gold and platinum working electrodes and analogous current versus square root of scan rate curves. This formed the basis for their assumption that similar numbers of electrons were involved in the oxidation of each of the tetracyclines, and oxidation occurred at structurally similar functional moieties. These similar properties were exhibited in the cyclic voltammetry (CV) and differential pulse voltammetry (DPV) work by Hou and Wang (1989), where OTC was included in a comparative study with tetracycline,

chlortetracycline and doxycycline. Yet as detailed further in Chapter 3, in-depth analysis of the electrochemical behaviour of OTC remains to be examined.

1.4 ELECTROCHEMICAL PRINCIPLES AND TECHNIQUES

1.4.1 Theory of voltammetry

Potentiostatic techniques are defined as measurements of current response resulting from an applied potential, which promotes the transfer of electrons to and from the electrochemically active compound (Wang, 1994).

A potential excitation waveform is maintained across an electrolyte solution. This facilitates the transfer of electrons either from the analyte to the working electrode (oxidation) or the opposite way (reduction) which in turn produces a measurable response in the form of current (Wang, 1994). A reversible rate-determined, single electron oxidation reaction can be illustrated as follows:

$$A \underset{k_b}{\overset{k_f}{\rightleftharpoons}} B + e^-$$

where A and B represent the reduced and oxidised form of the electrochemically active species respectively, K_f and K_b the rate constant of the forward and reverse reaction respectively, and e^- the single electron transferred.

A classical three-electrode electrochemical cell, commonly utilised in electro-analysis and used in this study, is represented by Figure 1.2. The electrochemical cell comprises a working electrode (WE), reference electrode (RE) and a counter (auxiliary) electrode (CE) submerged in an electrolyte solution, which is often a buffer.

In such an experimental setup, the function of the reference electrode is to maintain a controlled potential between itself and the working electrode, while the counter electrode completes the circuit allowing for the flow of electrons. This flow occurs between the counter- and the working electrode and is in turn responsible for the current peak observable in voltammograms (Wang, 1994; Kissinger and Heineman, 1996).

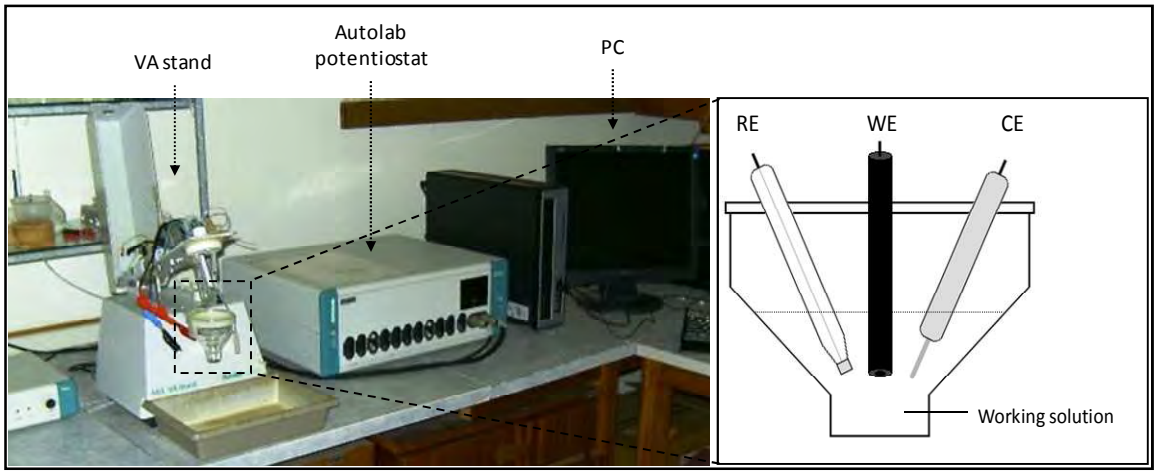

Figure 1.2 Autolab set-up with a standard three electrode electrochemical cell as used in this study. RE = reference electrode, WE = working electrode, CE = counter (auxiliary) electrode.

Taking into account the peak height and the potential at which it occurs, voltammetry can be used as a quantitative and qualitative tool respectively with regards to the analyte in question (Wang, 1994; Scholz, 2002).

1.4.2 Cyclic voltammetry

Cyclic voltammetry (CV) is one of the most commonly used electrochemical techniques, enabling determination of the nature of the redox reaction as well as electron kinetics. It offers qualitative and quantitative data about the analyte(s) in question (Wang, 1994). The technique is defined by a time-dependant, triangular, potential excitation waveform (Figure 1.3a).

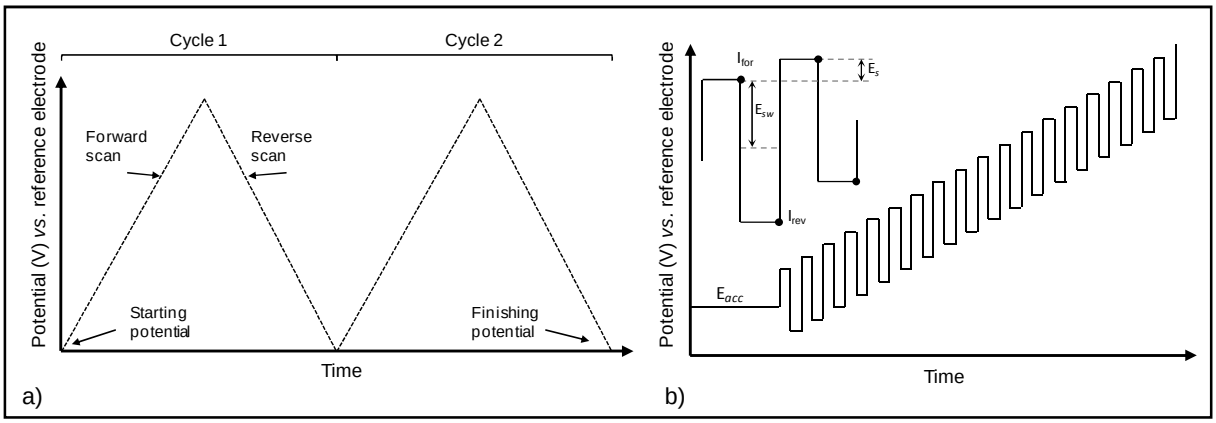

Figure 1.3 Excitation signal for a) cyclic voltammetry (CV) and b) square wave voltammetry (SWV). Adapted from Kissinger and Heineman, (1996). I_{for} and I_{rev} refer to the forward and reverse current sample points respectively as indicated by black dots; E_{sw} refers to the square wave amplitude; E_s refers to the step potential; E_{acc} refers to an arbitrarily long accumulation period at the starting potential.

The applied potential is cycled from an initial to a final potential and back to a finishing potential (often the same as the initial potential). The consequential current response is represented as a current vs. potential plot named a cyclic voltammogram (Wang, 1994).

1.4.3 Square wave voltammetry

The square wave voltammetric (SWV) technique consists of a regular square wave potential excitation waveform applied between the reference- and working electrode (Figure 1.3b). After an arbitrarily long waiting period (E_{acc}), which can serve as an accumulation step, the potential is shifted forward and then in reverse, according to the preset step height (E_s) and square wave amplitude (E_{sw}) (Wang, 1994). A current measurement is sampled twice during each cycle (forward half cycle, I_{for}, and reverse half cycle, I_{rev}), of which the difference (net current, I_{net}) is calculated as $I_{net} = I_{for} - I_{rev}$. I_{net} is plotted as the dependent variable versus the mean potential applied for each SW period, on what is known as a square wave voltammogram (Lovric *et al*., 1988; Miles and Compton, 2000).

The advantage of SWV can be found in its sensitivity and low detection limits (down to 1×10^{-8} M) due to differentiation between background currents (Wang, 1994).

1.5 ENHANCING SENSITIVITY: CARBON NANOTUBES

The nanoscale structure of carbon nanotubes (CNT) was described by authors including Iijima (1991). This author described CNTs as hollow cylinders consisting of one or more helically-formed tubules sharing a common axis, each made up of a graphite carbon hexagon network (Figure 1.4). Commonly, tubes with a single cylinder are referred to as single-walled carbon nanotubes (SWCNT), while those with multiple cylinders have been dubbed multi-walled carbon nanotubes (MWCNT) as shown in Figure 1.4a and 1.4b respectively (Hou *et al*., 2008).

Among many applications, CNTs have been shown: to improved load transfer (Qian *et al*., 2000) and increased strength and elasticity of composite and epoxy materials (Thostenson and Chou, 2002); have exceptional thermal conductive properties

(Nan *et al*., 2003; Ju and Li, 2006); and exhibit capabilities as a filtration material for bacterial and viral particles (Ajayan *et al*., 2006). With respect to their electrical properties, research has been performed into the use of CNTs as field-effect transistors (Martel *et al*., 1998; Bachtold *et al*., 2001) and field emission sources (Choi *et al*., 1999; Lee *et al*., 2001).

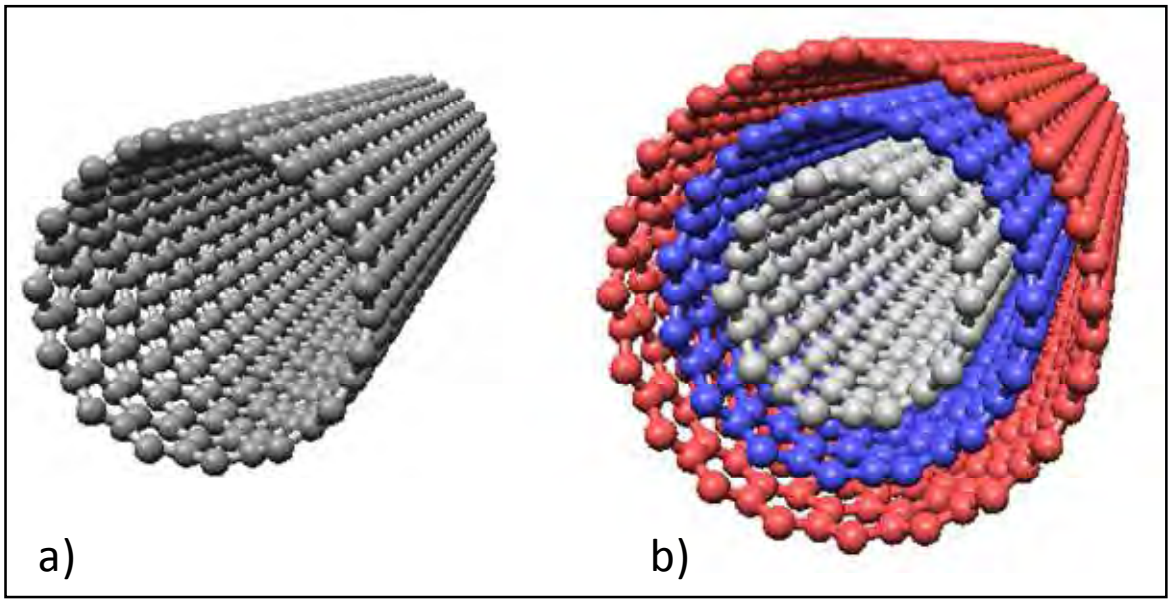

Figure 1.4 Conceptual diagrams of a) single-walled carbon nanotube and b) multi-walled carbon nanotube.
Modelled using Nanotube Modeller (Version 1.7.3, JCrystalSoft).

1.5.1 Electrochemical application of carbon nanotubes

The first application of CNTs towards enhancing an electro-oxidative response was reported for dopamine (Britto *et al*., 1996). Since then, CNTs have been applied to working electrode surfaces to improve the detection of a range of compounds including uric acid, hemoglobin, L-histidine, atenolol, propanol, dopamine, folic acid, glucose, ascorbic acid, tetracycline (TC) and OTC (Uslu and Ozkan, 2007; Vega *et al*., 2007; Guo *et al*., 2009; Zare and Nasirizadeh, 2011).

The literature around application of CNTs is dense and much yet remains to be understood to the nature of the benefits it affords for electro-analysis. Once believed to be catalytic, it is now understood that the enhanced oxidative and reductive signals observed are commonly ascribed to the edge-plane-like properties of the CNT tube ends and defect sites (Banks *et al*., 2005; Ji *et al*., 2006). These locations

of the CNT structure are referred to as edge-plane-like as they exhibited similar voltammetric behaviour as edge-plane pyrolytic graphite, while pristine tube wall behave similar to basal-plane electrodes and thus referred to as basal-plane-like (Holloway *et al*., 2008).

1.6 PROBLEM STATEMENT

The main research areas in electrochemical analysis are aimed at increasing sensitivity, enhancing specificity and decreasing fouling of the electrode surface. Analysis in complex media, such as microbiological growth media, present a particular challenge for electrochemical methods, owing to competitive interferents and fouling of the electrode surface due to adsorbed redox products or contaminants. Limited literature has explored voltammetry in growth media.

Processes in the literature that can achieve sensitivity and reduce fouling range from simple solutions to more complex methods, and include the use of derivatised nanomaterials. In this study, as detailed in Chapter 3 to 5 using OTC as a case study, simple solutions such as stirring and preconditioning potential are examined as well as simple solutions for voltammetric studies in growth media. Finally, we probe the role of MWCNTs in enhancing OTC detection. These studies serve to provide the platform for an ongoing study in developing methods for continuous detection by voltammetric methods, for OTC detection in antibiotic fermenters used in the industrial production of OTC.

1.7 OVERALL AIMS AND OBJECTIVES OF THIS STUDY

The work presented in subsequent chapters aimed to assess the applicability of voltammetric techniques, square wave voltammetry in particular, as a fast detection method for OTC. Emphasis is placed on improving sensitivity and OTC analysis in complex microbial growth media. A particular focus is developing methods that are simple and considered practical for real application in industry. The aims and objectives can be divided into the following three sections:

Aim 1 (Chapter 3): Evaluate simple operational parameters for enhancing sensitivity for OTC detection and reducing fouling

In light of limited literature available concerning the electro-analytical behaviour of OTC at a bare GCE, Chapter 3 examines the oxidative behaviour of OTC using CV and SWV. Operational parameters such composition and pH of the working solution, preconditioning potential and adsorption time were optimised. Electrode reusability, OTC reaction mechanism and detection limits were experimentally determined.

Aim 2 (Chapter 4): Establish viability of voltammetry as a monitoring system for OTC in complex microbiological growth media

As stated, the literature pertaining to voltammetry in growth media is limited. To address this knowledge gap, the voltammetric behaviour of commonly used microbiological growth media was assessed as examples of complex fermentation media used for commercial antibiotic production. As a case study of monitoring antibiotics in growth media, anodic and cathodic analysis of OTC was performed in sterile fermentation media. The influence of interfering growth media ingredients and electrode fouling on the recovery of OTC current signal and detection limit was investigated.

Aim 3 (Chapter 5): Asses the application of MWCNT-modified GCEs for enhancing detection of OTC

Literature concerning the application of MWCNT-modified GCEs towards the electro-analytical detection of OTC is scarce. In particular, minimal evaluation of MWCNT-GCE operational parameters has been performed. Chapter 5 aimed to assess the physical and chemical properties of MWCNTs, used for electrode modification, by Raman spectroscopy, CV and electrochemical impedance spectroscopy (EIS). Parameters assessed were acid functionalisation time and dispersal agent selection. The performance of MWCNT-modified GCEs towards OTC oxidation was evaluated based on MWCNT functionalisation time, dispersal agent selection, loading volume, detection limit and selective exclusion of interferents.

CHAPTER 2

General Experimental Approach

This chapter describes the general reagents, equipment and data analysis procedures used throughout the study. Subsequent results chapters detail the experimental approach relevant to those sections in further detail.

2.1 INSTRUMENTATION

2.1.1 Voltammetry

A Potentiostat/Galvanostat 30 (PGSTAT302, Autolab) linked to a Voltammetric Analytical stand (VA 663, Metrohm) via an Autolab IME 663 interface (Autolab) was used for all electrochemical analysis. Data analysis was performed using General Purpose Electrochemical System (GPES version 4.7.9, Eco Chemie B.V.), NOVA (version 1.5, Eco Chemie B.V.) and Microsoft® Excel 2007 software packages.

Glassy carbon electrodes (GCE, 3 mm diameter) from BioAnalytical Systems (BAS) were used in a standard three electrode electrochemical cell, serving as the working electrodes. A platinum wire and Ag/AgCl (3 M KCl, NaCl saturated) electrode served as the counter and reference electrode respectively. Electrodes were positioned equidistantly, prior to each analysis. All voltammetric experiments were performed at ambient temperature (21 ± 2°C) and solutions were quiescent.

2.1.2 Other equipment

A WTW inoLab pH 730 pH meter with WTW SenTix® 81 (KCl 3 M, Ag^+ free) reference electrode was used during buffer titrations.

2.2 MATERIALS

2.2.1 Reagents and solvents

The following reagents and solvents were of technical grade or higher, and are listed with their purities (%) and manufacturers from which they were obtained. Boric acid (> 99 %),nitric acid (65 %), potassium hexaxyanoferrate (III) (≥ 99 %) and citric acid

(≥ 99.5 %) from Merck; potassium hexacyanoferrate (II) trihydrate (≥ 99.5 %) from Fluka; phosphoric acid (> 85 %), acetic acid (glacial, > 99 %), sodium hydroxide (NaOH, > 98 %) and potassium hydroxide (KOH, > 85 %) from Saarchem; potassium chloride (KCl, > 99 %) and potassium dihydrogen phosphate (KH_2PO_4, ≥ 98 %) from Sigma Aldrich; Acetonitrile (for far UV HPLC, 99.9 %) from Riedel-de-Haën.

Nitrogen gas (N_2, > 99.999 % pure) was obtained from Afrox (South Africa) and purified using a gas dry trap from Chromatographic Research Supplies (CRS, USA) for the removal of moisture, oil and dust.

Double deionised MilliQ water (18 $M\Omega.cm^{-1}$) was used for all buffer and microbiological media preparations and wash steps. A 5 % nitric acid solution was used to clean all glassware followed by two wash steps with MilliQ.

2.2.2 Analyte

Oxytetracycline (OTC) hydrochloride (VETRANAL® grade, ≥ 98.1 % pure, CAS No. 2058-46-0) was purchased from Sigma Aldrich. OTC stock solutions were prepared weekly in the diluents specified and stored in dark containers at 4 °C when not used.

2.2.3 Electrochemical reagents

Britton-Robinson (BR) buffer (0.2 M boric acid, 0.2 M phosphoric acid, 0.2 M acetic acid) was titrated to the appropriate pH using NaOH. This buffer was selected for its buffering capacity across a wide pH range of 2 - 12 (Britton and Robinson, 1931). Potassium dihydrogen phosphate (PP) buffer (0.2 M) was titrated to either pH 2 or pH 7 as required using phosphoric acid and KOH respectively. Both buffers were used as supporting electrolytes and were stored at 4 °C between uses and warmed to room temperature before being employed.

For cathodic analyses, the electrolyte solution was degassed prior to measurements by purging with nitrogen gas for times specified in the respective sections. A nitrogen blanket was maintained over the solution during analysis to prevent oxygen from dissolving back into solution.

2.3 TECHNIQUES

2.3.1 Electrode preparation

The surface of the GCE was cleaned by rinsing with double deionised MilliQ water, followed by absolute ethanol and again with MilliQ water. The GCE surface was polished in an aluminium oxide slurry (< 10 micron, Sigma Aldrich) on a Buëhler felt pad (BAS) in a figure eight pattern followed by the same rinsing procedure as before. This cleaning routine was carried out between analyses unless otherwise stated.

2.3.2 Voltammetric techniques

Square-wave voltammograms (SWVs) depict current (I_{net}) as a function of potential applied unless otherwise stated, where $I_{net} = I_{for} – I_{rev}$ (Figure 2.1a). This is also referred to as the net square wave voltammetric response.

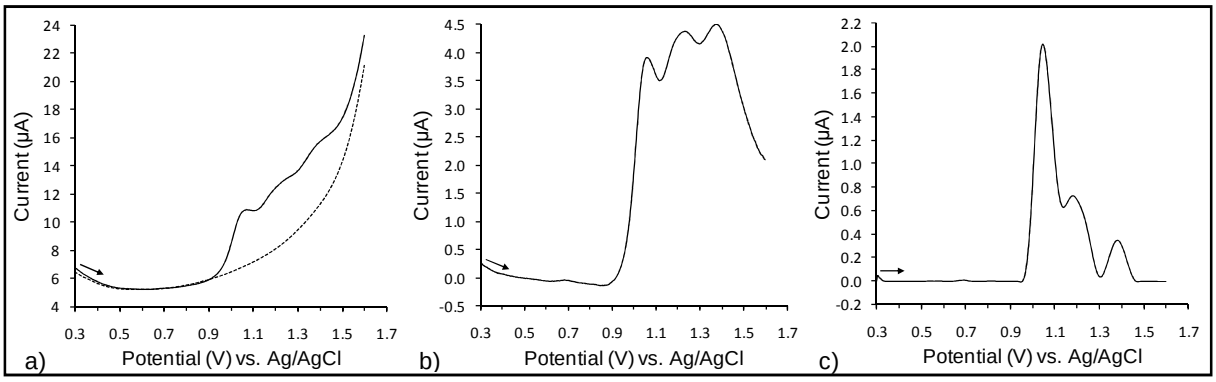

Figure 2.1 SWVs showing the difference between: a) normal SWV with dashed baseline, b) baseline subtracted SWV and c) baseline-corrected voltammograms as used in this study.

Quantitative data was obtained from baseline subtracted SWVs (Figure 2.1b). These were produced by subtracting the current response of a blank scan (containing no sample) from a scan containing the sample. Blank scans were obtained by ten successive scans in buffer or until a stable baseline was achieved.

Baseline-corrected (Figure 2.1c) SWVs are shown purely as visual aides to more clearly illustrate the individual peaks and were not used for quantitative analysis. Baseline corrected SWVs were produced in GPES using the Moving Average function (peak width: 0.005 V). Signal smoothing was used intermittently when

baseline subtracted data was presented, though this data manipulation was employed solely for visual purposes and not for data analysis.

Scan rate (υ) is calculated as the combined effect of step potential (E_s) and frequency (f) as follows: $\upsilon = E_s.f$ with E_s set at 5 mV and f at 20 Hz (Zachowski *et al*., 1986). With the square-wave amplitude, E_{sw}, at 20 mV, all parameters were maintained the same for every SWV experiment.

Cyclic voltammetry (CV) was used, where appropriate, to assess the kinetics of the redox processes involved in OTC and reversible redox probe detection. For both SWV and CV, all results were obtained and expressed as applied potential vs. Ag/AgCl reference electrode. Black arrows parallel to the voltammograms shown in this thesis indicate the scan direction for all CVs and SWVs.

Electrochemically reversible redox probes $Fe(CN)_6^{4-/3-}$ and $Ru(NH_3)_6^{2+/3+}$ were used to probe the electrode activity. For these electrochemically reversible reaction, the following scheme applies when the forward scan is in a positive direction:

$$R \rightleftharpoons O + e^-$$

where R represents the reduced form, O the oxidized form and e^- the single electron transferred in these reaction. These probes are commonly used to determine the effective electrode surface area, A_{exp}, (Van Benschoten *et al*., 1983) and examine GCE activity because of extensive work performed on the electron transfer kinetics of these probes (Brown, 1972; DeAngelis and Heineman, 1976; Hu *et al*., 1985).

2.3.3 Electrochemical Impedance Spectroscopy (EIS)

EIS is a powerful electrochemical tool used for probing corrosion mechanisms, the optimisation of batteries, and investigate the reaction mechanism occurring at an interfacial region (electrode/electrolyte interface in the case of this work) (Macdonald, 1990; Ferloni *et al*., 1996; Lisdat and Schäfer, 2008). By applying a sinusoidal excitation potential with a small amplitude (1-10 mV) to a electrolyte solution containing an equimolar concentration of the oxidised and reduced form of a redox molecule ($Fe(CN)_6^{3-/4-}$ and $Ru(NH_3)_6^{2+/3+}$ in this work), a sinusoidal current response is obtained (Macdonald *et al*., 1998).

Data modelling was performed using the frequency response analyser software (FRA, version 4.9.007, Eco Chemie B.V.), by fitting experimentally obtained data to an equivalent circuit. Data pertaining to the resistance of the solution, the charge transfer and the diffusion mass transport, as well as the capacitance of the electrode/electrolyte interface can be elucidated by individual circuit elements of the equivalent circuit (Park and Yoo, 2003). Properties of films on the electrode surface can be described by additional circuit elements.

Current flowing through resistors and capacitors experiences complex resistance called impedance (Park and Yoo, 2003). Impedance in this study is presented in complex impedance plots called Nyquist plots, as well as Bode plots. A frequency range of 100 mHz to 15 kHz was scanned logarithmically at an applied potential (V) equal to the observed open-circuit potential (OCP) for the respective sample, with an alternating voltage of 5 mV rms.

2.4 VOLTAMMETRIC DATA ANALYSIS

For all figures and tables, error bars and error margins represent standard deviation calculated with ≥ 3 replicates. For voltammograms, a scan rate of 100 mV/s was maintained for all experiments unless otherwise stated. Figure 2.2 shows analysis of typical SWV and CV data obtained.

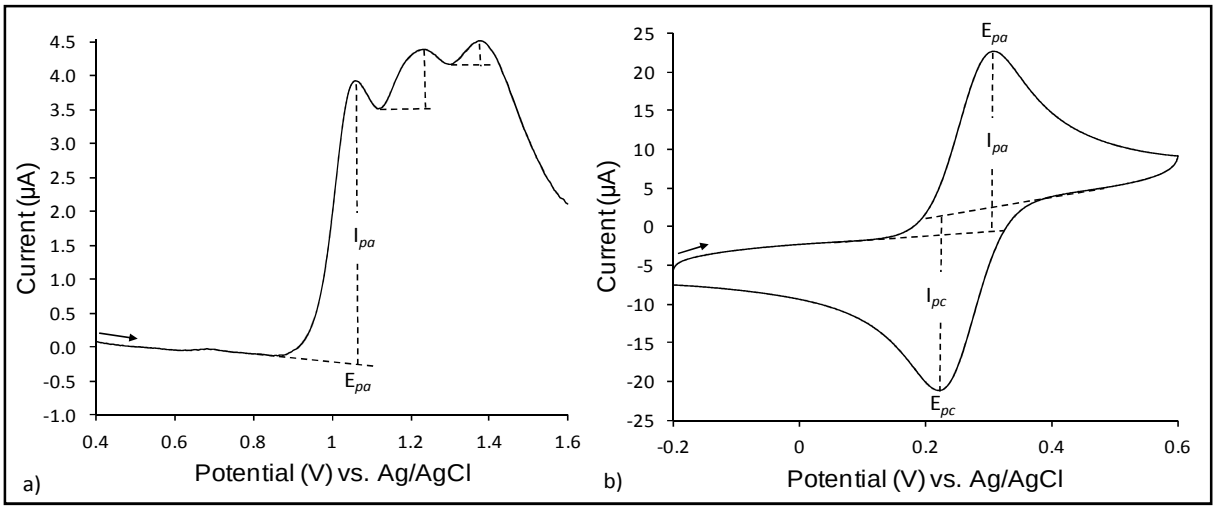

Figure 2.2 Data analysis for a) SWV analysis of OTC and b) CV analysis of a reversible redox couple. I_{pa} and I_{pc} refer to the height (µA) of the peak anodic and cathodic peak respectively, while E_{pa} and E_{pc} indicates the anodic and cathodic peak potential (V) respectively.

This figure shows how the peak current (I_p) and peak potential (E_p) obtained for SWV analysis of OTC and for CV analysis of reversible redox waves were measured (Figure 2.2a and 2.2b respectively).

2.4.1 Coefficient of variation and reproducibility

The calculated coefficient of variation (C_v) of scan replicates are presented periodically to enable comparisons of the variability observed between different experiments with dissimilar arithmetic means (Rosner, 2000):

$$C_v\ (\%) = \left(\frac{S}{\bar{x}}\right).100 \qquad \text{[Equation 2.1]}$$

where *s* represents standard deviation and $\bar{x}$ the mean of a set of replicates. C_v is expressed as a percentage value, where lower values represent greater reproducibility. Reproducibility can thus be calculated as follows:

$$\text{Reproducibility (\%)} = 100 - C_v \qquad \text{[Equation 2.2]}$$

Data sets with C_v values of ≤ 10 % (i.e. reproducibility ≥ 90 %) were deemed to have sufficiently high reproducibility for analytical purposes.

2.4.2 Electrode fouling

Fouling (also referred to as electrode passivation) refers to the decrease in current response observed without cleaning of the working electrode surface between successive scans. This can be illustrated by denoting the current response of the 1st scan as 100% and calculating the peak heights of subsequent scans in percentage format:

$$\text{Percentage fouling } (\%) = \left(\frac{I_{final}}{I_{initial}}\right).100 \qquad \text{[Equation 2.3]}$$

where I_{final} represents the peak current of the successive scans of a fouling study, while $I_{initial}$ corresponds to the current response of the first scan on a pristine electrode.

2.4.3 Detection and quantification limits

The limit of detection (LOD) was calculated as the lowest detectable analyte concentration and was calculated as follows:

$$\text{LOD} = \left(\frac{3.s}{\text{slope}}\right) \quad \text{[Equation 2.4]}$$

were LOD is three times the standard deviation (*s*) of the baseline current (blank scan) divided by the slope of the linear portion of the I_p vs. analyte concentration plot (Rufino *et al*., 2009). The limit of quantification (LOQ), as the lowest reliably quantifiable analyte concentration, was measured similarly with ten times *s*. Data was expressed in nM.

2.4.4 Sensitivity

The slope of the linear portion of I_p *vs.* analyte concentration was recorded as the gradient determined sensitivity.

Concentration specific sensitivities were calculated to enable comparisons between successive experiments to be performed for similar analyte concentrations. This was determined via the following equation:

$$\text{Concentration specific sensitivity} = \left(\frac{I_p}{c}\right) \quad \text{[Equation 2.5]}$$

expressed as μA/μM, where I_p refers to the current response and *c* the analyte concentration.

2.4.5 Data modelling for Langmuir isotherm

Concentration curves for OTC revealed a dependence between the current response and OTC concentration that could be expressed using an adaptation of the Langmuir isotherm (Bard and Faulkner, 2001):

$$\text{I} = \text{I}_\text{m}\left(\frac{Kc}{1+Kc}\right) \quad \text{[Equation 2.6]}$$

where I is used to represent the predicted current response (μA) for a given analyte concentration (c, expressed as μM), K is an adsorption coefficient while I_m corresponds to the maximum achievable current before the current signal plateaus (expressed as μA).

While these are not the standard units for the symbols expressed in the equation, they have been used previously to model the dependence of redox currents vs. analyte concentrations (Maeda *et al*, 1997; Perez *et al*., 2002).

Microsoft® Excel Solver was used to model the isotherm data and calculate I_m and K. The validity of using the Langmuir isotherm for a data set was tested using a $c.I_{exp}^{-1}$ vs c plot where linearity must be achieved (Perez *et al*., 2002). c is the analyte concentration and I_{exp}^{-1} the inverse of experimentally observed current for the respective analyte concentration.

2.4.6 Surface area measurements

Upon modification of the electrode surface through either suspected broth interference or carbon nanotube application, the electrode surface area was calculated using the Randles-Sevcik equation for reversible diffusion-controlled systems (Kissinger and Heineman, 1983):

$$I_{pa} = 2.69 \times 10^5 . n^{3/2} . A . C . D^{1/2} . v^{1/2} \qquad \text{[Equation 2.7]}$$

where I_{pa} is the anodic peak current (A) of $Fe(CN)_6^{4-}$, n the number of electrons transferred (one for this system), A the surface area (cm^2), C the analyte concentration (mol/cm^3), D the diffusion coefficient, 7.6×10^{-6} cm^2/s for $Fe(CN)_6^{4-}$ (Brown, 1972), and v the scan rate (V/s). Calculations of A were based on the assumption of a constant D.

2.4.7 Roughness factor (R_f)

Electrode surface roughness was calculated as the ratio of experimentally observed surface area to the geometrically calculated one:

$$\text{Roughness factor } (R_f) = \left(\frac{A_{exp}}{A_{geo}}\right) \quad \text{[Equation 2.8]}$$

where A_{exp} is the experimentally observed area (cm^2) calculated from the I_{pa} of the $Fe(CN)_6^{4-}$ and A_{geo} the geometric surface area (cm^2) of the glassy carbon electrode with a radius of 0.15 cm.

2.4.8 Peak current ratio and peak separation for reversible reactions

For fast reversible redox couples, the relationship between the anodic- and cathodic peak current can be described by:

$$\frac{I_{pa}}{I_{pc}} \cong 1 \quad \text{[Equation 2.9]}$$

where I_{pa} and I_{pc} refer to the anodic and cathodic current (μA) of the redox couple respectively (Kissinger and Heineman, 1983).

The following equation is used to calculate the peak separation (ΔE_p) of the aforementioned redox currents:

$$\Delta E_p = E_{pa} - E_{pc} \cong \frac{0.059}{n} \quad \text{[Equation 2.10]}$$

where E_{pa} and E_{pc} refer to the anodic and cathodic peak potential (V) respectively. This can be used to calculate the number of electrons (n) involved for a totally reversible reaction where a peak separation of 59 mV is expected (Kissinger and Heineman, 1983).

CHAPTER 3

Oxytetracycline Detection and Characterisation at a Bare Glassy Carbon Electrode using Cyclic- and Square Wave Voltammetry

3.1 INTRODUCTION

As a broad-spectrum antibiotic, oxytetracycline (OTC) has been used for a wide range of applications as both a therapeutic and preventative agent (Maia *et al*., 2008). Under favourable environmental conditions such as low temperature, low pH and dark settings, such as typically occurs during food storage, the stability of OTC is greatly improved (Doi and Stoskopf, 2000). This in turn, leads to a prolonged presence in the environment, as well as foodstuffs (Albright *et al*., 1961), allowing for increased risk of exposure to humans. The importance of accurate and reliable detection of OTC thus becomes clear. As discussed in Section 1.3, several techniques have been investigated in this regard.

The anodic electrochemical detection of OTC is thought to be due to the oxidation of the phenolic substituent at position C_{10} and di(methyl)amino group at position C_4 highlighted in Figure 3.1 (Kazemifard and Moore, 1997; Masawat and Slater, 2007).

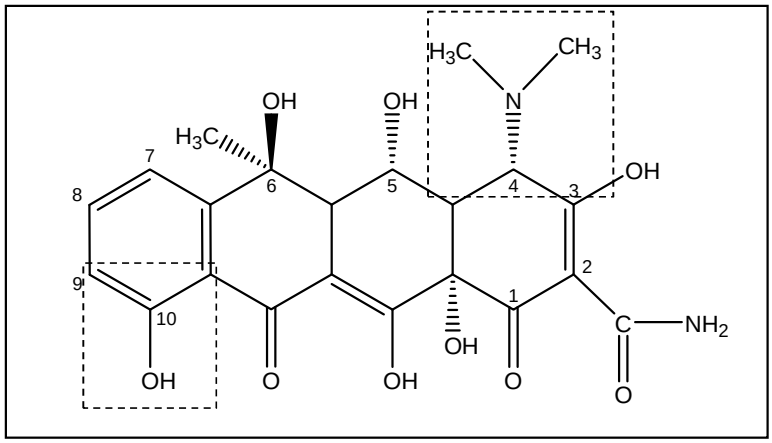

Figure 3.1 Oxytetracycline structure highlighting the proposed oxidation sites. Adapted from Kurzawa and Kowalcyk-Marzec (2004).

For the structurally similar tetracycline (TC) however, Chatten *et al*. (1979) proposed that the phenolic moiety is responsible for the primary anodic peak based on its

similar electrode fouling properties to that of phenols. This author proposed a 1 electron irreversible oxidation reaction for TC, based on data obtained at pH 4 where the amino groups of dimethylamine were protonated.

Hou and Wang (1989) previously described the presence of an irreversible peak starting at 1.0 V (*vs*. Ag/AgCl) during cyclic voltammetry (CV), and the occurrence of several peaks during differential-pulse voltammetry (DPV) at 0.99 V, 1.14 V and 1.35 V (*vs*. Ag/AgCl) respectively, the first being the most well-defined in a highly acidic medium.

In Table 3.1, electro-analytical data from literature for the detection and quantification of OTC is summarised together with tetracycline (TC) which exhibits similar electrochemical properties (Hou and Wang, 1989). In terms of Table 3.1, four methods of increasing sensitivity for OTC and TC detection have been investigated. These were a) electrode selection, b) CNT-coated electrodes, c) electrochemical electrode pre-treatment and d) coupled techniques. As data was presented in various forms, measurements were simplified in order to be comparable. All data is thus represented as molar concentration and peak potentials reported vs. Ag/AgCl reference electrode.

However, little work has been done on the electrochemical behaviour of OTC at a bare GCE and it is worth noting that none of the references cited, reported detection limits for unmodified GCEs in their studies. This has prompted further investigation in this regards, thereby allowing a greater understanding into its practical application.

Furthermore, the majority of methods cited in Table 3.1 were developed for the quantification of the primary anodic response of OTC (referred to as pa_1 in this thesis), though comparable detection limits (LODs) have been reported for cathodic analysis by Ni *et al*. (2011). The use of highly acidic electrolytes is also prevalent, many of which were KH_2PO_4. The LODs reported vary considerably due to the range of different analytical techniques used.

Table 3.1 Parameters and detection limits of electroanalytical techniques for the detection and quantification of OTC and tetracycline (TC) as found in literature. Data is standardised and all potentials are expressed *vs*. Ag/AgCl.

Analyte	Electrolyte	Electrode	pH	E_{det} (V)	Method	Linear range	LOD	Reference
OTC; TC	0.1 M KH_2PO_4	EP-GCE	2.5	+ 1.2	LCEC	0.4 – 8 nM; 0.4 – 8 nM	0.4 nM; 0.4 nM	Hou and Wang, 1989
OTC; TC	0.1 M KH_2PO_4	Au-SPE	2	+ 1.20	DC amperometry	1 – 500 µM; 1 – 500 µM	350 nM; 960 nM	Masawat and Slater, 2007
OTC; TC	0.05 M KH_2PO_4	MWCNT-GCE	2.5	+ 1.20	HPLC - amperometry	2.5-100 µM; 2.5-100 µM	90 nM; 310 nM	Vega *et al*., 2007
OTC; TC	0.1 M KH_2PO_4	Anodized BDD	2	+ 1.60	FI- amperometry	0.5 – 50 mM; 0.1 – 50 mM	10 nM; 10 nM	Wangfuengkanagul *et al*., 2004
OTC; TC	0.1 M Borate + 1 mM EDTA	Hg-film	8.7	~ - 1.40	Fast reductive CV	2.5 – 800 µM; 1 – 500 µM	1500 nM; 700 nM	Zhou *et al*., 1999
OTC	0.1 M Ammonium phosphate buffer	DNA - CNTPE	5.5	+ 0.18	SWASV	2 – 20 pM; 2 – 20 pM	0.0008 nM; 0.0008 nM	Ly *et al*., 2007
TC	0.1 M phosphate buffer	IL-MWCNT-film GCE	7	+ 0.58	LSV	0.11 – 22 µM; 0.11 – 22 µM	30 nM; 30 nM	Guo *et al*., 2009
OTC; TC	0.05 M KH_2PO_4 – Acetonitrile (84:16, $^{v}/_{v}$)	GCE	2.5	+ 1.2	HPLC - amperometry	0.02 – 10 µM; 0.02 – 10 µM	20 nM; 20 nM	Kazemifard and Moore, 1997
OTC, TC	0.04 M Britton Robinson buffer	HMDE	3.78	- 1.0	DPSV	40 – 322 nM; 40 – 201 nM	10.48 nM; 8.26 nM	Ni *et al*., 2011

Note: E_{det} = Detection potential, LOD = Limit of detection, EP-GCE = Electrochemically pre-treated GCE, LCEC = Liquid chromatography with electrochemical detection, Au-SPE = Gold screen printed electrode, DC = Direct current, MWCNT-GCE = Multi-walled carbon nanotube modified GCE, HPLC = High performance liquid chromatography, BDD = Boron-doped diamond, FI = Flow injection, Hg = Mercury, CNTPE = Carbon nanotube paste electrode, SWASV = Square wave anodic stripping voltammetry, IL = Ionic liquid, LSV = Linear sweep voltammetry, HMDE = Hanging mercury drop electrode, DPSV = Differential pulse stripping voltammetry.

3.1.1 Problem statement

While a range of well-defined methods for the electrochemical detection of OTC have been developed (Table 3.1), there exists a lack of information as to the redox properties of OTC at a bare unmodified glassy carbon electrode (GCE). There also exists limited information on the application of square wave voltammetry (SWV) as an analytical technique for OTC quantification. Britton Robinson (BR) buffer shows limited use as an electrolyte in quantitative OTC analysis, only having been applied in cathodic studies. Data relating to buffer and solvent selection, electrode fouling, adsorption and the reaction mechanism of OTC are scarce and incomplete.

3.1.2 Aims and objectives

This chapter aims to investigate the fundamental anodic electrochemical characteristics of oxytetracycline (OTC) at various pH solutions in two defined buffers. This chapter also probed simple methods for optimisation of anodic OTC current and decreasing electrode fouling.

Objective 1: To investigate the effect of electrolyte pH on the anodic electro-analytical behaviour of OTC using cyclic voltammetry (CV).

Objective 2: Square wave voltammetric (SWV) investigation of the effect of electrolyte solution and OTC diluent selection on anodic OTC detection.

Objective 3: Determine the influence of preconditioning potential and stir time on anodic SWV detection of OTC.

Objective 4: Investigate simple methods to reduce OTC fouling at the GCE surface.

Objective 5: Determine the dependence of the anodic OTC current on OTC concentration, using SWV.

Objective 6: Evaluate the mass-transport mechanism for OTC in acidic pH using CV.

Objective 7: Determine the oxidation mechanism of OTC in acidic pH.

3.2 EXPERIMENTAL APPROACH

Unless otherwise stated, all voltammetric experiments were conducted in accordance with Chapter 2. This includes electrode and buffer preparations, analysis and presentation of data and error margins for n ≥ 3. A scan rate of 100 $mV.s^{-1}$ was used unless otherwise specified. General reagent grades and suppliers specified in Section 2.2.

3.2.1 General OTC characterisation at pH 2 and 7

OTC stock solutions (1 mM) were prepared in MilliQ water and analysed in 0.2 M Britton Robinson (BR) buffer at pH 2 and 7 using both CV and SWV. A scan range of 0.3 – 1.6 V in the forward anodic direction was employed.

3.2.2 pH profile

The effect of pH on the anodic current response and peak potential of OTC was investigated. A pH range of 2 – 10 was established using 0.2 M BR buffer and 50 µM OTC.

3.2.3 Effect of solvent and electrolyte solution

The anodic current response of OTC was compared between two buffers, BR and potassium phosphate (PP) at a pH of 2 and 7 while simultaneously comparing a range of diluents for the preparation of OTC stock solutions. These included the respective buffers, MilliQ water, 20 % ethanol ($^{v}/_{v}$ in water) and 20 % acetonitrile ($^{v}/_{v}$ in water).

3.2.4 Preconditioning potential and stir time

The effect of the application of a preconditioning potential on the anodic response of OTC was investigated. This was achieved by placing the GCE in a stirred (1500 rpm) buffer solution for 40 seconds at potentials - 0.4 V, - 0.2 V, 0.0 V, 0.2 V, 0.4 V, 0.6 V and 0.8 V respectively. The preconditioning potential was applied prior to recording the SWV. Sample deoxygenation was performed when negative preconditioning potentials were applied.

Under the influence of a stirrer rotating at 1500 rpm, a range of stir times was compared from 10 – 50 seconds. At the time of stirring (after OTC addition), a conditioning potential of 0.0 V was maintained across the solution while the stir time was controlled through GPES software.

3.2.5 GCE fouling

The fouling effect of OTC at the GCE was investigated by performing successive scans without cleaning the working electrode between scans. The effect of stirring and a preconditioning potential was investigated as a means to decrease fouling.

3.2.6 OTC linear range and limit of detection (LOD) at pH 2 and 7

Using the selected electrolyte/solvent systems from Section 3.3.3, linear ranges of I_{pa1} *vs*. OTC concentration were established and LODs and LOQs were calculated according to Equation 2.4.

In addition, the data was modelled according to the Langmuir adsorption isotherm (Equation 2.6). The parameters I_m, which represents the theoretical maximum signal and K^{-1}, the inverse of the adsorption coefficient (K) used to represent the desorption affinity of OTC (Perez *et al*., 2002), were used to compare the model, as it was applied to I_{pa1} *vs*. OTC concentration plots obtained under different pH and buffer/solvent conditions.

3.2.7 Concentration-specific scan rate study

To determine the mode of mass transport of OTC, scan rate studies were performed. Tested scan rates ranged from 25 mV/s to 400 mV/s. The effect of low and high OTC concentration on mass transport was probed by performing studies at 3 µM and at 20 µM respectively.

3.2.8 OTC oxidation mechanism

Using the data obtained during the scan rate study, the reaction mechanism of OTC oxidation in 0.2 M BR buffer (pH 2) was determined for 3 µM and at 20 µM OTC. Tafel slope analysis was performed to determine the number of electrons involved in the rate-limiting step, n_a.

3.3 RESULTS AND DISCUSSION

3.3.1 General OTC characterisation at pH 2 and 7

For the purpose of initial OTC characterisation, studies were conducted at pH 2, based on its enhanced signal response as previously reported (Masawat and Slater, 2007; Vega *et al*., 2007) and pH 7, as this resembles physiological pH and is of relevance to analyses in biological systems. The effect of a broader pH range on I_{pa1} and E_{pa1} is reported in Section 3.3.2.

Figure 3.2 shows the electrochemical oxidation of OTC in pH 2 BR buffer (0.2 M). The cyclic voltammogram (CV) reveals three observable peaks, within the potential range 0.3 V to 1.6 V, starting at ~ 0.95 V.

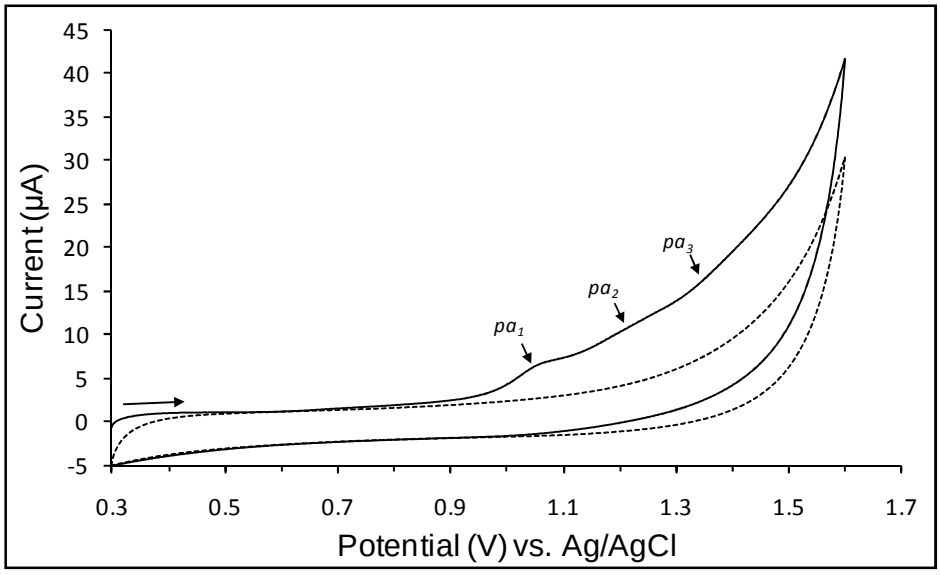

Figure 3.2 CV of 50 µM OTC in pH 2 BR buffer (0.2 M). Dashed line represents CV in buffer solution.

The anodic peaks were denoted as pa_1, pa_2 and pa_3 in order of appearance. Peaks possessed E_{pa} potentials of 1.05 V, 1.18 V and 1.39 V respectively, all occurring with standard deviation less than 10 mV. All peaks were observed to be irreversible as was found by Hou and Wang (1989) and Vega *et al*. (2007). Vega and co-workers reported a single anodic wave at ~ 1.5 V *vs.* Ag/AgCl in their CV analysis, possibly due to the high OTC concentrations (100 µM) employed in their studies (which could lead to peak masking), and the use of a multiwalled carbon nanotube modified-GCE.

In Figure 3.3, the unmodified and baseline corrected SWVs of OTC shows the individual anodic peaks at potentials 1.06 V, 1.23 V and 1.37 V for pa_1, pa_2 and pa_3 respectively, all with standard deviations of less than 10 mV.

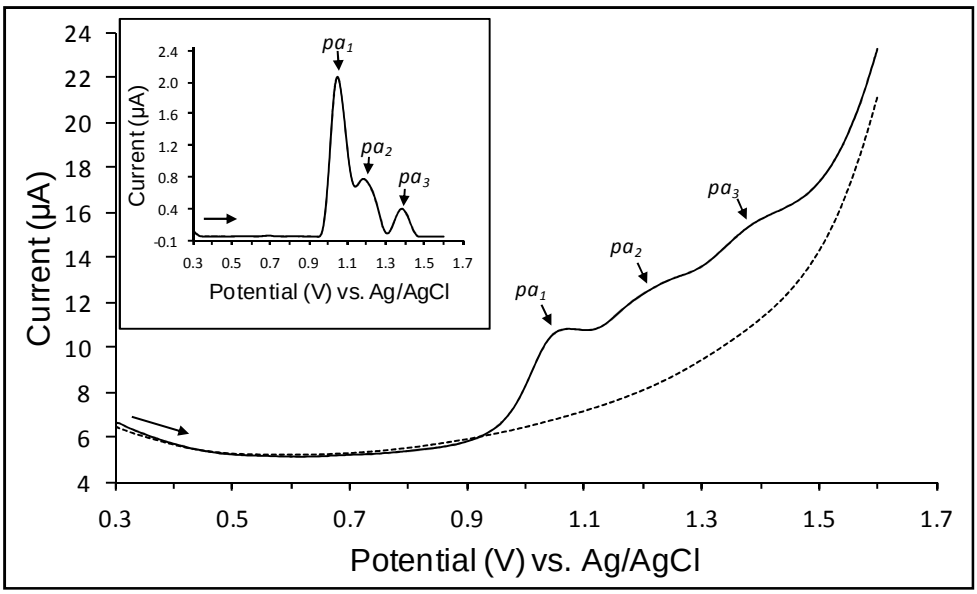

Figure 3.3 SWV of OTC (50 µM) in 0.2 M BR buffer (pH 2). Dashed line represents SWV in buffer solution. Inset shows baseline corrected scan.

Using differential pulse voltammetry (DPV), Hou and Wang (1989) found a similar set of peaks at 0.99 V, 1.14 V and 1.35 V (*vs*. Ag/AgCl) at pH 2.5 using a bare GCE. The slightly more negative peak potentials in their study are likely attributable to differences in pH and the lower scan rate employed in their studies, elaborated on in Section 3.3.2 and Section 3.3.7, respectively.

Under SWV detection, a fourth peak is observed to be masked by the right shoulder of pa_2 (visible in inset to Figure 3.3) in the baseline corrected voltammogram and referred to as pa_{2a}. While the baseline corrected SWV was not used for quantitative analyses, it illustrates pa_1 to be the largest and most defined peak and therefore, the most suitable for analytical purposes, as was found by Hou and Wang (1989) and others (Table 3.1). As such, pa_1 was utilised for analyses in these studies of OTC.

CV analysis of OTC at pH 7 (Figure 3.4) yielded similar results to that of pH 2. The same anodic triple peak structure was observed, occurring at more negative potentials of 0.79 V, 0.91 V and 1.057 V for pa_1, pa_2 and pa_3 respectively, all with

standard deviations less than 10 mV. Lower peak heights were observed at pH 7 compared to pH 2, as shown in Section 3.3.2. All observed peaks were irreversible, as reported by Vega *et al*. (2007) who reported no cathodic return signals across a pH range of 1.5 – 7.

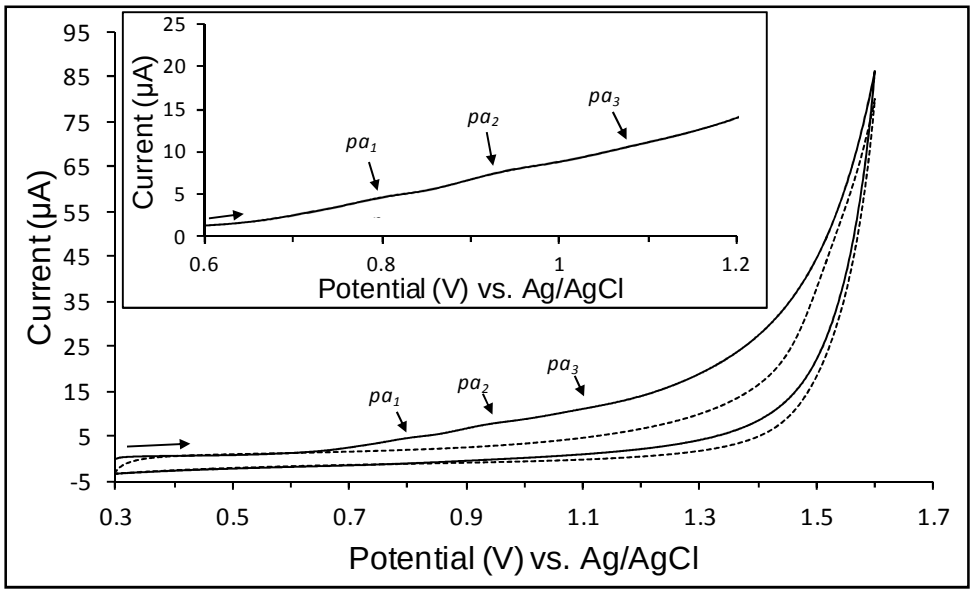

Figure 3.4 CV of OTC (50 µM) in 0.2 M BR buffer (pH 7). Dashed line represents CV in buffer solution. Inset shows magnified potential range containing pa_1, pa_2 and pa_3.

Figure 3.5 shows the corresponding SWV of OTC obtained at pH 7 in BR buffer.

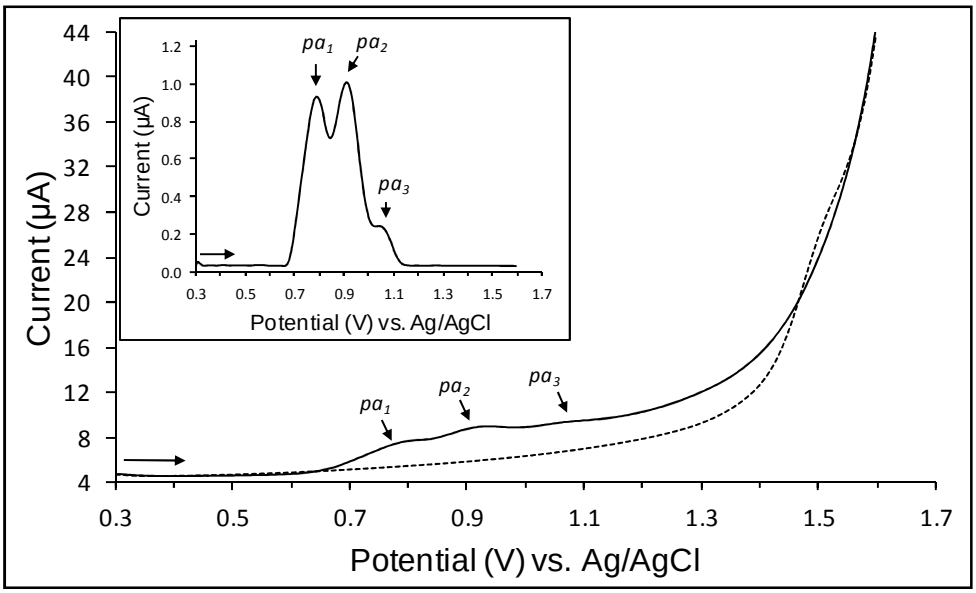

Figure 3.5 SWV of OTC (50 µM) in 0.2 M BR buffer (pH 7). Dashed line represents SWV in buffer solution. Inset shows baseline corrected scan.

Contrary to studies at pH 2, the second anodic peak, pa_2, at pH 7 appears larger in the baseline corrected SWV (inset of Figure 3.5), though this was believed to be due to tailing behaviour of pa_1. The I_p of the third anodic peak, pa_3, decreased due to increased current response of pa_2, which also lead to masking of the fourth peak (pa_{2a}).

3.3.2 Effect of pH on current response

Figure 3.6 shows the effect of electrolyte pH on the anodic response of pa_1. The highest I_{pa1} was recorded at pH 2, while the response at pH 10 was lowest. A decrease in I_{pa1} was observed from pH 2 to 6, followed by an increase until pH 8 before decreasing again. A C_v < 5 % was achieved for I_{pa1} at each pH unit, indicating high current response reproducibility. The peak positions were stable, with E_{pa1} varying less than 2 mV for each pH tested.

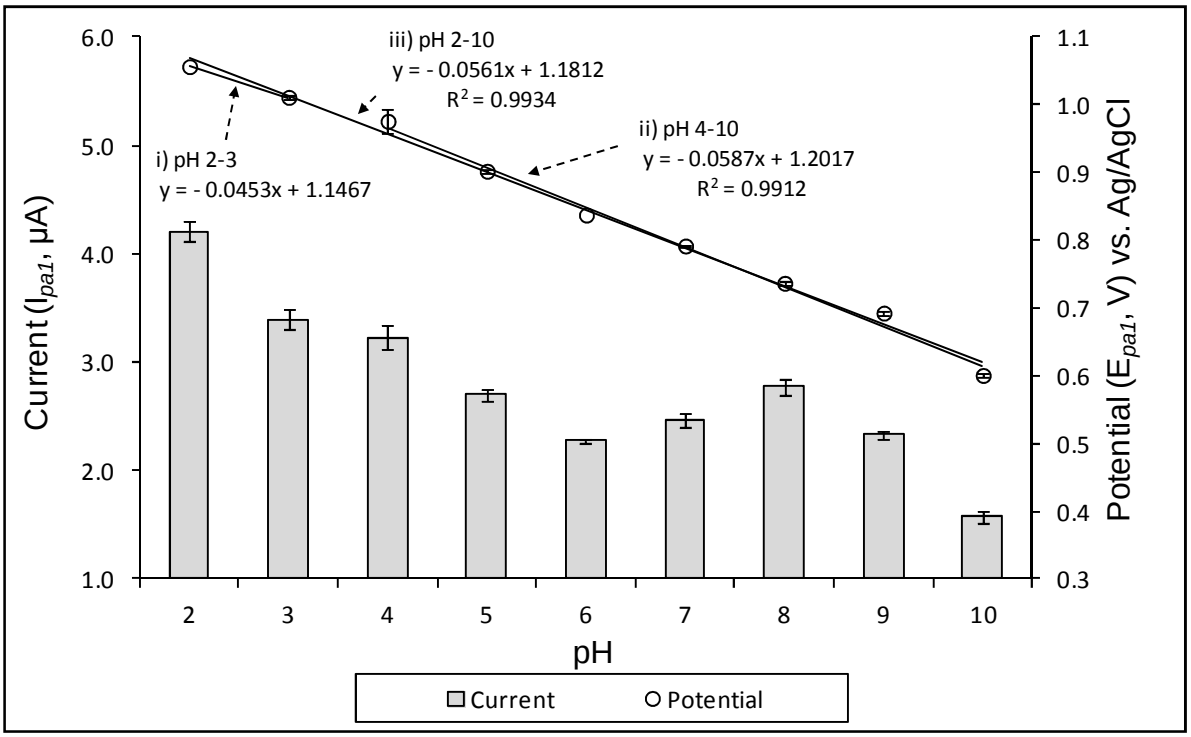

Figure 3.6 Effect of pH on the anodic CV response and peak potential of pa_1 of 50 µM OTC in 0.2 M BR buffer. E_{pa1} data was fitted according to three regression models encompassing i) pH 2 to 3, ii) pH 4 to 10 and iii) pH 2 to 10.

These results closely resemble those of Vega *et al*. (2007), who reported a decrease in current response from pH 1 to 7 using CV, whereas Figure 3.6 shows a decline up to pH 6 only. Wangfuengkanagul *et al*. (2004) reported deteriorating peak structure

and lowered current response with increasing alkalinity, up to pH 8. However, they did not present any voltammograms or data to indicate the precise effect of a near-neutral pH on I_{pa1}. With respect to literature (Table 3.1), Figure 3.6 constitutes the widest pH range tested for the anodic response of OTC.

The I_{pa1} values of pH sets 6 to 9 were compared in a one-way ANOVA test and found to be similar ($p < 0.05$) with the exception of pH 8. The lower anodic responses of OTC, which exists as a neutral and negatively charged species at a pH above 3.5 and 7.2 respectively, is believed to be due to limited electrostatic attraction and adsorption (Section 3.3.7) of OTC to the GCE surface. This attraction is proposed between cationic OTC species, in highly acidic buffer, and oxygen-containing functional groups on the GCE surface such as carboxylic- and quinone-like moieties (Dai and Shiu, 1996).

The E_{pa1} of OTC is seen to shift to a more negative potential with increase in alkalinity as observed by Hou and Wang (1989), indicating protons are involved in the oxidation process (Beilby *et al*., 1995). The slope of the E_{pa1} *vs.* pH plot is complex, as shown by three linear models applied in Figure 3.6. A regression line encompassing the entire pH range tested (2 – 10) provided the best fit ($R^2 = 0.9934$), yielding a 56.1 mV/decade shift, indicating an equal number of protons to electrons are exchanged during the redox reaction, as was seen by Guo *et al*. (2009) for tetracycline oxidation.

Slight deviations from the linear pattern of E_{pa1} *vs.* pH between pH 3 and 4, as well as 9 and 10 were observed. This could be due to two of the pK_a values of OTC, namely pK_{a1} at ~ 3.5 and pK_{a3} at ~ 9.58 (Sanli *et al*., 2009), though further investigation is needed to confirm this. No noticeable change is observed in the pH range of 7 to 8, which encompasses pK_{a2} at ~ 7.2. Inconsistencies for E_{pa1} *vs.* pH plots and the pK_a values of OTC were also noticed by Wangfuengkanagul *et al*. (2004) who provided no explanation.

This shift in E_{pa1} is illustrated in baseline corrected SWVs in Figure 3.7. This figure highlights the complicated peak structure of OTC, covering the range from highly

acidic to highly basic pH. While pa_1 is highlighted by the solid line, the complex nature and number of the succeeding peaks is evident from the dashed lines. An average of 2 - 3 peaks were observed, with pH 10 exhibiting 4 distinct peaks, as summarised in Figure 3.7.

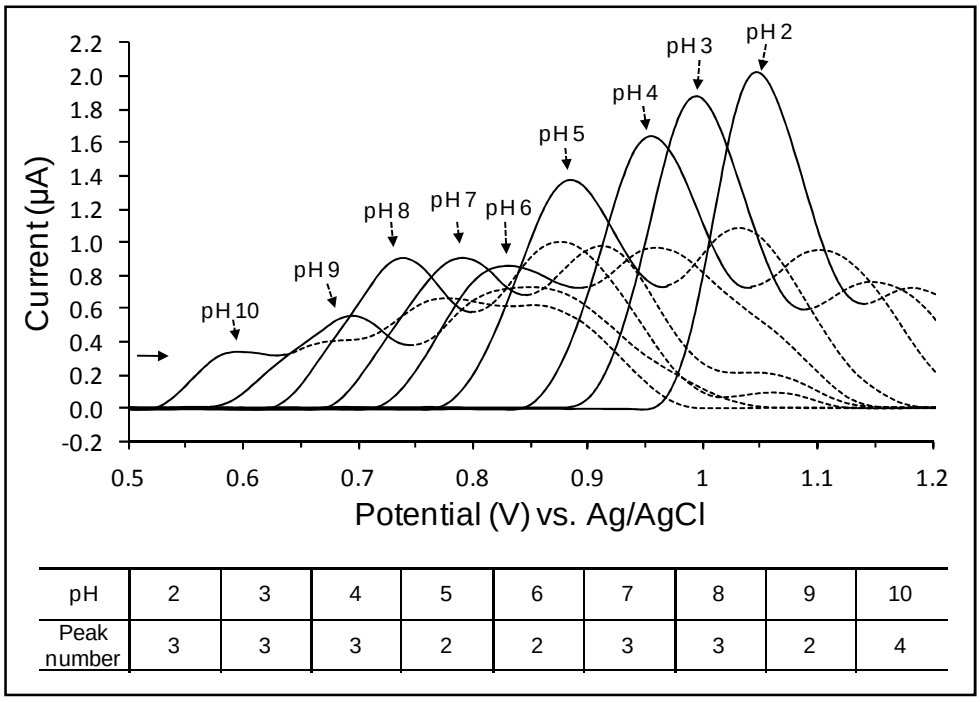

pH	2	3	4	5	6	7	8	9	10
Peak number	3	3	3	2	2	3	3	2	4

Figure 3.7 SWVs of 50 µM OTC in 0.2 M BR buffer with a pH ranging from 2 to 10. Solid line encompasses the first anodic peak (pa_1, at each pH), while dashed lines shows additional peaks. The number of observed peaks are tabulated for each pH. Voltammograms are baseline corrected.

A change in the occurrence and height of pa_2, pa_3 can also be observed. Figure 3.7 revealed a pH dependent change for I_{pa1} and shift of E_{pa1} for pa_2 and pa_3. This is more appropriately shown in Table 3.2 where the I_p and E_p of pa_1, pa_2 and pa_3 are compared at pH 2 and pH 7.

Table 3.2 I_p and E_p for anodic peaks of 50 µM OTC in 0.2 M BR buffer (pH 2 and 7) for CV analysis.

Anodic peaks	pH 2		pH 7		$\Delta E_p/\Delta pH$ ($mV.pH^{-1}$)
	I_p (µA)	E_p (V)	I_p (µA)	E_p (V)	
pa_1	4.209 (± 0.098)	1.056 (*)	2.470 (± 0.060)	0.791 (± 0.002)	53.0
pa_2	1.472 (± 0.087)	1.188 (± 0.002)	1.195 (± 0.024)	0.911 (± 0.003)	55.4
pa_3	1.266 (± 0.089)	1.387 (± 0.003)	0.525 (± 0.013)	1.059 (± 0.003)	65.6

* Standard deviation less than 1 mV.

Notably, the current for I_{pa1} was largest of all three peaks, with peak heights decreasing in the order of $pa_1 > pa_2 > pa_3$ at both pH 2 and pH 7. Similar $\Delta E_p/\Delta pH$ values demonstrate that the electrochemical reaction all three peaks involves the transfer of an equal number of protons and electrons.

3.3.3 Effect of solvent and electrolyte composition

Various solvents, used for the preparation of OTC stock solutions, were investigated for their effect on the current response and peak potential of pa_1 at pH 2 and pH 7. Furthermore, the choice of electrolyte was probed by comparing two different buffers at each pH.

In Figure 3.8, overlapping baseline corrected SWVs are presented for OTC analysis in different solvent systems and 0.2 M BR buffer or 0.2 M PP buffer, both at pH 2.

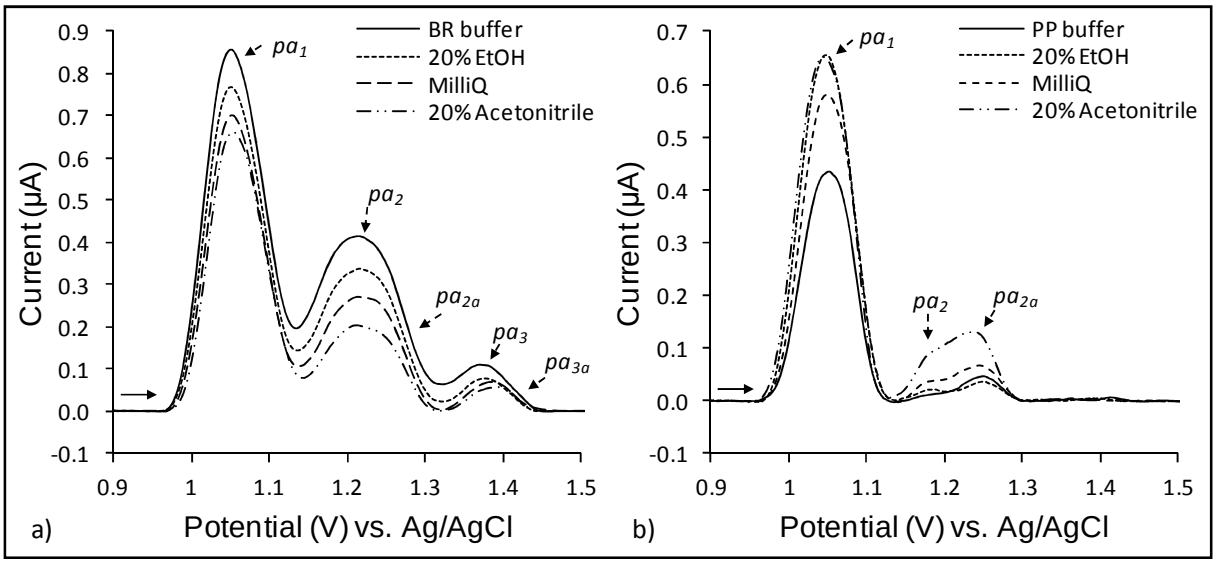

Figure 3.8 Baseline corrected SWVs of 20 µM OTC stock solutions prepared in various solvents analysed in a) 0.2 M BR buffer (pH 2) and b) 0.2 M potassium phosphate buffer (pH 2) as supporting electrolyte.

With respect to the choice of electrolyte, the separation between pa_1 and pa_2 is more distinct in PP buffer. This corresponds with a narrower pa_1 in PP. In BR buffer, an additional peak present on the right shoulder of pa_2 is observed for studies where OTC stock solutions were prepared in 20 % acetonitrile. This peak was previously referred to as pa_{2a} (Section 3.3.1). The occurrence of pa_{2a} is more clearly observed in PP buffer, where pa_2 and pa_{2a} are more resolved and are greatly enhanced in

20 % acetonitrile OTC stock solutions. A similar effect can be seen in BR buffer for pa_3, where a previously unseen additional peak is denoted as pa_{3a}. In PP buffer, pa_3 and pa_{3a} were not readily observed.

In both buffers however, an increase in current for pa_2 and pa_{2a} leads to peak merging, where both peaks contribute to a single peak that, at higher concentrations, becomes almost indistinguishable. The same is observed for pa_3 and pa_{3a} in BR buffer. For this reason, using pa_2 or pa_3 for the quantification of OTC at low concentrations is not recommended at pH 2.

Table 3.3 shows the results of SWV conducted at pH 2. The choice of solvent utilised for OTC stock solution preparation was found to have a minimal effect on the anodic response of OTC. A stable potential for all peaks was observed in both BR and PP buffer, for each of the solvents used for OTC stock solution preparation.

Table 3.3 Effect of solvent systems on the anodic SWV detection of 20 µM OTC (pa_1) at pH 2 in BR (0.2 M) and PP (0.2 M) buffer.

Solvent	BR buffer (BR)		PP buffer (PP)	
	I_{pa1} (µA)	E_{pa1} (V)	I_{pa1} (µA)	E_{pa1} (V)
Respective buffer	2.050 (± 0.092)	1.074 (± 0.03)	1.619 (± 0.111)	1.069 (± 0.008)
Ethanol (20 %)	1.952 (± 0.057)	1.074 (± 0.008)	2.042 (± 0.104)	1.070 (± 0.003)
MilliQ	1.852 (± 0.079)	1.081 (*)	1.876 (± 0.139)	1.071 (*)
Acetonitrile (20 %)	1.746 (± 0.075)	1.075 (± 0.007)	1.999 (± 0.087)	1.071 (*)

* Standard deviation less than 1 mV.

When BR buffer was used as electrolyte, the BR buffer as the diluent (or solvent) for OTC, yielded the highest current response, while for PP buffer, the largest average peak current was observed for OTC stock solutions prepared in 20 % ethanol. However, the difference between these two matrices was insignificant. More consistent I_{pa1} results were achieved for systems buffered by BR than by PP. A C_v of < 5 % was achieved for I_{pa1} in all BR buffered systems and < 10 % for all PP buffered systems. Statistically, the lowest response by a solvent system analysed in BR buffer was 20 % acetonitrile. For the use of PP buffer as electrolyte, PP buffer as a diluent of OTC performed weakest.

In Figure 3.9a, the overlapping SWV reveal the effect of different OTC solvents and electrolytes for analysis performed at pH 7. As for pH 2, the peak potentials were unaffected by the choice in stock solution diluent in both buffers tested.

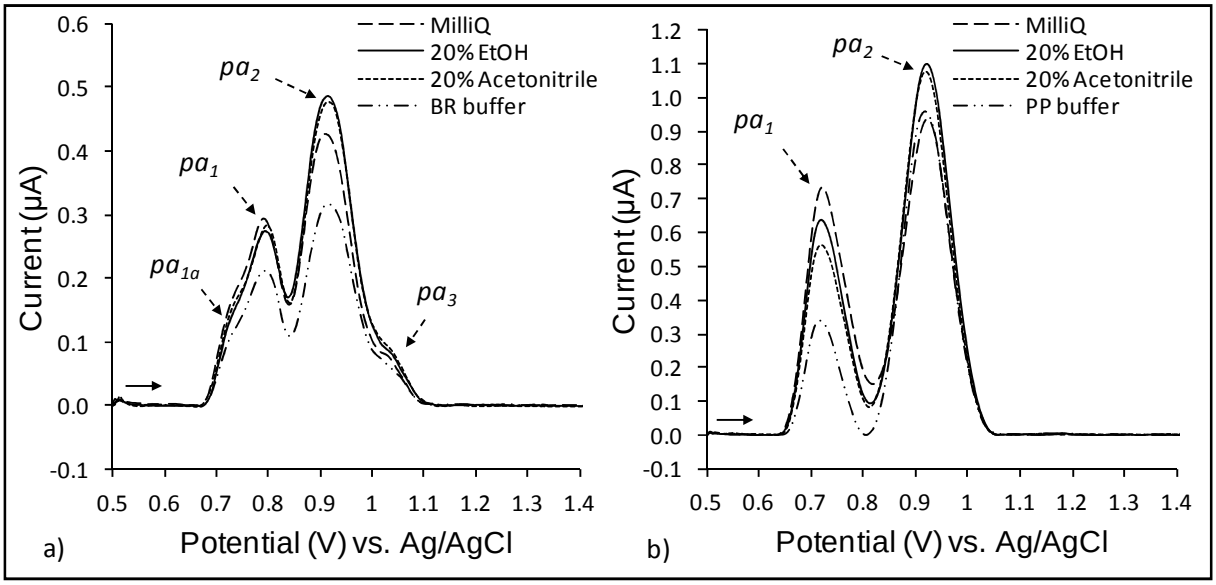

Figure 3.9 Baseline corrected SWVs of 20 µM OTC in stock solutions prepared in various solvents analysed in a) 0.2 M BR buffer (pH 7) and b) 0.2 M PP buffer (pH 7) as supporting electrolyte.

As observed before (Figure 3.5), the current response of pa_2 is higher than that of pa_1 for both BR and PP systems at pH 7. The separation between pa_1 and pa_2 is greater for PP buffer. As for studies at pH 2, pa_3 could not be observed in PP buffer, while it was found as a shoulder peak of pa_2 in BR buffer.

A shoulder peak to the left of pa_1 was observed, and was denoted pa_{1a}. This peak was not observed at higher OTC concentrations studies before (Section 3.3.2).It is proposed that these peaks merge at higher concentrations becoming indistinguishable from one another. This peak may cause the shift in E_{pa1} to a more positive potential in BR buffer, relative to studies in to PP buffer (Figure 3.9b). Varying peak potentials could lead to inaccurate readings at low concentrations making analysis in BR buffer unreliable at neutral pH.

Table 3.4 compares the effect of the solvents, used for OTC stock solution preparation, on I_{pa1} and E_{pa1} at both electrolytes tested at pH 7. For both BR and PP buffer systems, the highest current response was achieved for OTC stock solutions

that were prepared in MilliQ water. SWV analysis of OTC in PP buffer produced the greatest I_{pa1}, irrespective of the diluent used for stock solution preparation, when compared to BR buffer.

Table 3.4 Effect of solvent systems on the anodic SWV detection (pa_1) of 20 µM OTC at pH 7 in BR (0.2 M Britton Robinson) and PP (0.2 M Potassium phosphate) buffer.

Solvent	BR buffer		PP buffer	
	I_{pa1} (µA)	E_{pa1} (V)	I_{pa1} (µA)	E_{pa1} (V)
Respective buffer	0.969 (± 0.043)	0.805 (± 0.003)	1.182 (± 0.089)	0.736 (± 0.003)
Ethanol (20 %)	1.185 (± 0.099)	0.807*	1.426 (± 0.024)	0.726 (± 0.002)
MilliQ	1.219 (± 0.030)	0.805 (± 0.003)	1.577 (± 0.013)	0.730*
Acetonitrile (20 %)	1.186 (± 0.106)	0.805 (± 0.002)	1.302 (± 0.042)	0.736 (± 0.003)

* Standard deviation less than 1 mV.

As expected from pH studies, greater current responses were observed for analyses conducted at pH 2 compared to pH 7. However, contrary to pH 2, considerably greater differences were observed for the two electrolyte systems used at pH 7. While I_{pa1} and E_{pa1} were similar for BR and PP at pH 2, PP buffer is favoured at neutral pH with larger current responses, and more defined pa_1 at a lower oxidation potential.

Based on a combination of high peak currents and well-defined reproducible peak potentials observed under the conditions tested, further analysis at pH 2 and pH 7 was conducted using selected pH specific buffers and solvents for OTC stock solution preparation. For studies at pH 2, BR buffer with BR as solvent for OTC stock solutions and PP buffer with 20 % ethanol as solvent for OTC stock solutions were selected for further analyses based on the high I_{pa1} and clearly defined peak potential observed under these conditions.

For studies at pH 7, PP buffer with OTC stock solutions prepared in MilliQ was selected for further analyses as these resulted in the highest current response for all samples analysed at a neutral pH with a highly reproducible peak potential. BR buffer was not considered as an electrolyte at pH 7, as responses were significantly lower than that of PP buffer (pH 7) with higher I_{pa1} error margins and a more complex peak pattern for pa_1.

3.3.4 Preconditioning potential and stir time

Figure 3.10 shows the effect of applied preconditioning potentials, on the current response and oxidation potential of pa_1 for 35 µM OTC, during a waiting period prior to analysis.

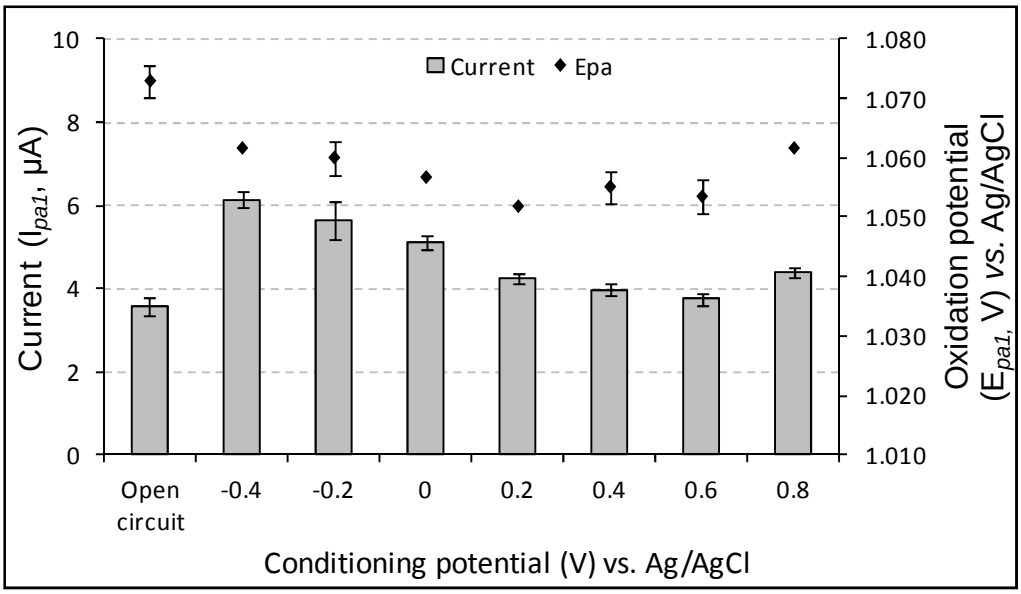

Figure 3.10 Effect of preconditioning potential on I_{pa1} and E_{pa1} for 35 µM OTC in 0.2 M BR buffer (pH 2). Preconditioning time was 40 seconds under stirred conditions. Result obtained by SWV.

With the exception of a preconditioning potential of + 0.8 V, there appears to be a trend of increasing signal response with decreasing preconditioning potential. For the open circuit, no potential was applied during the 40 second stir period, resulting in the lowest average current observed. The application of a preconditioning potential resulted in an average potential shift of 16 (± 4) mV for pa_1 towards a more negative potential when compared to the open circuit experiments suggesting that the reaction has become slightly more thermodynamically favourable (Mirceski *et al*., 2007).

If the preconditioning process is regarded as an electrochemical pre-treatment (ECP) process, it can be argued that this step has produced an electrode surface more suited for anodic OTC analysis. ECP processes are capable of removing adsorbed impurities while offering preferential ion exchange to cations (Kissinger and Heineman, 1996).

For the purposes of the proposed application of the sensor platform, a preconditioning potential of 0.0 V was chosen for all subsequent analysis owing to the sensitivity, reproducibility and lack of sample deoxygenation required at this potential. Even though a preconditioning potential of - 0.4 V gave a significantly higher response with good reproducibility, deoxygenation is a time- and equipment-consuming step not suited for on-site analysis. Sample deoxygenation is necessary to prevent oxygen reduction, the product of which may interfere with voltammetric studies (Reinke and Simon, 2002).

Figure 3.11 demonstrates the effect of conditioning time during the aforementioned preconditioning period. The anodic response of 20 µM OTC was seen to be greatly influenced over a range of stir times from 0 to 50 seconds, increasing gradually before stabilising.

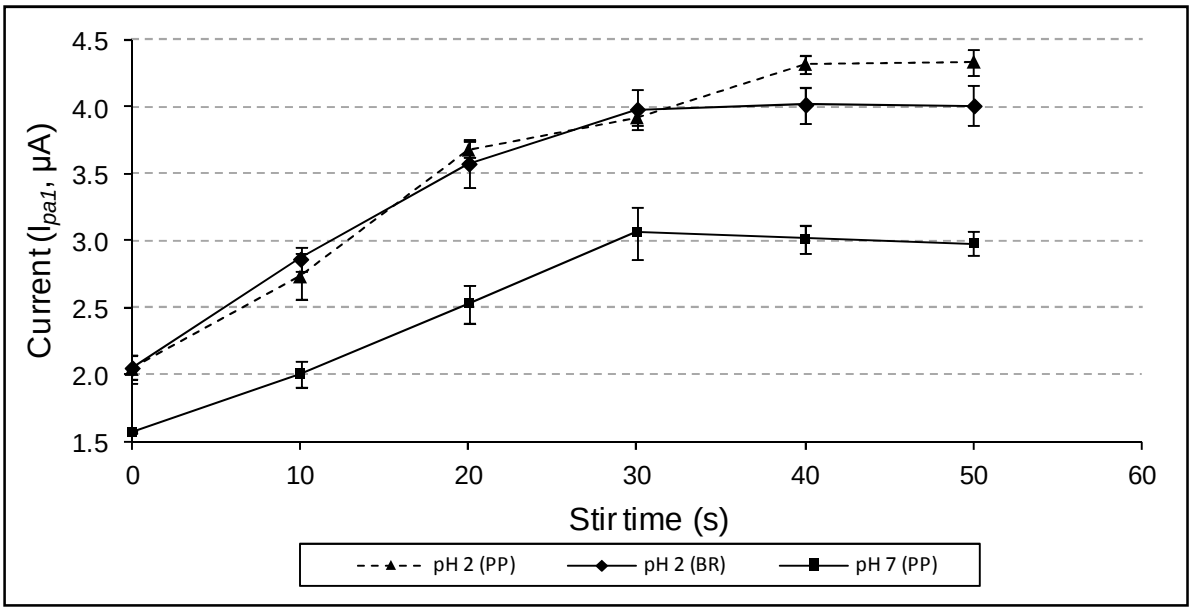

Figure 3.11 Current response of pa_1 of 20 µM OTC at various stir times obtained through SWV. pH 2 (BR) = BR buffer with BR stock of OTC; pH 2 (PP) = PP buffer with 20 % EtOH stock of OTC; pH 7 (PP) = PP buffer with MilliQ stock of OTC.
Note: A 0.0 V applied potential was maintained during the stir period.

For both pH 2 (BR) and pH 7 (PP), a maximum current response was obtained after 30 seconds of stirring at which stage the signal levels off. A similar result was reported by Guo *et al*. (2009) for tetracycline (TC) and was explained as saturation of the GCE surface by adsorbed TC.

Assuming the system is adsorption controlled, as indicated in the preceding text (Section 3.3.7), the increase in I_{pa1} can be attributed to an enhanced surface coverage of adsorbed analyte at the electrode surface (Lovric *et al*., 1988). This preconcentration was observed with prolonged stir times leading to increased current responses, until suspected surface saturation was obtained at longer stir times (~ 30 seconds) and the current response plateau plateaus.

To ensure more sensitive and reproducible data in future experiments, a 40 second stir time was adopted for analysis in BR buffer (pH 2). A similar approach was taken for studies conducted at pH 2 (PP) which showed the start of a stable current at 40 seconds. With slightly less variation in response, 50 seconds was chosen as the optimal stir time for PP (pH 7).

3.3.5 OTC fouling at bare GCE

Figure 3.12a shows the effect of consecutive SW voltammograms at a GCE without cleaning between subsequent scans in pH 2 BR buffer with 20 µM OTC. Figure 3.12b shows that in the absence of any pretreatment steps, I_{pa1} decreased to less than 20 % of the first scan (I_{max}). Following the fourth consecutive scan, no appreciable current could confidently be obtained from the voltammogram.

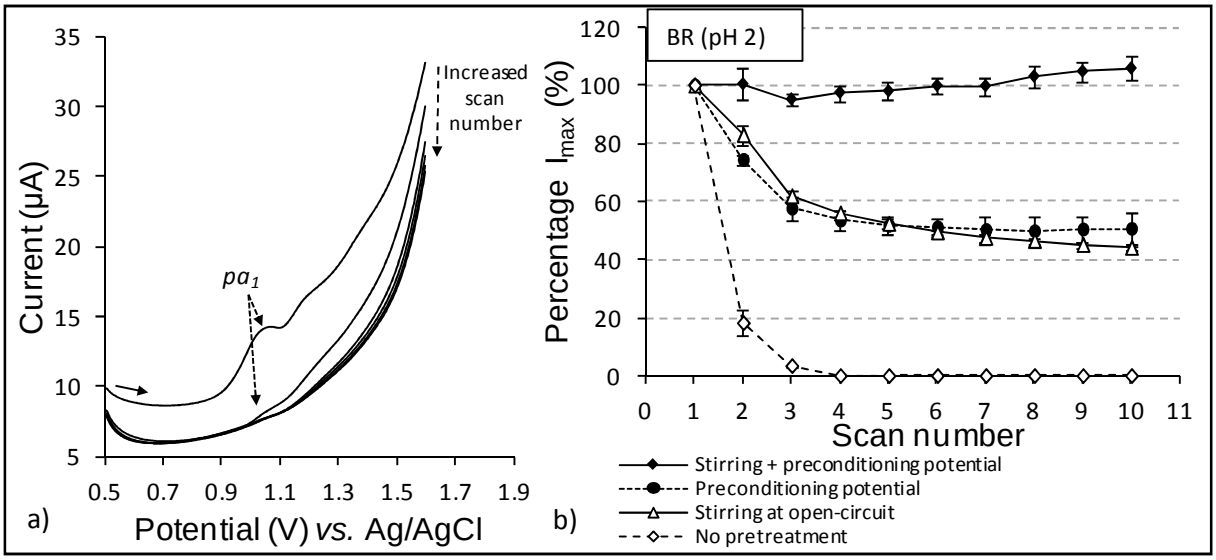

Figure 3.12 a) Effect of successive scans on SWVs of OTC without pretreatment between scans and b) comparison of I_{pa1} of 20 µM OTC fouling at bare GCE surface in 0.2 M BR buffer (pH 2) without and with preconditioning steps between successive SWV scans. OTC stock solution prepared in BR.
Note: Preconditioning potential (0.0 V) was maintained for 40 seconds across a quiescent solution.

The aforementioned preconditioning steps (preconditioning potential of 0.0 V), and stir time of 40 seconds (as per Figure 3.11), were applied individually and in combination between successive scans. The application of either the applied conditioning potential or the stirring procedure was shown to reduce GCE fouling, while maintaining acceptable reproducibility (Figure 3.12).

While stirring limited the fouling behaviour of OTC, I_{max} continued to decrease until the 10^{th} scan with a final current recovery of 44.1 (± 0.8) %. It is argued that the stirring procedure enabled migration of OTC oxidation product away from the surface, which mitigates the build-up of a fouling layer. Simultaneously, new oxidizable OTC species can replenish the electrode surface.

When the preconditioning potential alone was applied between successive scans, a value of 50 % of I_{max} was observed after 5 scans, stabilising after 5 scans at ~ 50 % of I_{max}. As mentioned previously (Section 3.3.4), the preconditioning potential could remove adsorbed oxidized OTC product, effectively renewing the electrode surface. Alternatively, OTC in electrolyte could be preferentially adsorbed over OTC oxidation product. As the preconditioning potential is applied for 40 seconds, a time-based replenishment of oxidizable OTC species to the electrode is also considered.

When both preconditioning steps were employed simultaneously, there was a reproducible pattern of current responses, which varied < 5 % to the first recorded scan (I_{max}), with the lowest and highest responses seen at scan 3 and 10 respectively. An average recovery of 100.4 (± 3.5) % was achieved across all scan numbers. These results report consistent and reproducible quantitative data can be obtained for OTC at a bare GCE for successive scans performed without electrode cleaning.

In Figure 3.13, consecutive voltammograms were recorded in PP buffer at pH 2 and 7 under similar experimental conditions as Figure 3.12. Under highly acidic conditions (pH 2), the fouling profile of OTC is similar for PP buffer (Figure 3.13a) as for BR buffer (Figure 3.12).

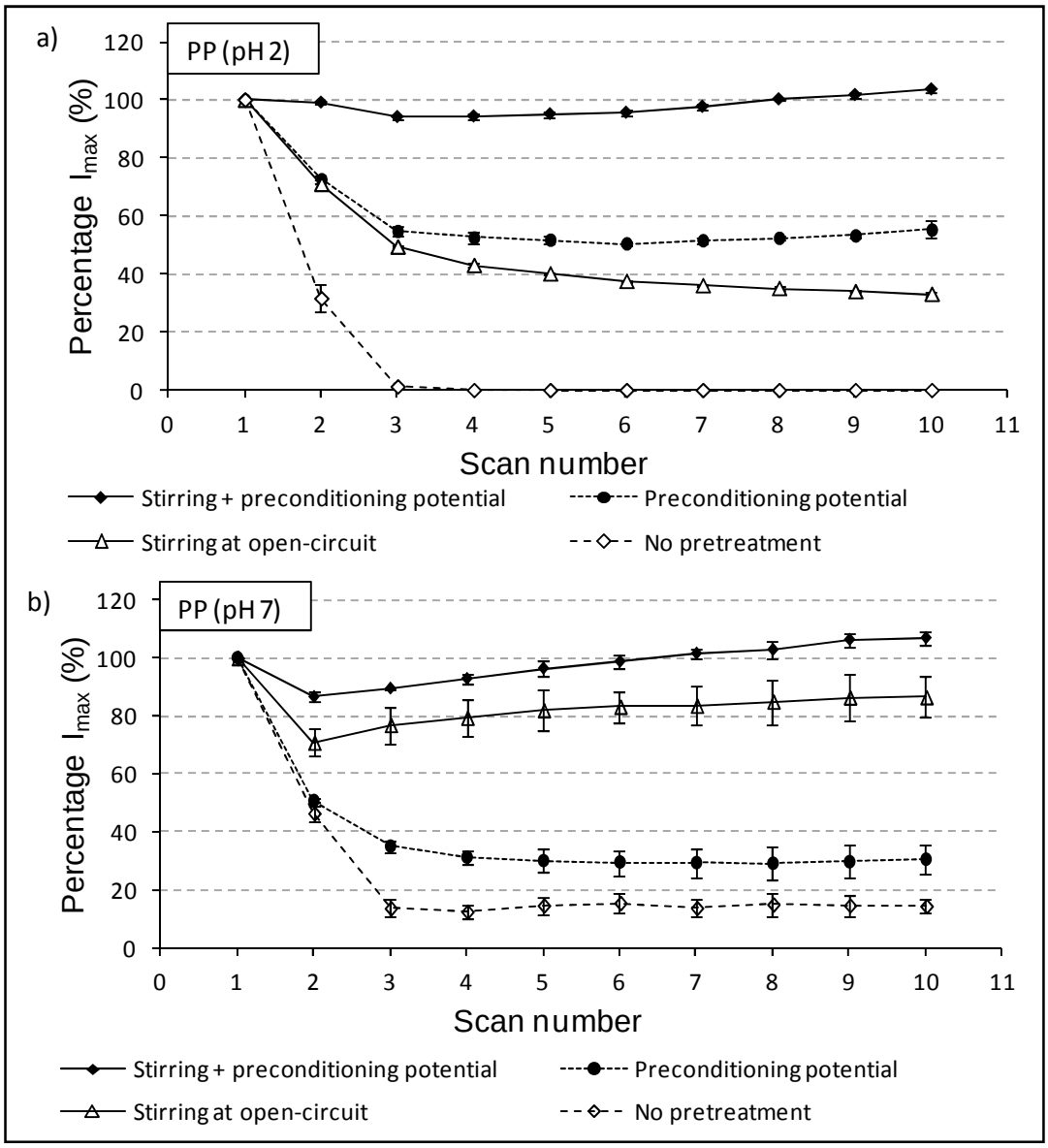

Figure 3.13 Comparison of I_{pa1} of 20 µM OTC fouling at bare GCE surface without and with preconditioning steps between successive SWV scans in a) 0.2 M PP buffer (pH 2) and b) 0.2 M PP buffer (pH 7).
Note: Preconditioning potential (0.0 V) was maintained for 40 seconds across a quiescent solution. OTC stock solutions prepared in 20 % EtOH and MilliQ for analysis at pH 2 and 7 respectively.

An average 97.9 (± 3.4) % current recovery was recorded across all scan numbers, when both stirring and a preconditioning potential was applied, relative to successive measurements without pre-treatment in 0.2 M PP buffer (pH 2).

In pH 7 PP buffer, fouling in the absence of any pretreatment steps was notably less than at pH 2 with recordable current recoveries of ~ 14 % after 10 successive scans. Stirring was shown to be effective in limiting fouling, retaining 76.9 (± 6.3) % of the

I_{max} after two scans and 86.5 (± 7.1) % at the 10th scan, suggesting that the fouled product is easily removed from the electrode surface and replenishment of oxidizable OTC species occurs rapidly in neutral solution.

The limited effect of the preconditioning on minimising fouling, 30.4 (± 5.2) % I_{max} after 10 scans, could be due to minimal effect of the applied potential 0.0 V on OTC oxidation at pH 7, as this potential was optimised for highly acidic conditions (Section 3.3.4). Secondly, a change in the charge of OTC at pH 7 (neutral charge) and pH-dependent electrode surface properties (Deakin *et al*., 1985; Chen and McCreery, 1996) could influence the fouling behaviour. Further investigation outside the scope of this research is required in this regard.

Under different experimental conditions, fouling and analytical reproducibility of OTC and TC has been investigated by various authors. Sensor stability was recorded on gold electrodes by Palaharn *et al*. (2003) for TC, and Masawat and Slater (2007) for OTC at 10 and 7 scans respectively, with relative standard deviation < 10 %. For flow-injection experiments at modified GCEs, reproducibility as high as 97 % after 30 scans for OTC at a nickel-modified GCE (Oungpipat *et al*., 1995) and 96.6 % after 100 scans for chlortetracycline (CTC) at a anodized boron doped diamond thin film GCE (Wangfuengkanagul *et al*., 2004) has been reported. No fouling data for OTC at a bare GCE has previously been presented.

Through the application of a time-based conditioning potential and stirring procedure, the GCE surface could thus be renewed to a state at which reasonably accurate, quantitative reading can be obtained at both pH 2 and 7 in BR and PP buffer.

3.3.6 OTC linear range and detection limits

In Figure 3.14, the relationship between I_{pa1} and OTC concentration was investigated using the optimised parameters in Section 3.3.3 and 3.3.4. A single linear range, as commonly reported (Masawat and Slater, 2007; Vega *et al*., 2007; Guo *et al*., 2009) was not obtained. Instead, two distinct intersecting ranges were observed. Linear ranges of I_{pa1} *vs.* OTC concentration were observed from 0.5 – 7 µM and from 7 – 30 µM in the BR buffer (pH 2). An intersection point of the two linear regressions

was calculated to be (6.97; 2.87) for the OTC concentration and I_{pa1} value respectively.

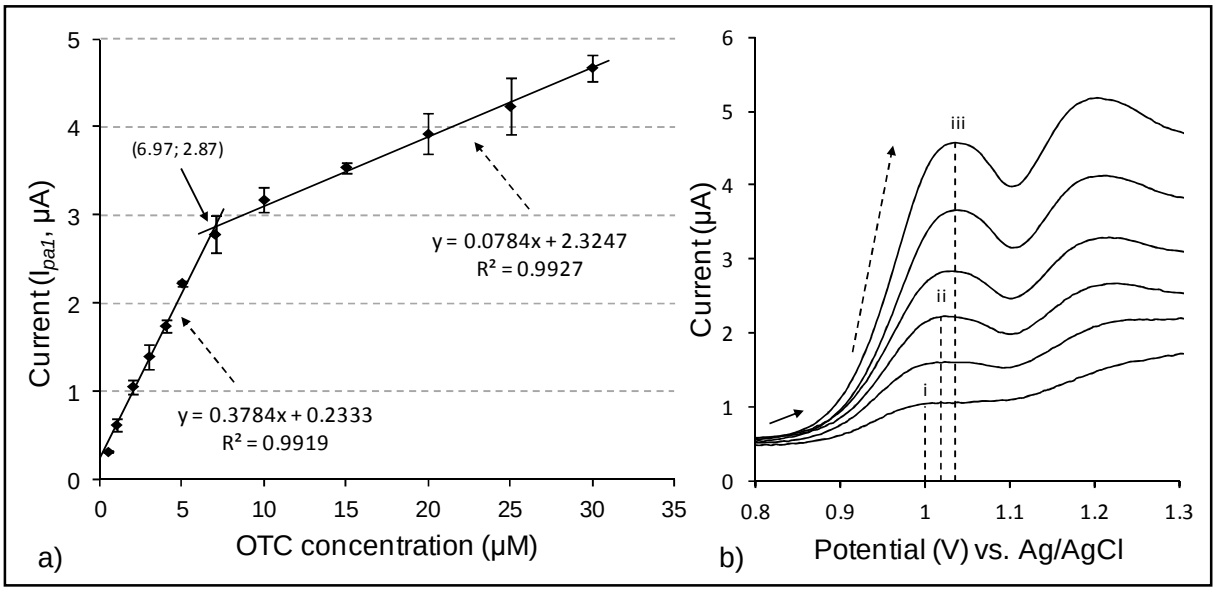

Figure 3.14 a) Standard curve of I_{pa1} *vs.* OTC concentration in 0.2 M BR buffer (pH 2) and b) baseline subtracted SWV overlay of increasing OTC concentration (1, 3, 4, 5, 10, and 20 µM) as indicated by the dashed arrow. Vertical dashed lines show E_{pa1} for OTC at 1 (i), 4 (ii) and 20 (iii) µM. A 40 second stir and applied potential (0.0 V) was maintained as the preconditioning procedure. OTC stock solution was prepared in BR buffer.

According to Abdel-Hamid (1998) in a study on phenolphthalein adsorption at a mercury electrode, a system comprising mixed diffusive and adsorptive behaviour is responsible for the observed non-linearity observed across the full concentration range. At low OTC concentrations, the current in Figure 3.14a is proposed to consist mainly of an adsorptive component due to adsorbed OTC on the GCE surface following the preconditioning step. However, at increasing OTC concentration, increased electrode coverage by the analyte may be achieved resulting in limited adsorptive current. At higher concentrations, the diffusive current contribution becomes more prominent as it does not suffer the same limitation. The same non-linear dependence of I_{pa} on analyte concentration was observed for anodic TC detection on a gold-modified tungsten microelectrode as reported by Wang *et al*. (2011). This author suggested irreversible adsorption of TC to the electrode to explain the decreased slope of the linear range encompassing higher concentrations of TC.

The oxidation peak potential, E_{pa1}, for OTC shifted non-linearly to a slightly more positive potential, as indicated by the vertical dashed lines in Figure 3.14b, from 1.019 V (± 0.003) for 0.5 µM to 1.040 V (± 0.004) for 30 µM.

Rather than many multiple linear regions, the current response of I_{pa1} at different OTC concentrations can be better described using an adsorption isotherm. The model used to describe the data obtained in this work was the Langmuir isotherm (Equation 2.6), a model regularly employed to describe electrode adsorption processes (Wang, 1994). The model was adapted to predict current responses for given analyte concentrations as described in Section 2.4.4.

Figure 3.15a shows the relationship between the experimentally observed data and predicted Langmuir model in overlapping curves.

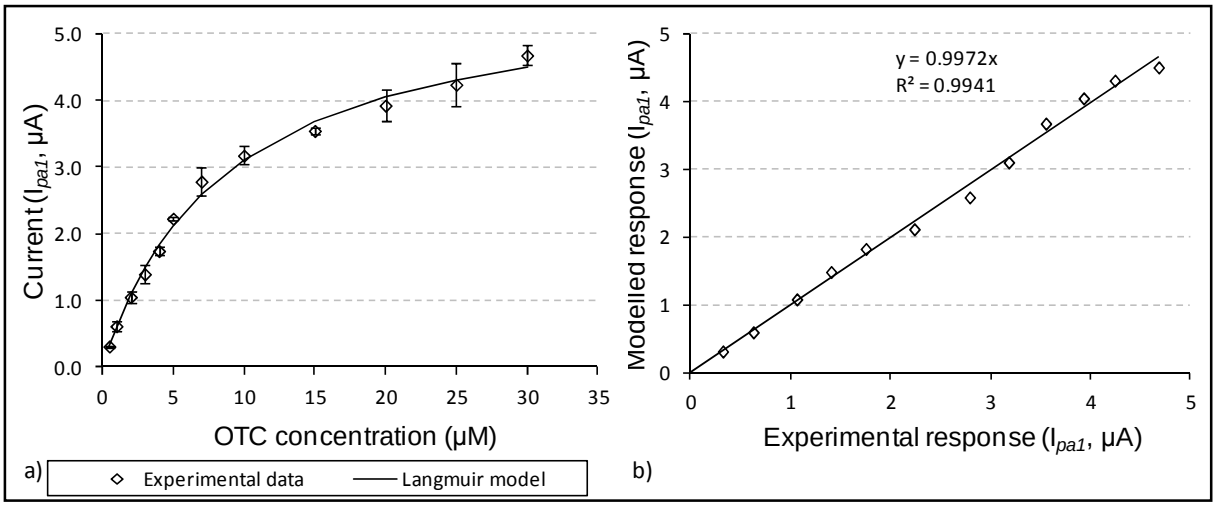

Figure 3.15 a) Overlay of the experimentally achieved OTC concentration curve and the Langmuir model predicted values for current and b) linear relationship between experimental and modelled (I) data (solid line represents linear correlation). Data obtained by SWV in 0.2 M BR buffer (pH 2) using a 40 stir time and 0.0 V applied potential. OTC stock solution prepared in BR buffer.

In accordance with the Langmuir isotherm, I was calculated as the modelled current response (µA) for a given concentration of OTC in solution. While the Langmuir isotherm assumes solely adsorptive processes are at play, which was found not to be the case for OTC (Section 3.3.7), reasonable fits were obtained for the experimental data presented. The model response closely matches that of the observed data. The accuracy of the modelled data is more appropriately shown in

Figure 3.15b where an R^2 value of 0.9941 was achieved when comparing the modelled and experimental current responses of I_{pa1}. The slope of 0.9972 is near 1 and is indicative of a good correlation between the data sets. For the Langmuir isotherm, I and K were obtained and discussed in Table 3.5.

Figure 3.16 and 3.17 show similar relationships between I_{pa1} and OTC concentration for analysis conducted in PP buffer at pH 2 and pH 7 respectively.

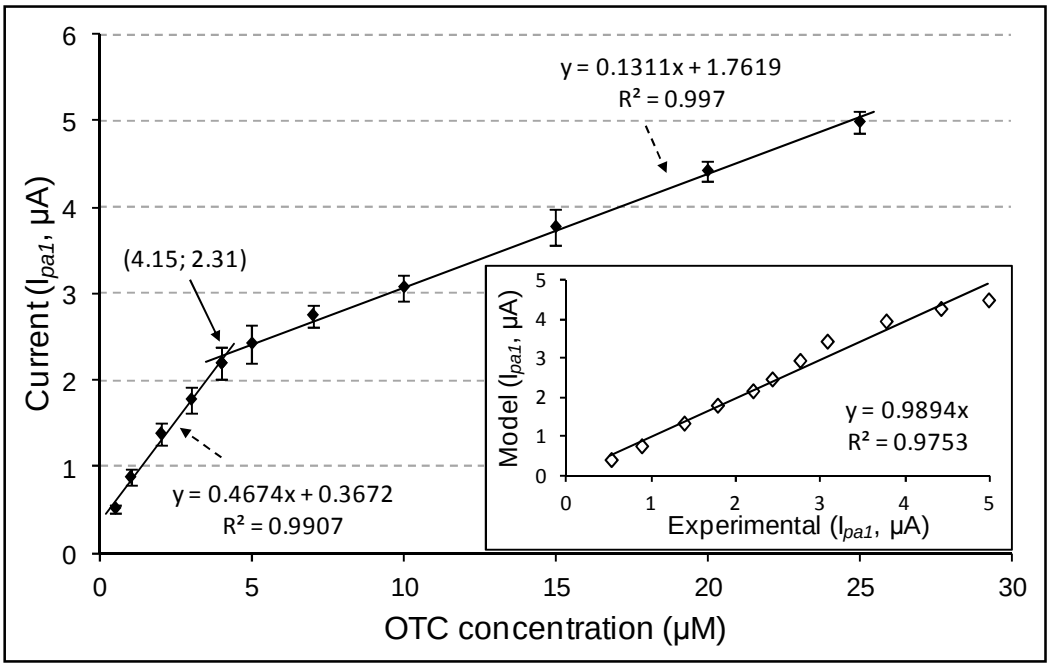

Figure 3.16 Standard curve of I_{pa1} *vs.* OTC concentration in 0.2 M PP buffer (pH 2). Inset shows linear relation between experimental and modelled (I) data using the Langmuir model. Data obtained by SWV in 0.2 M BR buffer (pH 2) using a 40 stir time and 0.0 V applied potential.OTC stock solution prepared in 20 % EtOH.

The linear relationships of I_{pa1} *vs.* OTC concentration were 0.5 – 4 µM and 4 – 25 µM for analysis in pH 2 PP buffer (Figure 3.16), and 1 – 8 µM and from 10 – 30 µM in PP (pH 7) (Figure 3.17).

When I_{pa1} *vs.* OTC concentrations plots for PP at pH 2 and pH 7 are compared, a noticeable increase in the concentration coordinate of the inflection point is observed at a higher pH.

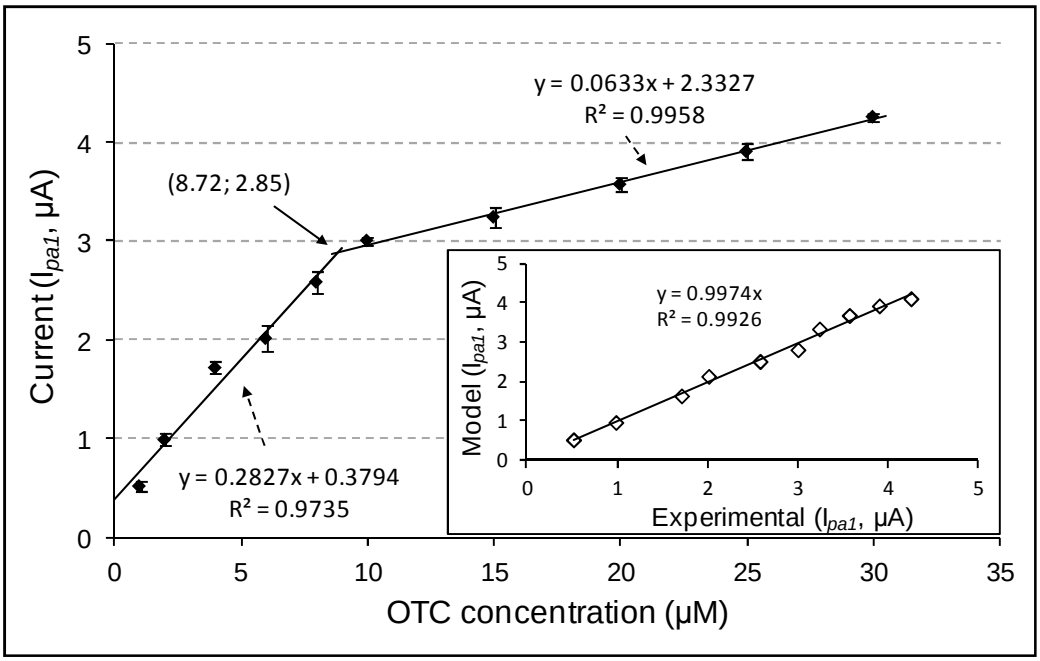

Figure 3.17 Standard curve of I_{pa1} *vs.* OTC concentration in 0.2 M PP buffer (pH 7). Inset shows linear relation between experimental and modelled (I) data. Data obtained by SWV in 0.2 M BR buffer (pH 2) using a 40 stir time and 0.0 V applied potential. OTC stock solution prepared in PP buffer.

Table 3.5 summarises results from the plots of I_{pa1} *vs*. OTC concentration of each of the three buffer sets (Figure 3.14 to 3.17). Both pH 2 buffer sets were calculated to have quantification limits in the lower nano-molar range while all three sets have detection limits below 50 nM.

Table 3.5 Data interpreted from I_{pa1} *vs*. OTC concentration plots in pH 2 and pH 7 buffer(s).

Buffer set	Range intercept (X;Y)	Slope (µA/µM)	Linear range		Standard deviation (µA)*	Model fit (R^2)	I_m (µA)	K^{-1} (µM)
			LOD (nM)	LOQ (nM)				
pH 2 (BR)	6.97 ; 2.87	0.378	24.3	80.8	0.126	0.9941	5.815 (± 0.003)	8.73 (± 0.81)
pH 2 (PP)	4.15 ; 2.31	0.467	16.6	55.4	0.141	0.9753	5.644 (± 0.009)	6.19 (± 1.34)
pH 7 (PP)	8.72 ; 2.85	0.283	42.4	141.5	0.074	0.9926	5.344 (± 0.001)	8.91 (± 0.82)

Note: LOD, LOQ and slope calculated from the lower linear ranges of the I_{pa1} *vs*. OTC concentration plots. The slope is used as a measure of sensitivity. I_m represents the theoretical current maximum of the adsorption model. K^{-1} indicates desorption affinity of OTC towards GCE surface.
*Calculated as the average of all standard deviation of the I_{pa1} *vs*. OTC concentration plots.

It is clear that analysis in pH 2 buffered solution yielded a higher signal response to that of pH 7, with detection limits more than twice that of pH 7 (PP). This is also

reflected in the sensitivity calculated by the slope of the linear range, which was 0.467 and 0.283 μA/μM for PP buffer at pH 2 and 7 respectively. As a simple detection method at a bare, unmodified GCE, this result compares favourably to other voltammetric techniques employed for OTC analysis (Table 3.1).

I_m represents the maximum signal achievable at which the current theoretically plateaus in an I_{pa1} *vs*. concentration plot due to electrode saturation by the adsorbate (Bard and Faulkner, 2001). It can be seen that these values are comparable between the different buffer sets ranging from 5.344 to 5.815 μA. The I_m for both PP buffer systems are lower than for BR. This serves to confirm that maximum signal response is influenced by both the pH and the choice of supporting electrolyte.

K^{-1} is derived from the adsorption coefficient, K, in Equation 2.6 and used to represent the desorption affinity of OTC towards the GCE surface (Perez *et al*., 2002). In a pH 2 buffered solution, K^{-1} was lower in PP buffer than in BR buffer. The effect of adsorption will thus be more pronounced in PP. This is in agreement with a lower LOD, as well as lower range intercept coordinates (X;Y) as a result of GCE surface monolayer formation at lower OTC concentrations in PP buffer (pH 2). This can also explain the increase in fouling observed at pH 2 for OTC in PP as opposed to BR (Section 3.3.5) due to increased adsorption in this buffer at this pH. K^{-1} was highest for OTC analysed in pH 7 PP buffer, correlating with the lower sensitivity and higher LOD (Table 3.5) observed for this buffer at a neutral pH.

While the fit to the Langmuir isotherm is indicative of a plateau effect where current response no longer increases due to full surface coverage (Kissinger and Heineman, 1996), this can not be held as true since the effect of diffusion, which becomes more prominent at higher concentrations, is not taken into account (Section 3.3.7). It is more likely that the upper linear range will continue to increase gradually due to the ever-increasing effect of diffusion, as a result of increasing OTC solution concentration (Abdel-Hamid, 1998). The higher the OTC solution concentration, the greater the diffusion gradient and the more pronounced the effect of diffusion would become. The Langmuir isotherm is thus only valid for the OTC concentration range examined here.

Figure 3.18 was plotted to probe the validity of the Langmuir isotherm for the system tested, and shows the relationship of the current function, $c.I_{exp}^{-1}$, *vs. c*, where *c* is the OTC concentration and I_{exp} the experimentally recorded current response for pa_1.

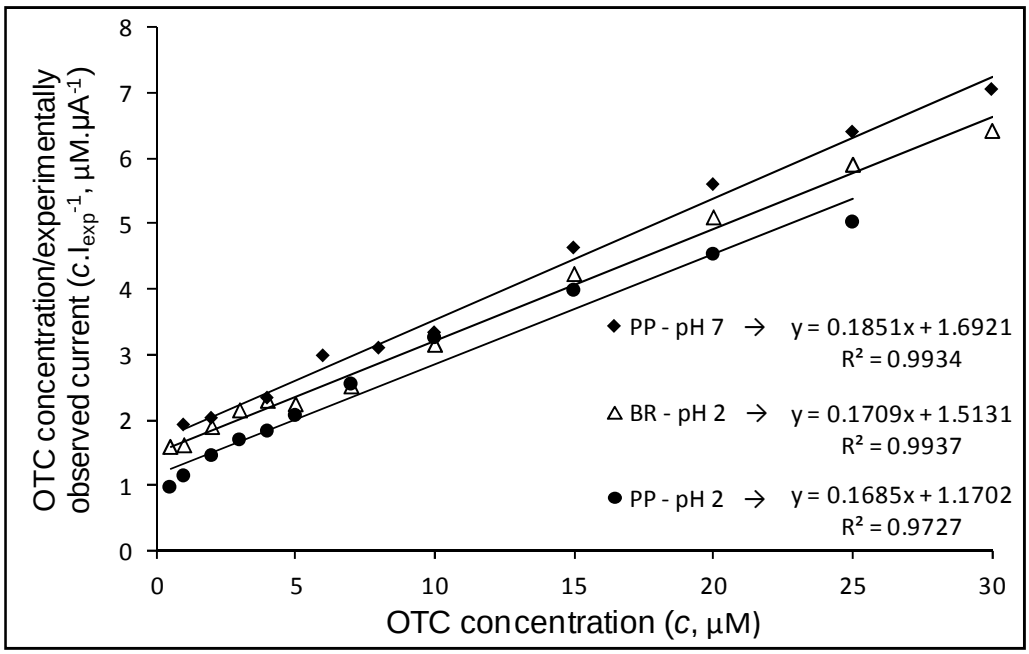

Figure 3.18 Linearised expression of $c.I_{exp}^{-1}$ *vs. c* for Langmuir isotherm validation. *c* is the adsorbate concentration (µM) and I_{exp} the experimentally observed current (I_{pa1}) for each respective OTC concentration.

According to Perez *et al*. (2002), linearity must be observed in this plot for the Langmuir isotherm to be applicable. Correlation coefficients of 0.97 and above were observed for all sets. It can be concluded that for the concentration ranges examined in this study, an adsorption isotherm can be applied to predict the relationship of I_{pa1} *vs*. OTC concentration, though was found to be most applicable to analysis in BR buffer (pH 2) and PP buffer (pH 7).

For further validation of the proposed mixed adsorption/diffusion process, a plot of current function, peak current/OTC concentration ($I_{pa1}.c^{-1}$) and log OTC concentration is presented in Figure 3.19. This current function is the inverse to that used in Figure 3.18 and more clearly illustrates the participation of the diffusive and adsorptive current components.

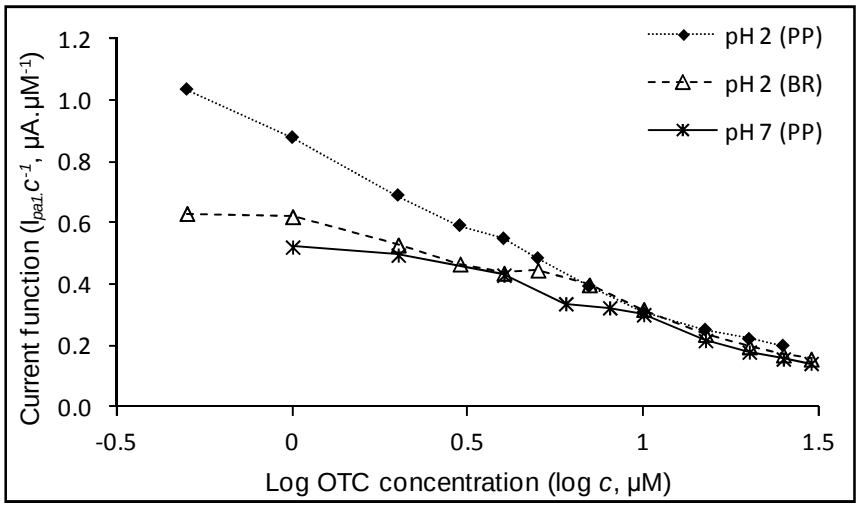

Figure 3.19 Relationship between current function ($I_{pa1}.c^{-1}$) and log OTC concentration (log *c*).

A decrease in OTC current function is observed for all buffers and pHs tested in Figure 3.19 with increasing log OTC concentration. For BR buffer (pH 2) and PP buffer (pH 7), limiting values are only observed for the current function at low analyte concentrations of 1 and 2 μM OTC respectively. According to Abdel-Hamid (1998), limiting values occur when the current function becomes independent of bulk concentration, i.e. in the absence of diffusive current. Thus, as OTC concentration increases, the current function decreases as a result of an ever more prominent diffusive current component. The absence of a limiting value for PP buffer (pH 2) compares well with the reduced linearity in Figure 3.18, suggesting diffusion contributed to the observed current for all concentrations tested in this acidic buffer, although accompanied by a strong adsorptive component at low concentrations (Figure 3.16).

This work offers the first use of the Langmuir isotherm to model the concentration-dependant adsorptive effect of OTC on its anodic current response, at a bare GCE.

3.3.7 Scan rate study

To further confirm adsorptive behaviour of OTC at the GCE surface, a scan rate study was performed in BR buffer (pH 2). Under varying experimental conditions, adsorption (Yarnitzky and Smyth, 1991; Guo *et al.*, 2009) and diffusion (Wangfuengkanagul *et al.*, 2004; Masawat and Slater, 2007) have both been implicated in the mass transport of OTC and other tetracyclines to the electrode

surface. Based on results obtained in the preceding section, both processes are believed to occur.

The scan rate study aimed to determine the contribution of adsorption and diffusion processes to the oxidation process of OTC for the operational parameters employed in this work. In particular, the 40 seconds stir time and 0.0 V applied conditioning potential which, when applied prior to analysis, were shown to enhance the anodic current, I_{pa1}, due to suspected adsorption of OTC onto the electrode surface.

The effect of altering the scan rate was determined using CV for two concentrations of OTC, i.e. 3 µM and 20 µM, as these fall within the first and second part of the aforementioned linear trends (Figure 3.14), respectively. From Figure 3.20, the effect of increasing scan rate becomes clear as current responses increase with scan rate.

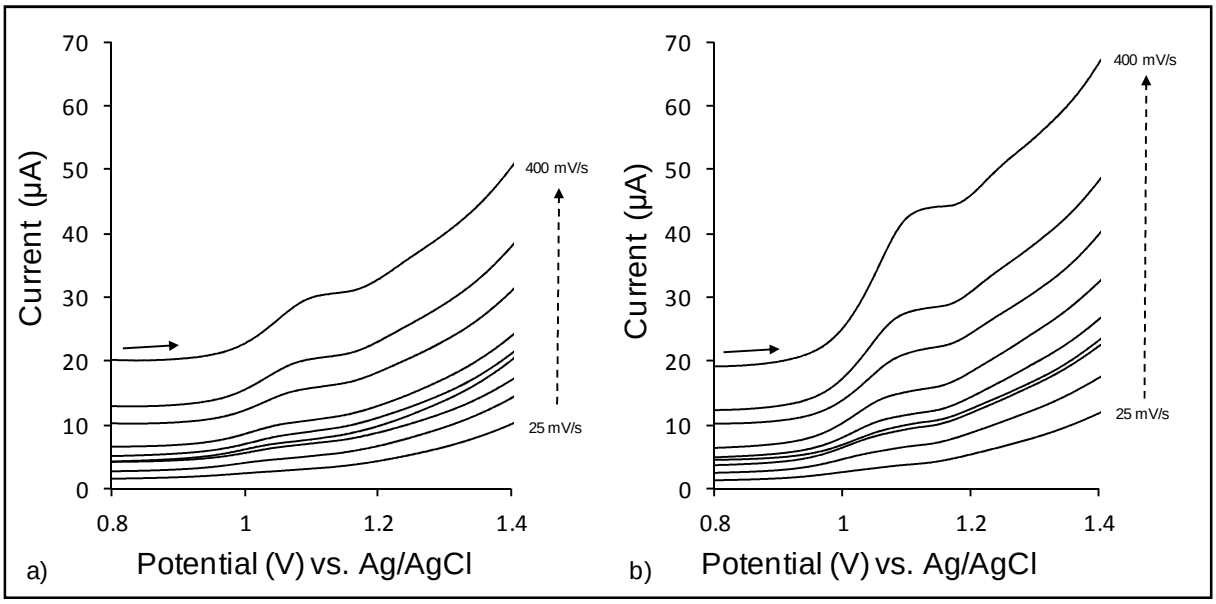

Figure 3.20 CV overlay showing the effect of changing scan rate on signal response for a) 3 µM and b) 20 µM of OTC in BR buffer (pH 2). Scan rates ranged from 25 to 400 mV/s, as indicated by the dashed arrow. Data obtained by CV in 0.2 M BR buffer (pH 2) using a 40 second stir time and 0.0 V applied potential.

As expected, the response for I_{pa1} increased with increasing scan rates, accompanied with an increase in charging current observed between 0.80 V and 0.95 V. This is due to increased background current originating from the electrolyte solution and electrode charging current (Kissinger and Heineman, 1996).

In Figure 3.21, plots for I_{pa1} *vs*. the square root of scan rate and I_{pa1} *vs*. scan rate for 3 µM and 20 µM OTC are shown. Only for the latter plot, could a linear relationship be established for the entire scan range tested (Figure 3.21b).

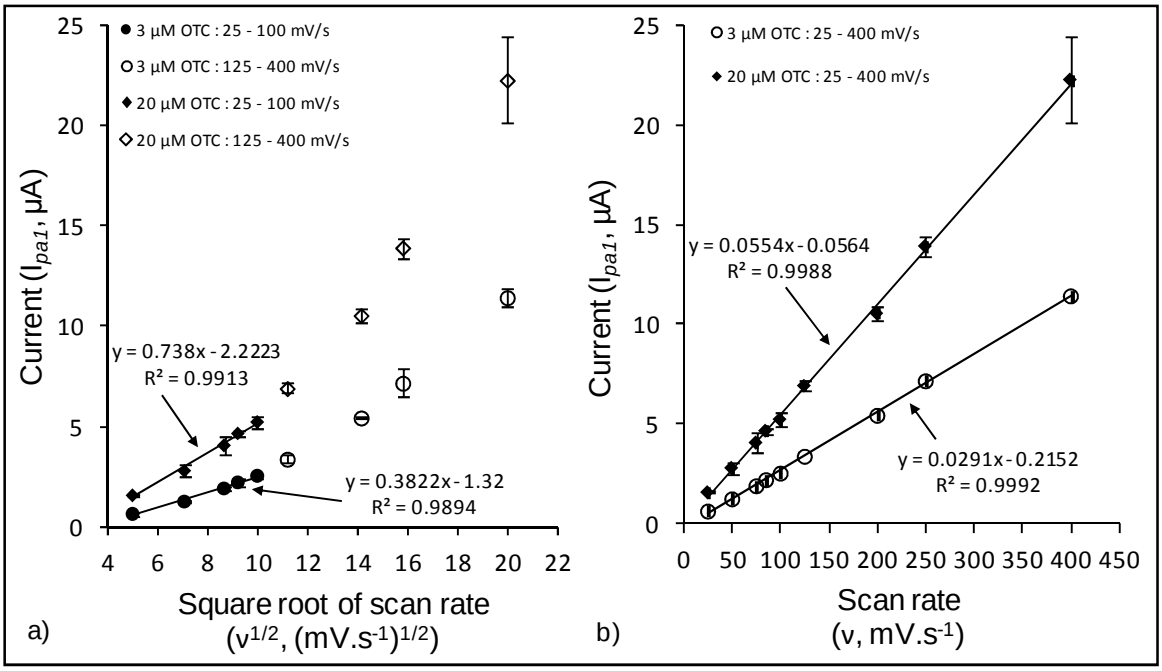

Figure 3.21 Relationship of a) I_{pa1} *vs.* square root of scan rate, $v^{1/2}$, and b) I_{pa1} vs. scan rate, *v*. CV analyses performed for 3 and 20 µM OTC in 0.2 M BR buffer (pH 2). Preconditioning step consisted of 40 second stir and 0.0 V applied potential prior to analysis.

The data was further interpreted to determine the mode of mass transport applicable for each concentration. For a diffusion controlled system, the relationship between peak current is linear to the square root of scan rate (Scholz, 2002). When however, peak height varies proportionally to scan rate, an adsorption controlled system is observed (Bard and Faulkner, 2001).

A linear relationship (with $R^2 > 0.99$) was obtained for a plot of I_{pa1} *vs*. the square root of scan rate in the range of 25 – 100 mV/s at both analyte concentrations (Figure 3.21a). This suggest diffusion controlled mass transport occurs in this scan rate range, above which it is controlled by adsorption governed by kinetics.

For the plots of I_{pa1} *vs*. *v*, a strong linear trend ($R^2 > 0.99$) could be extended from 25 mV/s to 400 mV/s for both concentrations of OTC (Figure 3.21b). This suggests adsorption of OTC occurs across the full scan rate range tested. This implies both

diffusive and adsorptive processes occur for each of the concentrations examined. To establish the extent to which each mass transport process participates in the transfer of analyte to the electrode surface, plots were drawn of log I_{pa1} *vs.* log scan rate. If the slope of this plot is close to 0.5, the system is said to be diffusion controlled (Compton *et al*., 1992; Zidan *et al*., 2010). A slope of 1.0 is indicative of an adsorptive process (Kalanur *et al*., 2008; Okumaru *et al*., 2011), whereas values falling between these points of reference are indicative of mixed adsorption and diffusion processes (Malinauskas *et al*., 2000; Lawrence and Wang, 2006).

From Figure 3.22 and 3.23, it is deduced that the mass transport of OTC to the electrode is strongly, but not solely, adsorptive as suggested by Figure 3.21. At a low concentration of 3 µM OTC, a good linear relationship was found for log I_{pa1} *vs*. log ν. While one linear regression can be used to describe the data, a higher correlation coefficient was found when two were drawn. In Figure 3.22, slopes of 0.9831 and 1.0737 for the ranges 25 – 100 mV/s and 100 – 400 mV/s respectively, the data suggests a system controlled primarily by adsorption at low analyte concentrations (3 µM OTC), as these values are close to the theoretical value of 1 (Kalanur *et al*., 2008; Okumaru *et al*., 2011).

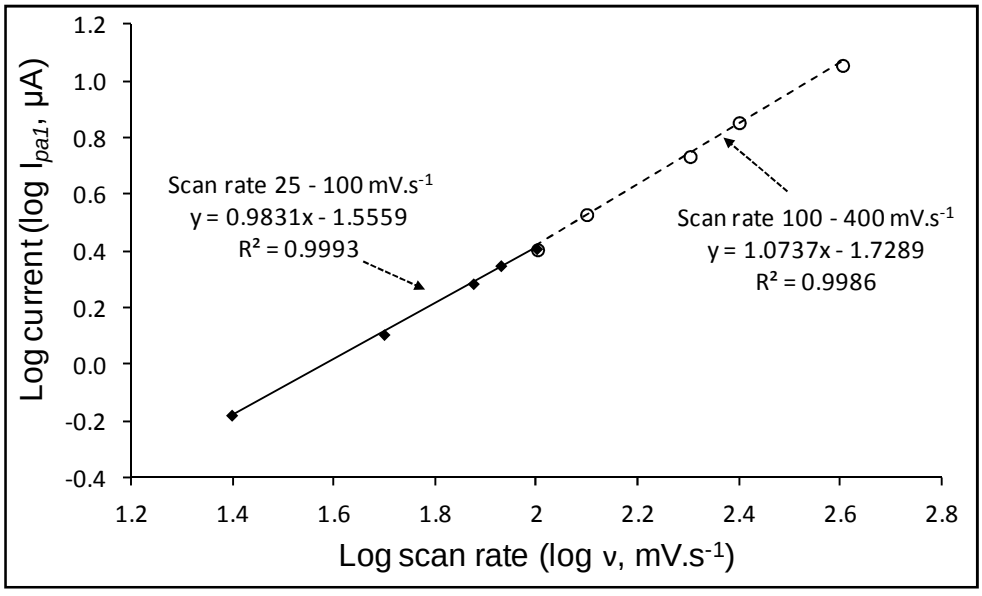

Figure 3.22 Plot of log I_{pa1} *vs.* log *v* at 3 µM OTC concentration. Linear relationships were observed from 25 – 100 mV/s and 100 – 400 mV/s. CV analysis performed in 0.2 M BR buffer (pH 2) with a 40 second stir and 0.0 V applied potential.

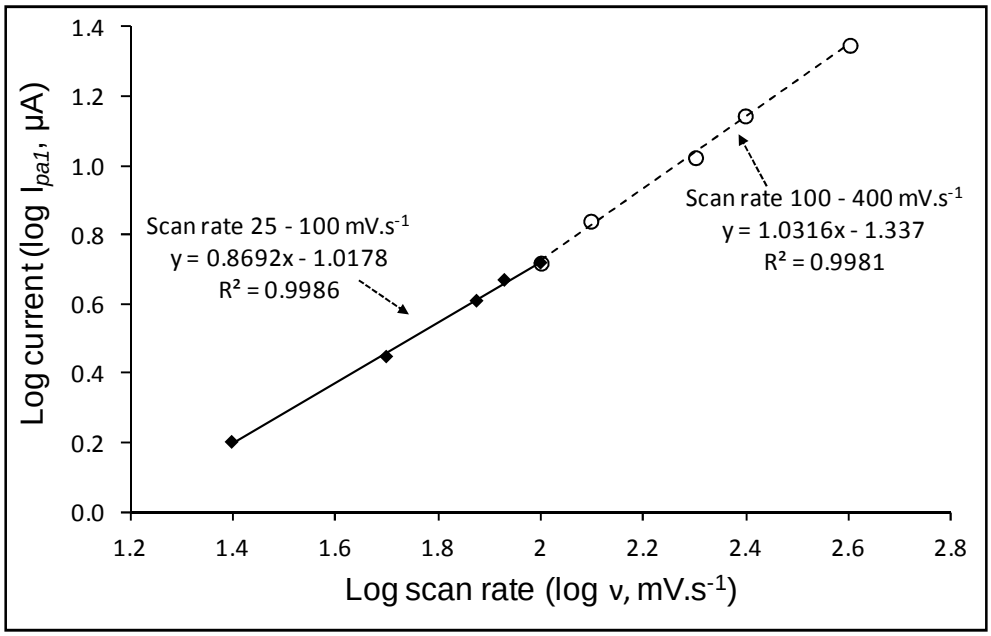

Figure 3.23 Plot of log I_{pa1} *vs.* log *v* at 20 µM OTC concentration. Linear relationships were observed from 25 – 100 mV/s and 100 – 400 mV/s. CV analysis performed in 0.2 M BR buffer (pH 2) with a 40 second stir and 0.0 V applied potential.

Figure 3.23 shows a slope of 0.8692 and 1.0316 recorded for the ranges 25 – 100 mV/s and 100 – 400 mV/s respectively at a high OTC concentration of 20 µM. This lower slope value of 0.8692 for the lower scan rate range suggests the system is influenced by adsorption as well as diffusion (Malinauskas *et al*., 2000; Lawrence and Wang, 2006) under lower scan rate conditions. This is because the current originating from diffused OTC (diffusive current) is proportional to the OTC concentration, but current arising from adsorbed OTC (adsorptive current) is not. Thus, as OTC concentration increases, the diffusive current increases, which results in a lower slope for log I_{pa1} *vs*. log ν plots at low scan rates.

Shaidarova *et al*. (2008) reported a slope of 0.75 for a plot of log I_{pa1} *vs.* log scan rate observed for 5 mM OTC, though no scan rate window is mentioned and analysis was performed at a ruthenium oxide: ruthenium cyanide film deposited GCE. At higher scan rates however, adsorption is the dominant form of mass transport as the slope is ~ 1.0.

The scan rate of 100 mV/s occurs at the inflection point for both log-log plots (Figure 3.22 and 3.23), incorporating both mass transport systems as was evident from

Figure 3.21 which suggests adsorption and diffusion both occur at this scan rate. As mentioned, mass transport of OTC has previously been attributed to either adsorption or diffusion in literature. The data presented above and in literature suggests the operational parameters (scan rate in this study) and analyte concentrations can slightly affect which mass transport process is favoured.

The scan rate studies complement data presented by the adsorption isotherm (Figure 3.15) and the relationship between the current function ($I_{pa1}.c^{-1}$) and OTC concentration (Figure 3.19). Under the conditions studied in this chapter, the information presented supports the view that adsorption is primarily responsible for the anodic signal observed for OTC at low and high concentrations.

It is believed that adsorbed OTC forms a monolayer on the electrode surface which, when it has sufficiently covered the GCE, partly obstructs more OTC from being oxidised due to this blocking layer (Bard and Faulkner, 2001), resulting in the second part of the standard curve of I_{pa1} *vs.* concentration, with a greatly reduced slope.

3.3.8 OTC oxidation mechanism

From the CV data obtained in the preceding scan rate study, the reaction mechanism for OTC, under highly acidic conditions, was examined.

Figure 3.24 presents the dependence of peak potential, E_{pa1}, and peak potential function, $E_{pa1}.v^{-1/2}$, on scan rate for high (20 μM) and low (3 μM) concentrations of OTC. A near-linear dependence on scan rate was observed for E_{pa1} at both concentrations (Figure 3.24a), with correlations (R^2) above 0.98. Linearity in this plot is described as being indicative of an EC mechanism (Niranjana *et al*., 2007; Char *et al*., 2008), where the redox step (E) is coupled to a follow-up irreversible chemical step (C_i) (Goyal *et al*., 2006; Hedge *et al*., 2008).

In Figure 3.24b, the current function, $E_{pa1}.v^{-1/2}$, when plotted against scan rate, produced a hyperbolically-shaped curve, supporting the presence of a succeeding chemical step (Kissinger and Heineman, 1996).

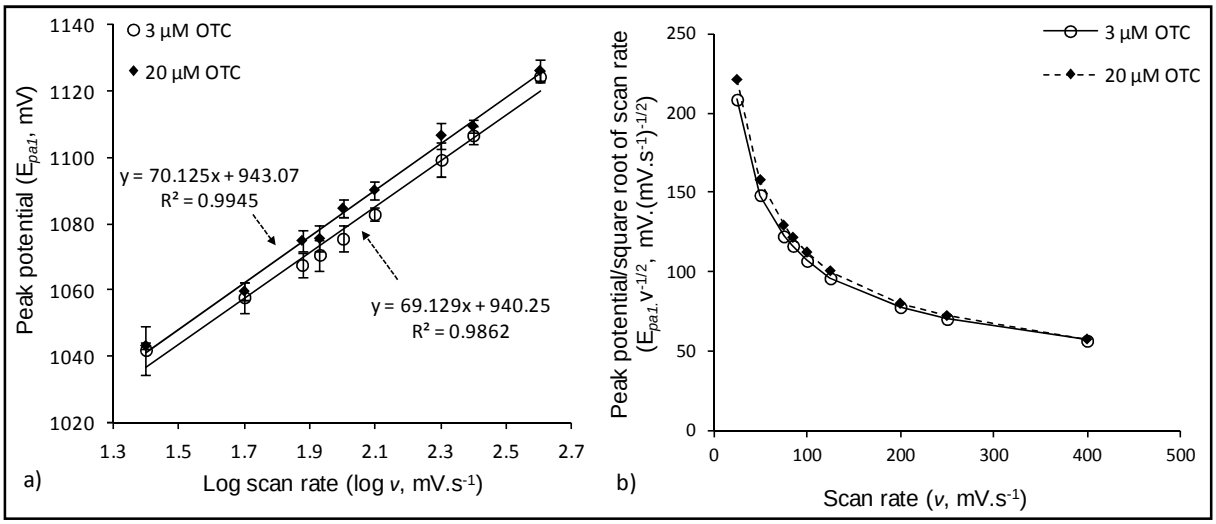

Figure 3.24 Dependence of a) peak potential, E_{pa1}, and b) peak potential function, $E_{pa1}.v^{-1/2}$ on scan rate. CV analysis performed for 3 and 20 µM OTC in 0.2 M BR buffer (pH 2).

The near-linear dependence of the ratio of I_{pa2} to I_{pa1} as a function of scan rate as shown in Figure 3.25, indicating pa_2 forms as a consequence of product formed during the primary oxidation process which yield pa_1 (Nicholson and Shain, 1964). Therefore, the reaction mechanism proposed for the oxidation of OTC is EC_iE.

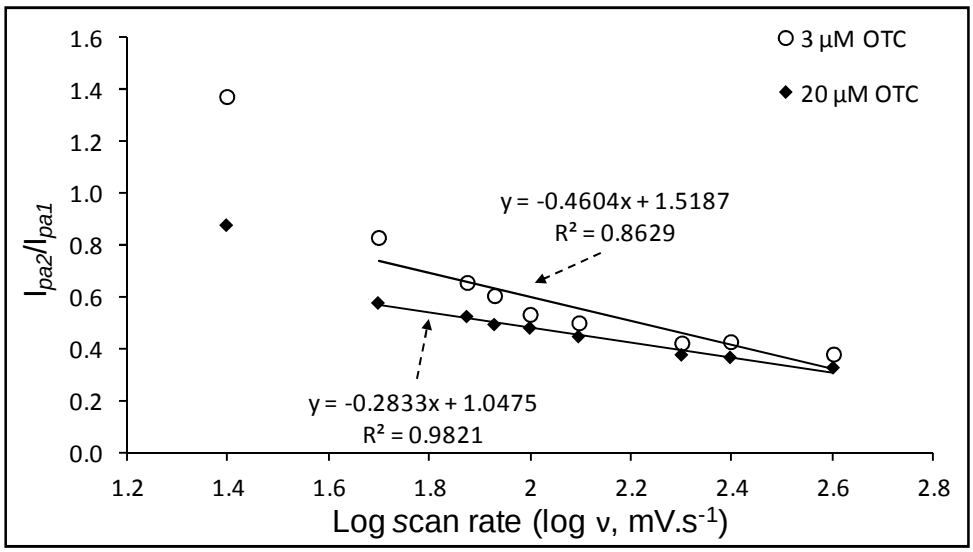

Figure 3.25 Ratio of I_{pa2} to I_{pa1} as a function of scan rate for 3 and 20 µM OTC in 0.2 M BR buffer (pH 2).

The number of electrons transferred in the rate limiting step (n_a), as well as the charge transfer coefficient (α) was determined using the slope of the E_{pa1} *vs.* log *v* plot (Figure 3.24a) in the following equation (Golabi and Irannejad, 2005):

$$b = 2\left(\frac{\Delta E_{pa1}}{\Delta \log v}\right) \quad \text{[Equation 3.1]}$$

where $\left(\frac{\Delta E_{pa1}}{\Delta \log v}\right)$ is the slope of the E_{pa1} *vs.* log *v* plot, and *b* the Tafel slope. Using the Tafel slope, calculated as 138.26 and 140.25 for 3 and 20 μM OTC respectively, the following equation can be solved to determine n_a and α (Bockris and Khan, 1993).

$$b = 2.303\ \frac{RT}{n_a .\alpha. F} \quad \text{[Equation 3.2]}$$

where *R* is the standard molar gas constant (8.31447 $J.mol^{-1}.K^{-1}$), *T* the temperature in Kelvin and *F* the Faraday constant (9.65 x 10^4 C). Thus, at room temperature (298 K), the equation can be simplified as follows:

$$b = \frac{59.1}{n_a.\alpha} \quad \text{[Equation 3.3]}$$

This results to $n_a.\alpha$ values of 0.427 and 0.421 for 3 and 20 μM respectively. By assigning a n_a value of either $1e^-$, $2e^-$ or $3e^-$, α can be determined as was done in Table 3.6.

Table 3.6 Determination of α for hypothetical values of n_a values of $1e^-$, $2e^-$ or $3e^-$ in the rate limiting step.

n_a	1	2	3
α for 3 μM OTC	0.427	0.214	0.142
α for 20 μM OTC	0.421	0.211	0.140

As values of α commonly vary between 0.3 and 0.7 (Yoshimoro *et al*., 1989), n_a consists of a $1e^-$ transfer process.

The total number of electrons transferred, n_t, was determined according to the following equation:

$$E_p - E_{p/2} = \frac{47.7}{n_t.\alpha} \quad \text{[Equation 3.4]}$$

where E_p and $E_{p/2}$ are the anodic peak potential and half peak height of pa_1 respectively, the difference of which represents the peak width at half peak height

(Scholz, 2002). Through the application of the averaged peak widths calculated for all scan rates at an OTC concentration of 3 and 20 µM, and the α values 0.427 and 0.421 for 3 and 20 µM OTC respectively (Table 3.6), n_t was calculated as 1.23 for 3 µM and 1.07 for 20 µM.

Therefore, according to the slopes of I_{pa1} *vs*. pH (Figure 3.6), which ranged between 45 and 59 mV/decade, and under the adsorptive conditions studied, the oxidation mechanism of OTC involves the transfer of $1e^-$ and 1 proton when studied in 0.2 M BR buffer (pH 2). This process is identical as was described for TC (Chatten *et al*., 1979; Guo *et al*., 2009). A single electron transfer is consistent with oxidation of the phenolic moiety at C_{10} (Figure 3.1) as proposed by Chatten *et al*. (1979), and supports this author's conclusion that the similar oxidative behaviour of tetracycline antibiotics is due to structural homology. Further investigation into the precise nature of the oxidative behaviour of OTC falls outside the scope of this research.

3.4 CHAPTER CONCLUSIONS

OTC exhibits itself as a group of three to four irreversible anodic peaks when observed using SWV depending on buffer pH. As noted in this work and in literature, pH 2 produces the highest current response across the range examined.

The response and potential for pa_1 appeared mostly independent of electrolyte solution and OTC stock solution solvent at pH 2, while a potassium phosphate buffer was preferred for analysis at physiological pH for reasons of sensitivity and peak sharpness. While the inclusion of a pre-conditioning potential has made accurate calculation of a LOD difficult due to the current response exhibiting OTC adsorption onto the GCE surface, as explained by the Langmuir isotherm, sensitivity was seen to increase considerably.

A brief summary in the form of Table 3.7 shows the extent to which each of the optimisation steps improved the anodic response, by comparing the detection sensitivity at 20 μM OTC.

Table 3.7 Comparative summary of concentration specific detection sensitivities of OTC after sequential optimisation steps for 20 μM OTC.

Optimisation step	Detection sensitivity (nA/μM)*		
	pH 2 (BR - B)	pH 2 (PP - E)	pH 7 (BR - M)
Baseline	82.8	**	50.6
Solvent and electrolyte selection	102.5	102.1	78.9
Stir time and pre-conditioning potential	200.8	216.7	150.6
Current increase	242 %	212 %	297 %

Note: BR = BR buffer as electrolyte, PP = PP buffer as electrolyte, B = respective buffer as stock diluent, E = ethanol as stock diluent, M = milliQ as stock diluent.
* Concentration specific sensitivity calculated using Equation 2.5.
** Baseline data refers to un-optimised analysis performed during the pH study in BR buffer only (Section 3.3.2).

A cumulative increase is observed for each optimisation step in Table 3.7, with current responses increasing up to 297 %, largely attributed to the application of a

stir and preconditioning potential step. As mentioned previously, this was believed to be due to an adsorptive process that allows for the accumulation of OTC at the electrode surface, which was confirmed through scan rate studies. OTC adsorption was favoured under low analyte and high scan rate conditions. The effect of OTC adsorption on I_{pa1} could be adequately described by the Langmuir isotherm for the analyte concentration tested. This previously unused method for modelling the effect of OTC concentration of the anodic current of I_{pa1}, offers an alternative means of calculating detection limits and quantifying unknown OTC-containing samples, when adsorptive complications are experienced.

Detection limits in the lower nano-molar range were calculated for each of the three systems tested (Table 3.5). Analysis at pH 7 was continued in order to determine its applicability for OTC analysis in real-world scenarios as seen in the following chapters.

The BR buffered (pH 2) detection matrix was selected for further analytical investigations for the following reasons:

- The greatest signal response for pa_1 was observed at pH 2 with a well-defined irreversible oxidation peak.
- Numerous literary sources have shown pH 2 to be favourable for OTC detection due to its chemical stability in acidic media (Table 3.1).
- Analysis at pH 2 displays well defined secondary and tertiary peaks, which could prove useful for future works.
- A lower overall standard deviation was achieved than for pH 2 (PP) for the I_{pa1} *vs*. OTC concentration plot.
- A lower stir time could be maintained than for the PP buffered system.
- Excellent surface renewal properties were observed in the fouling studies.
- The best correlation was found between the experimentally observed and Langmuir modelled data allowing for an alternative quantification strategy.
- The mass transport and reaction mechanism for this system was investigated and could provide further information if operational parameters are changed in subsequent experiments.

Scan rate studies showed the oxidation of OTC at pH 2 to be governed by an EC_iE reaction mechanism. N_a and N_t were found to be 1 electron, as reported for the structurally similar TC (Chatten *et al*., 1979).

This chapter has shown the applicability of voltammetry, and specifically SWV, in the detection and quantification of OTC in buffered matrix at an unmodified GCE. The detection limits of the above-mentioned system using an unmodified GCE compared favourably to methods summarised in Table 3.1. As no alternative techniques were coupled to SWV such as liquid chromatography (LC) and analysis was done on a bare GCE instead of mercury electrodes, the results in this chapter become even more significant. This also suggests further improvements through electrode modifications could produce an even more sensitive and versatile detection technique.

A strong fouling pattern is exhibited by OTC with signal loss of more than 50 % after two successive scans without surface renewal. The application of an *in vitro* preconditioning procedure (stirring and applied potential) was able to minimise this decrease in response, especially for pH 2. This suggests the possibility of a reusable electrode for successive sample analysis. Results of ten successive scans of OTC at a bare GCE, in the absence of electrode cleaning, were > 95 % reproducible, compared to > 90 % and > 93 % on an ionic liquid-MWCNT-GCE (10 scans for tetracycline; Guo *et al*., 2009) and a gold screen-printed electrode (7 scans for OTC; Masawat and Slater, 2007). The research presented in this chapter shows that while modification of the electrode surface can be an important improvement not only to sensitivity, but also to reusability, which is an important factor in the development of a continuous monitoring system, often overlooked simple stirring procedures and applied potentials can be effective in greatly improving reproducibility.

In the subsequent chapters, alternative matrices are tested in order to assess the versatility of the developed system. In addition, modification to the electrode surface in the form of nanomaterials was investigated in an attempt to improve signal response.

CHAPTER 4

Voltammetry in Complex Microbiological Growth Media:
A Case study of Oxytetracycline

4.1 INTRODUCTION

As described in Section 1.3.1, in order to improve the efficiency of antibiotic fermentation processes, production yields must be assessed either by on-line or off-line sampling techniques. While conventional disk-diffusion methods are reliable for measurements of antibiotic production, they offer no on-line application and are time-consuming (18 – 24 hours incubation period) (Riaz, 1986; Lunestad and Goksøyr, 1990; Yang and Lee, 2001). In light of the rapid fermentation processes of 5 - 10 days for oxytetracycline production by *S. rimosus* (Zygmunt, 1961; Yang and Lee, 2001), alternative techniques for measuring the production thereof within these short time-frames, have been investigated.

4.1.1 Fast antibiotic determination and monitoring in fermenters

An example of an attempt at developing a fast sensing technique for antibiotic fermentation yield was reported by Tunnemann *et al*. (2001). An optical glycopeptide antibiotic biosensor with a peptide recognition sequence was employed for the detection of vancomycin and balhimycin using reflectometric interference spectroscopy (RIfS). Among the issues highlighted by that study was the nonspecific binding of components within the fermentor to the sensor surface, which was solved through transducer coating and pre-analytical sample centrifugation and dilution. By the elimination and/or dilution of interacting broth constituents, detection accuracy was improved. This study highlighted the importance of a robust detection system that is able to analyse samples containing interfering organic molecules.

Optical biosensors for antibiotics have been reported by Höbel *et al*. (1992), where an immobilised or cross-linked penicillinase enzyme was utilised. When the enzyme is brought into contact with its substrate, penicillin G, a change in local pH occurs, causing both a measurable change in the colour of pH indicators immobilised within the biosensor as well as a change in the intensity of fluorescent light emitted by

fluorescence pH indicators. The degree of these changes was reported to be indicative of substrate concentrations.

High performance liquid chromatography (HPLC) has been reported for off-line analysis of tetracycline (TC) in fermentation media (Tsuji and Goetz, 1978). While this method was specific for TC, samples needed to be acidified, diluted and centrifuged prior to analysis.

For the specific detection of OTC, an automated system was developed relying on the colourimetric reaction that occurs after OTC complexation with ammonium molybdate, $(NH_4)_2MoO_4$, under heated and acidic conditions (Abdel-Azize *et al*., 1982). While this method is fast and accurate, the lowest reported detection level was only 200 μM, a concentration only observed after 24 – 48 hours of fermentation (Zygmunt, 1961; Yang and Yueh, 2001). Abdel-Azize and co-workers found $(NH_4)_2MoO_4$ did not complex with tetracycline (TC) or chlortetracycline (CTC). The method was thus not adaptable to other members of the tetracycline group, but showed promise as a selective detection method for OTC.

A similar colourimetric detection system was developed earlier by Grenfell *et al*. (1960) based on colour formation by OTC-$FeCl_3$ complexation, though no detection limit or specificity was mentioned. While both methods (Addel-Azize and Grenfell) employed Auto-Analyzer systems, each performed a manual, time-consuming, pre-analysis sample treatment stage to eliminate interferents. Indeed, even for complete on-line monitoring systems that incorporate an automated prefiltration step, filter membrane fouling due to high biomass concentration presents a frequently reported limitation for these methods (Kornmann *et al*., 2003).

4.1.2 Electrochemical monitoring of antibiotic production

Several electrochemical methods have been suggested for monitoring the production of antibiotics in complex growth media. These include differential pulse voltammetry (DPV) for saframycin A (Bersier and Jenny, 1988) and everninomicin detection (Kabasakalian *et al*., 1974), as well as polarography for trichothecin (Krugliak *et al*., 1977) and polarography as well as differential polarography for oleandomycin

(Kardo-Sysoeva *et al*., 1981) measured in fermentation media. Cathodic analysis at negative potentials was used as the primary method of antibiotic detection in these reported studies. Limited studies have explored voltammetry in the presence of growth media and none reported detection of OTC in complex fermentation media.

4.1.3 Problem statement

No voltammetric study has focused on the interfering effect of standard growth media on glassy carbon electrode activity. Literature concerning the presence of redox active molecules in these media is also lacking. Similarly, to the author's knowledge, electrochemical analysis of OTC in complex fermentation media has not previously been examined in the literature.

4.1.3 Chapter aims and objectives

The study aimed to explore the application of voltammetry in growth media through an assessment of interferents. Thereafter the study aimed to apply this knowledge to investigate the utilisation of voltammetric methods for the detection and quantification of OTC in complex growth media.

Objective 1: Investigation of the electrochemical behaviour of selected growth media using cyclic voltammetry (CV).

Objective 2: Assessment of the activity of a bare GCE in the presence of selected growth media through the use of a ferri-ferrocyanide redox probe.

Objective 3: Electrochemical impedance spectroscopy (EIS) study to probe surface fouling of different growth media onto the electrode surface.

Objective 4: Anodic square wave voltammetric (SWV) investigation of OTC in the presence of growth media and media components.

Objective 5: Cathodic SWV investigation of OTC in the presence of Abou-Zeid (AZ) media and AZ media components.

Objective 6: Investigating the role of pre-analysis treatment of growth media for cathodic detection, to enhance OTC current response in the presence of AZ media.

4.2 INSTRUMENTATION AND MATERIALS

4.2.1 Reagents

Grades and suppliers for general reagents are specified in Section 2.2.

The composition lists for the microbiological growth media can be found in Appendix A. These include the commercially available clostridium nutrient media (CNM, obtained from Fluka), Luria Bertani broth (LB, obtained from Biolab) and nutrient broth (NB, obtained from Biolab), as well as custom prepared media including minimal salts media (MSM), Abou-Zeid media (AZ) and malt extract media (MEM).

These growth media were selected for examination for their common use in the enumeration of bacterial species. Abou-Zeid (AZ) media, in particular, was selected for its high reported OTC yields during batch fermentation (Abou-Zeid *et al*., 1977). Due to its freely available components, it is also a likely media used for commercial OTC production.

4.2.2 Materials

All glassware used for microbiological media preparation was washed using a sequence of 5 % nitric acid and three MilliQ water rinses. All growth media was autoclaved at 121 °C for 15 min.

A microfuge® 16 centrifuge (Beckman Coulter, USA) was used for pre-treatment procedures of growth media samples.

4.3 EXPERIMENTAL APPROACH

Unless otherwise stated, all voltammetric experiments were conducted in accordance with Chapter 2. This includes electrode and buffer preparations, data analysis and presentation of data and error margins.

4.3.1 Voltammetry in complex microbiological growth media

CV analysis of a range of commonly used microbiological growth media (listed in Appendix A) were investigated voltammetrically. The presence of oxidizable and reducible media components was examined at both pH 2 and pH 7. The final concentration of growth media was 0.1 g/l in the buffered working solution.

The effect of different growth media on the activity of a bare GCE was by examination through the redox behaviour of a ferri-ferrocyanide ($Fe(CN)_6^{3-/4-}$) redox probe. A reference standard was established, using an equimolar solution (1 mM final redox probe concentration) of $K_4[Fe(CN)_6]$ and $K_3[Fe(CN)_6]$, analysed in 0.1 M KCl (pH 7). Buffer controls, in which no growth media was present, were prepared for both pH 2 (0.2 M BR buffer) and pH 7 (0.2 M PP buffer), followed by analysis of these buffers containing the various growth media. Both current- and potential-related parameters of $Fe(CN)_6^{3-/4-}$ were examined (Brown, 1972; Hu *et al*., 1985).

4.3.2 Electrochemical impedance spectroscopy (EIS) in selected growth media

EIS was performed in the presence of selected media to probe the effect of these complex samples on electrode performance. The electrode was scanned cyclically in the presence of the growth media, followed by a single scan after the addition of $Fe(CN)_6^{3-/4-}$ (1 mM) to confirm the open circuit potential (OCP) post scan using the GPES software. Operational parameters were as described in Section 2.3.3.

4.3.3 Anodic analysis of OTC in fermentation media

To assess the applicability of voltammetry as an analytical tool to quantify OTC in AZ media through its anodic response, the effect of the growth media on the current recovery of OTC was examined, relative to analysis performed in the absence of AZ media. The final concentration of AZ media in the working solution was 0.1 g/l.

4.3.3.1 Peptone and peptone substitutes

Substitute media components for peptone, an identified interferent and nutritive component of several media tested in these studies including AZ media, were investigated. These alternatives were in the form of yeast extract and malt extract and added to the same concentration as peptone, 5 g/l in AZ media (Abou-Zeid *et al*., 1977). After dilution in the working solution, the final concentration of each component was 0.1 g/l. Their effect on the anodic response of OTC was investigated at pH 2 (0.2 M BR buffer) and pH 7 (0.2 M PP buffer) under the respective buffer parameters highlighted in Chapter 3. Where peptone was replaced by malt extract, the media was referred to as malt extract media (MEM) (Appendix A).

4.3.3.2 OTC analysis in malt extract media (MEM)

OTC anodic signal recovery in the presence of MEM was compared for both acidic and pH neutral systems. Antibiotic stock solutions (1 mM) were prepared in MEM, a variation of AZ media in which peptone was replaced by malt extract (5 g/l) and supplemented with potassium nitrate (5 g/l). OTC anodic current recovery was compared to that observed for the appropriate standards performed in the respective buffers (Section 3.3.6).

4.3.3.3 Impact of MEM concentration on OTC signal response

The effect of MEM concentration on the anodic response of OTC was investigated. This was achieved by varying the final MEM concentration in the analysed buffer solution, including 0.1, 0.2, 0.5 and 1 g/l, while OTC was maintained at 20 µM.

4.3.3.4 OTC linear range in MEM

A linear detection range was established for OTC stock solutions prepared in MEM, to determine the relationship between I_{pa1} and OTC concentration in the presence of MEM. The LOD was calculated as before (Section 2.4.3) and compared to the standard curve of OTC in 0.2 M BR buffer (pH 2) in the absence of MEM, as reported in Chapter 3. OTC stock solutions prepared in MEM were diluted using freshly prepared MEM to maintain a consistent MEM concentration, while varying the amount of OTC analysed.

4.3.4 Cathodic analysis of OTC

The detection of OTC was investigated using both CV and SWV in 0.2 M BR buffer (pH 2), and in the presence of AZ growth media. A stir time of 40 seconds and scan rate of 100 mV/s was adopted for all cathodic studies.

4.3.4.1 Preconditioning potential

Similar to Section 3.3.4, a range of applied conditioning potentials were investigated for their effect on the cathodic peak of OTC, in particular the current response of the primary cathodic peak, pc_1.

4.3.4.2 Assessing the effect of O_2 reduction on OTC signal recovery

The minimal necessary sample de-aeration time by nitrogen purging, was established. Purging occurred prior to sample analysis while a nitrogen blanket covered the quiescent solution during analysis.

4.3.4.3 OTC analysis in AZ media

AZ media, as well as the individual components of this growth media, were probed for their effect on cathodic OTC analysis. A 0.4 M BR buffer (pH 2) was used for blank scans in mixtures of buffer and broth (1:1 $^{v}/_{v}$) to maintain a consistent buffer molarity of 0.2 M.

4.3.4.4 OTC sample preparation for cathodic analysis

Pre-treatment of AZ media samples containing OTC, were examined by performing the following six preparation procedures prior to cathodic analysis (Table 4.1). These simple procedures included combinations of sample acidification, centrifugation and filtration.

Table 4.1 Sample preparation as per prescribed method.

Pre-treatment	Method A	Method B	Method C	Method D	Method E	Method F
Acidification				X	X	X
Centrifugation		X			X	
Filtration			X			X

Note: Method A serves as a control and OTC stock solutions prepared in MEM were analysed without pre-treatment.

These methods are commonly used, either individually and in tandem, to remove cells, cellular debris and fermentation by-products (Ratledge and Kristiansen, 2001). They were performed prior to sample analysis for the purpose of improving the cathodic response of OTC by removal of interfering growth media components.

For sample acidification, a 1 mM OTC stock solution prepared in MEM was titrated to pH 2 using citric acid and phosphoric acid (1:1 $^{v}/_{v}$) and allowed to stabilize for 5 minutes prior to analysis (Yuan *et al*., 2010). Centrifugation was carried out at 8000 *g* for 4 minutes. Filtration was performed using 0.2 µm syringe filters (cellulose acetate membrane) (GVS, USA). Acidification was performed first when coupled with a second pre-treatment step.

Pre-electroanalytical parameters of 300 seconds de-aeration time and 40 seconds stirring at an open-circuit potential were employed for cathodic detection of pre-treated AZ media samples (Table 4.1) containing OTC. A control CV scan was performed with 20 µM OTC in 0.2 M BR buffer (pH 2) without the addition of fermentation broth. Recovery values for the above mentioned extraction methods were calculated with respect to this control.

4.4 RESULTS

4.4.1 Voltammetry in various microbial growth media – pH 2

The anodic and cathodic responses of each of the following media were investigated under both highly acidic (0.2 M BR buffer, pH 2) and neutral (0.2 M PP buffer, pH 7) conditions: AZ media, LB broth, MEM, MSM, NB and CNM. No OTC was present in any of these samples.

4.4.1.1 Broad potential range cyclic voltammetry

A wide potential range CV was used to identify anodic and cathodic peaks for each of the aforementioned media. In a pH 2 buffered electrolyte solution (0.2 M BR buffer), it is seen from Figure 4.1 that, apart from MSM, all the growth media contained components which are anodically detectable.

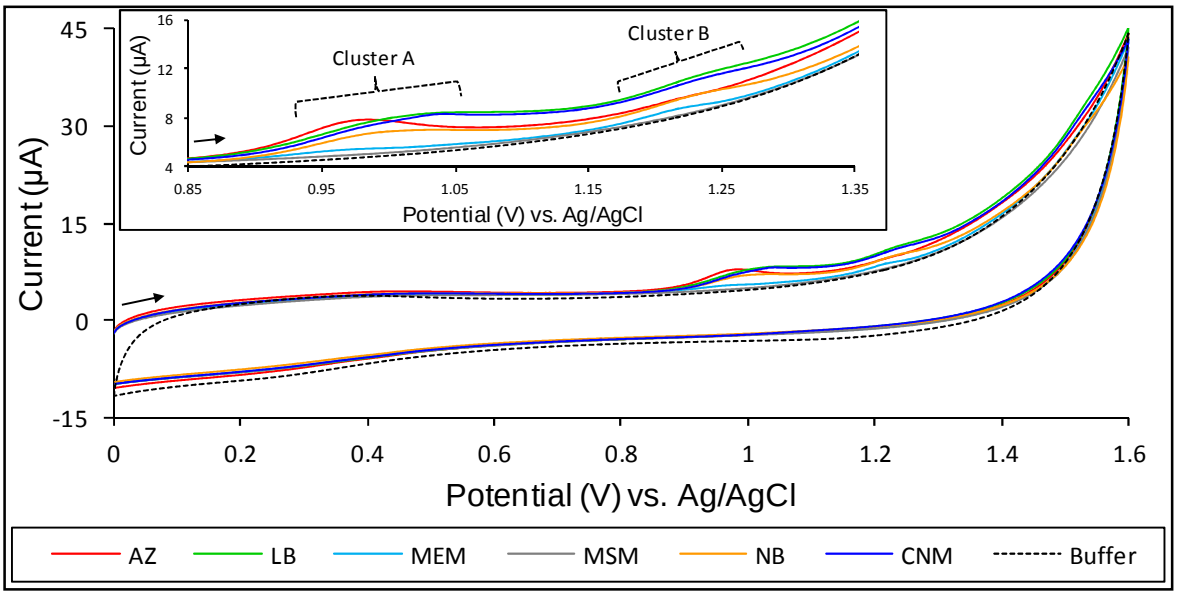

Figure 4.1 Anodic analysis of different media in 0.2 M BR buffer (pH 2). Magnification of peak-rich areas reported in inlay. Dashed line shows background scan performed in buffered solution. Final growth media concentration was 0.1 g/l.

The formation of the first group of peaks (referred to as Cluster A) begins at ~ 0.86 V while Cluster B formed after ~ 1.16 V (shown in inlay to Figure 4.1). There are no observable cathodic peaks in the potential range tested and the oxidation reactions are irreversible under the conditions tested. Analysis in the presence of these growth media can thus be performed in a highly acidic buffer solution without interfering

anodic peaks, across a limited potential range of 0 to ~ 0.86 V. Across the tested CV potential range (0.0 to 1.6 V), no electrochemically observable waveforms were seen for buffer containing MSM.

The anodic responses observed for the different media closely match those of the organic nitrogen sources described further (Section 4.4.4.1), which also produced two distinct anodic signals. The slight difference in the positions of peaks in Cluster A is attributed to varying compositions of each of the media (Appendix A).

Figure 4.2 shows CV analysis of the growth media under cathodic scans, where no observable peaks were observed in the range of 0 to - 1.3 V in a pH 2 buffered solution.

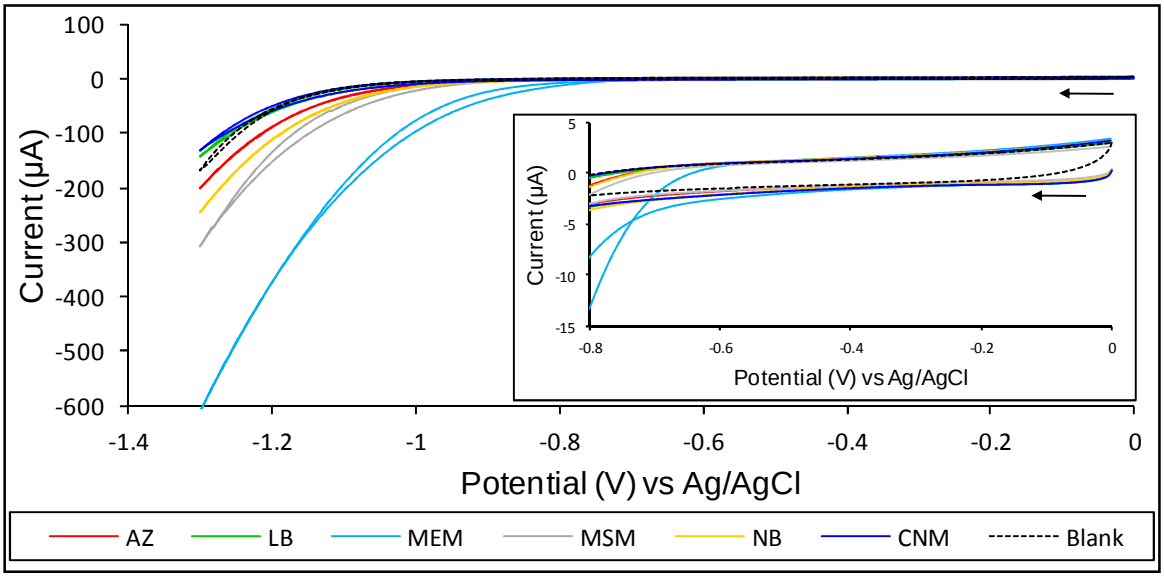

Figure 4.2 Cathodic analyses of different media in 0.2 M BR buffer (pH 2). Magnification of baseline reported in inlay. Blank scan was performed in BR buffer only. Final growth media concentration was 0.1 g/l.

With the exception of MEM, a similar response was observed for each of the media tested with varying magnitudes of faradaic current at highly negative potentials compared to the buffer blank. This effect was far more pronounced for MEM. From the inlay to Figure 4.2 it can be seen there is no faradaic behaviour in the range of 0 to - 0.8 V, and the CV of the growth media closely matches that of the buffered solution (blank).

4.4.1.2 Ferri-ferrocyanide redox probe analysis – pH 2

To further investigate the effect of growth media on the electrode response, a $Fe(CN)_6^{3-/4-}$ redox probe was used. CV analysis of $Fe(CN)_6^{3-/4-}$ was conducted in 0.2 M BR buffer (pH 2) spiked with microbiological growth media. The effect of the different media on the voltammetric behaviour of $Fe(CN)_6^{3-/4-}$ was measured with respect to an established baseline obtained in 0.1 M KCl.

These effects were grouped as either current related parameters, including peak current response, I_p, and thus effective surface area, A_{exp}, (in accordance with Equation 2.7), and I_{pa}/I_{pc} ratio (Equation 2.9), or the potential related parameter ΔE_p (Equation 2.10). For the purposes of this analysis, A_{exp} was calculated on the assumption that the diffusion coefficient (D) remains unchanged in the presence of different microbiological growth media.

Figure 4.3 shows the CV of $Fe(CN)_6^{3-/4-}$ in 0.2 M BR buffer (pH 2) and 0.1 M KCl (pH 7).

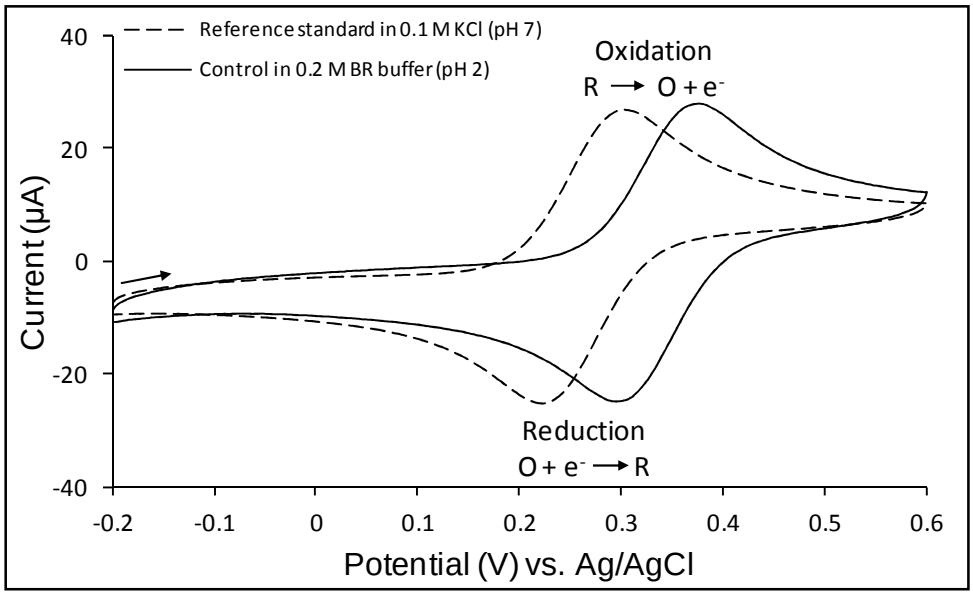

Figure 4.3 CV of 1 mM $Fe(CN)_6^{3-/4-}$ redox couple in 0.1 M KCl and 0.2 M BR buffer (pH 2). The oxidation and reduction schemes are included for the forward and reverse reaction respectively.

Analysis in BR buffer, referred to as the control, served to distinguish between electrolyte and growth media related changes in the redox parameters of $Fe(CN)_6^{3-/4}$. The shift of both the anodic and cathodic peak of $Fe(CN)_6^{3-/4-}$ towards a more

positive potential can be attributed to the lower pH of BR buffer (pH 2) compared to that in 0.1 M KCl (pH 7) (Martinez-Huitle *et al*., 2009). Table 4.2 compares the position of the anodic and cathodic peaks of $Fe(CN)_6^{3-/4-}$ as well as their peak separations (ΔE_p) under acidic conditions in the presence of different growth media and for the buffer controls.

Table 4.2 Comparative analysis of peak position and peak separation of 1 mM $Fe(CN)_6^{3-/4-}$ in various microbiological detection matrices with 0.2 M BR buffer (pH 2) as supporting electrolyte.

Detection matrix	E_{pa} (mV)	E_{pc} (mV)	ΔE_p (mV)
0.1 M KCl (pH 7)	302.3 (± 0.6)	232.0 (*)	70.3 (± 0.6)
0.2 M BR buffer (pH 2)	372.3 (± 0.6)	297.3 (± 0.6)	75.0 (*)
Growth media in BR buffer (pH 2)			
AZ media	372.7 (± 1.1)	297.0 (*)	75.7 (± 1.1)
NB	374.0 (± 0.2)	296.3 (± 0.6)	77.7 (± 2.5)
MSM	374.0 (*)	299.0 (*)	75.0 (*)
MEM	372.0 (*)	299.0 (*)	73.0 (*)
CNM	372.7 (± 1.2)	296.7 (± 0.6)	76.0 (± 1.0)
LB	374.0 (*)	297.0 (*)	77.0 (*)

Note: For analysis of growth media, 40 µl of the respective media was analysed with 1960 µl BR buffer (0.2 M, pH 2). The final growth media concentration was 0.1 g/l. ΔE_p calculated according to Equation 2.10.
* Standard deviation less than 0.1 mV.

ΔE_p serves as a measure of the reversibility of an electrochemical reaction, and is 58 mV for a totally reversible, one-electron reaction (Kissinger and Heineman, 1996). Noticeably, the ΔE_p in 0.1 M KCl (70.3 ± 0.6 mV) is larger than the theoretical value of 58 mV for this one-electron redox process (Kissinger and Heineman, 1983). This increase is due to a decreased reaction rate because of slower electron transfer between the WE and the redox species (Fagan *et al*., 1985; Kissinger and Heineman, 1996).

Fagan and co-workers (1985) have described ΔE_p values of 67.7 (± 1.0) mV for polished GC-20 carbon electrodes at scan rates of 1 V/s. They found ΔE_p would increase upon prolonged electrode storage due to deactivation of the GCE surface, which lead to slow electron transfer. Hu *et al*. (1985) found decreases in electrode properties such as surface cleanliness, surface roughness and electron mediating functional groups lead to reduced electron transfer rates.

An increase in ΔE_p was observed in 0.2 M BR buffer compared to 0.1 M KCl, with ΔE_p values varying between 73 and 77.7 mV in the presence of growth media. While all $Fe(CN)_6^{3-/4-}$ peaks recorded in BR buffer showed a significant shift towards a more positive potential with respect to KCl, only the presence of MEM and LB led to a statistically significant ($p < 0.05$) increase in ΔE_p compared to BR buffer in the absence of growth media. Overall, there was little variation in the values of E_{pa} and E_{pc} in BR buffer after the addition of growth media.

The anodic and cathodic responses of $Fe(CN)_6^{3-/4-}$ compared further in Figure 4.4a, show both the anodic and cathodic signal decreased in the presence of growth media when compared to the BR buffer control, which itself showed a lower response when compared to the reference standard in KCl.

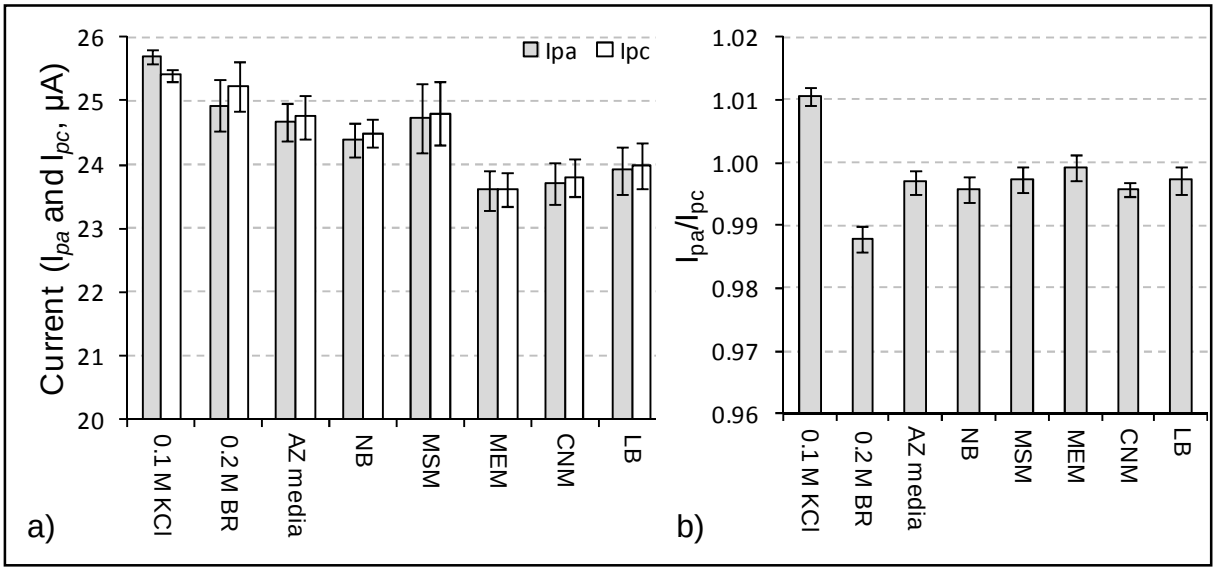

Figure 4.4 a) Anodic and cathodic response and b) I_{pa}/I_{pc} ratios of 1 mM $Fe(CN)_6^{3-/4-}$ analysed in 0.1 M KCl (pH 7) and 0.2 M BR buffer (pH 2) with and without microbiological media. Final growth media concentration was 0.1 g/l. I_{pa}/I_{pc} calculated according to Equation 2.9.
Note: Control refers to analysis performed in 0.2 M BR buffer (pH 2) in the absence of growth media.

However, only the I_{pa} and I_{pc} for $Fe(CN)_6^{3-/4-}$ analysed in MEM, CNM and LB were statistically lower ($p < 0.05$) than observed for analysis in BR buffer without media. Current responses for studies using MSM were most comparable to the BR buffer control. It has been suggested that adsorbed impurities on the electrode surface block electrochemically active sites, prohibiting electron transfer (Hu *et al*., 1985).

With respect to the work presented here, growth media components (peptone, yeast extract and malt extract in particular) are proposed to perform this action, leading to the observed decline of I_{pa} and I_{pc} for OTC when analysed in the presence of MEM, CNM and LB.

Figure 4.4b compares the I_{pa}/I_{pc} ratios, which indicate reaction reversibility, and is at unity for a totally reversible reaction (Kissinger and Heineman, 1996). Peak responses are more reversible in the presence of growth media and comparatively similar when contrasted to measurements in BR buffer only. A higher I_{pa}/I_{pc} ratio also implies a greater current response for I_{pa} compared to I_{pc}. As the anodic peak is recorded before the cathodic peak, due to the direction of the sweeping potential, additional time is available for proposed adsorption of growth media components. Increased surface passivation would decrease the cathodic response.

Adsorption of proteinacious media components may be a factor in the decreased reaction reversibility. A time-based increase in adsorption, though minimal, is supported by data published by Moulton *et al*. (2003), who reported impaired $Fe(CN)_6^{3-/4-}$ current responses for electrodes exposed to human serum albumin (HSA) and immunoglobulin G (IgG) after only 10 seconds.

The GCE surface area was established by CV analysis of an equimolar $Fe(CN)_6^{3-/4-}$ redox couple in 0.1 M KCl. Using the Randles-Sevcik equation (Equation 2.7), an experimentally observed surface area, A_{exp}, was calculated to be 0.1095 (± 0.0005) cm^2. This was larger than the geometric surface area, A_{geo}, of 0.0707 cm^2, resulting in a calculated roughness factor (R_f) of 1.549 (± 0.006) according to Equation 2.8.

In Table 4.3, the decline in A_{exp} and R_f, due to the presence of growth media, is presented. As governed by the Randles-Sevcik equation (Bard and Faulkner, 2001), the relation between A_{exp} is similar to that of I_{pa} values for analysis performed in various growth media (Figure 4.4). Analogous interpretations of the data can thus be made. These results show that on the assumption of a constant diffusion coefficient, *D*, the active surface area of the GCE decreased depending on the type of growth media introduced into the supporting electrolyte.

Table 4.3 Active surface area (A_{exp}) and roughness factor (R_f) of a GCE in the presence of different microbiological media with 0.2 M BR buffer (pH 2) as the supporting electrolyte.

Detection matrix	A_{exp} (cm^2)	R_f
0.1 M KCl (only)	0.1095 (± 0.0005)	1.549 (± 0.006)
0.2 M BR (pH 2)	0.1063 (± 0.0017)	1.504 (± 0.025)
Media in BR buffer (pH 2)		
AZ media	0.1052 (± 0.0013)	1.488 (± 0.018)
NB	0.1040 (± 0.0013)	1.471 (± 0.015)
MSM	0.1055 (± 0.0023)	1.492 (± 0.033)
MEM	0.1006 (± 0.0013)	1.424 (± 0.018)
CNM	0.1011 (± 0.0013)	1.430 (± 0.019)
LB	0.1020 (± 0.0016)	1.443 (± 0.023)

Note: A_{exp} calculated from the anodic current response of $Fe(CN)_6^{4-}$. Analysis in 0.1 M KCl was not performed in conjunction with either of the buffers or any of the media. Calculations performed on an assumed D of 7.6 x 10^{-6} cm^2/s for 1 mM $Fe(CN)_6^{4-}$. A_{exp} and R_f calculated according to Equation 2.7 and 2.8 respectively from the anodic peak current, I_{pa}. Final growth media concentration was 0.1 g/l.

In Table 4.3, the three lowest electrochemically active A_{exp} were noted for MEM, CNM and LB under acidic conditions, supporting findings of Figure 4.4a where these three media yielded the lowest I_{pa} values. The surface roughness matches these results, as a decrease in A_{exp} leads to a smaller R_f value, as seen in Table 4.3.

Similarly, when the assumption of a constant GCE surface area of 0.1095 cm^2 is made, values of D would show the same proportional relationship as A_{exp}, where a lower I_{pa} translates to lower D. Such an assumption would suggests no blocking of active sites on the GCE surface, but rather inhibited transfer of electroactive species to and from the working electrode as a result of an interfering adsorbed layer.

The data obtained for MSM indicated the least amount of interference with respect to electrode performance as A_{exp} and R_f closely match those obtained in BR buffer. This shows MSM, which appears electrochemically inactive across the wide potential range tested (0 – 1.6 V), to be the most favourable growth media for electrochemical analysis at pH 2.

4.4.2 Voltammetry in various microbial growth media – pH 7

As for pH 2, CV analysis of $Fe(CN)_6^{3-/4-}$ was replicated in a neutrally buffered 0.2 M potassium phosphate (PP) buffer solution containing the same microbiological growth media analysed in the preceding section.

4.4.2.1 Broad potential range cyclic voltammetry

In pH 7 PP buffer (Figure 4.5), a similar peak pattern was observed as for pH 2 (Figure 4.1). Three distinct anodic peak clusters were identified labelled A – C. Cluster A, forming at ~ 0.62 V, and Cluster B, forming at ~ 0.96 V, are the most pronounced of the three.

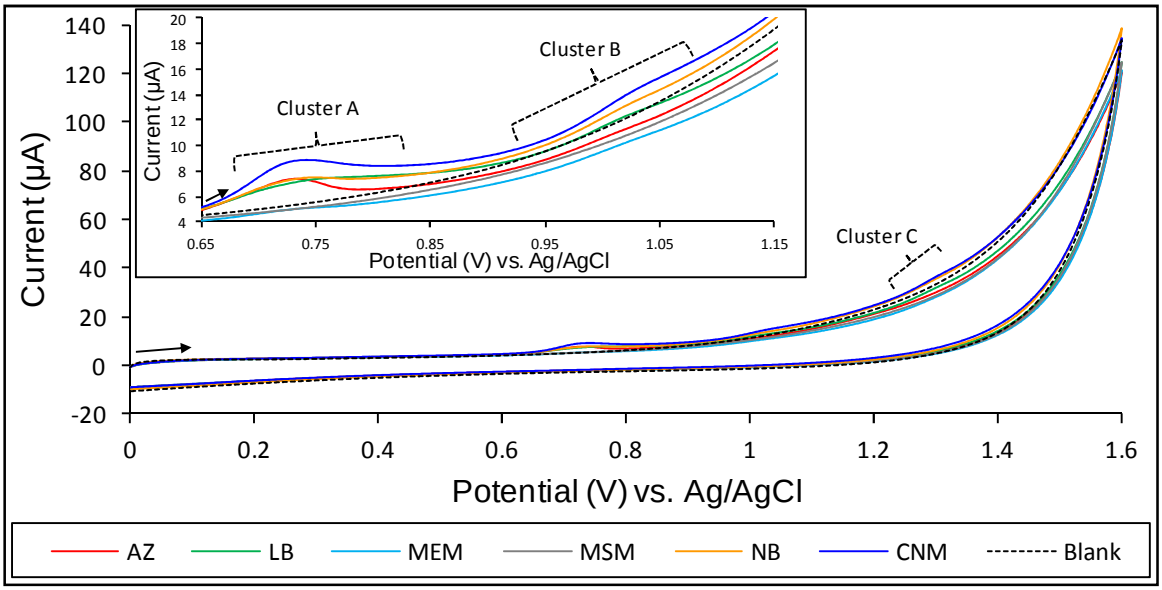

Figure 4.5 Anodic analyses of different media in 0.2 M PP buffer (pH 7). Magnification of peak rich area reported in inlay. Blank scan was performed in BR buffer only. Final growth media concentration was 0.1 g/l.

The separation of peaks from Cluster A and B of the respective growth media analysed in pH 7 buffered solutions, closely match that of the peaks found in pH 2 (Figure 4.1), but shifted to a less positive potential. Weak anodic peaks observed as Cluster C, became visible at ~ 1.3 V at this higher pH.

For CVs recorded with a positive sweep direction, the potential window in which no peaks were recorded was 0 to 0.6 V. As for pH 2, there is an absence of any return cathodic peaks across a potential window of 1.6 to 0 V.

In Figure 4.6, CV analysis of media in a negative potential range from 0 to – 1.3 V was tested in neutral PP buffer. The only cathodic wave observed in the presence of growth media, was identified for MSM at - 0.83 V. As observed in highly acidic buffer, MEM gave an increased non-faradaic response at potentials exceeding - 0.8 V.

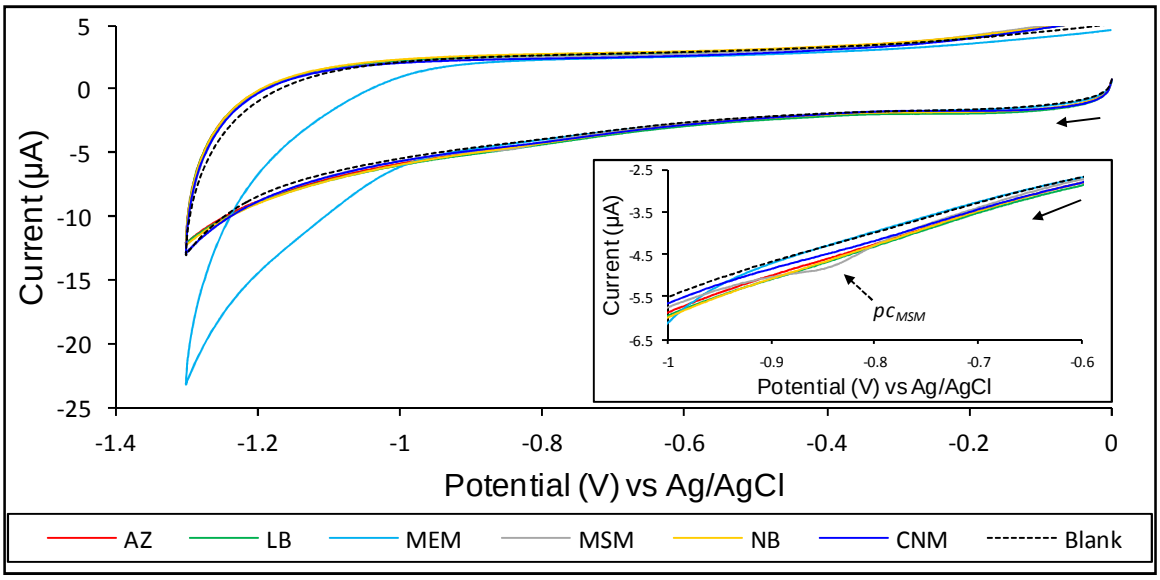

Figure 4.6 Cathodic analysis of different media in 0.2 M PP buffer (pH 7). Magnification of MSM peak reported in inlay. Blank scan was performed in BR buffer only. Final growth media concentration was 0.1 g/l.

With the exception of this increased non-faradaic response and the weak cathodic peak observed for MSM in Figure 4.6, cathodic analysis could be performed without hindrances across the wide negative potential range tested.

4.4.2.2 Redox probe analysis – pH 7

As performed for growth media at pH 2, the redox response of $Fe(CN)_6^{3-/4-}$ was evaluated to investigate the performance of a GCE in the presence of neutrally buffered electrolyte solution containing the various growth media (Figure 4.7).

In Figure 4.7, anodic and cathodic peak positions of $Fe(CN)_6^{3-/4-}$ shifted towards a more positive potential when analysed in 0.2 M PP buffer (pH 7) when compared to 0.1 M KCl of the same pH. This shift was to a lesser degree as compared to analysis at pH 2 (Figure 4.3), due to the similar pH of PP and KCl.

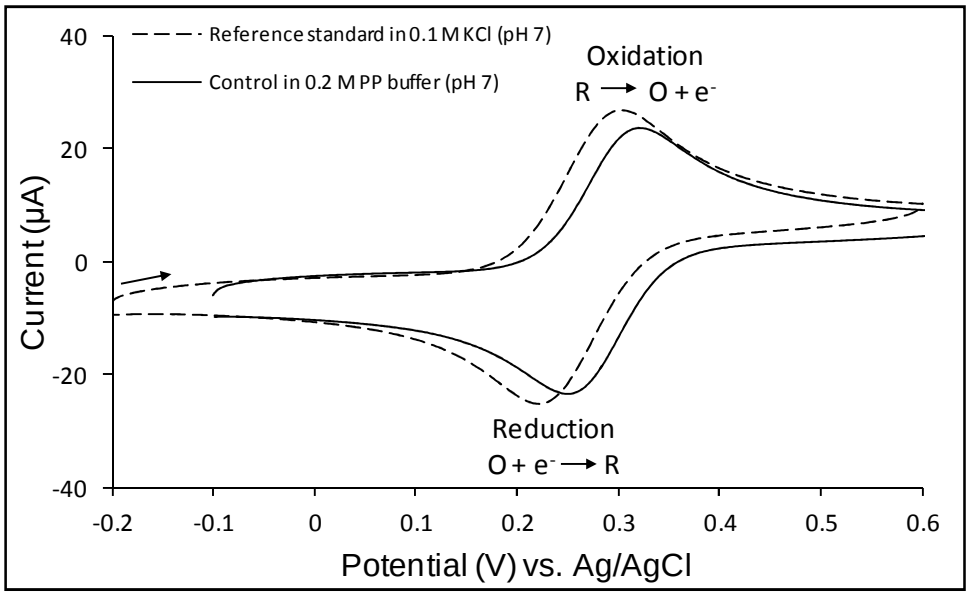

Figure 4.7 CV overlay of 1 mM $Fe(CN)_6^{3-/4-}$ redox couple in 0.1 M KCl and 0.2 M PP buffer (pH 7). The oxidation and reduction schemes are included for the forward and reverse reaction respectively.

Table 4.4 shows that at a neutral pH, ΔE_p is more varied across the data set than at pH 2. A ΔE_p of 68.3 (± 1.2) mV for analysis of $Fe(CN)_6^{3-/4-}$ in 0.2 M PP buffer closely matched the value obtained for 0.1 M KCl (70.3 (± 0.6) mV), while data obtained in the presence of growth media varies from 71 – 95 mV. With the exception of AZ media, the ΔE_p for the $Fe(CN)_6^{3-/4-}$ in each of the growth media was statistically larger ($p < 0.05$) than that of the PP buffer control, indicating reduced reversibility in the presence of growth media.

Table 4.4 Comparative analysis of peak position and peak separation of 1 mM $Fe(CN)_6^{3-/4-}$ in various microbiological detection matrices with 0.2 M PP buffer (pH 7) as supporting electrolyte.

Detection matrix	E_{pa} (mV)	E_{pc} (mV)	ΔE_p (mV)
0.1 M KCl (pH 7)	302.3 (± 0.6)	232.0 (*)	70.3 (± 0.6)
0.2 M PP buffer (pH 7)	320.3 (± 1.1)	252.0 (*)	68.3 (± 1.2)
Growth media in PP buffer (pH 7)			
AZ media	321.0 (*)	249.3 (± 1.1)	71.7 (± 1.2)
NB	330.0 (*)	241.0 (*)	89.0 (*)
MSM	321.0 (*)	250.0 (*)	71.0 (*)
MEM	325.7 (± 1.1)	246.0 (± 2.0)	79.7 (± 2.3)
CNM	332.7 (± 1.1)	237.7 (± 2.3)	95.0 (± 3.5)
LB	331.3 (± 1.1)	239.0 (*)	92.3 (± 1.2)

Note: For analysis of growth media, 40 µl of the respective media was analysed with 1960 µl PP buffer (0.2 M, pH 7). Final growth media concentration was 0.1 g/l. ΔE_p calculated according to Equation 2.10.
* Standard deviation less than 0.1 mV.

LB and NB are responsible for the 2nd and 3rd largest ΔE_p respectively, while CNM was responsible for the highest (95.5 (± 3.5) mV). These ΔE_p values compare well to data at pH 2, as reduced reversibility was observed for most growth media as shown by the increase in peak separation, while a positive shift for anodic and cathodic peaks suggests less thermodynamically favourable reactions (Wang, 2001).

Figure 4.8 shows a similar result for current response data at pH 7, as compared to pH 2. NB, CNM and LB yielded significantly lower current responses than the other media ($p < 0.05$) with lower standard deviation than at pH 2. The peak current ratios (I_{pa}/I_{pc}) in Figure 4.8b were dissimilar across the six growth media, though comparable to the PP buffer control. LB was the only outlier, with an I_{pa}/I_{pc} closer to unity.

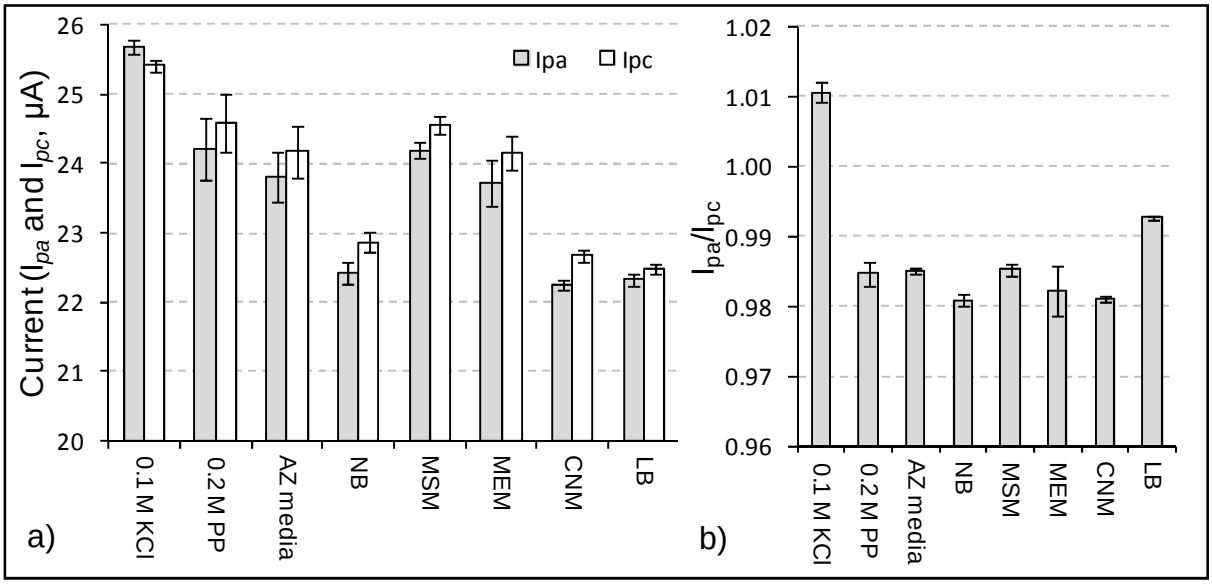

Figure 4.8 a) Anodic and cathodic response and b) I_{pa}/I_{pc} ratios of 1 mM $Fe(CN)_6^{3-/4-}$ analysed in 0.1 M KCl (pH 7) and 0.2 M PP buffer (pH 7) with and without microbiological media. I_{pa}/I_{pc} calculated according to Equation 2.9.
Note: Final growth media concentration was 0.1 g/l. Control refers to analysis performed in 0.2 M PP buffer (pH 7) in the absence of growth media.

As calculated for analyses at pH 2, Table 4.5 compares A_{exp} and R_f values for electrodes analysed in 0.2 M PP buffer in the presence of the various growth media. Under neutral pH conditions, the lowest A_{exp} and R_f were recorded for NB, CNM and LB, in keeping with the lower current responses observed in these media

(Figure 2.8a). As for pH 2, MSM showed a similar current response, surface area and surface roughness as compared to analysis in buffer (PP) without growth media.

Table 4.5 Active surface area (A_{exp}) and roughness factor (R_f) of a GCE in the presence of different microbiological media with 0.2 M PP buffer (pH 7) as the supporting electrolyte.

Detection matrix	A_{exp} (cm^2)	R_f
0.1 M KCl (only)	0.1095 (± 0.0005)	1.549 (± 0.006)
0.2 M PP buffer (pH 7)	0.1033 (± 0.0019)	1.461 (± 0.027)
Media in PP buffer (pH 7)		
AZ media	0.1015 (± 0.0015)	1.436 (± 0.022)
NB	0.0965 (± 0.0007)	1.353 (± 0.009)
MSM	0.1032 (± 0.0005)	1.460 (± 0.008)
MEM	0.1012 (± 0.0014)	1.431 (± 0.020)
CNM	0.0949 (± 0.0003)	1.343 (± 0.005)
LB	0.0952 (± 0.0003)	1.347 (± 0.005)

Note: A_{exp} calculated from the anodic current response of $Fe(CN)_6^{4-}$ Analysis in 0.1 M KCl was not performed in conjunction with either of the buffers or any of the media. Calculations performed on an assumed D of 7.6 x 10^{-6} cm^2/s for 1 mM $Fe(CN)_6^{4-}$. A_{exp} and R_f calculated according to Equation 2.7 and 2.8 respectively, from the anodic peak current, I_{pa}. Final growth media concentration was 0.1 g/l.
* Standard deviations were lower than 0.001 cm^2.

The following conclusions can be drawn when comparing analysis of growth media at pH 7 to pH 2 (Section 4.4.1). The introduction of growth media into an electrochemical working solution has more pronounced effect on the electrode activity. In particular, electrolyte solutions containing NB, MEM, CNM or LB dramatically reduced the electrochemically active surface area of the GCE, an effect more prominent at pH 7 than pH 2. MSM shows the most favourable behaviour as a complex detection matrix in both acidic and neutral pH relative to the respective buffer controls, and appears electrochemically inactive across a wide potential range, with only a small cathodic peak observed at approximately - 0.83 V in pH 7 buffer.

4.4.3 Electrochemical impedance spectroscopy (EIS) in buffer containing media

Electrochemical impedance spectroscopy (EIS) was used to further probe the effects of selected complex media on electrode performance in acidic (pH 2) conditions. This pH was selected for comparison with data obtained later where OTC was investigated in the presence of growth media. These analyses were performed primarily in a highly acidic pH, owing to the higher current response of OTC at pH 2.

Three microbiological media were selected, in part for their A_{exp} values from Section 4.4.1.2 and Section 4.4.2.2: MEM for its low A_{exp} and as it is used further as a complex matrix for OTC detection; MSM for its highest A_{exp} value most comparable to measurements in the absence of growth media; and NB as it is a commonly used microbial growth media.

As Figure 4.9 shows, the Nyquist plots and Bode plots for MEM and MSM closely matched those of the BR buffer control.

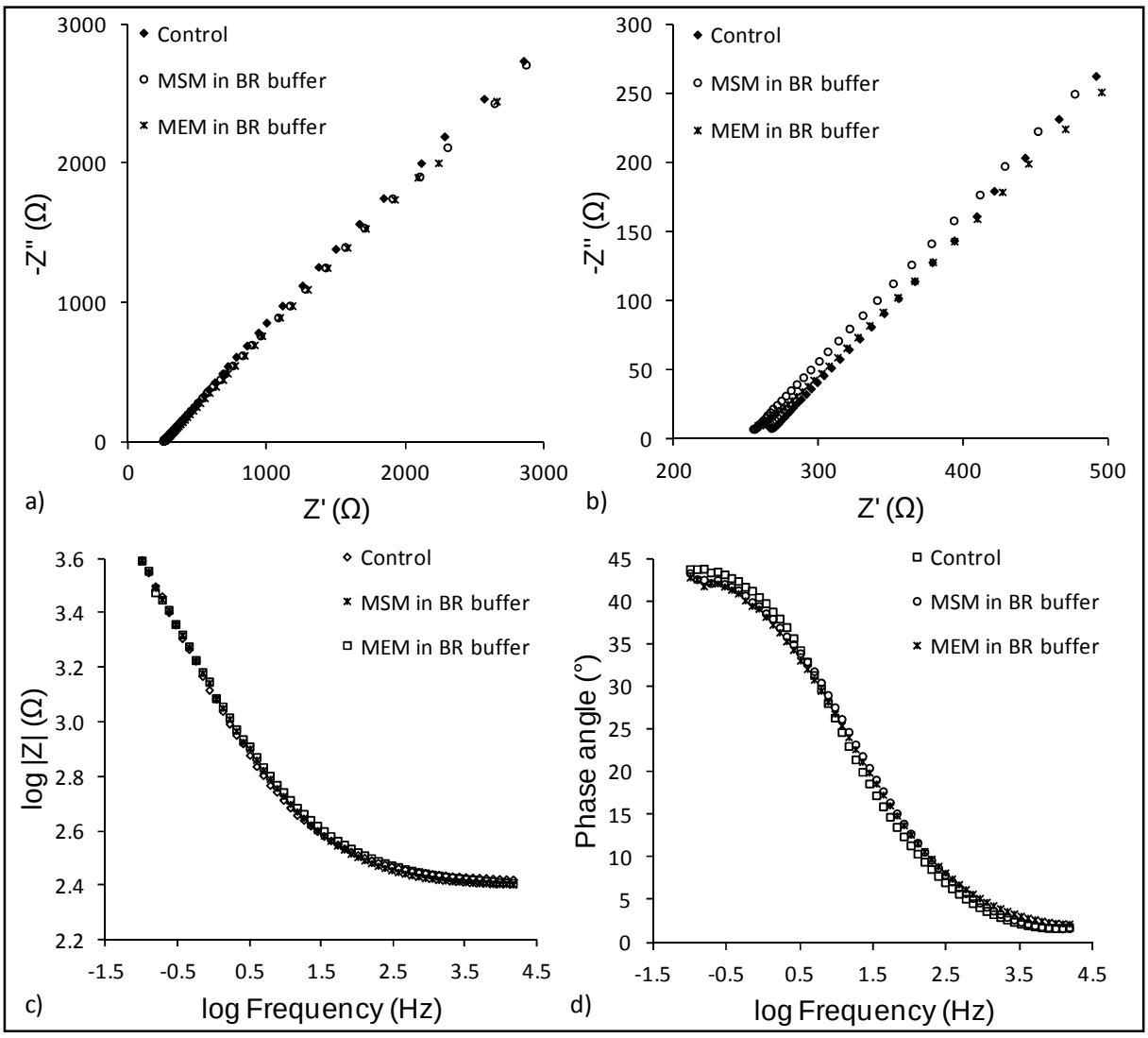

Figure 4.9 Impedance plots for a GCE in the presence of MEM, MSM and in 0.2 M BR buffer (pH 2) only (Control) using 1 mM $Fe(CN)_6^{3-/4}$. a) Nyquist plot of the whole frequency range from 100 mHz to 15 kHz and b) magnification of the higher frequency region, c) Bode plot of log impedance, |Z|, and d) phase angle, °, versus log frequency (Hz) respectively. Electrode potential was set at the respective OCP (V) for each set. Final MSM and MEM concentration was 0.1 g/l.

Only a difference in solution resistance (R_s), indicated by the intercept of the Z' axis, is visible in the Nyquist plot for the high frequency range (Figure 4.9b), as is confirmed through the use of data modelling (Table 4.6 and Table 4.7). The slope of the higher frequency range of the Nyquist plot was 1, indicating a faradaic process is described in the impedimetric profile (Lasia, 1999; Moulton *et al*., 2004). The Bode plot of impedance and phase angle plot (Figure 4.9c and 4.9d respectively) behaved similarly for BR buffer containing MEM and MSM, compared to the buffer without growth media.

As can be seen in Figure 4.10 and Figure 4.11 however, EIS data for buffer containing NB does not correspond with that of a NB free solution. From the Nyquist plot, an underlying semicircle is observed for BR buffer containing NB, in the higher frequency range (Figure 4.10b).

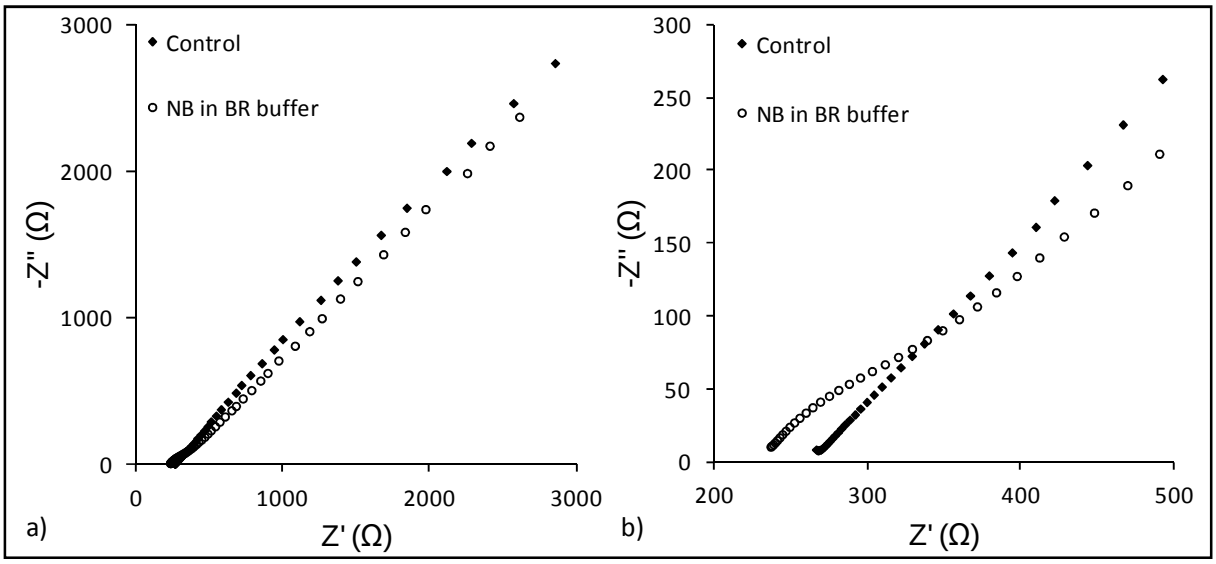

Figure 4.10 Nyquist plots for a GCE in the presence of NB and in 0.2 M BR buffer (pH 2) only (Control) using 1 mM $Fe(CN)_6^{3-/4-}$. a) Whole frequency range from 100 mHz to 15 kHz and b) magnification of the higher frequency region. Electrode potential was set at the respective OCP (V) for each set. Final NB concentration was 0.1 g/l.

In Figure 4.11b, in the high frequency range, an additional time constant can be seen in the phase angle *vs.* log frequency plot when compared to the BR buffer control. This time constant corresponds to the semicircle observed in Figure 4.10b.

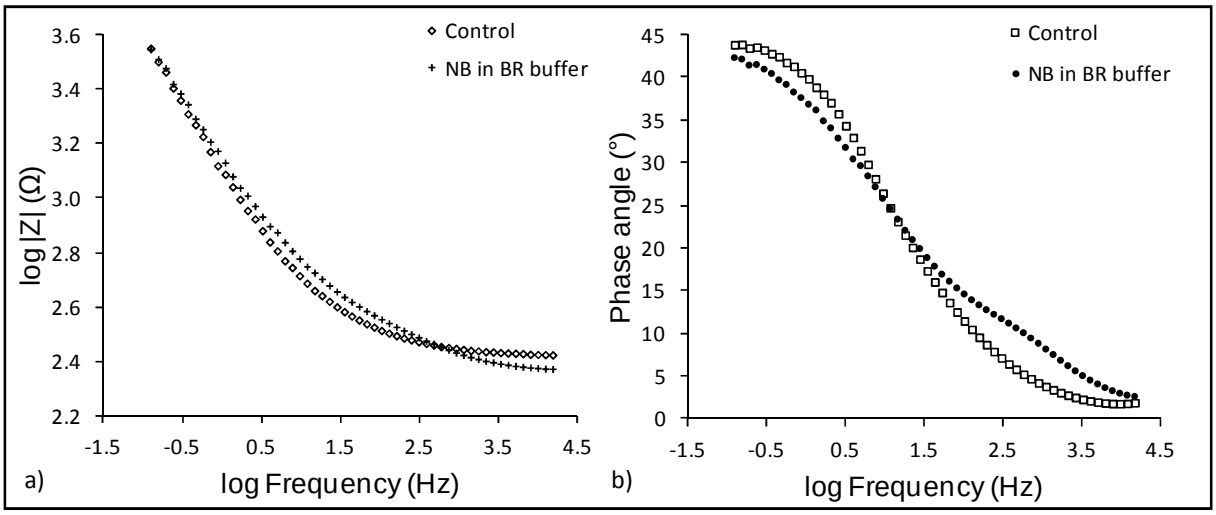

Figure 4.11 Bode plot for a GCE of a) log impedance, |Z|, and b) phase angle, °, versus log frequency (Hz) respectively, for 0.2 M BR buffer (pH 2) only (Control) and NB in BR buffer, using 1 mM $Fe(CN)_6^{3-/4-}$. The frequency range was 100 mHz to 15 kHz. Electrode potential was set at the respective OCP (V) for each set. Final NB concentration was 0.1 g/l.

A Randles equivalent circuit was used to model and evaluate the EIS data and is referred to as Circuit A (Figure 4.12a). R_s represents the solution resistance (Ω), R_{ct} the charge transfer resistance (Ω), C_{dl} the double layer capacitance (μF) and W the Warburg impedance (Suni, 2008; Harrington and Van den Driessche, 2011). A modified Randles cell (Figure 4.12b), was used with the capacitive element (C_{dl}) replaced by a constant phase element (CPE), for which the notation will be Q (Mho). This circuit is referred to as Circuit B. Table 4.6 and Table 4.7 summarise the circuit element data for Circuit A and B respectively.

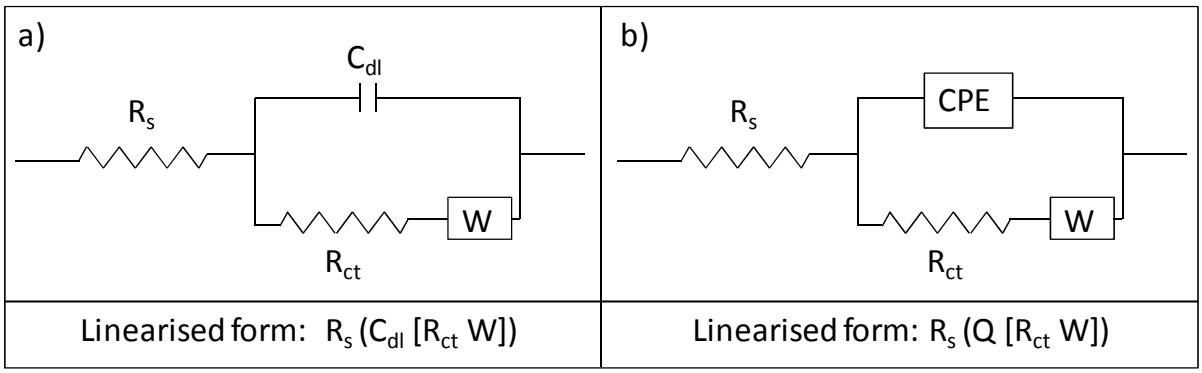

Figure 4.12 a) Randles equivalent circuit (Circuit A) and b) Randles equivalent circuit with CPE (Circuit B). Adapted from Suni, (2008). The linearised forms of the circuits are included, where round and square brackets indicate elements in parallel and series respectively. R_s is the solution resistance, R_{ct} the charge-transfer resistance, C_{dl} the double layer capacitance, CPE the constant phase element, Q, and W the Warburg impedance.

Table 4.6 EIS parameters for data modelled using Circuit A of $Fe(CN)_6^{3-/4-}$ in buffer and growth media.

Detection matrix	R_s (C_{dl} [R_{ct} W])					
	OCP (V)	R_s (Ω)	C_{dl} (μF)	R_{ct} (Ω)	W ($\Omega.s^{-1/2} \times 10^{-4}$)	χ^2 ($\times 10^{-2}$)
0.1 M KCl	0.260	194.6 (± 3.2)	4.83 (± 0.71)	*	3.588 (± 0.019)	2.673 (± 0.522)
Control in BR	0.333	264.4 (± 14.5)	8.94 (± 0.17)	*	3.529 (± 0.009)	7.829 (± 0.873)
NB in BR	0.331	228.3 (± 9.1)	2.11 (± 0.23)	59.2 (± 8.2)	3.389 (± 0.007)	1.324 (± 0.188)
MEM in BR	0.331	253.3 (± 9.7)	2.03 (± 0.37)	*	3.484 (± 0.040)	3.036 (± 0.205)
MSM in BR	0.331	254.7 (± 9.6)	4.91 (± 0.64)	*	3.473 (± 0.029)	3.077 (± 0.397)

Note: Analysis in 0.1 M KCl was performed in the absence of BR buffer or any growth media. Control in BR refers to EIS in 0.2 M BR buffer (pH 2) the absence of any growth media. Final growth media concentration was 0.1 g/l.
* Indicates where no appreciable value for R_{ct} could be established.

Most notable, there was an absence of R_{ct} values for all but the NB sample for Circuit A (Table 4.6). This is reflected in Circuit B where the R_{ct} for NB in BR buffer is more than double that of the BR buffer control (Table 4.7).

Table 4.7 EIS parameters for data modelled using Circuit B of $Fe(CN)_6^{3-/4-}$ in buffer and growth media.

Detection matrix	R_s (Q [R_{ct} W])						
	OCP (V)	R_s (Ω)	Q (μMho)	n	R_{ct} (Ω)	W ($\Omega.s^{-1/2} \times 10^{-4}$)	χ^2 ($\times 10^{-2}$)
0.1 M KCl	0.260	187.8 (± 3.3)	25.45 (± 4.14)	0.764 (± 0.008)	12.2 (± 1.0)	3.303 (± 0.027)	0.174 (± 0.057)
Control in BR	0.333	254.6 (± 13.6)	76.39 (± 12.4)	0.697 (± 0.024)	50.4 (± 6.4)	2.172 (± 0.129)	0.704 (± 0.163)
NB in BR	0.331	221.7 (± 9.0)	25.64 (± 2.78)	0.726 (± 0.018)	130.3 (± 9.5)	3.177 (± 0.041)	0.765 (± 0.149)
MEM in BR	0.331	244.2 (± 9.4)	38.66 (± 1.45)	0.671 (± 0.014)	28.5 (± 1.2)	3.037 (± 0.025)	0.706 (± 0.120)
MSM in BR	0.331	246.5 (± 9.5)	32.25 (± 0.54)	0.731 (± 0.026)	17.2 (± 8.4)	3.118 (± 0.030)	0.578 (± 0.132)

Note: Analysis in 0.1 M KCl was performed in the absence of BR buffer or any growth media. Control in BR refers to EIS in 0.2 M BR buffer (pH 2) the absence of any media. n is the dimensionless exponent of the Q. Final growth media concentration was 0.1 g/l.

R_{ct} is indicative of a change in the electron transfer rates between the redox-active species ($Fe(CN)_6^{3-/4-}$ in this study) and the surface of the working electrode (Moulton *et al*., 2004; Suni, 2008). It is measured as the change in faradaic current that arises due to a continual oxidation/reduction of the redox probe due to potential switching across the double layer (Harrington and Van den Driessche, 2011), in the form of the

applied sinusoidal waveform. The observed increase in R_{ct} for buffer containing NB, compared to buffer without growth media, is thus indicative of hindered electron transport. No such increase was observed for MEM or MSM (Table 4.6 and 4.7).

Increases in R_{ct} have been reported in literature, often due to the formation of an insulating layer on the surface of the GCE. In Section 4.4.5.3 it will be shown that growth media has a significant effect on the cathodic response of OTC in the absence of interfering peaks. In Section 4.4.1.2 and Section 4.4.2.2, it was observed that the presence of different microbiological media reduced the experimentally observed surface area (A_{exp}) as a result of lower I_{pa} for $Fe(CN)_6^{3-/4}$. It thus stands to reason that components in the media, in particular peptone, yeast extract and malt extract adhere to the electrode surface, forming such an insulating layer.

In Table 4.6 and 4.7, the element used to determine capacitance (C_{dl} or Q, depending on the circuit used) exhibits the opposite response to hindered electron transport, reducing as the insulating effect increases (Moulton *et al*., 2004; Suni, 2008). Moulton *et al*. (2003) showed solution pH, adsorption time and applied potential played a significant role in protein adsorption onto a gold (Au) electrode, which lead to increased ΔE_p and reduced I_{pa} and I_{pc} of $Fe(CN)_6^{3-/4-}$. In a subsequent paper, Moulton *et al*. (2004) used EIS to show substantial decrease in capacitance for their gold (Au) electrode (approximately 20 %, depending on protein and applied potential) after a 30 minute time-based adsorption of human serum albumin (HSA) and immunoglobulin G (IgG) at pH 7. This was accompanied by an increase in R_{ct} for solutions containing either protein. Moulton and co-workers concluded that an inert layer of proteins had adsorbed to the electrode surface hindering the passage of electrons between the redox probe and Au electrode.

Similar decreases in capacitance have been observed for a range of metal electrodes to which proteins were adsorbed, including bovine serum albumin (BSA) onto a platinum (Pt) electrode (Bernabeu *et al*., 1988), fetal bovine serum onto titanium (Ti) and CoCrMo alloy electrodes (Contu *et al*., 2002) and human cytochrome P450 2D6 onto a hybrid bilayer lipid membrane (HBM) coated silver (Ag) electrode.

While a linear relation between I_{pa} and R_{ct}, or capacitance (C_{dl} or Q) and R_{ct} could not be established, the presence of microbiological media did increase the charge transfer resistance for buffer containing NB (observed best for Circuit B), and decreased capacitance for buffer containing any of the tested growth media when, compared to the BR buffer control (Table 4.6 and Table 4.7). However, buffer containing MEM, which resulted in the lowest I_{pa} for $Fe(CN)_6^{3-/4-}$ (Section 4.4.1.2) did not produce the largest R_{ct}. This indicates the complexity in behaviour of the interaction of growth media with the electrode surface.

For more pronounced differences in both R_{ct} and C_{dl}, a longer exposure time might be necessary (Bernabeu *et al*., 1988; Moulton *et al*., 2004). An increase in protein size and its state of denaturation (usually pH related), has also been discussed as possible explanations for increased surface coverage and subsequent decrease of electrode activity (Jackson *et al*., 2000; Moulton *et al*., 2004). Further studies are required to this probe this process in more detail.

When CV data for $Fe(CN)_6^{3-/4-}$ (Section 4.4.1.2) is compared to EIS circuit element data, the following observation can be made. Only a slight increase in ΔE_p was observed for some of the media tested, indicating decreased reversibility compared to the BR buffer control. The decrease in I_{pa} was more noticeable, but only significant for MEM, CNM and LB. It is suggested that the decrease in I_{pa} is due to reduced access to the electrode surface (Downard and Roddick, 1995), as a result of an inert passivating layer composed of microbiological media (mainly proteinaceous molecules), as supported primarily by a decrease in capacitance, and an increase in R_{ct} for NB samples.

It is important to mention that the components present in the tested microbiological media which are referred to as proteinaceous (malt extract, peptone, meat extract, yeast extract and tryptone) are products of enzymatically or otherwise digested proteins. This would result in smaller peptide molecules with likely different electrode surface coverage properties than those of larger proteins.

4.4.4 Anodic analysis of OTC in AZ media

The following sections assess the applicability of voltammetry as an analytical technique to measure OTC yield in AZ media, a growth media similar to that used for the aerobic fermentation of *Streptomyces rimosus* for the production of OTC.

Figure 4.13a shows the voltammetric analysis of AZ media, with a pronounced primary anodic peak (pa_a) at ~ 0.96 V and a secondary peak (pa_b) at ~ 1.19 V in a pH 2 (BR) buffered solution, as reported in Figure 4.1. Further investigation revealed both peaks to be indicative of peptone, a principal AZ media constituent and nitrogen source for bacterial growth (Figure 4.13b). Peptone is accountable for all of the peaks observed in the broth as noted by the similar voltammograms of peptone and AZ media. There were also no observable peaks in the AZ media prepared without peptone.

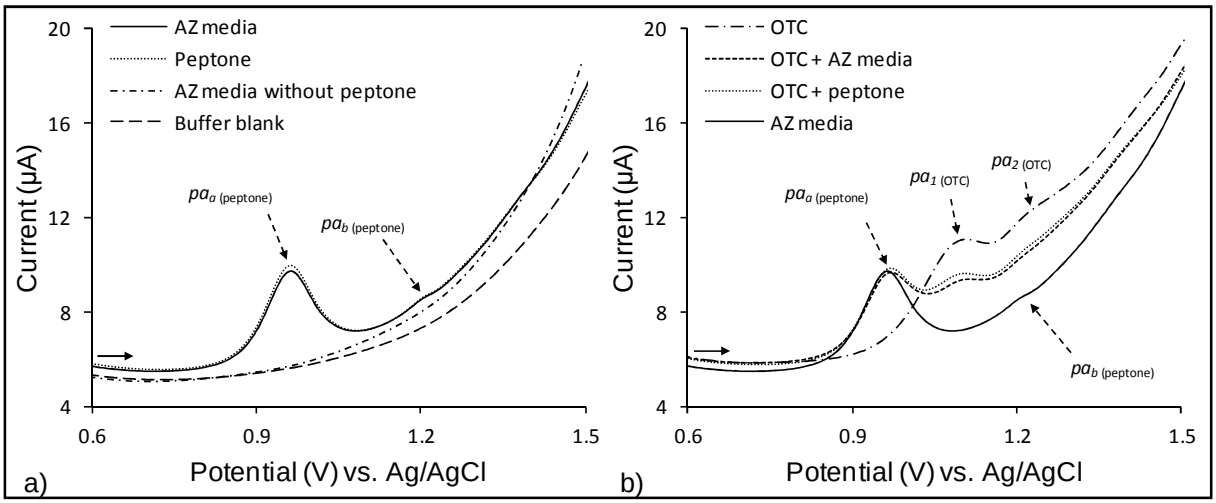

Figure 4.13 SWV overlays showing a) the anodic interference caused by the AZ media and one of the components, peptone, on b) the detection of OTC (20 µM) in 0.2 M BR buffer (pH 2). Subscripts of peaks (*pa*) represent peak number and the analyte undergoing oxidation. AZ media and peptone concentrations were 0.1 g/l.

The presence of peptone in the working solution represents substantial interference and reduces the OTC current response ($pa_{1(OTC)}$) to < 8 % of maximum response, compared to CVs of OTC in peptone-free AZ media. Based on this information, alternative organic nitrogen sources were investigated to replace peptone in AZ media.

4.4.4.1 Peptone substitutes

Substitute components for peptone were investigated, in an attempt to improve OTC signal recovery following anodic detection. These components were yeast extract and malt extract, and were used in the same concentration as peptone, i.e. 5 g/l for prepared media. Figure 4.14 shows the anodic electrochemical profile of peptone, yeast extract and malt extract in pH 2 buffer at a final concentration of 0.1 g/l after dilution in the working solution.

Two distinct peaks were observed for each of the growth media components and denoted $pa_{a(\text{components})}$ and $pa_{b(\text{components})}$ for the primary and secondary peak respectively. These sets correspond to the peak clusters identified earlier in other complex microbiological growth media (Section 4.4.1.1). The primary anodic peak, $pa_{a(\text{components})}$, for peptone and yeast extract were much larger than that of malt extract. Malt extract exhibited a third peak between $pa_{a(\text{components})}$ and $pa_{b(\text{components})}$.

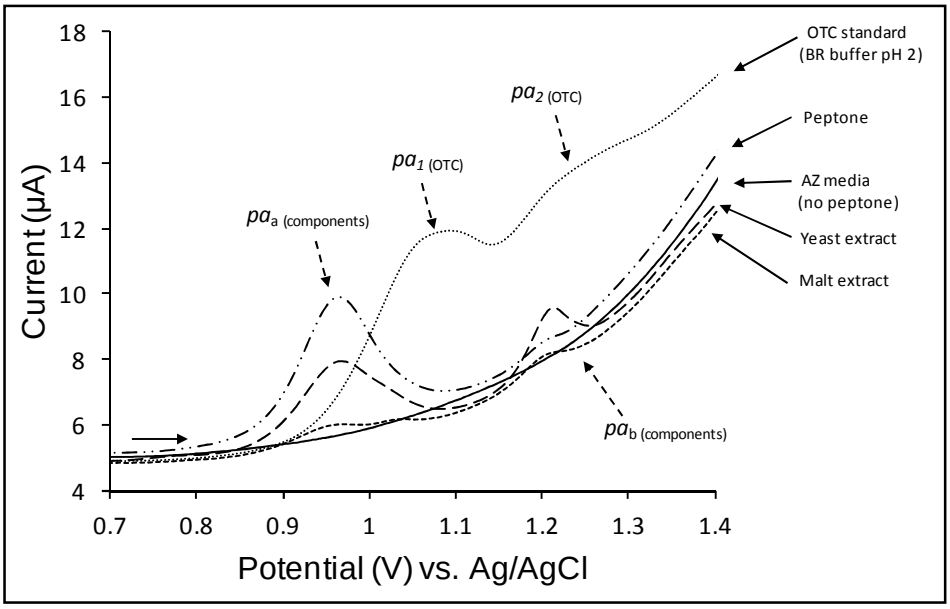

Figure 4.14 SWV overlay of peptone, yeast extract, malt extract and peptone-free AZ media in pH 2 BR (0.2 M) buffer. The OTC standard was recorded in BR buffer only. AZ media, peptone, yeast extract and malt extract concentrations were 0.1 g/l.

Each of the primary component peaks occurs at a more negative potential than the primary peak of the OTC standard, with an approximate separation of 100 mV between $pa_{a(\text{components})}$ and $pa_{1(\text{OTC})}$, indicating that these peaks would interfere with anodic analysis of OTC.

In Figure 4.15, analysis was performed in pH 7 (PP) buffer for each of the peptone substitute components. A similar result to that of pH2 was observed, though the primary component peaks, $pa_{a(\text{components})}$ were less separated (~ 30 mV) from $pa_{1(\text{OTC})}$. Again, the sets of peaks (pa_a and pa_b) correspond to complex growth media tested earlier at the same pH (Section 4.4.2.1). The component peaks shifted to a more negative potential as a result of the higher pH, 7, compared to pH 2.

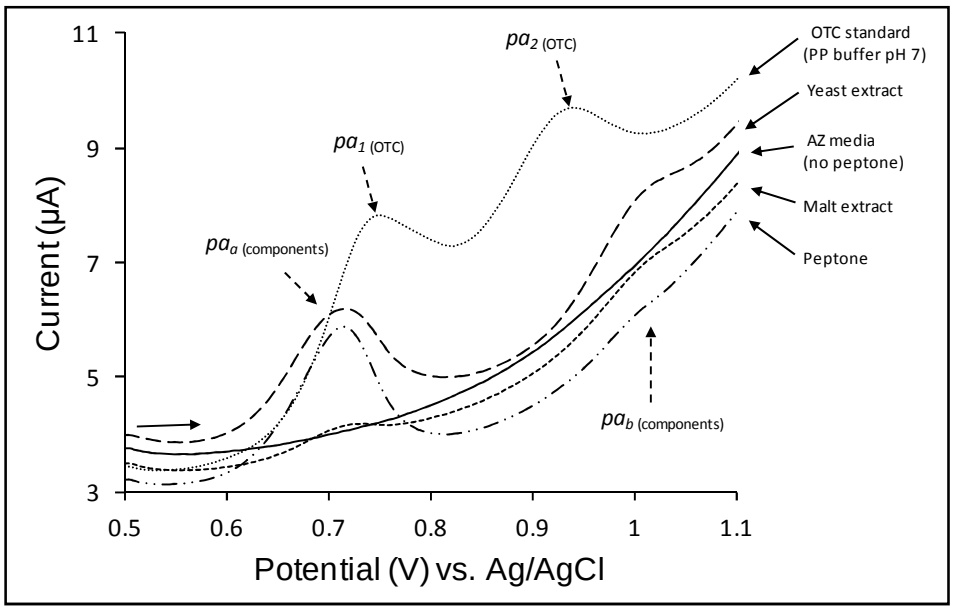

Figure 4.15 SWV overlay of peptone, yeast extract, malt extract and peptone-free AZ media in pH 7 PP (0.2 M) buffer. The OTC standard was recorded in PP buffer only. AZ media, peptone, yeast extract and malt extract concentrations were 0.1 g/l.

At pH 7, peptone and yeast extract exhibited the largest current responses for pa_a and pa_b, while those of malt extract was the smallest. Only a single peak was observed for malt extract at pH 7. Notably, the CV baselines at potentials less than 0.6 V at pH 7 were not as uniform as for pH 2.

Though complex chemical analysis would have to be performed to conclusively identify the interferent(s), it is proposed that the anodic profile of peptone, yeast extract and malt extract are due to their numerous constituents (Stokes *et al*., 1944; Fluckiger-Isler *et al*., 1994). In particular, the amino acids tyrosine (Huang *et al*., 2008; Shao *et al*., 2008) and L-cysteine (Zhou *et al*., 2007), and vitamins such as B_6 (Zhang and Wang, 2011) which have displayed anodic responses in the range of 0.6 to 0.75 V under neutral conditions at GCEs, are suspected.

The peaks of these organic molecules were reported to move towards less positive potentials with increasing pH, similar to the media components tested here. At a Pt electrode, tryptophan, tyrosine and cysteine produced anodic responses in the window of 0.5 to 0.8 V. A compositional breakdown of malt extract revealed at least 17 amino acids (including tyrosine and cysteine) and 6 vitamins (Fluckiger-Isler *et al*. 1994). Literary sources concerning the voltammetric analysis of complex microbiological growth media, at similar pH and potentials as shown in this work, could not be found.

4.4.4.2 Analysis in malt extract media (MEM)

Due to its minimal interference, malt extract was further explored as a replacement for peptone in AZ media. However, malt extract by itself is not an ideal replacement for peptone, which offers a range of vitamins and trace elements (Stokes *et al*., 1944), but also serves as the prime nitrogen source for the bacterial culture (Taskin and Kurbanoglu, 2011). As malt extract is commonly sold as a carbohydrate source, an additional inorganic nitrogen source in the form of electrochemically inert potassium nitrate (KNO_3) was added (5 g/l), while malt extract was maintained at the same concentration as peptone (5 g/l). This served to make the detection matrix more representative of a media used for culturing OTC producing bacteria (Abou-Zeid *et al*., 1981). This media is hereafter referred to as malt extract media, or MEM. Unpublished work has shown MEM to be a suitable growth media for *S. rimosus*.

Figure 4.16 shows an overlay of SWVs of OTC and MEM analysed in pH 2 BR buffer. Upon closer inspection, the anodic response of MEM exhibits three anodic peaks starting at ~ 0.85 V. The peaks were labelled $pa_{a1(\mathrm{MEM})}$, $pa_{a2(\mathrm{MEM})}$ and $pa_{b(\mathrm{MEM})}$, in order of increasing oxidation potential.

Due to the size and position of the malt extract peak, control experiments in a solution with growth media containing this component was not viable, as this caused substantial electrode fouling and subsequently hindered the detection of OTC due to their similar oxidation potentials. A blank scan was thus produced in BR buffer (pH 2), followed by MEM sample injection with and without OTC, shown in Figure 4.16b and 4.16a respectively.

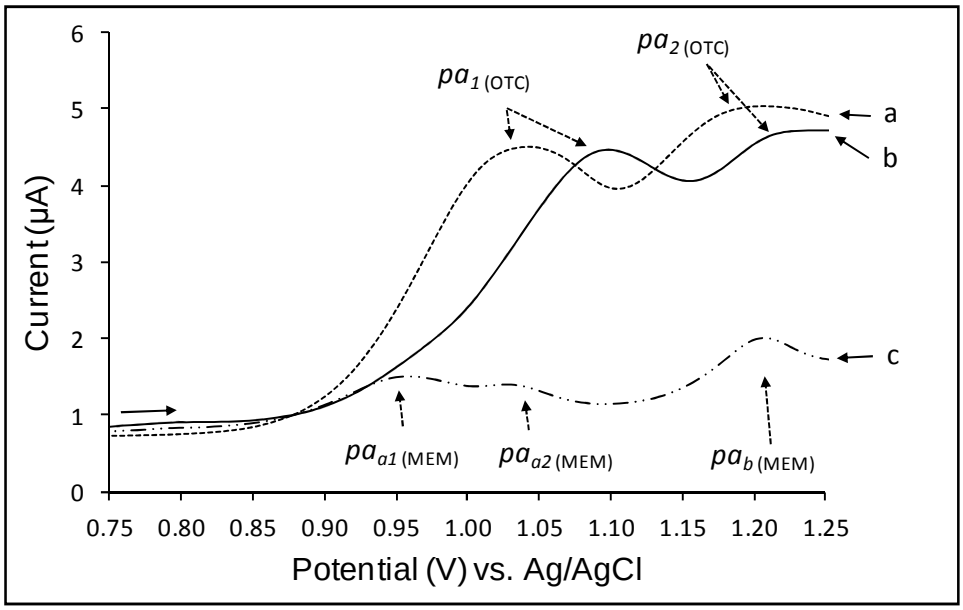

Figure 4.16 SWV overlay of OTC stock solutions prepared in a) 0.2 M BR buffer (pH 2) and b) MEM in 0.2 M BR buffer (pH 2), while c) shows the analysis of MEM without OTC in 0.2 M BR buffer (pH 2). OTC concentration was 20 µM, MEM was 0.1 g/l. Voltammograms presented are baseline subtracted.

CVs of OTC, when prepared as a stock solution in MEM), resulted in a potential shift of 55 (± 3) mV for $pa_{1(OTC)}$ relative to analyses in the absence of MEM (Figure 4.16b and 4.16a respectively), moving towards a more positive potential. A similar shift was observed for $pa_{2(OTC)}$. The presence of MEM can be observed in the left shoulder of $pa_{1(OTC)}$ for OTC stock solutions prepared in MEM, as well as broadening of $pa_{2(OTC)}$ attributed to the current contribution of $pa_{b(MEM)}$ (Figure 4.16b).

Without taking the effect of MEM into consideration, OTC anodic signal recovery of 96.8 % was achieved (Table 4.8). The peak current and peak potential of $pa_{1(OTC)}$ exhibited acceptable variation.

Table 4.8 Comparative SWV data for 20 µM OTC analysed in pH 2 BR buffer solutions. The position and current response of pa_1 is evaluated for OTC stock solutions prepared in BR buffer or MEM.

		OTC in BR buffer	OTC in MEM
E_{pa1}	E (V)	1.037 (± 0.005)	1.092 (± 0.002)
I_{pa1}	I (µA)	3.92 (± 0.23)	3.79 (± 0.33)
	C_v (%)	5.97	8.69
Signal recovery (%)		100	96.8

Note: MEM concentration was 0.1 g/l in the working solution. Signal recovery calculated as % I_{pa1} observed in the presence of MEM, relative to I_{pa1} measured in the absence of MEM.

Malt extract, as a nutrient, will be depleted by the bacteria during the fermentation process. This means a voltammogram with an identical amount of malt extract, as was present in the fermentation broth at the time of analysis, would have to be used for each sample taken if its involvement in the OTC signal response is to be accounted for. This is unpractical. Varying malt extract concentrations would also have an impact if not accounted for. However, this would require less time for sample analysis as appropriate MEM blanks do not have to be prepared.

Since bacterial systems are dynamic and substrate concentrations will vary (Kornmann *et al*., 2003), the amount of malt extract present would be ever variable and thus cannot be accurately accounted for. The aforementioned results are therefore confined to the conditions under which they were observed, meaning a final MEM concentration of 0.1 g/l. Signal recovery of 20 µM OTC in the presence of MEM was within 4 % of stock solutions prepared in BR buffer (Table 4.8).

Figure 4.17 shows a less favourable result when OTC was measured in the presence of MEM in a pH 7 (PP) buffered solution.

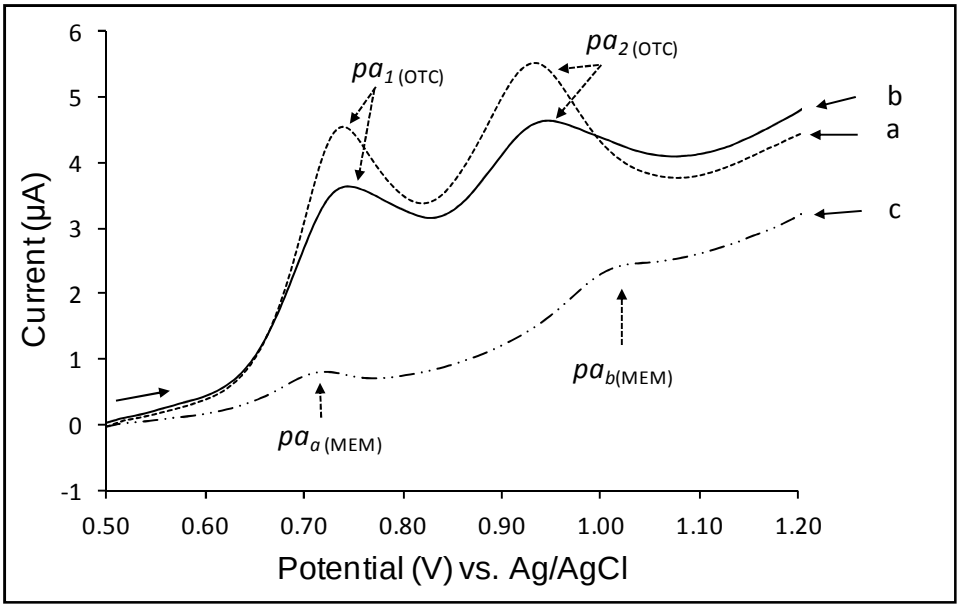

Figure 4.17 SWV overlay of OTC stock solutions prepared in a) 0.2 M PP buffer (pH 7) and b) MEM in 0.2 M PP buffer (pH 7), while c) shows the analysis of MEM without OTC in 0.2 M PP buffer (pH 7). OTC concentration was 20 µM, MEM was 0.1 g/l. Voltammograms presented are baseline subtracted.

In the presence of MEM, an additive effect of $pa_{b(MEM)}$ is observed on the right shoulder of $pa_{2(OTC)}$, broadening this peak, while the height of $pa_{1(OTC)}$ and $pa_{2(OTC)}$ decreased significantly compared to CV analysis of OTC in buffer solution (Figure 4.17b and 4.17a respectively).

$E_{pa1(OTC)}$ was constant with no observable shift between successive samples containing MEM, though a current recovery of only 84.1 % compared to analysis without MEM is reported in Table 4.9. The current response was stable (C_v < 2 %). The lower current recovery however, makes analysis under these conditions less favourable than at pH 2.

Table 4.9 Comparative data for 20 µM OTC analysed in pH 7 PP solutions. The position and response of pa_1 is evaluated for OTC stock solutions prepared in BR buffer and in MEM.

		OTC in PP buffer	OTC in MEM
E_{pa1}	E (V)	0.737 (± 0.002)	0.739 (*)
I_{pa1}	I (µA)	3.51 (± 0.07)	2.65 (± 0.05)
	C_v (%)	2.06	1.73
Signal recovery (%)		100	84.1

Note: MEM concentration was 0.1 g/l.
* Standard deviation less than 0.001 V.

In addition to a higher current recovery, OTC analysed in the presence of MEM at pH 2 offers an additional advantage over to pH 7. During sample acidification, which is performed to increase extraction yields from fermentation broths to increasing OTC solubility, pH values of 2.5 and less are commonly employed (Abou-Zeid *et al*., 1977; Abdel-Azize *at al*., 1982). Analysis at pH 2 would thus shorten analysis time by avoiding an additional titration step to a highly acidic pH *if required*, while maintaining OTC stability.

4.4.4.3 Effect of MEM concentration on OTC recovery

In the preceding experiment, 40 µl of OTC stock solution prepared in MEM was injected into the electrolyte solution to a total volume of 2 ml. This corresponds to a final MEM concentration of 0.1 g/l. Sensitivity is hereby impacted, as samples with lower analyte concentrations would possibly not exhibit OTC presence due to sub-

detection levels. A range of different OTC stock solutions, of decreasing concentrations, were prepared in MEM and injected into the working solution at increasing volumes respectively, to yield a similar final analyte concentration of 20 μM OTC, while increasing the final MEM concentration. In the absence of MEM, a value of 0 g/l MEM concentration was adopted. Analysis was performed in 0.2 M BR buffer (pH 2).

As shown in Figure 4.18a, with increasing final MEM concentration, the current response for $pa_{1(OTC)}$ decreased until it could no longer be accurately measured. As the final concentration of OTC was maintained at 20 μM, this decrease is attributable to the proportional increase of MEM present in the working solution as an interferent.

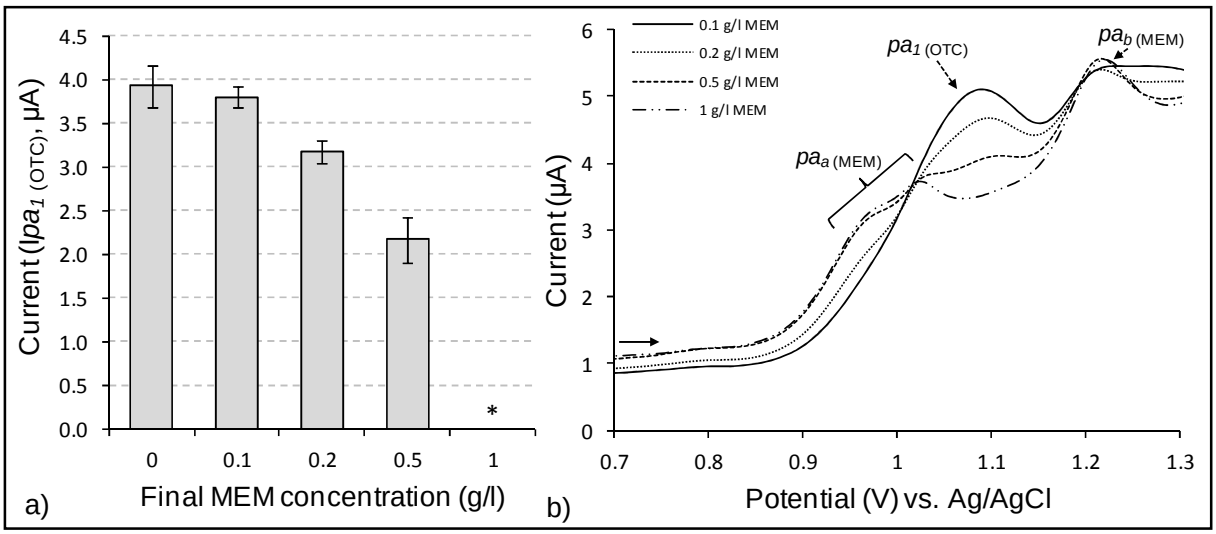

Figure 4.18 a) Signal response for 20 μM OTC at various MEM concentrations and b) baseline subtracted SWV overlay of representative scans for each MEM concentration in 0.2 M BR buffer (pH 2).
* No appreciable OTC signal could be obtained in the presence of 1 g/l MEM.

In Figure 4.18b, the primary anodic peaks of MEM ($pa_{a(MEM)}$) can be seen to increase for 0.2 g/l MEM, becoming more prominent for 0.5 g/l and 1 g/l MEM. The secondary peak of MEM ($pa_{b(MEM)}$) becomes more pronounced at increasing concentration accompanied with a decreased tailing effect indicating a reduced additive current effect from $pa_{2(OTC)}$ (Figure 4.18b).

With this increase in MEM and constant OTC concentration, the reliability of $I_{pa1(OTC)}$ measurements in the presence of MEM above 0.1 g/l becomes questionable.

In Figure 4.19a, the shift of $E_{pa1(OTC)}$ was plotted against the final concentration of MEM in solution. An increase in MEM concentrations closely correlates with a shift in the potential of the primary anodic peak of OTC towards a more positive potential. This indicates MEM kinetically limits OTC oxidation, and explains the aforementioned 55 mV shift for $E_{pa1(OTC)}$ (Section 4.4.4.2).

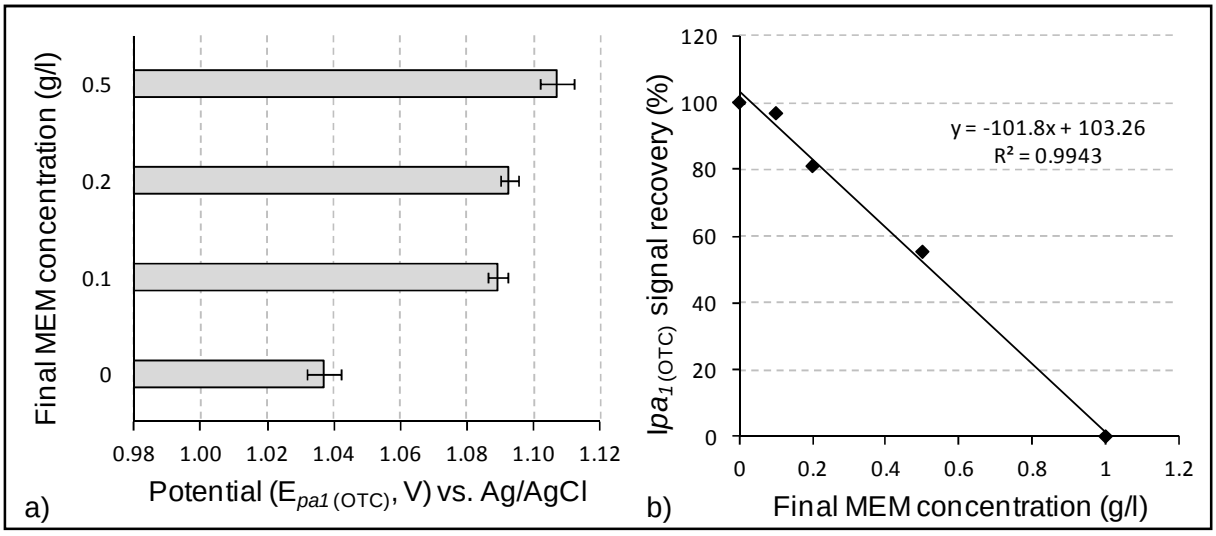

Figure 4.19 Effect of varying MEM concentration on a) the position (V) and b) signal recovery (%) of $pa_{1(OTC)}$ of 20 µM OTC in 0.2 M BR buffer (pH 2).

Figure 4.19b shows the effect of increasing MEM concentration on $pa_{1(OTC)}$ signal recovery. On the assumption of a negligible OTC current response in samples containing 1 g/l MEM, a strong correlation ($R^2 > 0.99$) was observed, showing a proportional decrease in OTC signal recovery with increasing MEM concentration. EIS studies have indicated a decrease in capacitance (C_{dl} and Q), suggesting some adsorption of MEM to the electrode surface (Table 4.6 and 4.7). As changes in $I_{pa1(OTC)}$ and $E_{pa1(OTC)}$ were observed for increasing MEM concentrations, increased adsorption of this growth media onto the GCE surface is likely attributable. This data corresponds with the EIS study, in which a decrease for C_{dl} and Q for buffer containing MEM was observed (Table 4.6 and 4.7 respectively).

Therefore, to maintain a high OTC current response, a 50-fold dilution was maintained for further experiments containing 0.1 g/l final MEM concentration.

4.4.4.4 Anodic linear range of OTC in MEM

In order to use the developed SWV procedure as a quantitative method for OTC production yield determination in MEM, a predictable relationship between $I_{pa1(OTC)}$ and OTC concentration is required. To determine the viability of this procedure, the effect of OTC concentration on the current response of $I_{pa1(OTC)}$ was investigated as shown in Figure 4.20a.

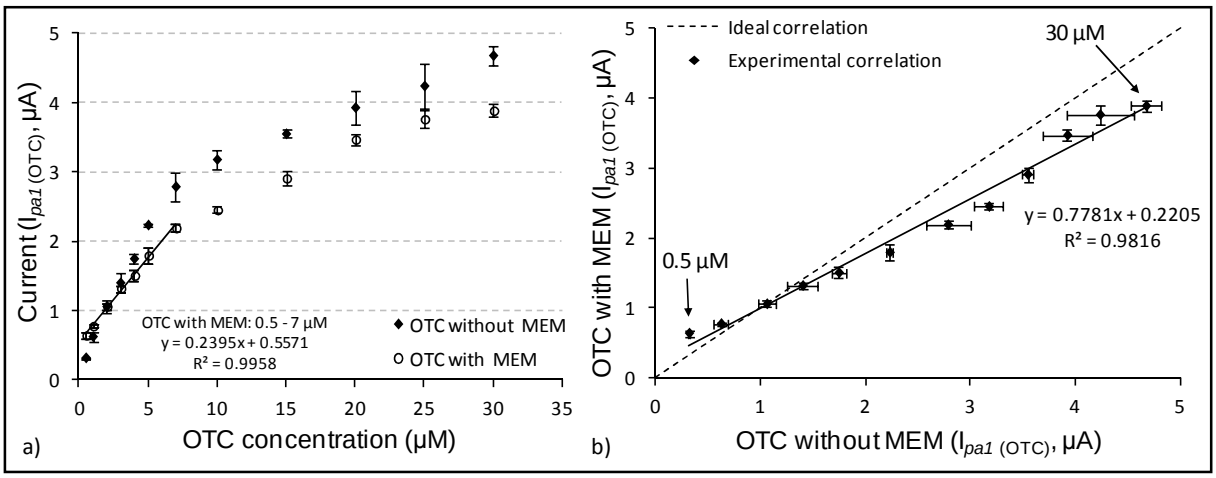

Figure 4.20 a) Standard curves of I_{pa1} *vs.* increasing concentrations of OTC, for which stock solutions were prepared in MEM and BR buffer (pH 2) and b) I_{pa1} correlation between OTC stocks prepared in BR buffer and in MEM across the OTC concentration range tested (0.5 – 30 µM from left to right). The dashed line indicates an ideal correlation, whereas the solid line represents the linear trend for the experimental correlation. SWV analysis performed in 0.2 M BR buffer (OTC stock solution in MEM:BR buffer, 1:50 $^{v}/_{v}$) as electrolyte solution. The final MEM concentration was 0.1 g/l for OTC stock solutions prepared in this growth media.

OTC samples prepared in MEM were prepared according to Method E (Table 4.1), which involves acid treatment and a centrifugation step. This is an adaptation to common practices for OTC extraction from fermentation media (Abou-Zeid *et al*., 1977; Yang and Ling, 1989) to obtain particle-free samples while improving OTC solubility (Tongaree *et al*., 1999). This data is compared to results observed in BR buffer in the absence of MEM (Section 3.3.6).

To evaluate current recovery of $pa_{1(OTC)}$, the current responses in 0.2 M BR buffer (pH 2) in the absence of MEM were assigned a recovery value of 100 %. When compared to analysis in the absence of MEM, a current recovery for OTC of ~ 77 % was achieved, with an average recovery of 85.9 (± 7.3) % for the OTC concentration

range of 2 - 30 µM. For the two lowest OTC concentrations, 0.5 µM and 1 µM, current recovery was 203 and 125 % respectively in the presence of MEM.

Figure 4.20b compares the OTC current response in the presence of MEM to the response observed in BR buffer only. A 100 % current recovery for OTC samples containing MEM compared to analysis in BR buffer is plotted as the ideal correlation. It is evident that at low analyte concentrations, the current response is greater in the presence of MEM than for BR buffer only, with the opposite being true for high concentrations of OTC where the experimental correlation falls below the ideal correlation in the presence of MEM. This leads to an overestimation of OTC at low concentration and an underestimation at high concentrations. These high recoveries at low OTC concentration are thought to be due to an additive effect of masked malt extract peaks becoming more pronounced as $I_{pa1(OTC)}$ decreases.

Overall, a good correlation ($R^2 > 0.98$) was observed between the two data sets, i.e. OTC in the presence and absence of MEM (Figure 4.20b). Low standard deviation was achieved for the current responses of OTC stock solutions prepared in MEM, with an average $C_v < 4$ %. Within the OTC concentration range examined (0.5 – 30 µM) and under the stated conditions, OTC could be measured with confidence in the presence of MEM, with concentration specific current values comparable to those observed in BR buffer controls.

As in Chapter 3, the Langmuir isotherm was used to describe the experimentally observed data (Section 3.3.6). Table 4.10 compares the LOD, data variability and Langmuir model parameters for OTC measured with and without MEM (Figure 4.20).

For OTC analysed in the presence of MEM, a reasonably good correlation was observed between the experimentally obtained data and the Langmuir model. I_m decreased by more than 1.3 µA for buffer with MEM compared to buffer without, indicating a lower maximum signal achievable before the current is predicted to plateau.

Table 4.10 Detection limits and Langmuir isotherm parameters of OTC measured in the absence and presence of MEM.

OTC stock preparation	Lower linear range (0.5 – 7 µM)		Slope (µM/µM)	Standard deviation (µA)*	Langmuir model parameters		
	LOD (nM)	LOQ (nM)			Model fit (R^2)	I_m (µA)	K^{-1} (µM)
OTC without MEM	24.3	80.8	0.378	0.126	0.9941	5.815 (± 0.003)	8.73 (± 0.81)
OTC with MEM	966.4	3221.4	0.240	0.071	0.9738	4.496 (± 0.03)	6.82 (± 2.8)

Note: Analysis performed in 0.2 M BR buffer (pH 2). Final MEM concentration was 0.1 mg/ml. LOD and LOQ calculated according to Equation 2.4. Langmuir isotherm modelled according to Equation 2.6. The slope was taken from the I_{pa1} vs. OTC concentration plots (Figure 4.20).
* Calculated as the average of all standard deviation of the I_{pa1} vs. OTC concentration plots (Figure 4.20).

K^{-1}, as the inverse of adsorption affinity, was lower in the presence of MEM, suggests more OTC adsorption to the electrode surface. However, this is not reflected by the large LOD of 0.97 µM, which is substantially larger than 0.081 µM for analyses in the absence of MEM (Table 4.10). The LOD of 0.97 µM is also higher than the lowest experimentally measured concentration, 0.5 µM. Therefore, 0.5 µM was adopted as the experimentally obtained LOD. Again, this emphasises the inaccuracy of OTC detection at low concentrations, as interference by MEM becomes more pronounced at low OTC concentrations, affecting detection precision.

A lower slope for the plot of I_{pa1} *vs.* OTC concentration (Figure 4.20) shows OTC detection sensitivity to be lower in the presence of MEM compared to analyses in BR buffer.

OTC can thus be monitored quantitatively in the presence of a constant MEM concentration, though with a substantially increased detection limit relative to analysis in the absence of MEM.

4.4.5 Cathodic analysis of OTC

As an alternative detection method to overcome anodic interference of growth media, cathodic analysis of OTC was investigated. Figure 4.21 shows a CV of 0.2 M BR buffer (pH 2) containing OTC. This shows a distinct primary cathodic peak (pc_1) at - 0.89 V as well as a secondary peak (pc_2) at - 1.05 V. Both peaks appear irreversible in the potential window tested.

These cathodic peak positions are comparable to data reported by Ni *et al*. (2011) who used CV and differential pulse stripping voltammetry (DPSV) in their studies. A pH study performed by Ni *et al*. (2011) for OTC and other tetracyclines revealed a shift in the cathodic peaks towards a more negative potential with increasing pH. They also showed a decrease in current response with increasing alkalinity over a pH range of 2 - 9.6. Reported as having the most positive peak potential and offering the greatest sensitivity, pH 2 was selected for cathodic analysis of OTC.

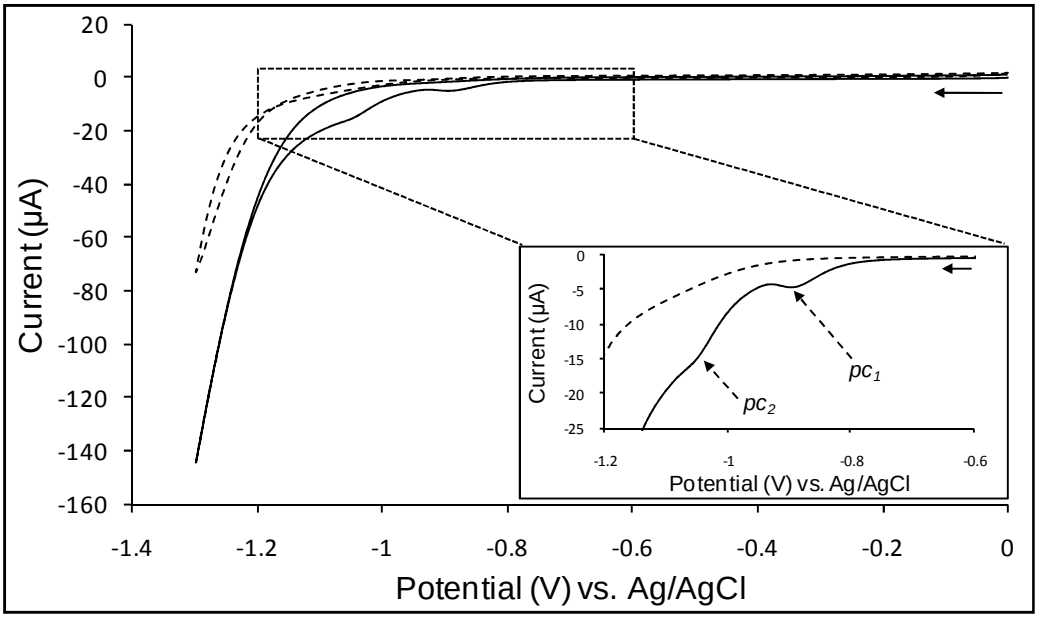

Figure 4.21 Cathodic CVs of 20 µM OTC in 0.2 M BR buffer (pH 2). Enlarged insert shows only reverse scan to show the primary (pc_1) and secondary peak (pc_2) more clearly. Dashed line shows scans performed in BR buffer only.

Figure 4.22 shows the cathodic SWV for OTC. A third cathodic peak (pc_3) was observed at approximately - 1.25 V (inlay of Figure 4.22). This third peak however, is also present in working solutions devoid of analyte and is believed to be due to an unrelated process, associated either with the supporting electrolyte or the electrode itself. The latter seems more likely as a GCE was used in this study while Ni *et al*. (2011) used a hanging mercury drop electrode (HMDE) while BR buffer was common in both studies. The origin of the third peak is attributed to the complex surface chemistry of GCEs (Engstrom and Strasser, 1984; Beilby *et al*., 1995).

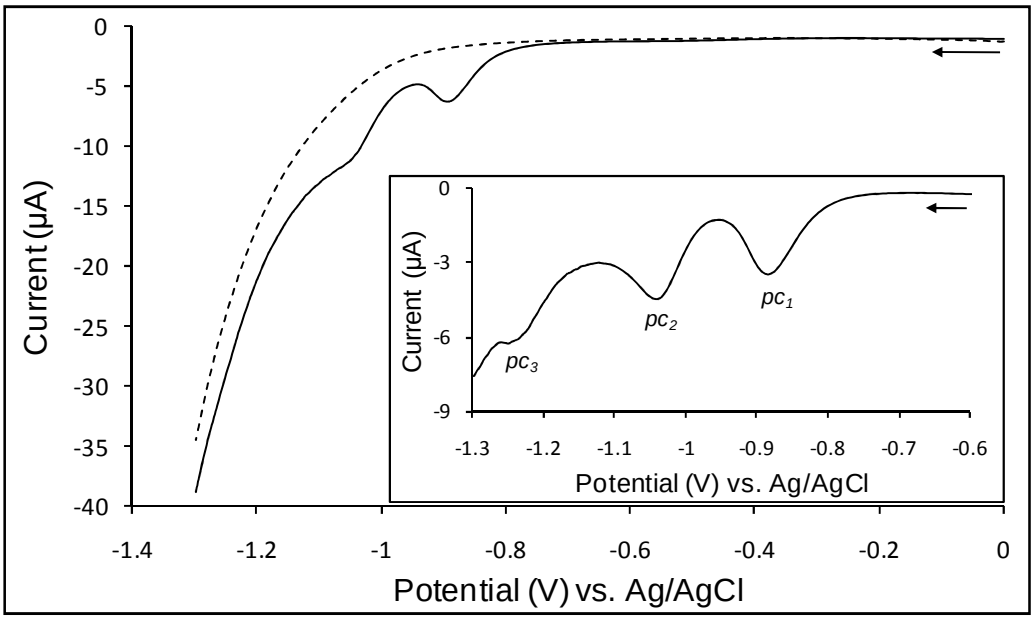

Figure 4.22 Cathodic SWVs of 20 µM OTC in 0.2 M BR buffer (pH 2). A cropped baseline subtracted SWV is included as an inlay, showing three (pc_1, pc_2 and pc_3) cathodic peaks. Dashed line shows scans performed in BR buffer only.

Due to the use of SWV, the primary and secondary peaks are well defined, with the primary peak displaying an approximate increase in response of 20 % over CV data. The primary cathodic peak, pc_1, was selected for further analyses.

4.4.5.1 Preconditioning potential

As was seen in the preceding chapter (Section 3.3.4), the application of a preconditioning potential can be immensely valuable in increasing anodic signal responses of electroactive compounds, in this case OTC. As Figure 4.23 shows, the same is true for the cathodic signal of OTC.

With the exception of 0.0 V and - 0.2 V, all potentials tested showed a significantly improved signal response ($p < 0.05$) accompanied by varying levels of standard deviation when compared to an open circuit system.

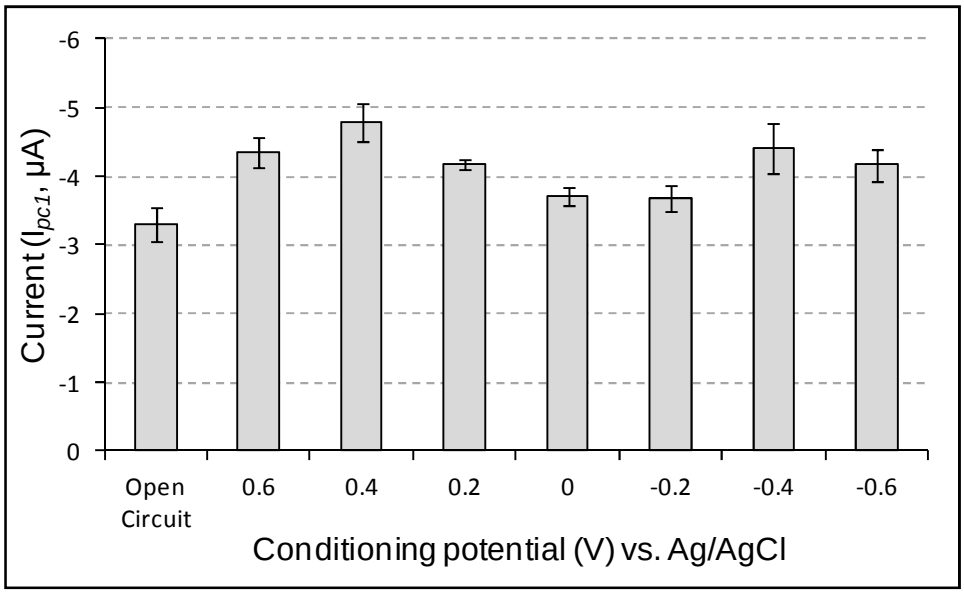

Figure 4.23 Consequence of a 40 second applied preconditioning potential on the cathodic SWV detection of 12 µM OTC in 0.2 M BR buffer (pH 2).

However, irregularities were observed in voltammograms where conditioning potentials were applied in the form of peak and troughs in plain buffered solutions. These were found to play a profound role in subsequent analysis of AZ media. For this reason, the adopted adsorption process consisting of a 40 second stirring procedure prior to analysis, was performed under open circuit conditions.

4.4.5.2 Interference of dissolved oxygen

For fast and accurate sample analysis, time-consuming steps such as de-aeration of the working solution must be optimised. To determine the interfering effect of dissolved oxygen (dO_2) on the cathodic current of pc_1, solutions were de-aerated for various lengths of time. The effect of dO_2 is clearly illustrated by Figure 4.24.

For a de-aeration time of 0 seconds, the SWV shows a large cathodic peak starting at ~ - 0.15 V and peaking at - 0.43 V (Figure 4.24a). This peak is indicative of oxygen reduction (Reinke and Simon, 2002) and can be seen to interfere with pc_1 of OTC when nitrogen purging was omitted. After only 120 seconds of de-aeration, the baseline can be seen to stabilise, though a measurable response for pc_1 is only obtained after 240 seconds (Figure 4.24b).

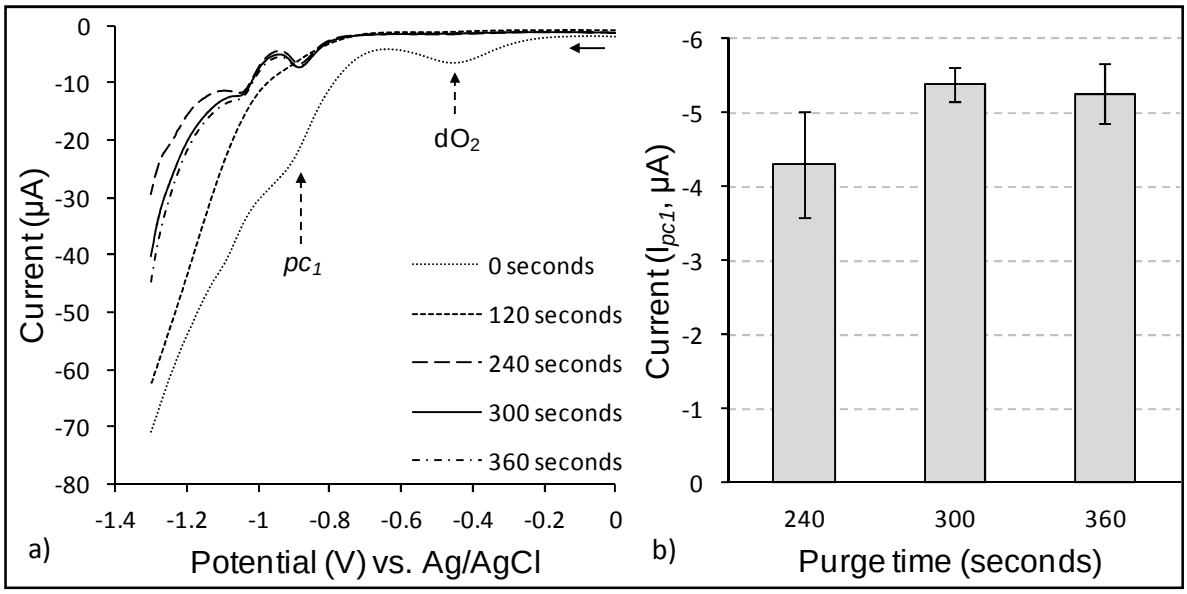

Figure 4.24 a) Superimposed SWVs showing the effect of varying purge times on the cathodic analysis and b) signal response of 20 µM OTC in 0.2 M BR buffer (pH 2). The volume of the working solution was 2 ml.

After a subsequent minute of de-aeration (300 seconds in total), the OTC signal increased even further, while the standard deviation decreased. Additional de-aeration did not improve current response and 300 seconds was adopted as the standard de-aeration time for subsequent experiments. In order to reduce analysis time, a narrower potential window was selected from 0.0 to - 1.1 V, wide enough to encompass both cathodic OTC peaks.

4.4.5.3 Cathodic OTC analysis in AZ media

As mentioned in Section 2.3.2, background voltammograms obtained in buffer devoid of analyte, measured and subtracted from voltammograms of analyte containing buffer. This served in these studies to remove background current associated with the working solution. In Figure 4.25, AZ media, as used previously, was examined for its effect on the cathodic detection of OTC in highly acidic BR buffer (pH 2, 0.2 M). This figure shows the effect on SWVs obtained following the injection of OTC into solutions, where the background scan differed. It also examines the effect of OTC stock solutions prepared in either BR buffer of AZ media.

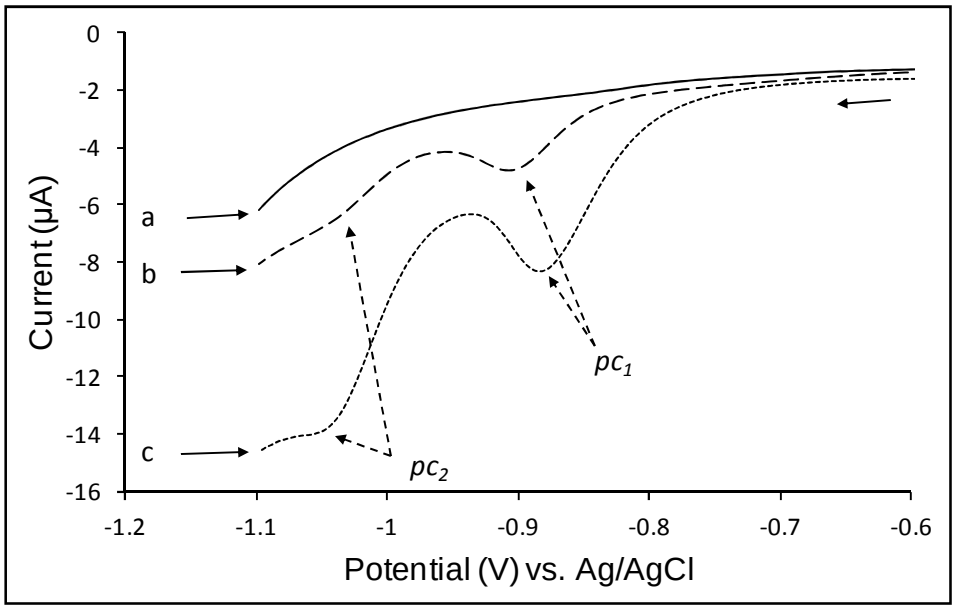

Figure 4.25 Effect of AZ media on the cathodic SWV response of 20 µM OTC. a) Background SWV obtained in mixture of AZ media (2.5 g/l) and 0.2 M BR buffer (1:1, $^{v}/_{v}$) followed by injection of OTC stock solutions prepared in BR buffer, b) background SWV obtained in BR buffer followed by injection of OTC stock solutions prepared in AZ media (0.1 g/l), c) background SWV obtained in BR buffer followed by injection of OTC stock solutions prepared in BR buffer.

Figure 4.25a shows recording of a background scan in the presence of AZ media prior to OTC analysis, resulted in no observable cathodic signal for OTC samples prepared in BR buffer. When the background current was recorded in BR buffer, followed by injection of OTC samples prepared in AZ media (Figure 4.25b), the current for pc_1 was diminished to 37 % when compared to analysis performed in BR buffer in the absence of AZ media (Figure 4.25c). The decrease in cathodic OTC current is believed to be due to fouling of the electrode surface by AZ media components (Appendix A).

The position of pc_1 shifted to a slightly more negative position (~ 21 mV), indicating a thermodynamically less favourable reduction process compared to analysis in an electrolyte devoid of AZ media. The presence of AZ media, either used for the preparation of OTC stock solutions, or part of the working solutions, compromised the cathodic response of OTC.

To explain the effect of AZ media on the current response of OTC when used for stock solution preparation, Figure 4.26 examines the effect of each individual growth media component on the cathodic detection of OTC.

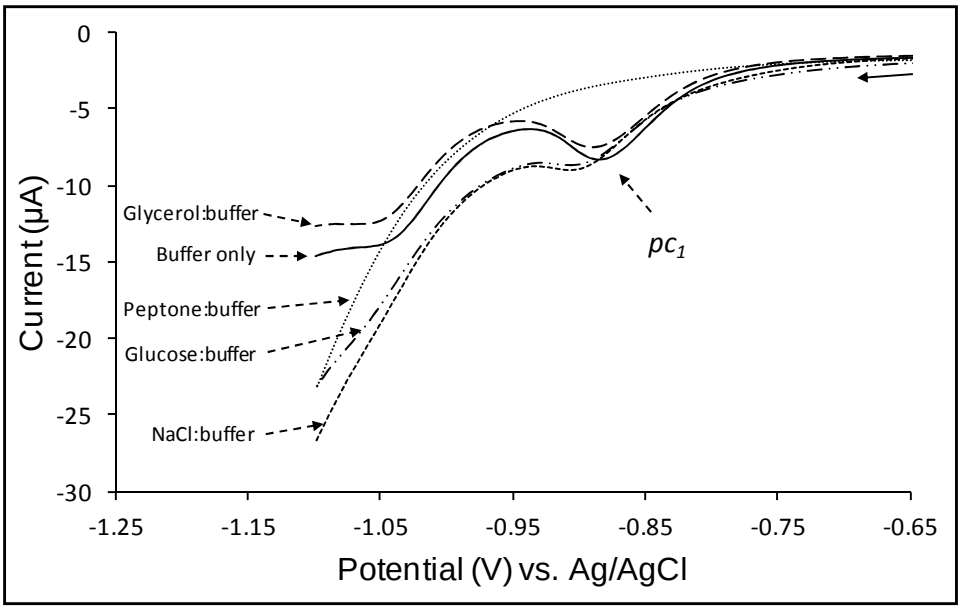

Figure 4.26 Effect of AZ media components (2.5 g/l) on the SWV response of 20 µM OTC. Analysis performed after background SWVs were obtained in mixtures (1:1, $^{v}/_{v}$) of 0.4 M BR buffer (pH 2) and individual AZ media components. Voltammogram obtained in the absence of media components served as control and denoted "Buffer only".

To determine the cause of the poor signal response, each AZ media component was prepared separately and used in a 1:1 ratio ($^{v}/_{v}$) with BR buffer (pH 2, 0.4 M) to produce a blank scan. This was followed by injection of an OTC stock solution (prepared in BR buffer). Peptone was shown to be the major interfering component, the presence of which resulted in no observable cathodic response for OTC.

While peptone does not exhibit any observable cathodic wave in the potential window investigated (data not shown), it is clear that this growth media component is responsible for the quenched signal of *pc*$_1$ as observed by the absence of a peak for OTC in Figure 4.26. This is likely due to peptone coating the GCE surface and limiting the OTC from coming into contact and exchanging electrons with the electrode (Section 4.4.3). The use of AZ media for background voltammograms recorded prior to OTC sample analysis to generate a baseline was thus precluded. For further analyses, background voltammograms were obtained in BR buffer devoid of AZ media followed by injection of OTC stock solutions prepared in AZ media.

4.4.5.4 Sample preparation

Using cathodic detection of OTC as a means to overcome the limitations of AZ media, the effect of simple sample pre-treatment steps (Table 4.1) was examined. Figure 4.27 compares six pre-treatment procedures to determine if signal recovery could be improved by removal of interfering components from AZ media, as well as evaluate the efficacy of pre-treatment procedures employed for OTC extraction from fermentation media.

Method A (no pre-treatment of OTC stock prepared in AZ media) produced a 37 % current recovery compared to analysis in the absence of AZ media (relative to the control) as per Figure 4.25. None of the pre-treatment methods (B - F) produced a statistically significant increase in current response ($p < 0.05$) compared to method A. An average recovery of 38.6 (± 2.5) % was observed for all the methods examined.

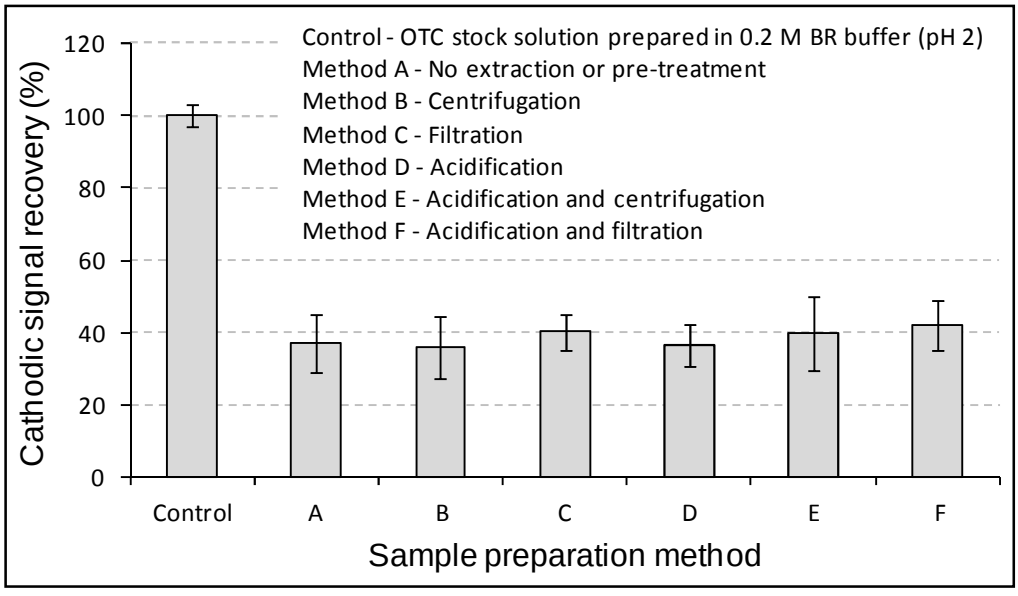

Figure 4.27 Cathodic signal recovery of I_{pc1} of 20 µM OTC stock solutions prepared in AZ media following several sample preparation methods. "Control" consisted of OTC stock solutions prepared in 0.2 M BR buffer (pH 2). Analysis performed in working solution of 0.2 M BR buffer (pH 2). AZ media concentration was 0.1 g/l, and added to the working solution at a ratio of 1:50 ($^{v}/_{v}$; OTC stock prepared in AZ media:BR buffer).

Thus, Figure 4.27 shows that none of the sample preparation methods was able to remove peptone from the sample as confirmed by the consistently low signal recovery for OTC relative to Method A. The low cathodic response in the presence of

AZ media combined with the need for de-aeration does not offer any improvement over anodic analysis of OTC in this complex growth media.

However, OTC current responses were not observed to decrease for any of the extraction methods tested. This result was expected as filtration and centrifugation are commonly employed for the purpose of sample purification in the downstream process of antibiotic production (Ratledge and Kristiansen, 2001), and suggests these simple pre-treatment methods could prove useful as a biological sample clean-up procedure to remove whole cells and cellular debris observed in fermentation media without compromising OTC extraction efficiency. This is important within the context of further such studies.

4.5 CHAPTER CONCLUSIONS

The complex composition of the different growth media tested is reflected by their electrochemical behaviour. Not only were many of the growth media components electrochemically active, adsorption of growth media to the electrode surface was observed. This represents a particular challenge for electrochemical analysis in complex growth media.

Minimal published data on the voltammetric behaviour of complex growth media or analysis of metabolic products in the presence of growth media possibly reflects the interfering nature of these complex matrices, forcing investigators to either perform extensive sample pre-treatment procedures, avoid operational conditions and potentials prone to interference, or use alternative analytical techniques to overcome this problem. This study represents the first focussed investigation to interrogate these challenges, probing the anodic and cathodic analysis of OTC in a case study.

While the exact nature of the anodic and cathodic peaks of the tested growth media is unclear, components such as peptone, yeast extract and malt extract were shown to oxidise irreversibly at potentials exceeding 0.6 V at pH 7 or lower. It is speculated that these peaks are attributable to amino acids and vitamins, as contained within these components (Stockes *et al*., 1944; Fluckiger-Isler *et al*., 1994).

Through the use of a $Fe(CN)_6^{3-/4-}$ redox probe, the adsorptive effect of growth media onto the electrode surface was investigated. The potential and current related parameters used to assess the reversibility of a redox reaction, ΔE_p and I_{pa}/I_{pc} respectively, suggest the presence of an adsorbed layer on the electrode surface, hindering electron transfer between the redox probe and electroactive surface sites of the GCE. A decrease in the A_{exp}, supports this notion.

The presence of adsorbed impurities on the GCE surface was confirmed by impedance spectroscopy, evident from a decline in the double-layer capacitance, C_{dl}, for measurements performed in electrolyte solutions containing growth media. A decline in C_{dl} and anodic current of $Fe(CN)_6^{3-/4-}$ for measurements in the presence of

adsorbed proteinacious molecules has been reported (Moulton *et al*., 2003; Moulton *et al*., 2004). This forms the basis for the argument that proteinacious molecules present in the growth media analysed in this work (Appendix A), adsorb to the GCE surface reducing the electrode performance due to a passivating surface layer.

In light of the constraints mentioned here, analysis in minimal salts media (MSM) is recommended when voltammetry in growth media is attempted. MSM exhibited no anodic response in a positive potential window of 0 to 1.6 V, and showed minimal interference to $Fe(CN)_6^{3-/4-}$ analysis, suggesting little to no adsorption of impurities onto the electrode surface. This is likely due to the low concentration of yeast extract (2 mg/l) in this growth media.

The primary anodic peak of OTC, $pa_{1(OTC)}$, was noticeably influenced by the anodic current responses of nitrogenous sources contained within the tested growth media. The small separation between interfering peaks and OTC peaks led to underestimation of $pa_{1(OTC)}$ and thus a reduced signal. These nitrogenous sources include peptone, yeast extract and malt extract, the latter exhibiting the least amount of interference for the anodic signal of OTC with a 96.8 % $pa_{1(OTC)}$ signal recovery in pH 2 BR buffer and 84.1 % in pH 7 PP buffer compared to analysis in the absence of growth media components, prompting its use for further anodic studies. Malt extract was replaced as the nitrogen source in AZ media, and this media was referred to as malt extract media (MEM). High OTC current recovery and well-defined oxidation parameters (Chapter 3) prompted further studies to be conducted in pH 2 BR buffer.

At a constant MEM concentration of 0.1 mg/ml in the working solution, the concentration of OTC could be adequately measured. The plot of $I_{pa1(OTC)}$ versus OTC concentration exhibited a similar OTC adsorption behaviour as described by the Langmuir isotherm in Section 3.3.6. Due to the interference of MEM at low OTC concentrations, a detection limit (LOD) was calculated to be 996.4 nM, compared to 24.3 nM in the absence of MEM.

Less favourable results were observed for the cathodic analysis of OTC, which took the form of two cathodic peaks, pc_1 *and* pc_2. A minimal de-aeration period of 300

seconds had to be maintained to achieve reproducible responses, a procedure not well suited for on-line analysis. While no interfering cathodic peaks were observed for AZ media, a lower pc_1 current is reported for OTC measured in the presence of AZ media. Protein adsorption, as confirmed by CV and EIS experiments using $Fe(CN)_6^{3-/4-}$, is suspected to be the cause of this lower current for pc_1. Adsorption was not mitigated through pretreatment procedures, as peptone could not be removed. For these reasons, cathodic analysis of OTC in the presence of complex microbiological growth media was not investigated further.

Pre-treatment of OTC samples prepared in MEM and AZ media did not appear to improve the current response of OTC. This indicates neither peptone nor malt extract, associated with the decline in OTC current, was effectively removed from the growth media samples by centrifugation, acidification or filtration. To overcome the effect of proteinacious interferents, solvent extraction of OTC, or protein precipitation by means of a neutral salts, organic solvent of pH change, could be employed to separate OTC and interfering media components (Ratledge and Kristiansen, 2001).

For voltammetry to be used as a viable on-line sensor, further studies would have to be performed to determine the effect of *S. rimosus* bacteria, bacterial cell debris and metabolic products (present in the fermentation growth media), on the operational parameters of a GCE. Additional interferents for the OTC signal would likely be encountered. While fouling of the electrode with OTC oxidation product and adsorbed impurities would occur, mechanical regeneration of the electrode surface by self-cleaning electrodes has been reported (Olsson *et al*., 2006). This could minimise OTC signal decline and prolong the working life of the electrode surface. OTC detection limits would also need to be improved.

To conclude, the experiments performed within this chapter have elucidated the difficulty of voltammetry in the presence of complex detection matrices, in particular bacterial growth media. OTC could accurately be determined in the presence of MEM, with an experimentally determined LOD of 0.5 µM. The dependence of I_{pa1} on OTC concentration in the presence of MEM was comparable to measurements obtained in the absence of MEM (Section 3.3.6).

CHAPTER 5

Oxytetracycline Analysis at Chemically Oxidised Multi-Walled Carbon Nanotube Modified Glassy Carbon Electrodes

5.1 INTRODUCTION

Since the application of carbon nanotube-modified electrodes to the enhancement of the electro-oxidative response of dopamine by Britto *et al*. (1996), an abundance of applications for single (SWCNT) and multi-walled carbon nanotubes (MWCNT) in the field of electro-analytical chemistry have been reported (Banks and Compton, 2006; Wildgoose *et al*., 2006; Agüí *et al*., 2008; Yanez-Sedeno *et al*., 2010).

MWCNT modified GCEs have been investigated for their ability to improve tetracycline antibiotics detection sensitivity. Guo *et al*. (2009) used MWCNT/ionic-liquid film coated GCEs in their linear sweep voltammetry (LSV) studies to enhance the anodic response of tetracycline (TC), resulting in an estimated LOD of 30 nM. Vega *et al*. (2007) employed HPLC-amperometry with a MWCNT-modified GCE, reporting a LOD of 90 nM, 120 nM, 310 nM and 440 nM for OTC, TC, chlortetracycline (CTC) and doxycycline (DC) respectively. Both studies showed substantially improved anodic signals for OTC analysed at MWCNT coated electrodes, though no mention is made of the LOD achieved at bare electrodes.

However, several key operational parameters for the two systems dealing with tetracycline oxidation at MWCNT-modified electrodes were not examined in detail, forming the motivation for the work performed in this chapter. These parameters include a) the effect of duration of acid functionalisation, which is known to affect structural and chemical properties of MWCNTs (Gonzales-Guerrero *et al*., 2008), b) dispersal agent selection for effective MWCNT application (Ribeiro *et al*., 2011), and c) MWCNT loading volume for effective electron transfer (Huang *et al*., 2003). The role of MWCNTs in enhancing the anodic current is poorly understood for tetracyclines and examined here in detail.

5.1.1 Acid functionalisation of MWCNTs through chemical oxidation

Acid functionalisation of MWCNTs serves multiple purposes of which two will be discussed. Firstly, acid functionalisation aids in the removal of metal catalysts and amorphous graphite found as impurities resulting from the manufacturing process. This occurs as the graphite is oxidised while the catalyst dissolves in the highly acid mixture (Su *et al*., 2008), which can be removed subsequently by centrifugation.

Secondly, chemical oxidation of the MWCNTs improves water dispersion because of the increase in oxygen-containing functional groups (Osswald *et al*., 2007; Lau *et al*., 2008). This leads to an overall negative surface charge aiding in aqueous distribution (Datsyuk *et al*., 2008). These groups include carbonyl, carboxyl and hydroxyl functional groups at defect (disordered) sites on the MWCNT surface (Osswald *et al*., 2007). Tube shortening has been reported because of prolonged chemical oxidation (Gonzales-Guerrero *et al*., 2008), as well as improved conductivity (Lau *et al*., 2008). As will be discussed later, chemical oxidation and the formation of oxygen-containing groups are advantageous for the electrochemical analysis of cationic species.

5.1.2 Raman spectroscopy

The effect of acid functionalisation on the structural properties of MWCNTS is often investigated using Raman spectroscopy (Gonzales-Guerrero *et al*., 2008; Holloway *et al*., 2008). Raman spectroscopy offers insight into the structural disorder and purity of acid treated MWCNTs (Holloway *et al*., 2008; Su *et al*., 2009) which, when used in conjunction with Fourier-transform infrared (FTIR) spectroscopy and X-ray photoelectron spectroscopy (XPS), can be linked to surface chemical properties (Osswald *et al*., 2007; Datsyuk *et al*., 2008).

Raman, as a spectroscopic technique, is used to study low frequency modes, including the rotational and vibrational mode, of molecular systems (Smith and Dent, 2005). A monochromatic laser light with a frequency v_0, is used to excite molecules to a virtual energy state (Petry *et al*., 2003). Photons are absorbed temporarily, before being scattered at three different frequencies (Smith and Dent, 2005) as shown in Figure 5.1.

In the first case, when the photons are incident on non Raman-active modes, the basic vibrational state of these modes is excited to a virtual state before emitting scattered light of the same frequency (v_o) as the incident light with a resulting return to the initial vibrational state (Wilson *et al*., 1980). This is referred to as elastic Rayleigh scattering (v_R). The majority (99.999 %) of photons are elastically scattered, offering no sample data (Petry *et al*., 2003).

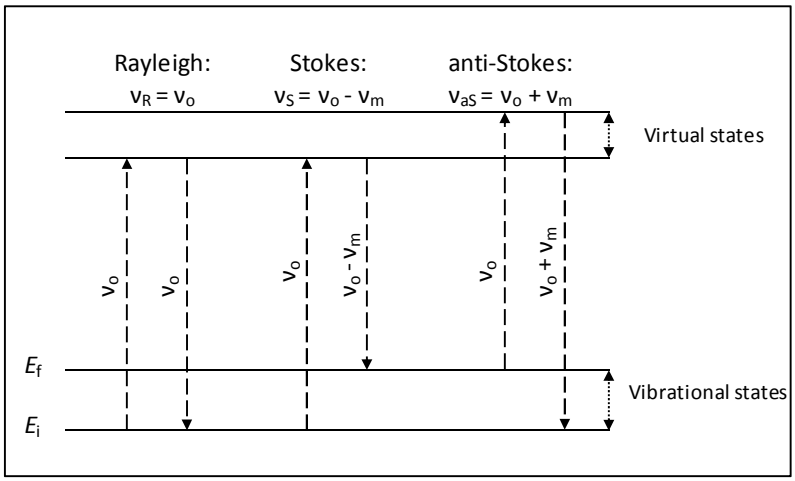

Figure 5.1 Schematic of Rayleigh, Stokes and anti-Stokes Raman scattering. Adapted from Gardiner *et al*. (1989) and Petry *et al*. (2003).

In the second and third case, light is directed toward Raman-active modes, where photons are inelastically scattered and possess a different frequency to the incident light (Wilson *et al*., 1980). Stokes frequency (v_S) is observed when the frequency of scattered light is lower (v_o - v_m) than that of the incident light (Petry *et al*., 2003). This is as a result of a net decrease in energy of incident photons after partial transfer of energy (v_m) to the Raman-active mode. This increases the energy of the vibrational state of Raman-active modes from an initial state (E_i) to an elevated state (E_f) (Ferraro and Nakamoto, 2003). In the event where scattered light has a higher frequency (v_o + v_m) than the incident light, it is referred to as the anti-Stokes frequency (v_{aS}) (Wilson *et al*., 1980). Incident photons gain energy (v_m) from E_f, reducing the vibrational state of the mode to E_i (Petry *et al*., 2003).

5.1.3 Selection of MWCNT acid functionalisation time and dispersal agents

The surface charge of MWCNTs as well as the charge exhibited by MWCNT dispersal agents must be considered when selecting either for modifying a GCE

surface used for the detection of cationic or anionic analyte species. For example, a Nafion® film applied to an electrode surface is known to behave as a cation-exchange membrane due to its negatively charged sulphonate groups (De Betono *et al*., 1999). Electrostatic interaction between charged MWCNTs and cationic and anionic species was observed by Maldonado *et al*. (2006). As shown later for $Fe(CN)_6^{3-/4-}$ (negative) and $Ru(NH_3)_6^{2+/3+}$ (positive) probes however, electrostatic interaction is not always solely responsible for the change in signal observed at coated electrodes.

5.1.4 Problem statement

The complex interaction between analytes and a) MWCNTs, b) the functional groups on their surface formed after acid treatment and c) the dispersal agent used for MWCNT application is not well understood. Specifically, the possibility of charge-based interaction between MWCNTs and charged analytes has been debated in literature. Also, the effect of MWCNT-modified GCEs on the anodic current response of OTC is poorly understood.

5.1.5 Chapter aims and objectives

This chapter aimed to investigate the role of MWCNT-modified electrodes for the anodic detection of OTC. This was done by examining the structural properties of acid functionalised MWCNTs, and their effect on the operational parameters of coated GCEs. Additionally, the interaction between functionalised MWCNTs and charged molecules, was investigated. Where possible, distinction is made between charge-based and surface area related changes in current response of the analyte in question.

Objective 1: Raman spectroscopy to examined the effect of prolonged acid functionalisation on the structural properties of MWCNTs.

Objective 2: Probing the effect of acid functionalisation on the operational parameters of GCEs using the reversible redox probe $Fe(CN)_6^{3-/4-}$.

Objective 3: Investigation of interaction between MWCNT-coated GCEs with charged molecules for selected GCE coatings by CV and EIS using the anionic $Fe(CN)_6^{3-/4-}$ and cationic $Ru(NH_3)_6^{2+/3+}$ redox probes.

Objective 4: Selection of optimal MWCNT acid functionalisation time and dispersal agent for CV analysis of anodic response of OTC.

Objective 5: As a frequently used electroanalytical technique, SWV was investigation for MWCNT-modified GCEs. MWCNT loading volume and LOD for the anodic detection of OTC were examined.

Objective 6: To assess the exclusion properties of MWCNT-Nafion®-coated GCEs towards interfering analytes of OTC current responses.

5.2 INSTRUMENTATION AND MATERIALS

5.2.1 Reagents

Multi-walled carbon nanotubes (> 90 % pure, internal diameter 110 – 170 nm, length 5 – 9 μm) and Nafion® (5 % wt. in lower aliphatic alcohols) were obtained from Sigma Aldrich. KBr (99.5 % pure) for Raman sample preparation was obtained from Riedel-de-Haën. Hexaammineruthenium (III) chloride (98 % pure) and hexa-ammineruthenium (II) chloride (≥ 99.9 % pure) were sourced from Aldrich.

5.2.2 Instrumentation

Three different glassy carbon electrodes (GCEs, 3 mm diameter) were employed in the study of MWCNT modified electrode surfaces, unless otherwise stated, in order to probe the variability between different GCEs.

An Elmasonic S10 (H) ultrasonic bath (Elma, Germany) was used during MWCNT functionalisation.

An Avanti J-E centrifuge (Beckman-Coulter, USA) equipped with a JA-20 rotor was used for centrifugal purification of MWCNTs after chemical oxidation.

Electrodes modified with MWCNT suspensions through the drip-dry method, were dried in a PL001 oven (Prolab Instruments, Switzerland).

A Bruker RAM II FT-Raman spectrometer (Bruker Optic GmbH, Germany) equipped with a Nd:YAG laser (1064 nm) was employed for Raman spectroscopy. Data was analysed using OPUS software (version 6.5, Bruker Optic GmbH, Germany).

5.2.3 Raman data interpretation

In Figure 5.2, a typical Raman spectra of MWCNTs is shown. Raman spectra were analysed using OPUS (version 6.5) software, as shown by the fitted curves for the D, G and D’ band superimposed on the raw data (shown by the dashed lines in Figure 5.2).

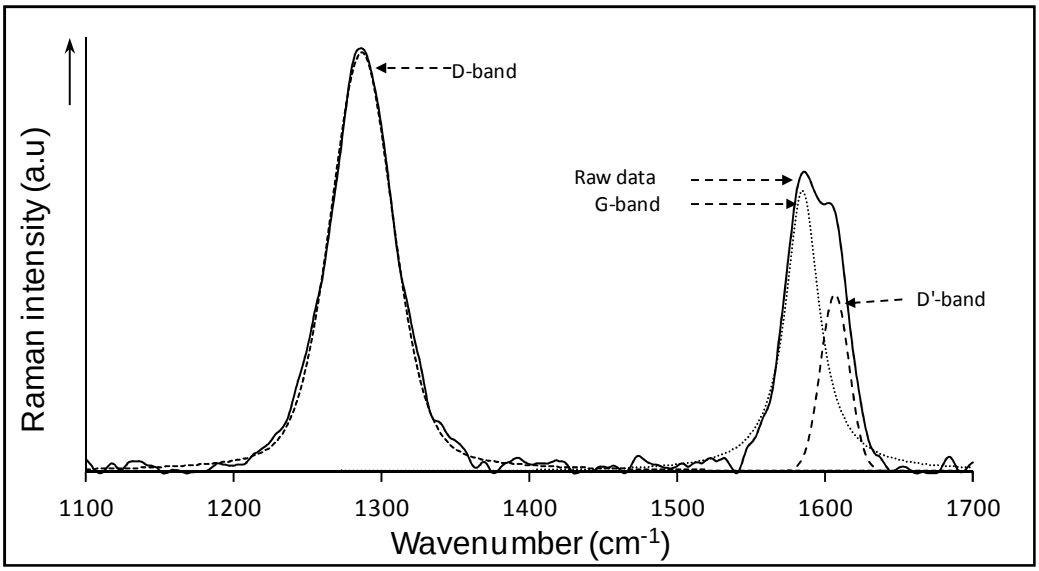

Figure 5.2 Curve fit analysis of typical Raman spectra of MWCNTs analysed using OPUS. Fitted curves for D, G and D'-band are superimposed on the experimental data. The solid black line represents experimentally obtained data while various dashed line styles indicate fitted models for bands.

The D and G-bands were fitted according to Lorentzian curves, while a Gaussian curve was used to fit the D'-band (Antunes *et al*., 2006; Osswald *et al*., 2007). Contrary to single-walled carbon nanotubes (SWCNT), the radial breathing modes in the wavenumber range of 100 – 400 cm^{-1} are not visible for MWCNTs due to their large tube diameter (Jorio *et al*., 2003; Datsyuk *et al*., 2008).

The ration of D-band to G-band intensity was calculates as follows:

$$I_D/I_G = \frac{\text{D-band intensity}}{\text{G-band intensity}} \qquad \text{[Equation 5.1]}$$

where the ratio I_D/I_G is represented by an arbitrary unit.

5.3 EXPERIMENTAL APPROACH

An applied potential of 0.0 V was maintained for 40 seconds while stirring prior to each CV and SWV scan. Scan rate was 100 mV/s.

5.3.1 Functionalisation and Raman characterisation of MWCNTs

MWCNT were functionalised in a mixture of nitric acid and sulphuric acid (1:3 $^{v}/_{v}$). MWCNT were added to micro-centrifuge tubes with the acid mixture to a concentration of 1 mg/ml, and sonicated for periods of 2, 5 and 10 hours respectively. Untreated MWCNTs are referred to as unfunctionalised and denoted as *u*-MWCNTs. Functionalised MWCNT are denoted as x hr *f*-MWCNTs where x represents the length of acid functionalisation time (either 2, 5 or 10 hours).

Following acid functionalisation, washing steps were performed to remove the functionalisation agents (acids) and impurities. The content of the micro-centrifuge tube was added to 39 ml of MilliQ water and centrifuged for 5 min at 10 000 *g*. The supernatant was discarded and the pellet re-suspended in 40 ml fresh water followed by another centrifugation step. This cycle was repeated until the pH of the re-suspended pellet was near-neutral (~ 7). *f*-MWCNT pellets were oven-dried (100 °C) and re-suspended in DMF (1 mg/ml). Subsequently functionalised MWCNTs were tested at a reference concentration of OTC, and deemed comparable when current responses varied less than 5 % from the first prepared MWCNTs.

Using Raman spectroscopy, the effect of different functionalisation times on the structural properties of the MWCNTs was probed. Samples were diluted using KBr to 0.1 % ($^{w}/_{w}$). Measurements were taken using a Nd:YAG laser (1064 nm) at an intensity of 100 mW for an average of 1024 scans. The instrument was pre-cooled using liquid nitrogen.

5.3.2 MWCNT-modified electrodes: $Fe(CN)_6^{3-/4-}$ analysis of functionalisation time

GCEs were cleaned as before (Section 2.3.1) and dried in an oven at 70 °C for two minutes. 2 µl of MWCNT suspensions (1 mg/ml in DMF) were casted onto the surface of a freshly cleaned and dried GCE surface through physical adsorption

(also called the drip-dry method). The electrode was placed back in the oven and dried for 1 minute. This deposition was repeated until the required layering of nanotubes was achieved. The MWCNT solutions in DMF were sonicated for 1 hour prior to use. The changes in physical and chemical properties of the GCEs, as brought on by the deposition of MWCNT, were investigated using CV with 1 mM $Fe(CN)_6^{3-/4-}$ redox probe in 0.1 M KCl (pH 7).

5.3.3 EIS of 10 hr f-MWCNT-GCE using anionic and cationic redox probe

The impedimetric properties of several different electrode coatings was examined. These analyses were performed using the negatively charge $Fe(CN)_6^{3-/4-}$ and positively charged $Ru(NH_3)_6^{2+/3+}$ redox probes. Both probes were prepared as 1 mM final concentration and EIS performed in a 0.1 M KCl (pH 7) working solution. Operational parameters were as described in Section 2.3.3.

Impedance studies were conducted on the following surfaces: Nafion®, Nafion®-MWCNTs, DMF, DMF-MWCNT and bare GCEs. These coating were selected for their use in further studies. The loading volume for coated GCEs was 4 µl, and 10 hr *f*-MWCNTs were used.

5.3.4 OTC analysis at a MWCNT modified GCE

The effect of MWCNT functionalisation time on the anodic response of OTC (pa_1) was investigated using CV. The same coating procedure was used as in Section 5.3.2. As a result of this study, 10 hr *f*-MWCNTs were selected for subsequent OTC analysis. Measurements were performed in 0.2 M BR buffer (pH 2).

5.3.5 Effect of MWCNT dispersal agents on OTC response

Different MWCNT dispersal agents were investigated for their effect on the anodic response of OTC. Dried MWCNTs were dispersed in water or Nafion® solution, and compared to DMF. Nafion® solutions were prepared by diluting a 5 % wt. solution to 0.5 % wt. using ethanol. MWCNTs were added to dispersants to a concentration of 1 mg/ml and sonicated for 1 hour before use. Results of this study prompted the use of 0.5 % wt. Nafion® as the dispersal agent of choice for OTC analysis.

5.3.6 SWV at MWCNT-GCEs

The applicability of SWV for OTC analysis at MWCNT-GCEs was assessed and compared to CV. A method to normalise the current response between electrodes, based on the separation of the SWV current components, was investigated.

5.3.7 Optimal MWCNT loading volume

The effect of MWCNT loading volume was investigated. The loading volume was adjusted in 2 µl increments and deposited onto the electrode surface as before (Section 5.3.2). A 4 µl loading volume was maintained for subsequent OTC experiments, based on the results of this study.

5.3.8 Linear range of OTC

The effect of OTC concentration on I_{pa1} was studied at the optimised modified electrode surface (10 hr *f*-MWCNT in Nafion®, 4 µl loading volume). The forward and net current components were evaluated separately.

5.3.9 Exclusion of interferents based on charge-charge repulsion

To evaluate the exclusion properties of the optimised MWCNT-coated electrode towards interfering molecules, the anodic response of OTC was probed at pH 6.44 in the presence of ascorbic acid (AA) and uric acid (UA). At this pH, AA and UA are present mainly in a negatively charged state, while OTC has a neutral charge as reported in literature (Zen and Hsu, 1998; Roy *et al*., 2003; Sanli *et al*., 2009). This leads to diminished transport of AA and UA to the electrode surface, as Nafion® acts as a cation exchange membrane. Electrode coatings examined were Nafion® and 10 hr *f*-MWCNT-Nafion® (4 µl loading volume each).

5.4 RESULTS AND DISCUSSION

5.4.1 Effect of acid functionalisation on MWCNT dispersion

Figure 5.3 shows solubilised MWCNTs, dispersed in water, following acid functionalised for various lengths of time. Following 15 minutes sonication to disperse the MWCNTs in water, the bottles were left to rest. One hour after sonication, unfunctionalised MWCNTs in the bottle labelled 0 hr, are seen to settle out of suspension, while those treated in acid (functionalised) for 2, 5 and 10 hours remain suspended (Figure 5.3b).

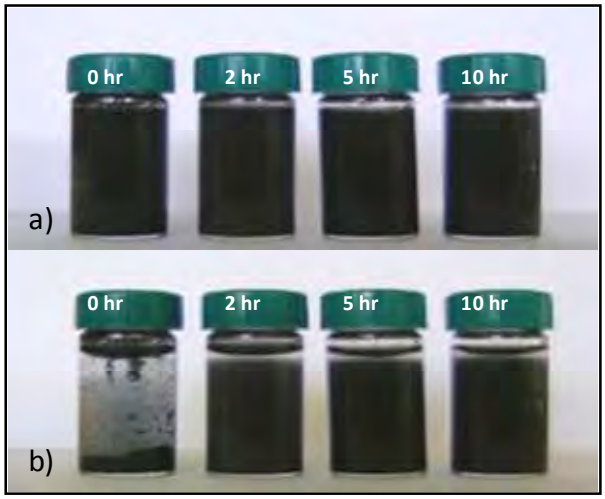

Figure 5.3 Dispersion of acid functionalised MWCNTs in water (1 mg/ml). a) MWCNT suspensions directly after 15 min sonication and b) after 60 minutes at rest. The numbers indicated the length of acid treatment in hours, where "0 hr" refers to untreated as-received MWCNTs (*u*-MWCNTs).

Improved water dispersion of MWCNTs serves as an indicator of the degree of end-cap and sidewall functionalisation because of the increased oxygen-containing moieties such as carbonyls, carboxyls and hydroxyls (Osswald *et al*., 2007; Lau *et al*., 2008; Coccini *et al*., 2010). This increased negative surface charge results in hydrophilicity and enhanced MWCNT distribution, while reducing aggregation (Datsyuk *et al*., 2008). The acid functionalisation process has thus improved the dispersal of the MWCNT.

5.4.2 Raman characterisation of acid functionalised MWCNTs

Figure 5.4 shows the Raman spectrum of untreated and acid functionalised MWCNT samples. In the spectrum window of 1100 – 1700 cm^{-1}, three distinct bands were

visible. Two peaks, at wavenumber 1583.1 cm^{-1} (± 1.6) and 1605.3 cm^{-1} (± 1.4), are attributed to the G- and D'-band respectively (Antunes *et al*., 2006; Datsyuk *et al*., 2008). The third peak at 1286.8 cm^{-1} (± 1.6) was assigned as the D-band, though this band has been reported at a slightly lower wavenumber of ~ 1330 cm^{-1} by Osswald *et al*. (2007) and Su *et al*. (2008) using excitation wavelengths of 633 nm and 325 nm respectively. The observed downshift of the D-band can be explained by the lower excitation wavelength used in these studies compared to 1064 nm in this work (Antunes *et al*., 2006).

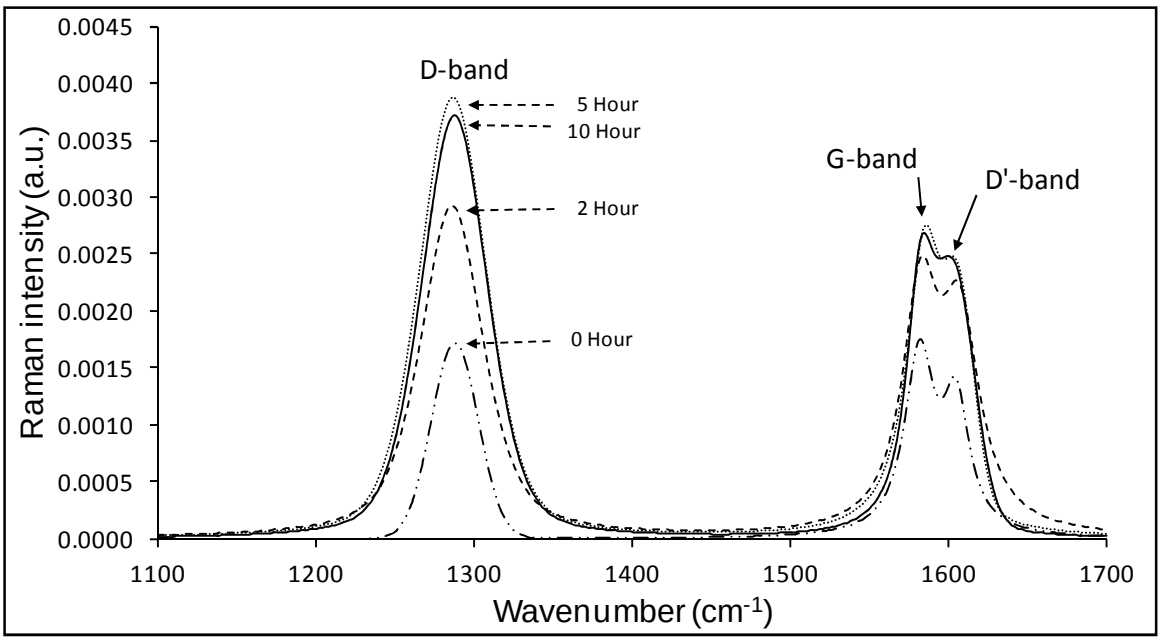

Figure 5.4 Raman spectrum of acid-functionalised MWCNT for various functionalisation times. Samples diluted to 0.1 % wt. with KBr. Measurements were taken using a Nd:YAG laser (1064 nm) at an intensity of 100 mW for an average of 1024 scans.

Table 5.1 summarises the Raman spectral parameters of the three bands, which were fitted according to Section 5.2.3. An increase in the D-band intensity is observed for acid functionalisation times in the order of 0 hr < 2 hr < 10 hr < 5 hr. This band is used as a measure of structural disorder (Su *et al*., 2008) and commonly ascribed to disordered and amorphous carbon (Lau *et al*., 2008; Datsyuk *et al*., 2008). The increased intensity for the D-band (Table 5.1) indicates acid functionalisation led to a time-dependant increase in disorder in the MWCNT structure, compared to unfunctionalised MWCNTs.

Table 5.1 Raman spectral parameters of MWCNTs acid-functionalised for prolonged times.

Time	D-band			G-band			D'-band			I_D/I_G ratio
	Position (cm^{-1})	Intensity (x 10^{-5})	FWHM (cm^{-1})	Position (cm^{-1})	Intensity (x 10^{-5})	FWHM (cm^{-1})	Position (cm^{-1})	Intensity (x 10^{-5})	FWHM (cm^{-1})	
0 hrs	1286.7	313	40.96	1582.9	257	29.99	1606.7	158	20.24	1.218
2 hrs	1287.2	346	40.95	1582.3	277	30.00	1604.9	154	19.02	1.250
5 hrs	1286.1	411	50.71	1585.3	275	29.99	1606.1	144	19.01	1.495
10 hrs	1287.3	396	45.82	1581.7	261	25.12	1603.6	179	25.11	1.516

Note: Intensity is reported as an arbitrary unit. FWHM describes the full-width at half-peak maximum. I_D/I_G calculated according to Equation 5.1. Measurements were taken using a Nd:YAG laser (1064 nm) at an intensity of 100 mW for an average of 1024 scans.

The G-band intensity increased as follows: 0 hr < 10 hr < 5 hr < 2 hr. The origin of this band is found in the stretching vibrations of carbon-carbon bonds of the tangential (in-plain) mode of the graphene structure (Jorio *et al*., 2004; Rosca *et al*., 2005). The D'-band decreases from 0 hr to 5 hr before increasing and reaching a maximum after 10 hrs. This band occurs as a shoulder on the G-band at a higher wavenumber, and is indicative of graphitic defect sites (Jorio *et al*., 2004). The full-width at half peak maximum (FWHM) values tracks the band intensity data, where an increase in intensity is accompanied by an increase in peak width. In particular, increases in D-band width have been attributed to increased MWCNT sidewall functionalisation (Holloway *et al*., 2008).

The ratio of the D-band intensity (I_D) to G-band intensity (I_G) were compared to determine defect density of the MWCNTs. Values of I_D/I_G near zero indicate high purity and flawless MWCNTs, while a ratio above one indicates a high degree of disorder as well as extensive functionalisation of the MWCNT sidewall (Holloway *et al*., 2008). Table 5.1 shows I_D/I_G increased with prolonged functionalisation time, indicating an increased defect density. The functionalisation-time dependant increase in I_D/I_G is due to increased bends and kinks in the graphene bonds of the MWCNT structure, as well as defect sites containing oxygen-containing moieties (Lau *et al*., 2008). These defect sites can occur as holes in the graphene sheet making the surrounding area more susceptible to further oxidation (Gonzalez-Guerrero *et al*., 2008).

A similar I_D/I_G result was described by Osswald *et al*. (2007), who reported an increase in carboxyl and carbonyl functional groups using Fourier-transform infrared

(FTIR) spectroscopy. X-ray photoelectron spectroscopy (XPS) studies by Datsyuk *et al*. (2008) and Lau *et al.* (2008) support these findings. Although an initial drop in I_D/I_G can be expected for short functionalisation times due to the oxidation of amorphous carbon, continuous regeneration of amorphous carbon during the acid treatment process appears to compensate for this loss (Rosca *et al*., 2005).

Gonzalez-Guerrero *et al*. (2008) also reports on the increase of I_D/I_G ratio with increased acid reflux time. In their study, this increase was most prominent in the first 6 hours of the reflux process. Using double-backward titration, the Raman disorder ratio was shown to correlate to the total concentration of acidic sites on the MWCNTs, which levelled off after 6 hours. This indicated stable acid-group coverage of the MWCNT surface. The total concentration of carboxylic acid groups however, increased for the full 12 hour duration of the study showing a lag period between 4 and 8 hours where the total acid concentration plateau was reached. The subsequent increase after 8 hours occurs as available ketone groups are converted to carboxylic acid moieties (Gonzalez-Guerrero *et al*., 2008). Similar work by Kim and Sigmund (2004) showed carboxylic acid concentration plateau after only 7 hours, though acid reflux was performed in H_2SO_4:HNO_3 (3:1) mixture while Gonzalez-Gurrero *et al*. (2008) used 65 % HNO_3.

To summarise, Raman spectroscopy revealed structural disorder and oxygen-containing surface functional groups for acid treated MWCNTS increased with functionalisation time, as expected.

5.4.3 MWCNT-modified electrodes: Effect of functionalisation time on electroanalytical detection of $Fe(CN)_6^{3-/4-}$

To assess the effect of MWCNT acid functionalisation time on the operational parameters of GCEs, Figure 5.5 shows CVs obtained for $Fe(CN)_6^{3-/4-}$ using a GCE coated with MWCNTs functionalised for increased periods of time. The significantly broader and smaller anodic and cathodic waves for $Fe(CN)_6^{3-/4-}$ at *u*-MWCNT-GCE relative to a bare GCE is suggestive of smaller electroactive surface area (Kissinger and Heineman, 1983) and is related to the structure of the *u*-MWCNT (Ji *et al*., 2006).

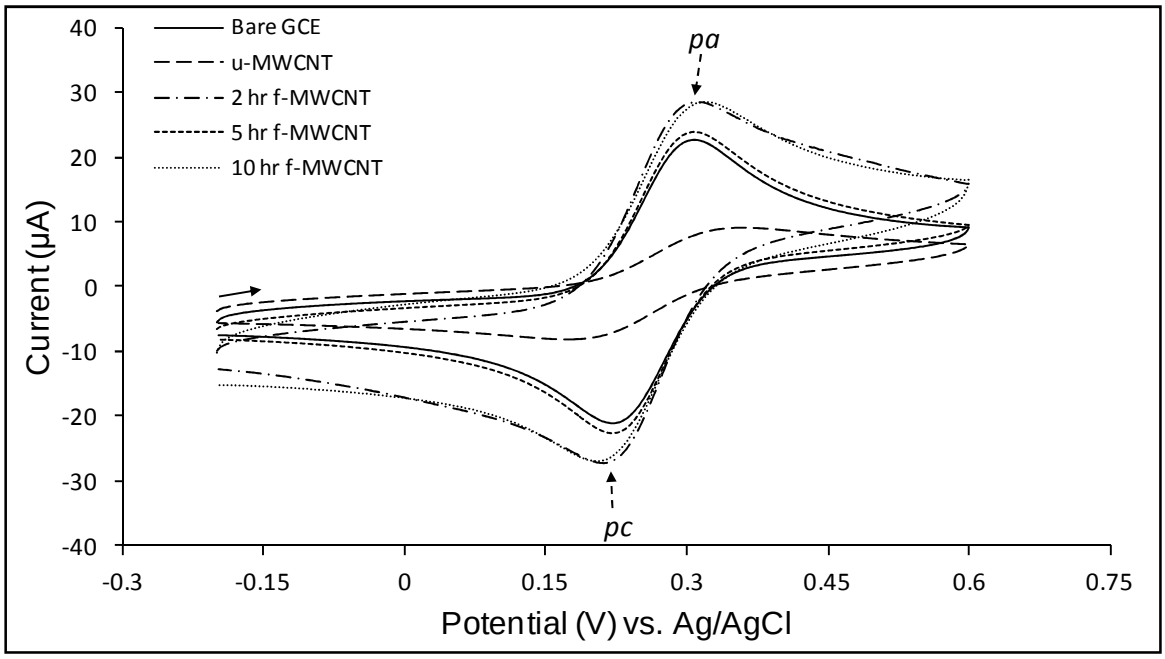

Figure 5.5 CV overlay showing the effect of different MWCNT functionalisation times on the redox behaviour of 1 mM $Fe(CN)_6^{3-/4-}$ in 0.1 M KCl. Typical CV scans were obtained at GCE 1.

In essence, depressed peak heights and enlarged peak separation at *u*-MWCNT-GCEs bears resemblance to CVs obtained by Moore *et al*. (2004) and Ji *et al*. (2006) at basal-plane pyrolytic graphite (BPPG), while the CV shapes obtained at a bare GCE and *f*-MWCNTs-GCEs bear resemblance to edge-plane pyrolytic graphite (EPPG). The implication of edge-plane-like defect sites is discussed in detail further in this section. Based on the shape of the CV for *u*-MWCNT-GCE, partial blocking of the electrode surface with a slower electron transfer is likely (Banks *et al*., 2005), while peak shape and separation for all *f*-MWCNT-coated GCEs was comparable to bare GCEs.

Table 5.2 compares the potential related parameter, ΔE_p, for the three GCEs used. An enlarged ΔE_p accompanied the increase in MWCNT functionalisation time, all of which were larger than the ΔE_p at bare GCEs. *u*-MWCNT-GCEs exhibited the largest ΔE_p, and hence the most sluggish electrode kinetics (Fagan *et al*., 1985), indicating the functionalisation of MWCNTs (2, 5 and 10 hrs) improved electron transfer. This improvement was greatest for 2 hr *f*-MWCNTs, followed by 5 and 10 hr functionalisation times, which were statistically similar ($p < 0.05$) for each electrode used.

Table 5.2 ΔE_p for 1 mM $Fe(CN)_6^{3-/4-}$ in 0.1 M KCl at MWCNT-modified GCEs.

Electrode	ΔE_p (mV) Electrode surface coating				
	Bare	*u*-MWCNT	2 hr *f*-MWCNT	5 hr *f*-MWCNT	10 hr *f*-MWCNT
GCE 1	77.7 (± 5.5)	149.3 (± 15.8)	87.7 (± 6.7)	96.3 (± 16.3)	106.7 (± 10)
GCE 2	70.7 (± 1.2)	161.3 (± 12.1)	84.7 (± 3.1)	107.3 (± 29.9)	125.3 (± 6.5)
GCE 3	95.7 (± 3.2)	143.7 (± 11.1)	123.7 (± 4.5)	144.7 (16.8)	163.3 (± 9.7)
Average	81.3 (± 12.9)	151.4 (± 9.0)	98.7 (± 21.7)	116.1 (± 25.3)	131.8 (± 28.9)

Note: ΔE_p was calculated as the average of three electrodes, n = 9, according to Equation 2.10.

For a fast one-electron reversible redox process of $Fe(CN)_6^{3-/4}$, a theoretical ΔE_p of 58 mV is expected (Kissinger and Heineman, 1983). As explained in Section 4.4.1.1 however, electrode deactivation and surface properties affect peak separation, even for the bare GCE, which ranged between 70 and 96 mV for the three electrodes used here. This mitigated the electron transfer process resulting in the quasireversible peaks observed in this study (Figure 5.5). The increase in ΔE_p accompanying the addition of MWCNT to GCE surfaces indicates further decrease in reversibility with ΔE_p as high as 163 mV (± 9.7) observed for 10 hr *f*-MWNCT-GCE3. For *u*-MWCNT-GCEs, this parameter nearly doubled with respect to the respective bare GCEs, indicating greatly diminished reversibility, which correlates with the value for $I_{pa}/I_{pc} > 1$ (Hu *et al*., 1985; Wang, 2001) reported in Figure 5.6.

Figure 5.6 compares the anodic signal, I_{pa}, of $Fe(CN)_6^{3-/4-}$ and simultaneously reports the I_{pa}/I_{pc} ratio for the different *f*-MWCNT-GCEs. The 2 hr *f*-MWCNT-GCEs produced the most consistent increase in I_{pa}, being the only modified surface to cause a statistically significant increase ($p < 0.05$) in I_{pa} as compared to the bare GCEs, while I_{pa} results for 5 hr and 10 hr *f*-MWCNTs were statistically similar to the uncoated electrodes. Since increases and decreases in I_{pa} of $Fe(CN)_6^{3-/4-}$ are reflected in a proportional manner by the experimentally observed surface area, A_{exp} (Equation 2.7), and the surface roughness factor, R_f (Equation 2.8), analogous interpretations can be made for these three parameters. Therefore, electrodes coated with 2 hr *f*-MWCNTs exhibit an increased A_{exp} and R_f relative to the bare GCE.

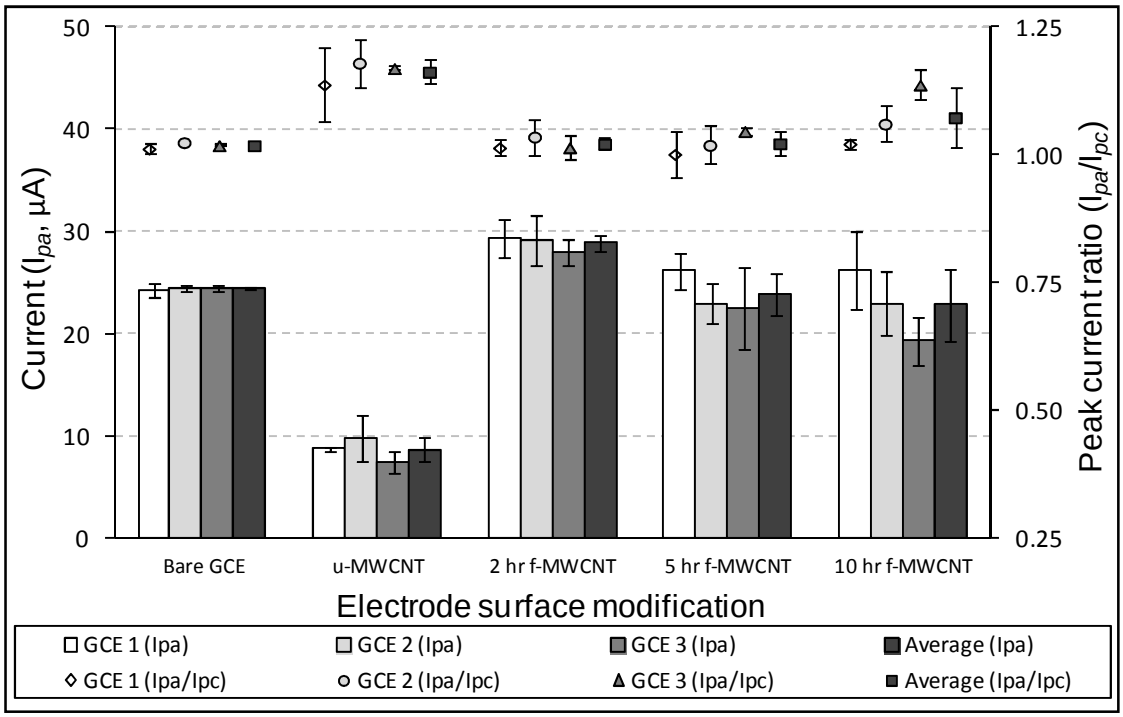

Figure 5.6 CV analysis of I_{pa} and I_{pa}/I_{pc} for 1 mM $Fe(CN)_6^{3-/4-}$ in 0.1 M KCl. I_{pa}/I_{pc} was calculated using Equation 2.9 and represents a dimensionless number.

$Fe(CN)_6^{3-/4-}$ at a *u*-MWCNT-GCEs showed an I_{pa} current decrease of more than 64 % compared to the bare GCEs. An air film was observed on the surface of the *u*-MWCNT-DMF layer when submerged into the electrolyte solution. This is due to the highly hydrophobic nature of unfunctionalised MWCNTs (Li *et al*., 2002), which decreases the electrode area actively involved in electron transport. This air film was not observed for any of the functionalised MWCNTs, supported by the dispersive properties of *f*-MWCNTs (Figure 5.3).

An increase in I_{pa}/I_{pc} is observed with increased functionalisation time and diminishing anodic current response (Figure 5.6). A larger I_{pa}/I_{pc} ratio is indicative of slower electron transfer process (Kissinger and Heineman, 1983), where the oxidation reaction is favoured over the reduction reaction. It is proposed that both the variation in I_{pa} and the ratio I_{pa}/I_{pc} can be explained in terms of the edge-plane-like regions present on the functionalised MWCNTs. The absence of these sites mitigates electron transfer processes for the *u*-MWCNTs, resulting in a lower I_{pa} and even lower I_{pc} as evident by the increased I_{pa}/I_{pc} ratio. Similarly, with increased oxygen-containing functional group concentration associated with increased functionalisation time as shown by Raman studies previously (Table 5.1), the I_{pa}

decreased in the order of 2 hr > 5 hr > 10 hr. This order is reversed for the increase in I_{pa}/I_{pc}.

Similar to the edge-plane sites of graphite and the glassy carbon structure of GCEs, the majority of electron transfer occurs along edge-plane-like defect sites found on tube ends and defect sites along the tube wall of acid functionalised MWCNTs (Kissinger and Heineman, 1983; Ji *et al*., 2006; Holloway *et al*., 2008). It was shown however by Holloway *et al*. (2008), that increased concentrations of oxygen-containing functional groups at these defect sites and tube ends, which form as a result of the chemical oxidation process, greatly inhibit the electron transfer process. The combined Raman and CV studies indicate 2 hr *f*-MWCNTs have proportionally more un-functionalised edge-plane-like sites, while prolonged chemical oxidation for 5 and 10 hour *f*-MWCNTs leads to saturation of these electron-mediating sites by carbonyl and carboxyl moieties, and a subsequent decrease in I_{pa} (Figure 5.6) and increased ΔE_p (Table 5.2) for $Fe(CN)_6^{3-/4-}$ with increasing functionalisation time. This data offers the first proposed reason for the smallest ΔE_p and largest electrochemically active surface area for $Fe(CN)_6^{3-/4-}$ at 2 hr *f*-MWCNTs.

Alternatively, enhanced electrostatic repulsion of the anionic $Fe(CN)_6^{3-/4-}$ probe by increased negatively charged functional groups at 5 and 10 hr *f*-MWCNTs is an appealing and simple solution. This mechanism was also proposed by Ji *et al*. (2006) to explain increased peak separation of the $Fe(CN)_6^{3-/4-}$ couple. This mechanism was however questioned by Holloway *et al*. (2008), who could not observe a decrease in ΔE_p for a cationic $Ru(NH_3)_6Cl_3$ probe used by this author, though no mention of variations in current response were made. This mechanism is not ruled out.

The manner in which interaction between these probes and MWCNT-modified GCEs occurs, could lead to a biased conclusion when surfaces are compared (Holloway *et al*., 2008). If redox probe interactions with specific MWCNT surface groups influences the electroactive surface area, as reported in this section, this data does not necessarily apply to other analytes as shown in Section 5.4.5.

Variation between the three electrodes used, is noted in Table 5.2 and Figure 5.6. Electrode variability is not unusual, and has been reported on and linked to pre-treatment history (Heiduschka and Dittrich, 1992), surface deactivation through impurities (Hu *et al*., 1985) and chemical and structural properties of the electrode surface (Engstrom and Strasser, 1984). GCE variability was also observed for *f*-MWCNT-GCEs by Niland *et al*. (2012), who reported intra- and inter-electrode variability (C_v) as high as 57.1 and 101.9 % respectively, for anodic current responses of the mycotoxin citrinin.

5.4.4 Redox probe and EIS analysis of select modified surfaces

To further probe the interfacial properties of the modified electrode surfaces, CV and EIS was conducted for selected GCE coating, analysed with both the anionic $Fe(CN)_6^{3-/4-}$ and cationic $Ru(NH_3)_6^{2+/3+}$ redox probes. These coatings, selected for comparison to further studies involving anodic OTC detection later in this chapter, were DMF, Nafion®, and either dispersal agent containing 10 hr *f*-MWCNTs.

In Figure 5.7, the degree of reversibility for each of the probes at the modified GCE surfaces, as well as their current responses, was evaluated using CV.

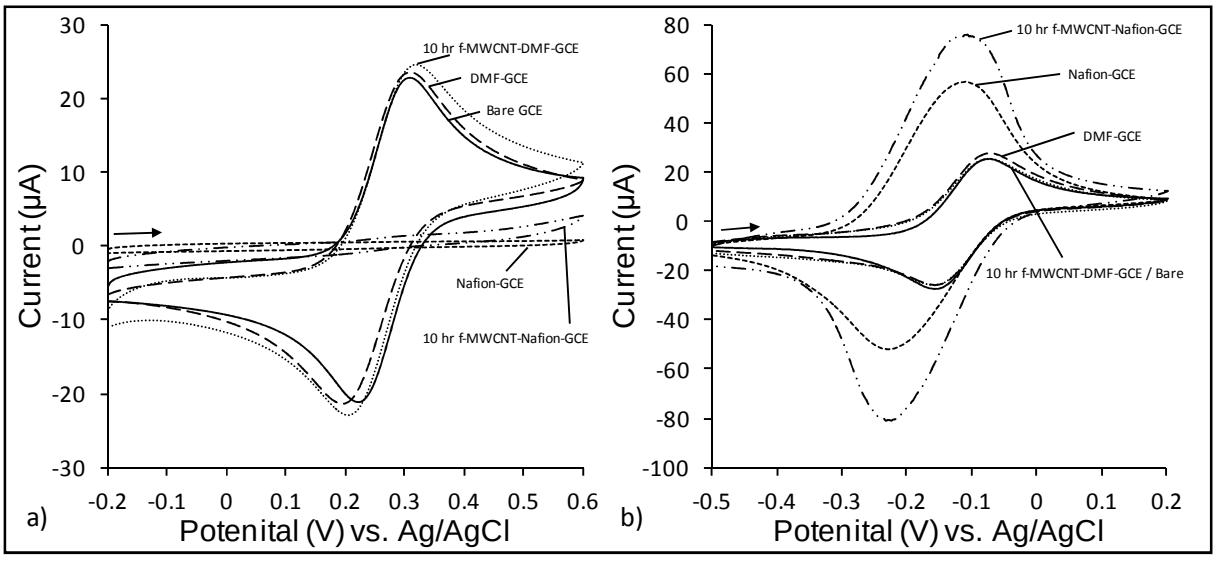

Figure 5.7 CVs of a) 1 mM $Fe(CN)_6^{3-/4-}$ and b) 1mM $Ru(NH_3)_6^{2+/3+}$ analysed at a bare GCE, DMF-GCE, 10 hr *f*-MWCNT-DMF-GCE, Nafion®-GCE and 10 hr *f*-MWCNT- Nafion®-GCE in 0.1 M KCl.
Note: CVs for $Ru(NH_3)_6^{2+/3+}$ at 10 hr *f*-MWCNT-DMF-GCE closely match those obtained at a bare GCE.

Figure 5.7a shows a minimal $Fe(CN)_6^{3-/4-}$ current response at a Nafion®-GCE due to the negatively charged Nafion® layer, which acts as a cation-exchange membrane forming an insulating layer (Zhang *et al*., 2008). Though minimal, an increase in both the anodic and cathodic peaks for $Fe(CN)_6^{3-/4-}$ was observed at MWCNT-Nafion®-coated GCEs, relative to Nafion®-GCEs. This is similar to the result for uric acid at near-neutral pH (Section 5.4.10), supporting the idea by Tsai *et al*. (2004) of Nafion® bridging by protruding MWCNTs, enabling electron transport to occur across the anion-repelling film. The anodic and cathodic peaks for $Fe(CN)_6^{3-/4-}$ were similar when analysed at a bare GCE, a DMF-GCE and a MWCNT-DMF-GCE, though peak separation increased for the modified layers, relative to the bare GCE (Table 5.3).

In Figure 5.7b, CVs for $Ru(NH_3)_6^{2+/3+}$ show the effect of surface modifications was more substantial for this probe. While voltammograms for the bare GCE, DMF-GCE and MWCNT-DMF-GCE were similar, the I_{pa} and I_{pc} increased for analysis at Nafion®-GCE and even more at MWCNT-Nafion®-GCE relative to bare GCEs and DMF-based surface modifications.

Table 5.3 compares ΔE_p and I_{pa}/I_{pc}, parameters indicative of the reversibility of the redox reaction, for each of the redox probes at the selected modified surfaces.

Table 5.3 ΔE_p and I_{pa}/I_{pc} for 1 mM $Fe(CN)_6^{3-/4-}$ or $Ru(NH_3)_6^{2+/3+}$ in 0.1 M KCl at modified GCE surfaces

GCE modified surface	$Fe(CN)_6^{3-/4-}$ probe		$Ru(NH_3)_6^{2+/3+}$ probe	
	ΔE_p (mV)	I_{pa}/I_{pc}	ΔE_p (mV)	I_{pa}/I_{pc}
GCE (freshly polished)	70.3 (± 0.6)	1.011 (± 0.001)	78.0 (± 0.2)	0.958 (± 0.032)
DMF-GCE	109.0 (± 4.2)	1.062 (± 0.004)	79.0 (± 0.4)	1.065 (± 0.007)
10 hr *f*-MWCNT-DMF-GCE	107.7 (± 5.5)	1.092 (± 0.027)	84.0 (± 0.4)	1.009 (± 0.037)
Nafion®-GCE	148.0 (± 36.8)	2.274 (± 0.303)	125.0 (± 0.5)	1.055 (± 0.030)
10 hr *f*-MWCNT-Nafion®-GCE	115.5 (± 2.1)	1.461 (± 0.125)	122.0 (± 1.3)	0.897 (± 0.100)

Note: I_{pa}/I_{pc} and ΔE_p calculated as the average of three electrodes, n = 9., according to Equation 2.9 and 2.10 respectively.

Electrode surfaces coated with DMF and Nafion® hindered the electron transport of $Fe(CN)_6^{3-/4-}$, as shown by increased ΔE_p and I_{pa}/I_{pc}. Similar to work by Tsai *et al*. (2004), the addition of MWCNTs improved $Fe(CN)_6^{3-/4-}$ reaction reversibility when

Nafion® was used as a dispersal agent, reducing ΔE_p by ~ 32.5 mV and I_{pa}/I_{pc} by ~ 0.813. When MWCNTs were dispersed in DMF, ΔE_p and I_{pa}/I_{pc} did not decrease significantly and reversibility was not improved.

Table 5.3 shows minimal increases for these parameters when $Ru(NH_3)_6^{2+/3+}$ was analysed at a DMF-GCE or MWCNT-DMF-GCE compared to a bare GCE, as is reflected by their similar CVs (Figure 5.7b). Analysis at a Nafion®-GCE increased ΔE_p, while the addition of MWCNTs to Nafion® lowered the I_{pa}/I_{pc} ratio to less than unity, indicating the reverse reaction (cathodic peak) was larger than the forward reaction (anodic peak). The effect of MWCNTs on ΔE_p and I_{pa}/I_{pc} was divided for $Ru(NH_3)_6^{2+/3+}$. For DMF-coated GCEs, ΔE_p increased and I_{pa}/I_{pc} decreased with the addition of MWCNTs, while both parameters decreased for Nafion®-coated GCEs after including MWCNTs.

While ΔE_p increase by 77.7 mV and I_{pa}/I_{pc} by 1.263 for $Fe(CN)_6^{3-/4-}$ at a Nafion®-coated GCE compared to analysis at a bare GCE, these increases were 47 mV and 0.097 for the respective parameters when $Ru(NH_3)_6^{2+/3+}$ was analysed. The lesser increases for ΔE_p and I_{pa}/I_{pc} for the positively-charged $Ru(NH_3)_6^{2+/3+}$ suggest charge-based attraction towards the Nafion®-film for this probe, while repulsion is proposed for $Fe(CN)_6^{3-/4-}$. After the addition of 10 hr *f*-MWCNTs, the difference in ΔE_p and I_{pa}/I_{pc} between MWCNT-Nafion®-GCEs and bare GCEs decreased to 45.2 mV and 0.45 respectively for $Fe(CN)_6^{3-/4-}$ and 44.0 mV and - 0.06 for $Ru(NH_3)_6^{2+/3+}$ for the respective parameters. A decrease for both parameters for both probes after the addition of MWCNTs does not support any charge-based interaction between the nanotubes and the probes. As changes in ΔE_p and I_{pa}/I_{pc} were small for DMF-containing coatings after the addition of MWCNTs, no conclusions could be drawn from that data for either redox probe.

Figure 5.8 compares the anodic response, I_{pa}, for $Fe(CN)_6^{3-/4-}$ and $Ru(NH_3)_6^{2+/3+}$ at the selected modified GCE surfaces. Compared to bare GCEs, the current response for $Fe(CN)_6^{3-/4-}$ remains unchanged for DMF-GCEs and increases slightly for MWCNT-DMF-GCE. As mentioned, the peaks for $Fe(CN)_6^{3-/4-}$ observed at Nafion®-GCEs and MWCNT-Nafion®-GCEs were diminished due to the cation-exchange

properties of Nafion®. In the case of both dispersal agents, the addition of MWCNTs increased I_{pa} of $Fe(CN)_6^{3-/4-}$ relative to electrodes coated with the dispersants only.

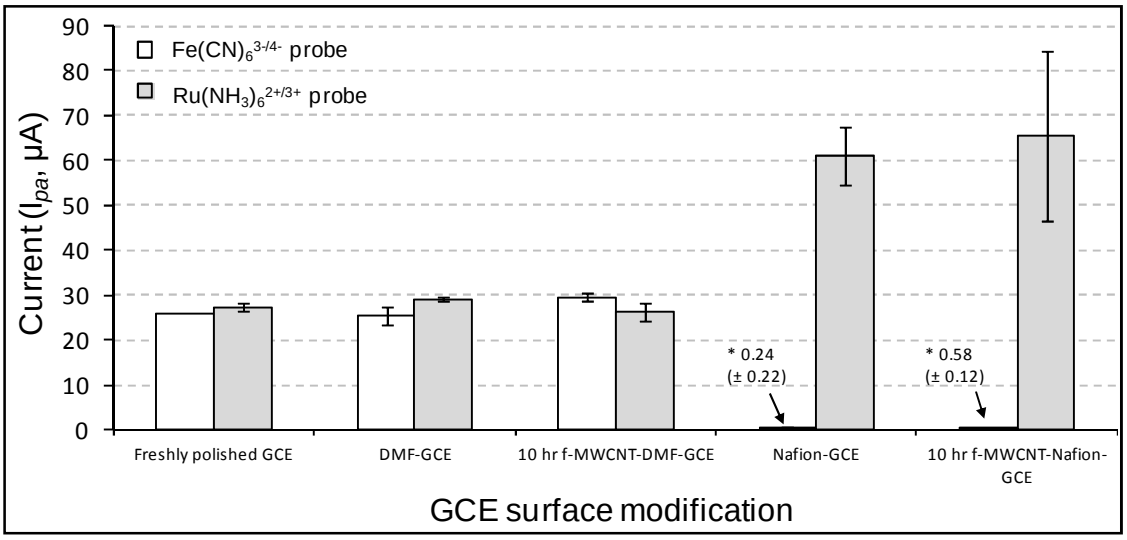

Figure 5.8 Anodic current response, I_{pa}, of $Fe(CN)_6^{3-/4-}$ and $Ru(NH_3)_6^{2+/3+}$ at selected modified electrodes. Redox probes (1 mM) were analysed in 0.1 M KCl. I_{pa} calculated as the average of three electrodes, n = 9.
* As the current responses for $Fe(CN)_6^{3-/4-}$ at Nafion®-containing films were low, I_{pa} and standard deviation were inserted.

For $Ru(NH_3)_6^{2+/3+}$, similar current responses were obtained for the bare GCEs, DMF-GCEs and MWCNT-DMF-GCEs. When analysed at a GCEs with Nafion®-containing films, a quantitative increase in I_{pa} was measured relative to bare GCEs. However, the difference in I_{pa} between Nafion® without and with MWCNTs was insignificant due to large standard deviations, though appeared larger for the latter. As no increase in I_{pa} for $Ru(NH_3)_6^{2+/3+}$ was observed at electrodes coated with DMF-containing film after the addition of MWCNT, the increased I_{pa} at Nafion®-GCE and MWCNT-Nafion®-GCE is ascribed to a higher transport rate for $Ru(NH_3)_6^{2+/3+}$ through the Nafion® film, as reported by Leddy and Vanderborgh, (1987). Accumulation of $Ru(NH_3)_6^{2+/3+}$ in the film layer, due to electrostatic attraction by the cation-exchange membrane, is also considered.

While charge-based interaction between $Ru(NH_3)_6^{2+/3+}$ and Nafion® is suggested by the increased I_{pa} compared to bare GCEs, the nature of interaction between MWCNTs and the charged redox probes remains unclear due to inconclusive data

from the CV analysis. To further probe any possible charge-based interaction, electrochemical impedance spectroscopy (EIS) was performed.

EIS was conducted for each of the surfaces, to improve understanding of the effect of GCE-coatings on redox probe analysis and electrode performance. In Figure 5.9, the EIS profile of $Fe(CN)_6^{3-/4-}$ is displayed in the form of Nyquist plots and Bode plots. The Nyquist plots in Figure 5.9a and 5.9b are presented separately due to the larger impedance observed for Nafion® and MWCNT-Nafion®-coated GCEs. For the bare GCE, a straight line is observed, which is characteristic of a diffusion limited electron transport process (Huang *et al*., 2006). Neither the bare GCE nor the MWCNT-DMF-GCE displayed a semi-circle in the high frequency range, as was observed for DMF-GCE. These semi-circles were greatly enlarged for MWCNT-Nafion®-GCE and even larger for Nafion®-GCE, as expected for increased electron transport resistance, due to cation-exchange properties of Nafion® (Liu *et al*., 2006; Tsai *et al*., 2010). According to Zhang *et al*. (2008), the diameter of the semi-circles is directly related to the charge-transfer resistance, R_{ct}, indicating an electron blocking effect for both the DMF and Nafion® film.

This behaviour is reflected in plots of phase angle and Bode modulus (Figure 5.9c and 5.9d respectively). Both the phase angle and magnitude of impedance is reduced for the DMF and Nafion® film when MWCNTs are added to the coating. The time-constant observed for DMF-GCE in the phase angle plot, which corresponds to the semi-circle in Figure 5.9a, is no longer visible when analysed at a MWCNT-DMF-GCE.

Figure 5.10 consists of the Nyquist, phase angle and Bode modulus plots for the cationic probe $Ru(NH_3)_6^{2+/3+}$, obtained at the selected modified surfaces. For DMF-containing coatings, there appears to be little difference in terms of their Nyquist profile when compared to a bare GCE (Figure 5.10a). Similarly, the phase angle for DMF-GCE and MWCNT-DMF-GCE were similar to a bare GCE (Figure 5.10c), with larger total impedance, |Z|, for the Bode modulus plot, mostly at high frequencies (Figure 5.10d).

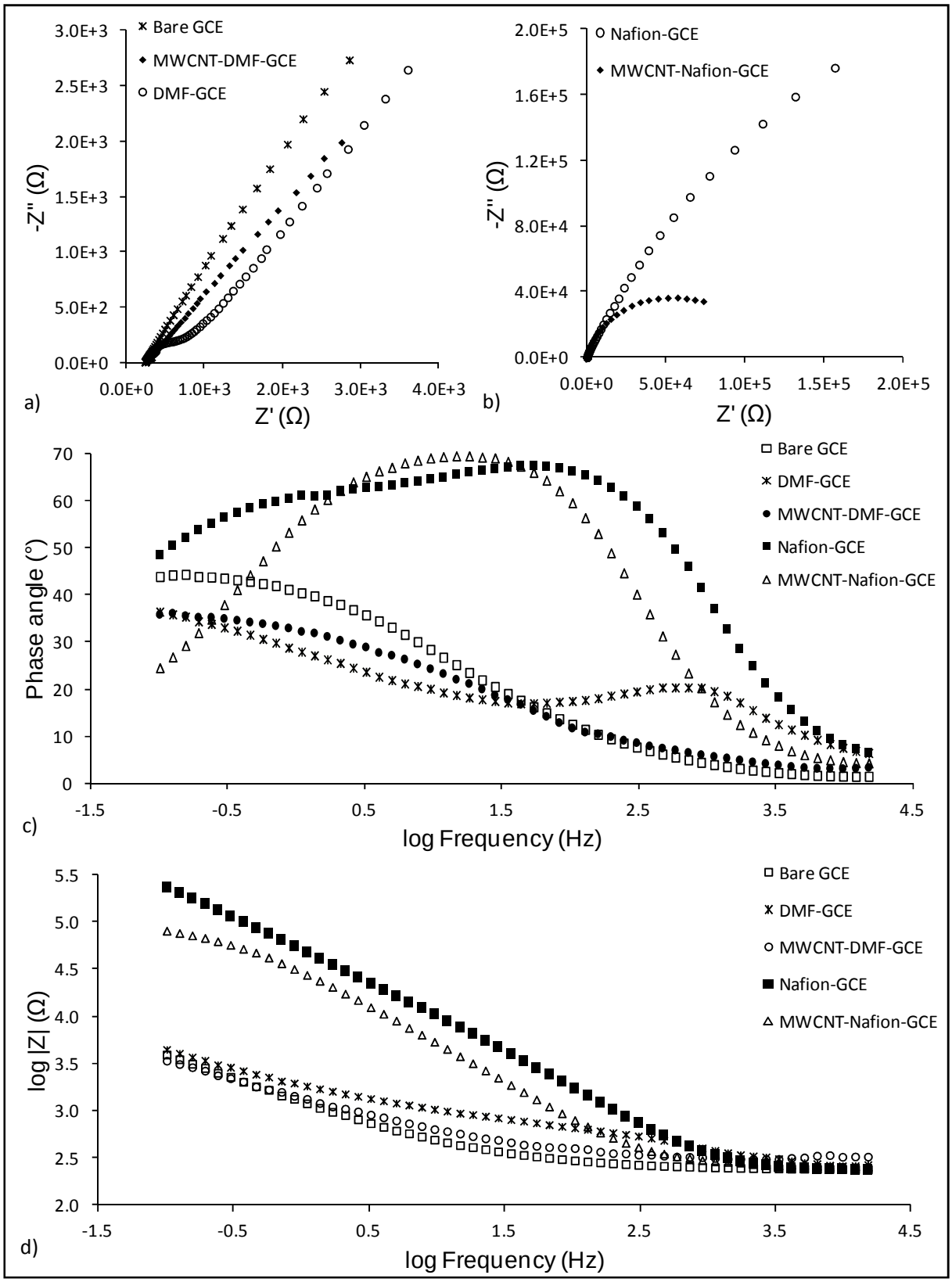

Figure 5.9 Impedance profile of 1 mM $Fe(CN)_6^{3-/4-}$ for various modified surfaces displayed in the form of a and b) Nyquist plots, c) Bode phase and d) Bode modulus. Analysed in 0.1 M KCl. Nyquist plots were separated for scaling purposes.

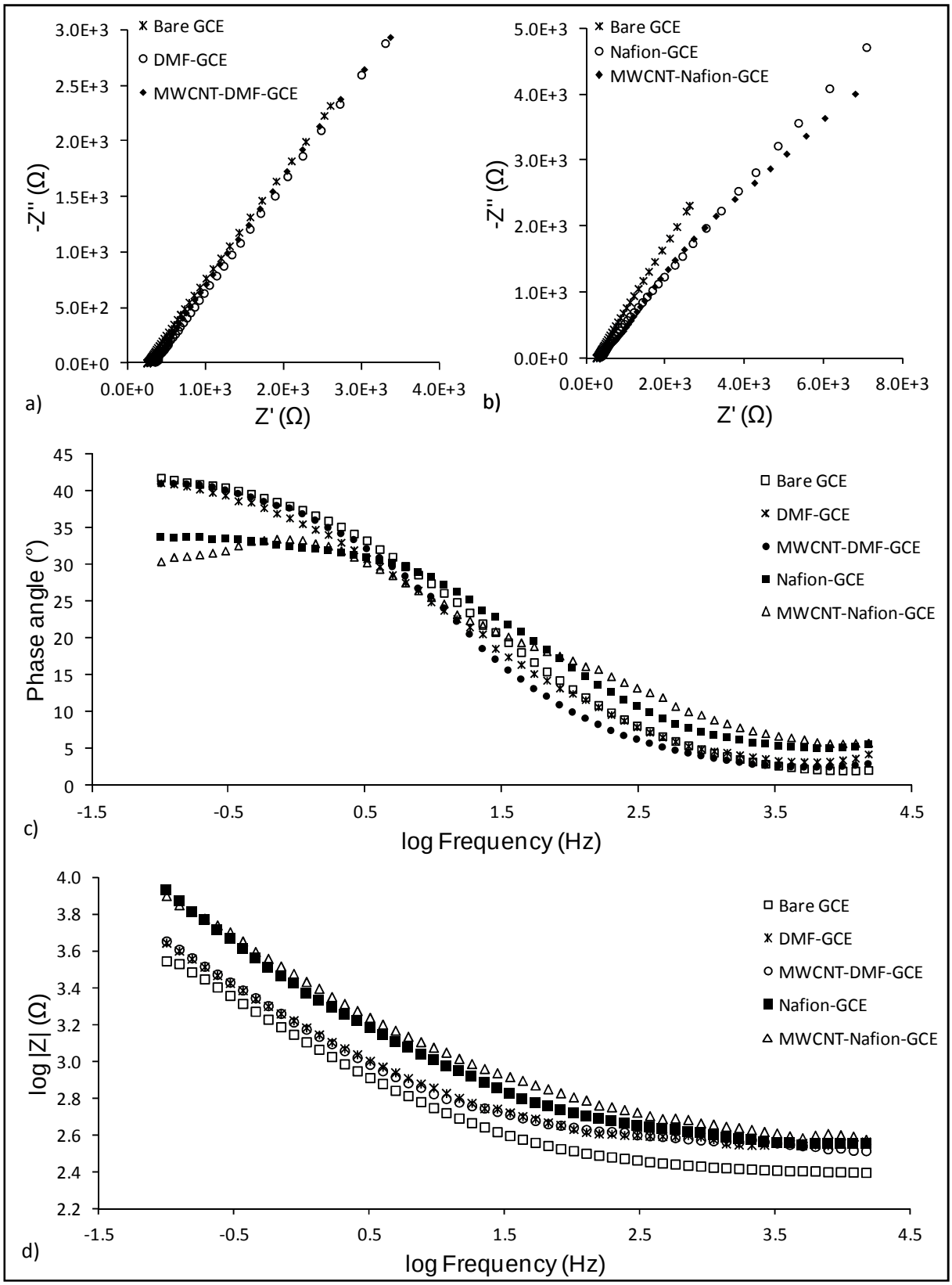

Figure 5.10 Impedance profile of 1 mM $Ru(NH_3)_6^{2+/3+}$ for various modified surfaces displayed in the form of a and b) Nyquist plots, c) Bode phase and d) Bode modulus. Analysed in 0.1 M KCl. Nyquist plots separated based on dispersal agent used.

Figure 5.11 shows the circuits used to fit the data presented in Figure 5.9 and 5.10. A Randles equivalent cell (Circuit A) was used to model the data obtained at a bare GCE, while a modified Randles cell (Circuit C), with an additional resistor and CPE (in parallel) to define the properties of the electrode coating, was used for analysis of modified surfaces.

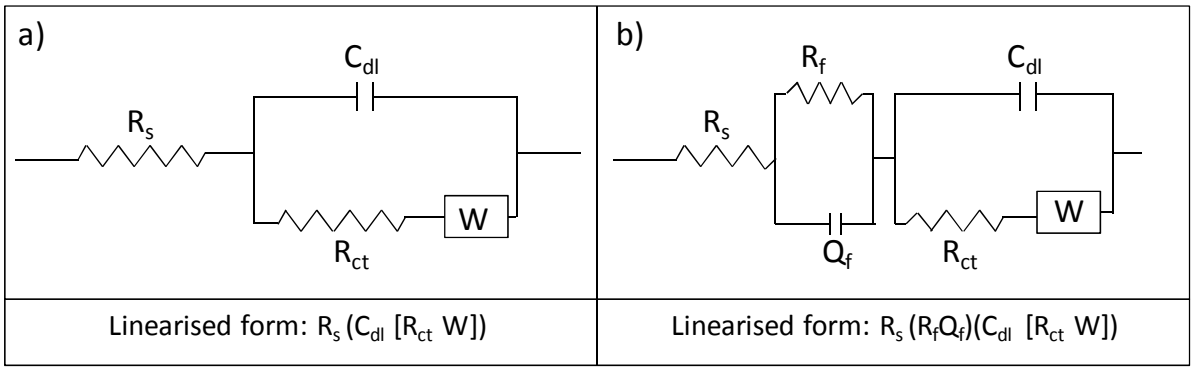

Figure 5.11 Equivalent circuits used for EIS data modelling. a) Randles cell used for bare GCE data fitting and b) modified Randles cell for coated electrode data fitting. R_s represents solution resistance, R_f the film resistance, R_{ct} the charge-transfer resistance, C_{dl} the double layer capacitance, Q_f the film capacitance and W the Warburg impedance. In the linearised form, round brackets and square brackets indicate circuit elements in parallel and series respectively.

Table 5.4 presents data obtained from the EIS data fitting procedure for both $Fe(CN)_6^{3-/4-}$ and $Ru(NH_3)_6^{2+/3+}$. Most notable is the large standard deviation for most of the parameters. This is attributed to variability between individual coatings, as observed by Niland *et al*. (2012). Even so, a pattern can be observed when comparing dispersal agent with and without MWCNTs.

Firstly, the large increases in R_{ct} and R_{tot} when analysing $Fe(CN)_6^{3-/4-}$ at Nafion®-coated GCEs, compared to bare GCEs, is supported by the large increases in ΔE_p and I_{pa}/I_{pc}, and confirms prior assumption of charge-based repulsion between the anionic probe and cation-exchange film. This is further supported by the small increase in R_{ct} and R_{tot} for $Ru(NH_3)_6^{2+/3+}$ at the same coated surface. The increase in Q_f and C_{dl} for Nafion®-films after the addition of MWCNTs (for both probes) is suggestive on an increase in surface area.

Table 5.4 Fitted EIS parameters for 1 mM $Fe(CN)_6^{3-/4-}$ and 1 mM $Ru(NH_3)_6^{2+/3+}$ at selected modified electrode surfaces in 0.1 M KCl.

Redox probe and surface modification		R_s (kΩ)	R_f (kΩ)	Q_f (μF)	R_{ct} (kΩ)	R_{tot} (kΩ)	C_{dl} (μF)	W ($\Omega.s^{-1/2}$ x 10^4)	χ^2 (x 10^{-2})
$Fe(CN)_6^{3-/4-}$	Bare GCE	0.19 *	n/a	n/a	**	**	4.8 (± 0.7)	3.588 (± 0.019)	2.673 (± 0.522)
	DMF-GCE	0.23 (± 0.01)	0.52 (± 0.01)	153.8 (± 86.7)	0.23 (± 0.52)	0.75 (± 0.05)	1.1 (± 0.2)	3.365 (± 0.013)	1.309 (± 0.150)
	MWCNT-DMF-GCE	0.29 (± 0.02)	12.10 (± 9.48)	820.3 (± 227.4)	0.01 (± 0.01)	12.11 (± 9.49)	14.7 (± 1.7)	6.062 (± 1.789)	2.713 (± 1.490)
	Nafion-GCE	0.23 (± 0.01)	10.10 (± 2.16)	5.7 (± 0.5)	76.56 (± 54.75)	86.66 (± 56.62)	2.5 (± 0.2)	0.039 (± 0.011)	2.823 (± 0.930)
	MWCNT-Nafion-GCE	0.25 (± 0.03)	99.20 (± 21.98)	8.57 (± 0.8)	2.49 (± 0.71)	101.69 (± 22.69)	11.8 (± 1.6)	0.939 (± 0.224)	1.713 (± 0.447)
$Ru(NH_3)_6^{2+/3+}$	Bare GCE	0.24 (± 0.03)	n/a	n/a	**	**	1.4 (± 0.5)	3.430 (± 0.277)	0.718 (± 0.327)
	DMF-GCE	0.35*	0.05 (± 0.01)	2.5 (± 0.7)	0.09 (± 0.01)	0.14 (± 0.02)	10.6 (± 0.3)	3.008 (± 0.094)	1.507 (± 0.221)
	MWCNT-DMF-GCE	0.30*	0.07 (± 0.03)	4.5 (± 3.7)	0.12 (± 0.04)	0.18 (± 0.02)	10.7 (± 1.1)	2.789 (± 0.421)	0.901 (± 0.271)
	Nafion-GCE	0.43 (± 0.07)	0.132 (± 0.05)	2.2 (± 1.4)	0.40 (± 0.17)	0.53 (± 0.22)	6.6 (± 3.3)	1.670 (± 0.346)	38.325 (± 8.075)
	MWCNT-Nafion-GCE	0.27 (± 0.08)	3.68 (± 1.15)	106.7 (± 90.1)	1.87 (± 0.93)	5.55 (± 0.52)	106.6 (± 54.8)	3.569 (± 0.198)	7.146 (± 5.341)

n/a - No R_f and Q_f values were recorded for bare GCEs according to Circuit A. R_{tot} calculated as sum of R_f and R_{ct}.
* Standard deviation less than 0.01 kΩ.
** R_{ct} and R_{tot} values for bare GCE were negligible.

Analysis with $Fe(CN)_6^{3-/4-}$ show an increase of R_f, Q_f and C_{dl} for MWCNT-containing electrode coatings compared to the dispersal agents only (DMF-GCE and Nafion®-GCE), while the R_{ct} decreased dramatically from 76.56 to 2.49 kΩ. Thus, while the resistance imposed by the various coatings increased with the addition of MWCNTs, the added capacitance was sufficient to improve electron transfer, as supported by the increase in I_{pa} of $Fe(CN)_6^{3-/4-}$ observed for MWCNT-containing coatings in Figure 5.8. This is further supported by lowering of ΔE_p and I_{pa}/I_{pc} for $Fe(CN)_6^{3-/4-}$ when MWCNTs were added to Nafion® (Table 5.3).

When analysed with the $Ru(NH_3)_6^{2+/3+}$, Q_f, R_{ct} and C_{dl} increase for MWCNT-containing coatings compared to the dispersal agents alone, R_{ct} increasing from 0.40 to 1.87 kΩ when MWCNTs were added to Nafion®. Compared to DMF-GCE, R_f decreases for MWCNT-DMF-GCE while it increases for MWCNT-Nafion-GCE when compared to Nafion-GCE. From Figure 5.8, the slight decline in I_{pa} for $Ru(NH_3)_6^{2+/3+}$

for surfaces modified with DMF with MWCNT compared to DMF alone, is due to the minimal increase in both film- and double-layer capacitance. Contrarily, an increased I_{pa} at MWCNT-Nafion®-coated GCEs compared to Nafion®-GCEs was due to greatly increased capacitance, despite increased film- and charge-transfer resistance.

When comparing DMF-GCEs and MWCNT-DMF-GCEs, the increase in R_f for $Fe(CN)_6^{3-/4-}$ and decrease for $Ru(NH_3)_6^{2+/3+}$ for the latter modified electrode could be due to charge-based interaction between the redox probes and the MWCNTs. As the MWCNTs are covered in negatively charged oxygen-containing moieties, they repel the anionic $Fe(CN)_6^{3-/4-}$, while attracting $Ru(NH_3)_6^{2+/3+}$. A similar charge-based attraction is proposed for OTC analysis at 10 hr *f*-MWCNT-coated GCEs. This could explain the improved signal compared to a bare GCE, while no substantial increase in current was observed for $Fe(CN)_6^{3-/4-}$ for MWCNTs functionalised for 10 hours.

Based on the data presented in this section, charge-based interaction is not excluded, though appears to occur exclusively between the Nafion® coating and the charged probes, where $Fe(CN)_6^{3-/4-}$ is repelled and $Ru(NH_3)_6^{2+/3+}$ is attracted. No charge-based interactions were observed between the MWCNTs and either probe.

5.4.5 Anodic response of OTC at MWCNT-GCEs

In the succeeding sections, the effect of MWCNTs and their dispersal agent on the anodic response of OTC was assessed. Figure 5.12 shows OTC analysed at a GCE modified with different *f*-MWCNTs dispersed in DMF. A notably increased baseline compared to the bare GCE was observed at potentials ranging from 0.5 to 0.9 V, where no faradaic current was observed. The background charging current increased in order of increasing MWCNT functionalisation times, and is attributed to the increased electroactive surface area (Britto *et al*., 1996) and MWCNT functional group density (Holloway *et al*., 2008) revealed by Raman spectroscopy (Section 5.4.2), which increase with functionalisation time.

DMF-coated GCEs, *u*-MWCNT-GCEs and bare unmodified GCEs share similar low non-faradaic currents between 0.5 and 0.9 V (emphasised by inlay to Figure 5.12).

The DMF and *u*-MWCNT surfaces also shared the same weak OTC peak shape and intensity (Figure 5.13), their CVs being nearly indistinguishable.

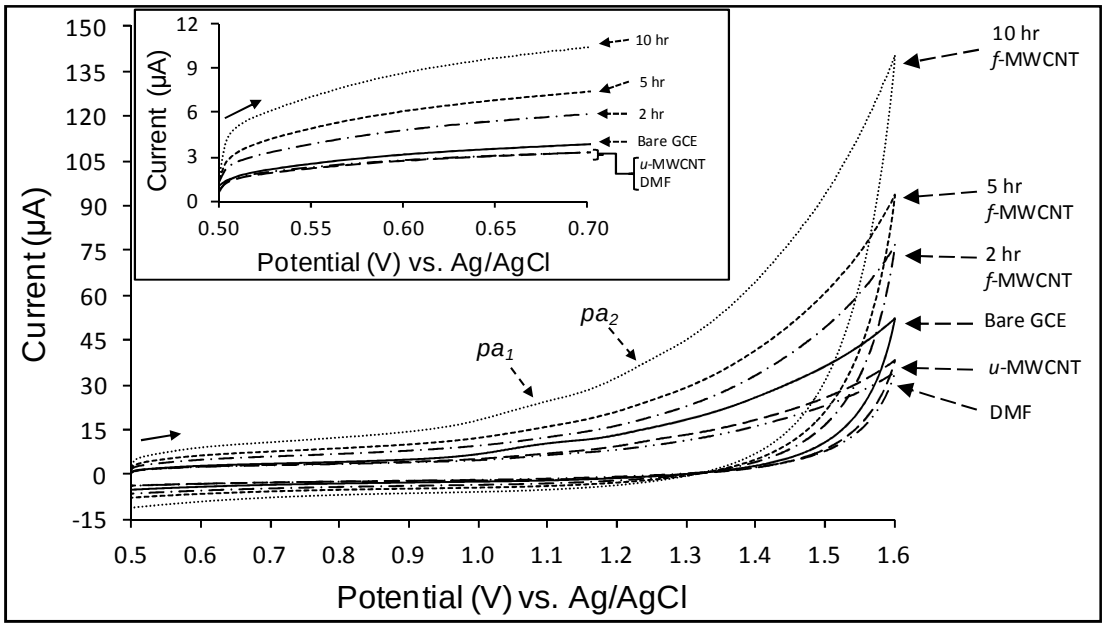

Figure 5.12 Overlay of CVs for GCE modified with MWCNT of different functionalisation times in the presence of 20 µM OTC in 0.2 M BR buffer (pH 2). Inlay shows charging current in the lower potential range.

In Figure 5.13, the anodic responses of OTC, I_{pa1}, are compared for each of the different modified surfaces.

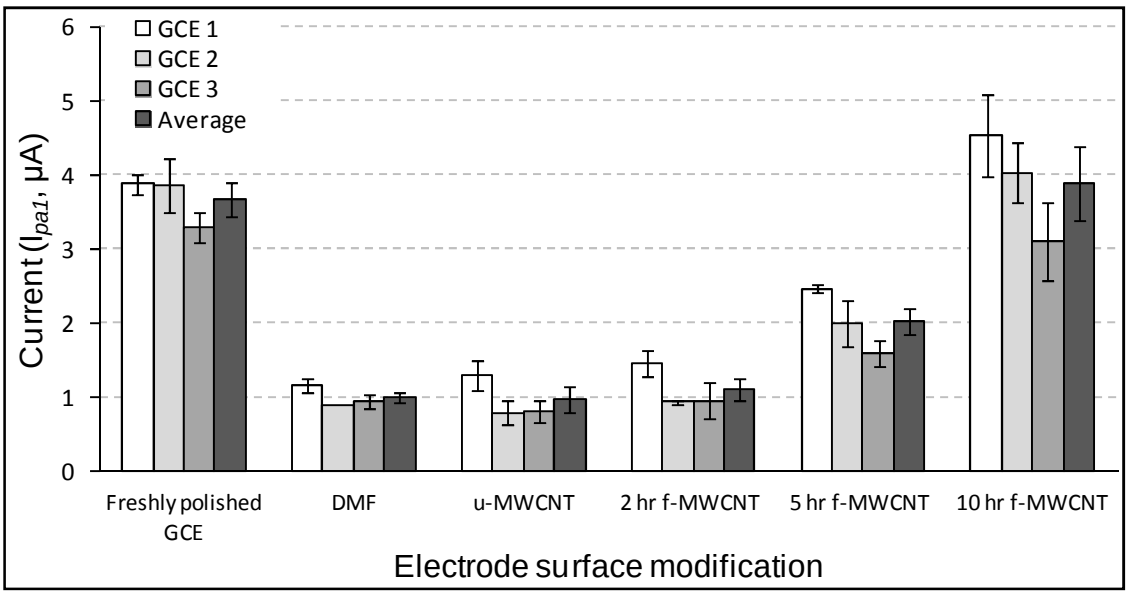

Figure 5.13 Anodic CV response of 20 µM OTC in 0.2 M BR buffer (pH 2) at electrodes modified with MWCNT of different functionalisation times. "DMF" data for electrodes coated with DMF only.

With the exception of 10 hr *f*-MWCNT-GCEs, the anodic response for OTC at each of the modified surfaces was statistically lower ($p < 0.05$) than that observed at the respective bare GCEs.

Firstly, the effect of a DMF coated GCE is considered. While the current response at the DMF-GCEs was greatly reduced compared to a freshly polished electrode, no significant increase was observed when *u*-MWCNTs or 2 hr *u*-MWCNTs were included in the DMF. An electron transfer limitation, applicable to DMF-, *u*-MWCNT- and 2 hr *f*-MWCNT-coatings for OTC oxidation, seems likely in light of their similar behaviours.

At this point, it must be reiterated that each of the modified electrodes was stored in a 70 °C oven, in order to allow the dispersal agent DMF to evaporate. The surface of the freshly polished GCEs however, was renewed through mechanical polishing and rinsing, before being placed immediately into the electrolyte solution to start the CV. Thermal electrode deactivation is proposed, leading to a reduction in the number of GCE active sites that aid in the electro-oxidation of OTC. The increase in functionalisation time, resulting in more carboxyl and carbonyl groups on the MWCNT surface (assumed from the Raman data, Table 5.1), likely compensated for this GCE deactivation leading to increased current response for 5 and 10 hr MWCNT-GCEs relative to 2 hr *f*-MWCNT-GCEs. The absence of such behaviour for $Fe(CN)_6^{3-/4-}$ at 2 hr *f*-MWCNT-GCEs suggest a strong dependence of OTC anodic current on the degree of MWCNT acid functionalisation. In fact, an increase in current response with increased acid functionalisation time, would indicate the enhanced signal is due to more than merely increased surface area considering, a loading volume of 8 µl was maintained for all MWCNTs (Kumar and Shanmugam, 2011).

The increase in I_{pa1} for functionalised MWCNT-GCEs occurs in the order of 2 hr < 5 hr < 10 hr, which was exactly opposite to the order observed for $Fe(CN)_6^{3-/4-}$ (Figure 5.6). Taking into account that OTC is fully protonated at pH 2, the aforementioned proposal of electrostatic attraction for OTC to the negatively charged MWCNTs, and repulsion for $Fe(CN)_6^{3-/4-}$ seems plausible.

The 10 hr *f*-MWCNTs-GCEs were selected for their statistically higher average I_{pa1} response compared to bare GCEs, compared to other MWCNTs analysed, and used for further OTC analysis.

5.4.6 Effect of different MWCNT dispersal agents

Due to the near-insignificant increase in anodic response of OTC at GCEs modified with 10 hr *f*-MWCNT dispersed in DMF, two additional dispersal agents were investigated. These were MilliQ water and Nafion® (0.5 % wt. in ethanol). MWCNT concentrations were maintained at 1 mg/ml in dispersal agent as before in DMF. Dispersal agents without MWCNTs were casted onto the electrode and dried to evaluate their effects on the anodic peak current of OTC.

Figure 5.14a and 5.14b shows CVs recorded using electrodes coated with either the dispersal agents only or MWCNT-dispersal agent mixture, respectively. Increased charging current, associated with MWCNTs, was observed for each of the dispersal agents containing MWCNTs.

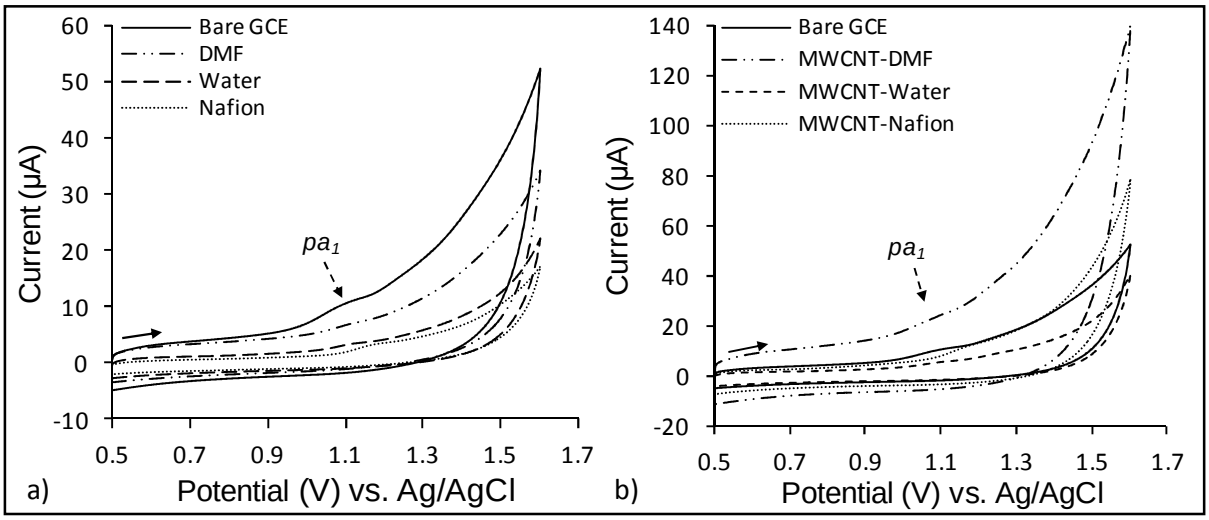

Figure 5.14 CVs of OTC analysed at a) dispersal agent and b) MWCNT-dispersal agent coated electrodes. Analysis performed for 20 µM OTC in 0.2 M BR buffer (pH 2).

Table 5.5 compares the anodic potential of the primary OTC peak, pa_1, analysed at different modified electrodes.

Table 5.5 E_{pa1} of OTC at different electrode surface modifications.

GCE surface	DMF	Water	Nafion®	MWCNT-DMF	MWCNT-water	MWCNT-Nafion®	Bare GCE
E_{pa1} (V)	1.108 (± 0.002)	1.125 (± 0.006)	1.181 (± 0.007)	1.105 (± 0.001)	1.115 (± 0.007)	1.184 (± 0.005)	1.037 (± 0.005)

Note: E_{pa1} expressed as average of three GCEs with C_v < 1 %, n = 9. Analysis conditions identical to Figure 5.14.

Notably, for each of the modified electrodes, including those coated with the dispersal agents only, a positive shift of the E_{pa1} was observed compared to the bare GCE. This indicates less thermodynamically favourable conditions, complicating OTC oxidation (Wang, 1994). For water and DMF, the addition of MWCNT lowered the oxidation potential slightly, though this was not statistically significant (p < 0.05). The largest positive shift of E_{pa1}, relative to a bare GCE, occurred for Nafion® and MWCNT-Nafion® coated GCEs.

Figure 5.15 details the anodic response of OTC at each of the modified GCE surfaces.

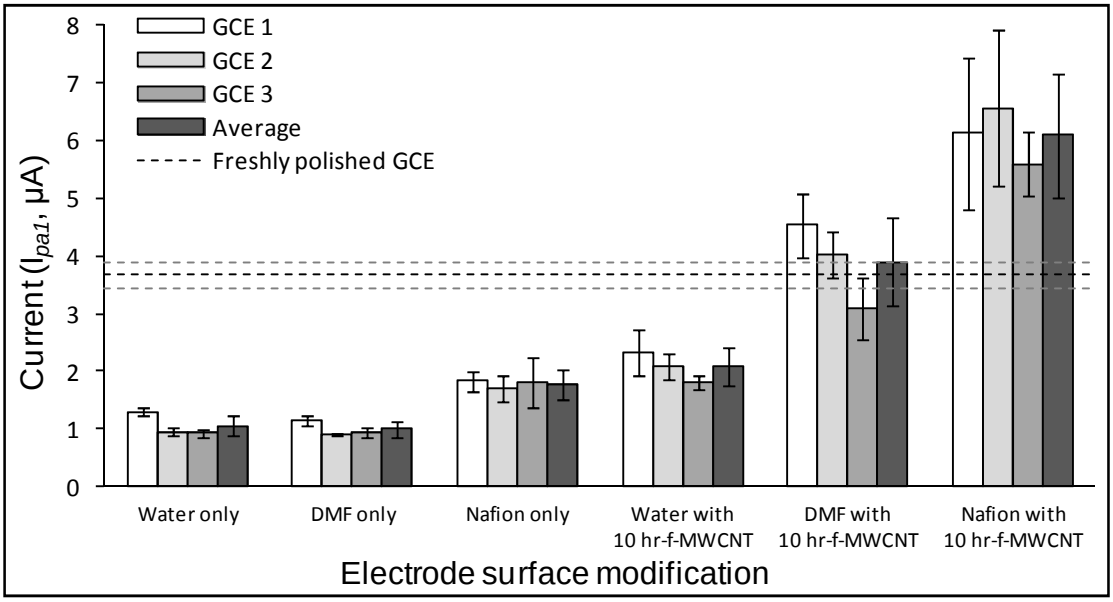

Figure 5.15 Effect of different MWCNT dispersal agent on the CV response of 20 µM OTC in 0.2 M BR buffer (pH 2). The average is calculated from all replicates of the three electrodes. Vertical dashed black line and grey lines represents the average I_{pa1} response and standard deviation respectively, for measurements at three freshly polished GCEs.

The dispersal agents alone performed poorly, unable to produce anodic currents equal to that of the freshly polished bare GCE. The addition of 10 hr *f*-MWCNTs led

to a consistent improvement in OTC signal for each of the dispersal agents. The greatest signal was observed for 10 hr *f*-MWCNT-Nafion®-coated GCEs.

While the Nafion®-coated GCEs exhibit a similar decrease in current response compared to the freshly polished bare GCE, this decrease is less than for DMF and water. This suggests accumulation of OTC occurs in the Nafion® film, due to the cation-exchange properties of this layer (Szentirmay and Martin, 1984; Xie *et al*., 2008). As the pK_a of Nafion® is reported as ~ - 6 (Kreuer *et al*., 2000), sulphonate groups in the polymeric structure of Nafion® are negatively charged at pH 2, and aid in the accumulation of cationic species through electrostatic attraction (De Betono *et al*., 1999). This accumulation would occur mainly during the 40 second preconditioning period, and to a lesser extent during the potential sweep of the voltammogram for the non-faradaic portion prior to OTC oxidation.

These results are similar to Vega *et al*. (2007) who used unmodified MWCNT dispersed in an aqueous 0.1 % Nafion® solution for anodic TC and OTC analysis. As no acid functionalisation of the MWCNTs was performed in their studies, and no decrease in E_{pa1} was observed, the author ascribed the enhanced current response to increased surface area of the GCE used. It is worth noting unmodified MWCNTs have metal particle impurities (such as catalysts) which could aid in their observed increased I_{pa}.

This section has highlighted the importance of selecting an appropriate MWCNT dispersal agent. Nafion® not only enhances I_{pa1} after the oven drying procedure, it also enhances the dispersal of MWCNTs as evident from an additional increase in I_{pa1} (Figure 5.15).

Figure 5.13 and 5.15 shows *f*-MWCNTs, dispersal agents and combinations thereof can enhance anodic signals in an analyte-specific manner. For the experimental conditions maintained in this work, the combination of 10 hr *f*-MWCNTs dispersed in Nafion® provided the greatest anodic current for I_{pa1} of OTC and was used for further OTC analysis.

5.4.7 SWV analysis of OTC at MWCNT modified GCEs

In Figure 5.16, the use of SWV for analysis at 10 hr *f*-MWCNT-Nafion®-GCEs was investigated. It is clear that the charging current for the modified GCE is higher than that of a freshly polished bare GCE. A shift in oxidation peak for pa_1, pa_2 and pa_3 towards a more positive potential was observed for the 10 hr *f*-MWCNT-Nafion®-GCE as for CVs in the preceding section.

From the overlay, pa_1 appears smaller at the modified electrode, as compared to the bare GCE. This is in contradiction to the results observed for the aforementioned CV analysis (Figure 5.15) where 10 hr *f*-MWCNT-Nafion®-GCEs produced a marked increase in current response as compared to bare GCEs. This suggests that in the presence of MWCNTs, SWV responses are more complex and its application as a waveform requires detailed interrogation if it is used for the quantification of OTC.

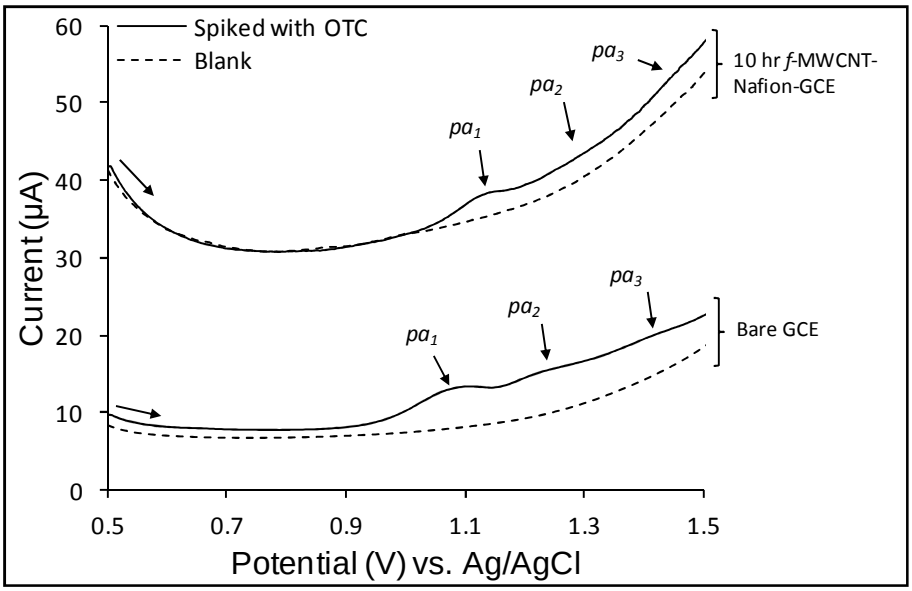

Figure 5.16 SWV overlay for the oxidation of 20 µM OTC in 0.2 M BR buffer (pH 2) at bare and 10 hr *f*-MWCNT-Nafion®-GCE. Dashed line represents SWV in buffered solution. Electrode used was GCE 1.

Table 5.6 compares I_{pa1} and E_{pa1} results for OTC obtained by CV and SWV. For CV analysis, the anodic OTC signal increased by 65 % relative to bare GCEs after the addition of 10 hr *f*-MWCNT to the electrode. For SWV, the OTC current decreased by 42 %.

Table 5.6 I_{pa1} and E_{pa1} of OTC obtained for CV and SWV at bare and 10 hr *f*-MWCNT-Nafion®-GCEs.

	Current, I_{pa1} (µA)		Potential, E_{pa1} (V)	
	Bare GCEs	10 hr *f*-MWCNT-Nafion®-GCEs	Bare GCEs	10 hr *f*-MWCNT-Nafion®-GCEs
CV	3.686 (± 0.363)	6.089 (± 1.068)	1.104 (± 0.002)	1.184 (± 0.005)
SWV	3.914 (± 1.071)	2.306 (± 1.360)	1.097 (± 0.008)	1.143 (± 0.007)

Note: Values are represented as the average of three replicates of three electrodes (n = 9). Analysis of 20 µM OTC in 0.2 M BR buffer (pH 2).

The variation in current response was also significantly higher for SWV than for CV. A C_v of 9.8 % and 27.4 % for I_{pa1} was observed at bare GCEs for CV and SWV respectively, and 17.5 % and 59.0 % for MWCNT-GCEs for CV and SWV respectively. The oxidation potential of pa_1 was also compared in Table 5.6, showing a shift towards a more positive potential of ~ 80 mV and ~ 46 mV for CV and SWV, respectively, with the addition of MWCNTs in Nafion®.

To investigate the decrease in current response for SWV after GCE modification with MWCNT, the complex current signal for SWV was examined. As mentioned, all SWVs depict ΔCurrent (I_{net}) as a function of potential applied, where $I_{net} = I_{for} - I_{rev}$ (Section 2.3.2). This is because of the square-wave potential excitation signal applied, where current is sampled at two distinct points (Section 1.4.3). Thus, two current profiles, depicting the forward (I_{for}) and reverse (I_{rev}) current response, are generated for SWV each scan (Osteryoung and Osteryoung, 1985).

In Figure 5.17, the three current components are presented for GCE 1 and 3 at a bare (freshly polished) and 10 hr *f*-MWCNT-Nafion®-GCEs. The presence of an OTC oxidation signal in the reverse half-period, I_{rev}, is expected for an irreversible redox process governed primarily by adsorption (Lovric *et al*., 1988). The I_{rev} current is smaller than I_{for}, as it is sampled at a more negative potential at which OTC oxidation is less thermodynamically favourable and more OTC depletion has occurred because of the initial oxidation at I_{for} (Nuwer *et al*., 1991).

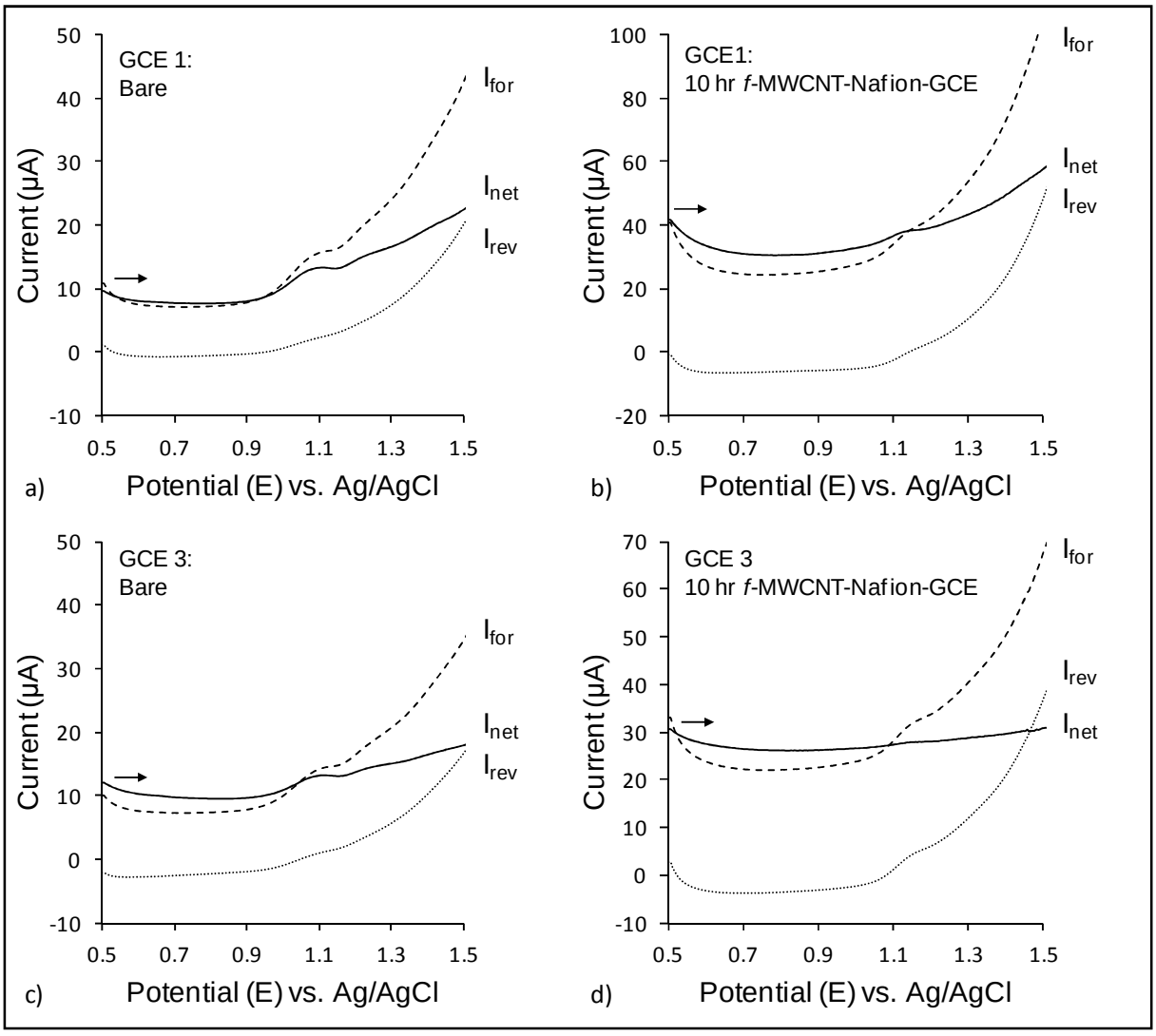

Figure 5.17 SWV current components (I_{net}, I_{for} and I_{rev}) in 0.2 M BR buffer (pH 2) with 20 µM OTC. Voltammograms obtained for GCE 1 and GCE 3 at freshly polished bare electrodes (a and c respectively) and 10 hr *f*-MWCNT-Nafion® modified GCEs (b and d respectively).

The charging current separating the I_{for} and I_{net} is as a result of a relatively high square-wave amplitude, E_{sw}, and indicates the upper limit of this operational parameter (Nuwer *et al*., 1991). Increasing E_{sw} has been shown to increase I_{net} peak currents (Lovrick *et al*., 1988). However, Nuwer and co-workers explain that while increasing E_{sw} can lead to improved I_{net} peak resolution, as the forward and reverse currents separate with regard to their oxidation potential, increased charging current, as is observed between I_{for} and I_{rev} in Figure 5.17, as well as reduced baseline resolution indicate the upper limit for E_{sw}. As decreasing E_{sw} would lead to poorer I_{net} peak resolution due to an increased I_{rev}, parameters were maintained as before.

Due to the manner in which I_{net} is calculated and the adsorptive nature of OTC oxidation, an increase in I_{rev} for GCEs after coated with MWCNTs reduces I_{net}, resulting in a lower current response for OTC at MWCNT modified GCEs for SWV when compared to CV. A similar result was reported by Bobrowski *et al*. (2009) for adsorptive stripping voltammetry (AdSV) of accumulated palladium, which based on the voltammograms shown, lost approximately 30 % of their anodic signal due to subtracted I_{rev} current contributions.

In Figure 5.18, each of the current components is compared for bare and MWCNT-coated GCEs. These values were obtained by separating the current components for SWV scans in the presence and absence of OTC for each of the three electrodes used. The components for analysis in the absence of OTC were subtracted from the respective components in the presence of OTC, allowing I_{pa1} to be calculated for I_{net}, I_{for} and I_{rev} independently.

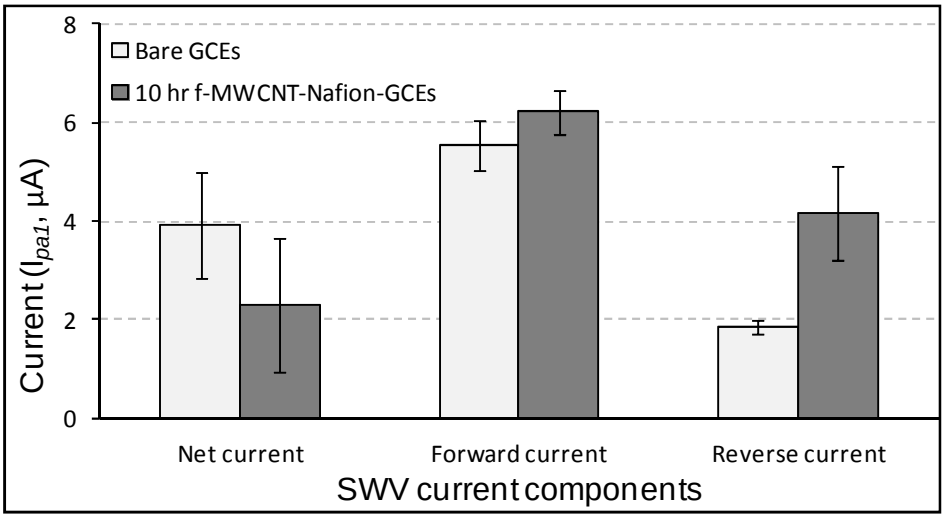

Figure 5.18 SWV current components for pa_1 of 20 µM OTC in 0.2 M BR buffer (pH 2) at bare and 10 hr *f*-MWCNT-GCEs. Responses were separated into net current (I_{net}), forward current (I_{for}) and reverse current (I_{rev}) and averaged for three electrodes, n = 9.

In Figure 5.18, the I_{net} shows the aforementioned decrease for OTC measured at MWCNT-GCEs as compared to bare GCEs using SWV, while the opposite is true for I_{for}. This is due to the greatly enlarged I_{rev} for MWCNT-GCEs. I_{rev} is responsible for a loss in I_{net} of 29.9 % and 62.9 % for the bare and modified GCEs respectively. Thus, by analysing the forward current independently, an enhanced response for pa_1 could be achieved. The variability (C_v) of I_{pa1} was reduced significantly from 27.4 % to

9.3 % for bare electrodes, and from 59.0 % to 7.3 % for MWCNT-GCEs between I_{net} and I_{for} respectively. I_{for} analysis could thus be a means of standardising responses between variable electrodes when SWV is applied.

In summation, due to increased current recorded in the SWV reverse step, increases in I_{pa1} observed for I_{for} are negated through the subtraction process that yields I_{net}. This has prompted further investigation into the usefulness of I_{for} for quantitative purposes for this irreversible adsorption controlled process. Due to the lower variability between the electrodes, the shorter analysis time and the more defined oxidation peaks as compared to CV, SWV was adopted for further analysis of OTC. GCE 3 was excluded from further analysis due to non-uniform behaviour.

5.4.8 MWCNT loading volume

From Figure 5.18, it was clear that the use of 8 µl MWCNT, which was casted onto the GCE surfaces in the preceding experiments, did not statistically improve the current response of I_{pa1} when SWV was employed. Figure 5.19 shows the effect of varying MWCNT loading volumes on the anodic response of pa_1 for OTC. The three SWV current components were examined individually as before (Figure 5.18).

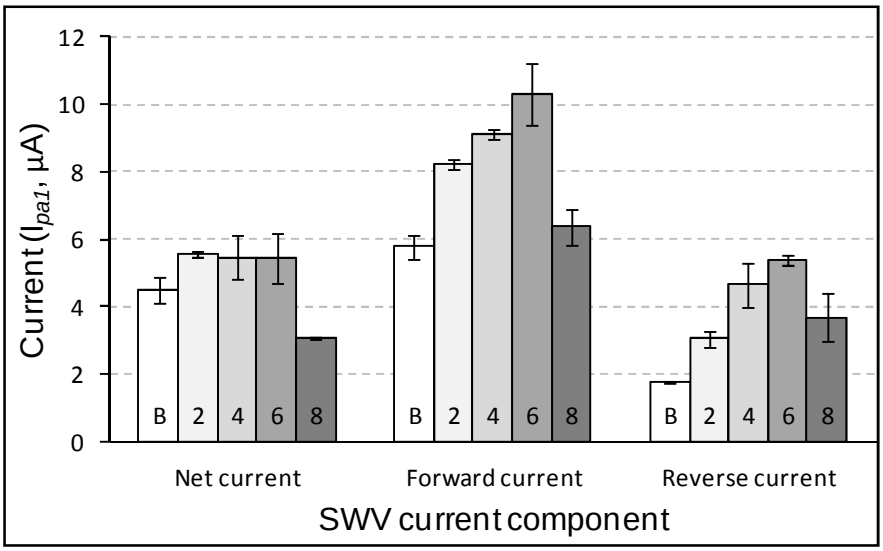

Figure 5.19 Effect of MWCNT loading volume on response of I_{pa1} for 20 µM OTC in 0.2 M BR buffer (pH 2). Responses were separated into net current (I_{net}), forward current (I_{for}) and reverse current (I_{rev}) and averaged for two electrodes, n = 6.
Legend: Numbers represent length of MWCNT acid functionalisation (hours) and B the I_{pa1} values at bare GCEs.

A relationship between the three current components is observed, where an increase in I_{for} is associated with a near-proportional increase in I_{rev}, resulting in minimal improvement in current for I_{net} and increased standard deviation. Lowering the loading volume from 8 µl, an increase in I_{for} was observed, with statistically higher current responses observed for 2, 4 and 6 µl compared to the bare GCEs. Huang *et al*. (2003) and Kumar and Shanmugan (2011) reported a similar trend, both reporting limiting loading volumes of 10 µl Nafion® containing MWCNTs. These authors suggest an excessive MWCNT loading volume could result in instability of the modified layer, while a thicker film layer leads to blocking of electron transfer.

While the amount of deposited MWCNT decreases with lower loading volumes, so does the Nafion® film thickness. Zen and Hsu (1998) and Yang *et al*. (2008) pointed out that the Nafion® film deposited on the electrode can impose diffusional constraints, even for cationic species. As shown in Section 3.3.7, though minimal, diffusion does participate as a mass transport system for OTC oxidation. Therefore, additional diffusive current at lower loading volumes of MWCNTs is also considered as an explanation for the observed increase in I_{pa1} for the I_{for} current component.

Figure 5.19 shows that while the anodic peak (I_{net}) for OTC was greatest for electrodes coated with a 6 µl coating (10.29 µA ± 0.92), a 4 µl coating showed less variation (9.11 µA ± 0.17). A loading volume of 4 µl was maintained for future work, based on excellent reproducibility for I_{for} (> 98 %), and a I_{for} anodic current response of 9.11 µA (± 0.17) for 20 µM OTC, constituting a current increase of > 57 % as compared to bare GCEs.

5.4.9 Effect of OTC concentration on I_{pa1} of OTC at MWCNT-Nafion® coated GCEs

Osteryoung and Osteryoung (1985) have likened the I_{for} and I_{rev} to the forward and reverse current obtained in CV, offering important qualitative data. While this has become evident in the preceding sections, the following experiment probed both the I_{net} as well as I_{for} response for a range of OTC concentrations, to determine the quantitative importance of I_{for} data. In Figure 5.20, the effect of OTC concentration on the anodic response of OTC at a 10 hr *f*-MWCNT-Nafion®-GCEs was investigated.

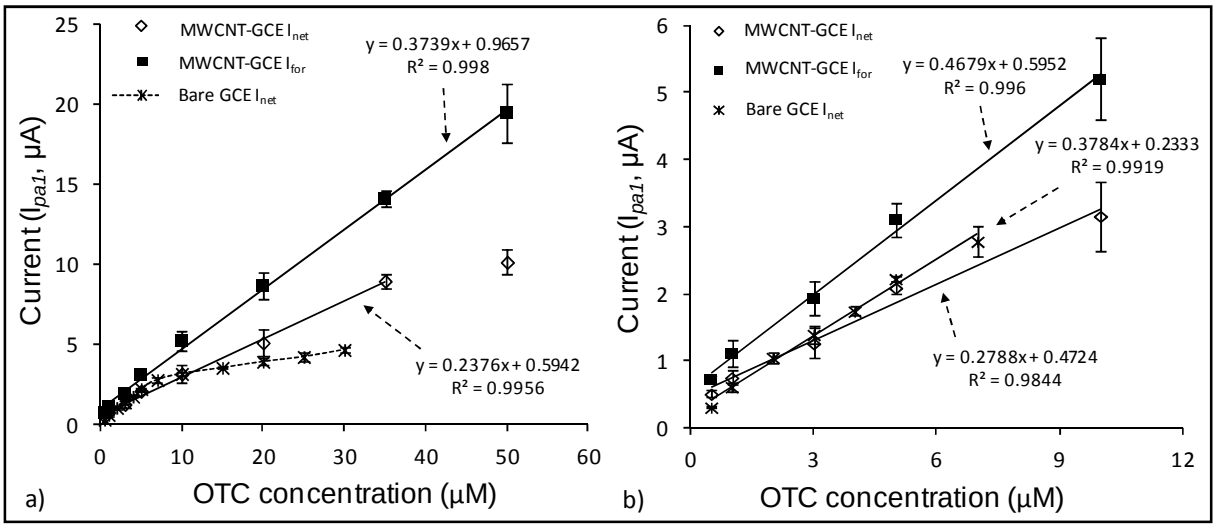

Figure 5.20 Plot of I_{pa1} *vs.* OTC concentration for 10 hr *f*-MWCNT-Nafion® coated GCEs in 0.2 M BR buffer (pH 2) for OTC concentration range a) 0.5 – 50 µM and b) 0.5 – 10 µM. Current presented as the I_{net} and I_{for} component for the MWCNT-coated electrodes. I_{net} data for bare GCE included for comparative purposes. Solid black lines indicate correlations.

The forward ($I_{for\text{-}CNT}$) and net current component ($I_{net\text{-}CNT}$) were plotted together with I_{net} results obtained for OTC in Chapter 3 (Section 3.3.6) for a freshly polished bare GCE ($I_{net\text{-}CGE}$). Contrary to the OTC current at a freshly polished bare GCE ($I_{net\text{-}GCE}$) which could be described by a Langmuir isotherm, linearity was observed for $I_{for\text{-}CNT}$ across the entire concentration range tested (0.5 – 50 µM), and up to 35 µM for $I_{net\text{-}CNT}$ (Figure 5.20a). $I_{for\text{-}CNT}$ results for pa_1 do not appear to exhibit the plateau effect observed for the bare GCE ($I_{net\text{-}GCE}$), previously associated with monolayer coverage of the electrode surface.

A possible plateau effect for $I_{net\text{-}CNT}$ was seen to emerge at high concentrations of OTC, where current values at 50 µM could not be fitted to the straight-line correlation for this data set. This would indicate an increase in the concentration required to form a monolayer compared to a bare GCE, because of the increased surface area due to the MWCNTs. This is supported by the increased signal observed for OTC at 10 hr *f*-MWCNTs (Figure 5.15) as well as increased charging current (Figure 5.12) which, due to the lack of catalytic effect observed (Table 5.5), indicates an enhanced electroactive surface area (Britto *et al*., 1996; Holloway *et al*., 2008).

In Table 5.7, the LOD and LOQ were calculated as before (Section 3.3.6) for $I_{net\text{-}CNT}$ and $I_{for\text{-}CNT}$, for the concentration ranges in which linearity was observed for Figure 5.20a and 5.20b.

Table 5.7 OTC detection limit and sensitivity for unmodified and MWCNT-Nafion®-coated GCEs.

Current component	OTC concentration range (μM)	Standard deviation (μA)*	LOD (μM)	LOQ (μM)	Slope (μA/μM)
$I_{net\text{-}CNT}$	0.5 – 35	0.367	1.167	3.121	0.2376
$I_{for\text{-}CNT}$	0.5 – 50	0.558	0.896	2.395	0.3739
$I_{net\text{-}GCE}$	0.5 – 7	0.126	0.024	0.081	0.3784

Note: $I_{net\text{-}GCE}$ data obtained in Section 3.3.6 for a bare GCE. $I_{net\text{-}CNT}$ and $I_{for\text{-}CNT}$ data obtained for 10 hr *f*-MWCNT-Nafion®-GCE (Figure 5.20). The slope of the I_{pa1} *vs.* OTC concentration is used as a measure of sensitivity and taken from Figure 5.20b. LOD and LOQ calculated according to Equation 2.4. Analysis performed in 0.2 M BR buffer (pH 2).
* Calculated as the average of all standard deviation for the I_{pa1} *vs*. OTC concentration plots.

When analysed at a MWCNT-Nafion®-GCE, a less sensitive and higher detection limit for OTC was witnessed, relative to analysis at a bare GCE. While I_{pa1} for individual OTC concentrations were significantly higher in the I_{for} current component, the slopes of $I_{for\text{-}CNT}$ and $I_{net\text{-}GCE}$ were similar across the concentration ranges tested indicating similar detection sensitivity. Caution is warranted when comparing slopes of unequal concentration ranges, but serves merely to compare detection sensitivities of the largest linear segment for I_{pa} *vs*. OTC concentration plots. The standard deviations for $I_{for\text{-}CNT}$ and $I_{net\text{-}CNT}$ were greater than for $I_{net\text{-}GCE}$, impacting on determine LOD and LOQ (Equation 2.4), where variation in current response is accounted for.

Work in this section as well as Section 5.4.7 and Section 5.4.8 highlight the complications associated with SWV detection of OTC at a MWCNT-coated GCE, which arose from increased I_{rev} current contributions. While accurate data could be obtained from the I_{for} current components, which was not affected by rising I_{rev}, caution is warranted when this approach is considered. Using only the forward SWV current component eliminates the advantage of this pulsed technique, which serves to minimise charging current contributions (Bard and Faulkner, 2001). As mentioned by Bobrowski *et al*. (2009), higher precision may be obtained at the loss of sensitivity when using I_{net}.

The merits of MWCNTs and Nafion® coated GCEs must however not be ignored. A linear relationship of I_{pa1} *vs.* OTC concentration was observed for a much larger OTC range for $I_{net\text{-}CNT}$ and $I_{for\text{-}CNT}$, far exceeding that of the bare electrode ($I_{net\text{-}GCE}$). Larger currents at lower OTC concentrations also enable easier and more reliable determination of I_{pa1} and E_{pa1}.

5.4.10 Charge-based exclusion of interfering analytes

To investigate the exclusion properties of the MWCNT-Nafion® film deposited on the GCEs, model anionic interferent species were investigated for their effect on the anodic response of OTC at bare and coated electrodes. These interferents were ascorbic acid (AA) and uric acid (UA).

In Figure 5.21, the ionization states of AA, UA and OTC are indicated by different shaded regions, accompanied by the net charge of the molecule for the pH range covered by each region. In the demarked window spanning pH 5.40 – pH 7.49, both AA and UA exist primarily as anionic species while OTC is neutrally charged.

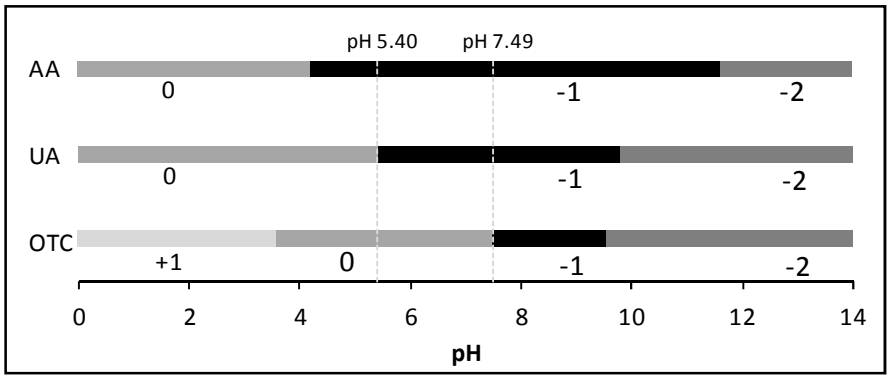

Figure 5.21 pH dependant ionization states of AA, UA and OTC. Vertical dashed lines demark pH window where AA and UA have a net negative charge (-1) and OTC a net neutral charge (0). Data sourced from Zen and Hsu (1998), Roy *et al*. (2003) and Sanli *et al*. (2009).

To examine the charge-based exclusion of Nafion® towards anionic species, analysis was performed in PP buffer (pH 6.44), to ensure a satisfactory proportion of AA and UA were negatively charged, while maintaining a sufficiently high proportion of neutrally charged OTC to prevent excessive exclusion of the analyte of interest.

Figure 5.22 shows CVs for AA, UA and OTC individually, as well as a combination of the three, hereafter referred to as the complex sample.

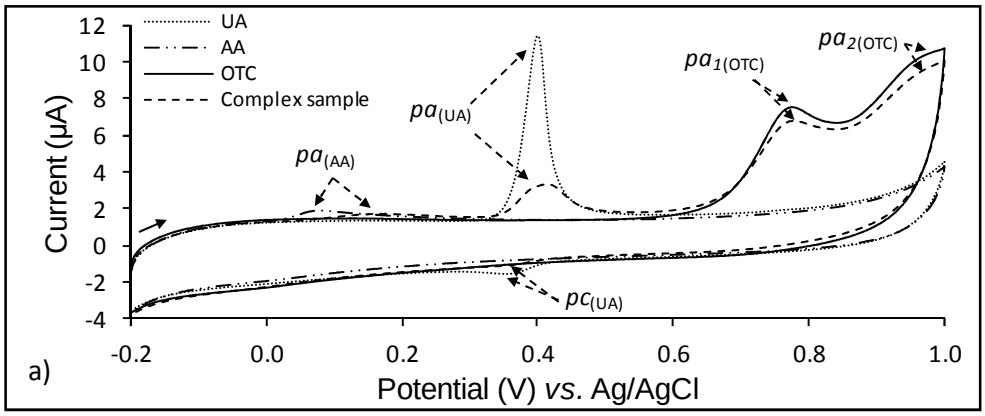

Figure 5.22 Effect of interfering analytes ascorbic acid (AA) and uric acid (UA) on the anodic response of OTC at a bare GCE. Each analyte analysed at 20 µM in 0.2 M PP buffer (pH 6.44). Complex sample contained OTC, AA and UA (all 20 µM).

At a bare GCE, AA oxidised irreversibly ($pa_{(AA)}$) at a potential of 0.079 V (± 0.005) at pH 6.44. This potential is lower than 0.350 V and 0.600 V reported by Roy *et al*. (2003) and Zare and Nasirizadeh (2011) respectively, for bare GCEs at pH 7. Uric acid exhibits a large, sharp anodic peak, $pa_{(UA)}$, and a small cathodic peak, $pc_{(UA)}$, at 0.340 V (± 0.001) and 0.357 V (± 0.003) respectively. This is similar to results shown by Sharath Shankar *et al*. (2009), though the oxidation potential is lower than reported by Zare and Nasirizadeh (2011), who observed no cathodic peak for UA at a bare GCE. However, Zare and Nasirizadeh (2011) explain the importance of GCE activation in lowering the oxidation potential of AA and UA, indicating the potential sweep range and accumulation potential (0.0 V) applied in Figure 5.22, provides a unique electrode activation, giving rise to more well defined and separated peaks at lower oxidation potentials. Under near-neutral pH conditions, $pa_{1(OTC)}$ oxidation occurred at 0.777 V (± 0.002).

There is a noticeable difference in peak heights for each of the analytes when analysed simultaneously in the complex sample (Figure 5.22). The AA and UA peaks decreases to 74.9 % and 23.6 % respectively when analysed together, relative to when measured individually. As shown later in Figure 5.24, $I_{pa1(OTC)}$ decreased to 79.6 % relative to analyses in the absence of UA and AA, and constitutes a statistically significant decline ($p < 0.05$). Nafion®- and MWCNT-Nafion®-coated

GCEs were investigated to improve the current response of OTC in the presence of these interfering molecules.

Figure 5.23a shows OTC measured at Nafion®-coated electrodes (4 µl coating without MWCNTs). A substantially diminished I_{pa1} for OTC is observed at a more positive potential of 0.898 V (± 0.015) compared to 0.777 V (± 0.002) at a bare GCE. When the complex sample was analysed, there was no observable peak attributable to AA, while only the anodic peak for UA was observed in baseline subtracted scans. AA and UA were excluded through electrostatic repulsion by the negative charged sulphonate groups in the Nafion® structure (Zen *et al*., 1998; De Betono *et al*., 1999).

Figure 5.23b examines the effect of MWCNT-Nafion® coating of GCEs on the anodic responses of OTC, UA and AA.

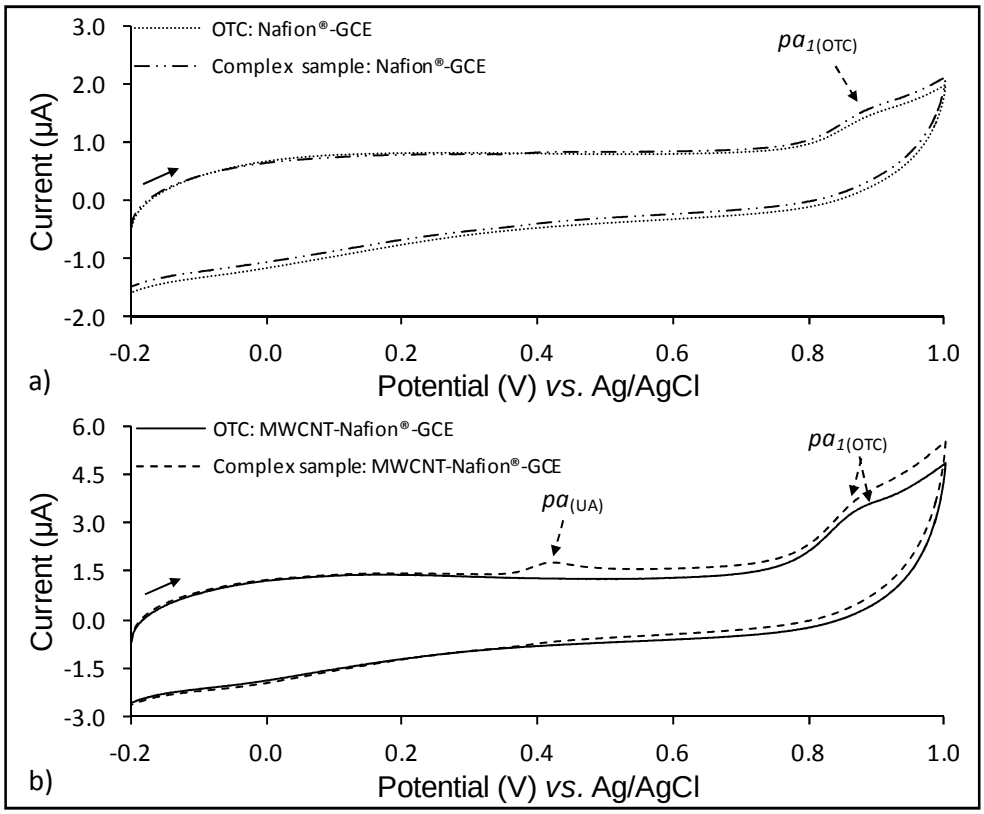

Figure 5.23 Effect of interfering analytes ascorbic acid (AA) and uric acid (UA) on the anodic response of OTC at a) Nafion® coated GCEs and b) 10 *f*-MWCNT-Nafion® coated GCEs. Each analyte analysed at 20 µM in 0.2 M PP buffer (pH 6.44). Complex sample contained OTC, AA and UA (20 µM each).

The presence of the anodic UA peak at the MWCNT-Nafion®-GCE, which was near absent at the Nafion®-GCE, indicated either poor electrode coating or the formation of channels in the Nafion® film by the MWCNTS enabling UA to penetrate the deposited layer. Poor film coatings can be attributed to the inconsistent film thickness due to the manual casting process. Conductive channels through the Nafion® film, formed by the MWCNTs could enable electron transport between UA and the electrode surface to occur (Zare and Nasirizadeh, 2007). This is similar to $Fe(CN)_6^{3-/4-}$ in Section 5.4.4.

Table 5.8 summarises the effect of Nafion® and MWCNTs on the anodic responses $I_{pa1(OTC)}$, $I_{pa(UA)}$ and $I_{pa(AA)}$ for complex samples containing all three analytes, as compared to bare electrodes. A decrease in all anodic current is reported for Nafion®-GCEs, while the addition of MWCNTs improves these peak responses.

Table 5.8 Anodic current response for OTC, UA and AA in complex samples obtained by GCEs at various stages of surface modification.

Electrode surface	I_{pa} of UA in complex sample (μA)	I_{pa} of AA in complex sample (μA)	I_{pa1} of OTC in complex sample (μA)
Bare GCE	2.127 (± 0.230)	0.372 (± 0.009)	5.197 (± 0.734)
Nafion®-CGE	0.048 (± 0.039)	-	0.499 (± 0.121)
10 hr *f*-MWCNT-Nafion®-GCE	0.328 (± 0.072)	-	1.645 (± 0.377)

Note: Complex sample contained 20 μM UA, AA and OTC and was analysed in 0.2 M PP buffer (pH 6.44). No current was observed for AA at Nafion®-GCE or 10 hr *f*-MWCNT-Nafion®-GCE.

Figure 5.24 details the anodic current response for OTC at the three electrode coatings in the presence and absence of UA and AA. A significant decrease ($p < 0.05$) in $I_{pa1(OTC)}$ is seen for measurements at bare electrodes in the presence of UA and AA. The addition of Nafion® and Nafion®-MWCNTs to GCE surfaces, though decreasing $I_{pa1(OTC)}$, improved current responses for OTC in the presence of UA and AA to within statistically similar range as OTC analysed individually.

The data indicates that while charge-based exclusion of possible interferents can be achieved by the application of a Nafion® coating to the GCE surface, the enhanced signal response observed for OTC in the presence of AA and UA is achieved under

conditions that lead to severe reduction in I_{pa1} signal. This decline in $I_{pa1(OTC)}$ of OTC is due primarily to the pH of the solution in which OTC exists mostly as a neutral molecule, and is therefore no longer preferentially adsorbed into the Nafion® layer by electrostatic attraction.

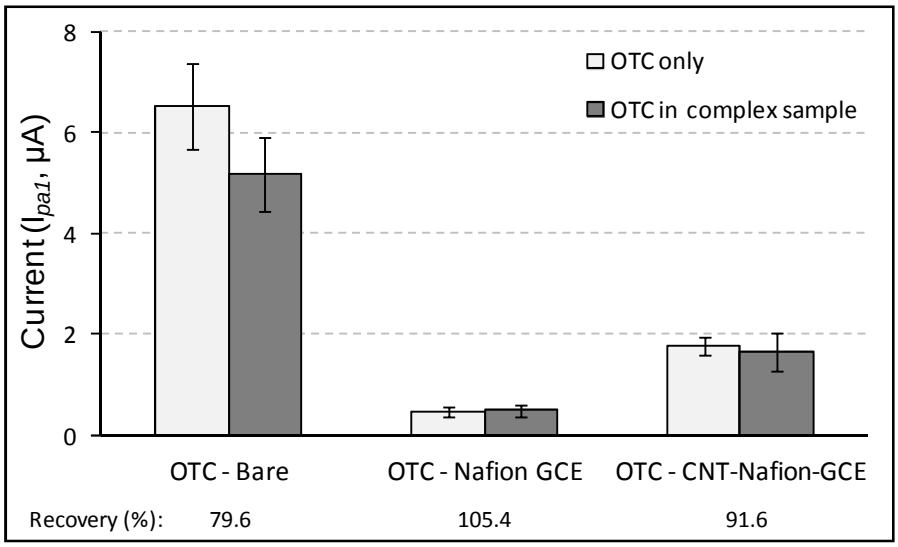

Figure 5.24 Current of OTC (I_{pa1}) in the presence of AA and UA analysed at bare, Nafion® and 10 hr *f*-MWCNT-Nafion® coated GCEs. Data calculated from I_{net} current component. All analytes were 20 µM and analysed in 0.2 M PP buffer (pH 6.4). Nafion®-GCEs were coated with 4 µl Nafion® without MWCNTs. Complex sample contained 20 µM UA, AA and OTC. Percentage current recovery (%) calculated for OTC in the presence of UA and AA with respect to OTC analysed individually.

Based on results shown in Table 5.8 and Figure 5.24, it can be concluded that while the anodic current for OTC is diminished at Nafion®- and MWCNT-Nafion®-coated GCEs, this response is not excluded to the same extent as for UA and AA. Interferents that are negatively charged at highly acidic conditions, where the addition of MWCNTs and Nafion® was shown to increase the response of OTC, would similarly be excluded while maintaining a high I_{pa1} current.

While the MWCNT-Nafion®-GCEs were applied in an attempt to reduce the interfering effect of MEM, as shown in Section 4.4.4.2, no decrease in the anodic MEM response was observed for coated electrodes relative to bare GCEs (data not included). This was expected if the interfering components of MEM are suspected to be proteinacious in nature with similar pK_a values to OTC (McMurry, 2000), and thus charged similarly at pH 2 thus negating charge-based exclusion by Nafion®. This work is the basis for further investigation.

5.5 CHAPTER CONCLUSIONS

Raman spectroscopy revealed prolonged acid functionalisation increased the oxygen-containing functional groups that covered defect sites, produced at the tube-end and tube walls during this chemical oxidation process. This was evident from an increase in I_D/I_G ratio and MWCNT dispersion, which indicates increased structural defects.

The effect of MWCNT-coatings on GCEs was initially investigated using the anionic $Fe(CN)_6^{3-/4-}$ redox probe. GCEs modified with unfunctionalised MWCNTs (*u*-MWCNTs) showed a greatly increased peak current ratio, I_{pa}/I_{pc}, and the peak separation, ΔE_p, while the anodic response was reduced dramatically compared to bare GCEs. MWCNTs that were acid functionalised for 2 hours showed a decrease in ΔE_p and I_{pa}/I_{pc}, indicating a more reversible reaction, while the current response was higher than that of both the *u*-MWCNT-GCEs and bare GCEs. However, prolonged functionalisation beyond 2 hours led to less reversible reactions with lower current responses.

However, caution is advised when using redox probes as a fast measure of modified electrode performance, as is evident from the contrary results obtained for OTC for which the greatest response at MWCNT-modified GCEs was observed after 10 hours of acid treatment. Based on EIS data, the charge of the analyte molecule cannot be overlooked when assessing the reasons for enhanced electrode performance.

EIS revealed the interplay between resistance and capacitance of both the film coating and electrode surface, where sufficiently high capacitance negated the effect of increased film and charge-transfer resistance. This increased capacitance originates from the negative-charge covered MWCNTs embedded in the respective dispersal agent films. The data obtained for the cationic $Ru(NH_3)_6^{2+/3+}$ and anionic $Fe(CN)_6^{3-/4-}$ suggests the possible affinity of certain modified surfaces towards either positive or negatively charged molecules.

Based on the results obtained for the redox probes, and the literary sources cited, the following table was constructed to summarise the proposed effects of MWCNTs and their dispersal agents on the operational parameters of coated GCEs, as well as their effect on the anodic response of $Fe(CN)_6^{3-/4-}$, $Ru(NH_3)_6^{2+/3+}$. These effects are categorised as a) charge-based interactions (repulsion and attraction), b) a change in the number of oxygen-containing functional groups present on the electrode surface and c) a change in the active electrode surface area. In Table 5.9, these three categories are compared for CV data obtained for both $Fe(CN)_6^{3-/4-}$ and $Ru(NH_3)_6^{2+/3+}$ at various coated GCEs.

Table 5.9 Effect of MWCNTs and dispersal agents on GCE surface area for $Fe(CN)_6^{3-/4-}$ and $Ru(NH_3)_6^{2+/3+}$ analysis.

Probe	Electrode surface	Charge-based interaction	Oxygen groups	Surface area
$Fe(CN)_6^{3-/4-}$ (Section 5.4.3 CV data)	2 hr *f*-MWCNT-DMF-GCE *vs.* bare GCE	~	+	+
	5 and 10 hr *f*-MWCNT-DMF-GCEs *vs.* bare GCE	~	++	~
$Fe(CN)_6^{3-/4-}$ (Section 5.4.4 CV data)	Nafion®-GCEs *vs.* bare GCE	++ repulsion	~	- -
	10 hr *f*-MWCNT-Nafion®-GCEs *vs.* bare GCE	+ repulsion	+	-
$Fe(CN)_6^{3-/4-}$ (Section 5.4.4 EIS data)	Nafion®-GCEs *vs.* bare GCE	++ repulsion	~	-
	10 hr *f*-MWCNT-Nafion®-GCEs *vs.* bare GCE	+ repulsion	+	+
$Ru(NH_3)_6^{2+/3+}$ (Section 5.4.4 CV data)	Nafion®-GCEs *vs.* bare GCE	++ attraction	~	+
	10 hr *f*-MWCNT-Nafion®-GCEs *vs.* bare GCE	++ attraction	+	++
$Ru(NH_3)_6^{2+/3+}$ (Section 5.4.4 EIS data)	Nafion®-GCEs *vs.* bare GCE	Inconclusive	~	+
	10 hr *f*-MWCNT-Nafion®-GCEs *vs.* bare GCE	Inconclusive	+	++

Legend:
+ Slight increase
++ Larger increase
- Slight decrease
- - Larger decrease
~ No substantial change

Table 5.9 indicated that while charge-based interaction does occur with different surface modifications, it is only decisively observed during interaction between the

charged redox probes and the Nafion® film. Increases in oxygen-containing functional groups constitutes a minor role in improving $Fe(CN)_6^{3-/4-}$ current responses. Primarily, increases and decreases in modified electrode surface area relative to uncoated GCEs are responsible for the increased and decreased I_{pa} observed for both probes.

The far greater increase in OTC current response for DMF or Nafion® containing MWCNTs, compared to films composed of the dispersal agent was found to be due to an increase in active electrode surface area as shown in Table 5.10. This is similar to the redox probes in Table 5.9. Charge-based interaction between OTC and Nafion® is proposed, through adsorption of OTC into the cation-exchange film.

Table 5.10 Effect of MWCNTs and dispersal agents on GCE surface area for OTC analysis.

Experiment	Electrode surface	Charge-based interaction	Oxygen groups	Surface area
MWCNT functionalisation time (Section 5.4.5)	2 hr *f*-MWCNT-DMF-GCE *vs.* bare GCE	No evidence	+	+
	5 and 10 hr *f*-MWCNT-DMF-GCEs *vs.* bare GCE	No evidence	++	++
Dispersal agent selection (Section 5.4.6)	Nafion®-GCEs *vs.* bare GCE	+ attraction	~	-
	10 hr *f*-MWCNT-Nafion®-GCEs *vs.* bare GCE	+ attraction	+	+

Legend:
+ Slight increase
++ Larger increase
- Slight decrease
- - Larger decrease
~ No substantial change

Based on the superior current response observed for OTC, Nafion® was selected as the preferred dispersal agent for MWCNTs. The increased signal was in part due to the cation-exchange properties of Nafion®, which is proposed to have led to OTC adsorption. The proposition of increased adsorption is supported by larger current responses in the reverse current component, I_{rev}, for SWV, as well as greatly enhanced linearity observed in I_{pa} *vs*. OTC concentration plots. Increase adsorption appears to prolong the onset of the plateau behaviour observed for a bare GCE in

Chapter 3 (Section 3.3.6). However, due to increased background noise, detection limits were higher than for a bare GCE.

Using uric acid, UA, and ascorbic acid, AA, as model anionic interferents, selective nature of the MWCNT-Nafion®-coating was probed. The anion-repelling properties of Nafion® were found remove interference of UA and AA, while able to improve OTC current response when analysed in conjunction with both interferents. The addition of MWCNTs significantly improved the current response of OTC.

In conclusion, the improved signal obtained at MWCNT-coated GCEs does not necessarily originate merely from an increased surface area. Distinction must be made between physical surface area, and electrochemically active surface area that appears to be specific for the analyte in question.

While 10 hr *f*-MWCNTs was able to improve the anodic signal of OTC when dispersed in Nafion®, detection limits did not improve due to increased background noise.

This work offers a focused study into the charge-based interaction between charged analytes and a MWCNT-modified GCE surface using both positively and negatively charged redox probes. In addition, this work offers a more in-depth understanding into the beneficial application of MWCNTs as electrode surface modifiers for the anodic voltammetric detection of OTC.

CHAPTER 6

Overall Conclusions and Future Recommendations

6.1 OVERALL CONCLUSIONS

The core aim of this thesis was to examine the voltammetric analysis of oxytetracycline (OTC). This was done while addressing limitations within the literature regarding the electrochemical behaviour, fouling, detection in complex media, and finally the application of multi-walled carbon nanotubes (MWCNTs) for OTC analysis. While probing these limitations at a practical level, the study also sought to examine and introduce key fundamental information to the body of literature concerning voltammetry in complex media as well as probing the application of MWCNTs for enhanced detection of analytes.

Firstly then, the electro-analytical behaviour of OTC was characterised by cyclic voltammetry (CV) and square wave voltammetry (SWV). This was followed by investigating the viability of using voltammetry as a quantitative analytical technique in complex microbial growth media samples, using OTC in a case study. The third aspect investigated was the application of acid functionalised multi-walled carbon nanotubes (MWCNTs) in order to enhance the anodic detection of OTC.

6.1.1 Voltammetry of OTC

Voltammetry of OTC was investigated primarily at a very acidic pH, both to improve its stability and to enhance the anodic current for this analyte. Through the optimisation of often overlooked simple operational parameters, the following method of analysis was developed: OTC stock solutions were prepared in 0.2 M BR buffer (pH 2) and analysed in an electrolyte solution of the same buffer. By stirring the working solution and applying a preconditioning potential (0.0 V) for 40 seconds prior to analysis, a LOD of 24.3 nM was achieved. This LOD is lower than the maximum residue level (MRL) established by the European Union for food products (EC, 1996), thus showing the applicability of this method as a quality-assurance tool.

Renewal of the electrode surface was necessary between successive scans, due to OTC fouling at the GCE surface, which led to loss of current response (Figure 3.12). This was achieved in the form of simple pretreatment steps. By stirring the working solution and applying a 0.0 V preconditioning potential between scans, the electrode could accurately be used for 10 scans without requiring mechanical polishing. Such simple surface renewal methods are unique for anodic analysis of OTC, where other authors have only investigated the use of modified GCE surfaces to overcome fouling (Oungpipat *et al*., 1995; Masawat and Slater, 2007).

As has been suggested for the structurally similar antibiotic tetracycline (TC) (Guo *et al*., 2009), the oxidation of OTC was found to involve an equal number of electrons and protons. This work also confirms for the first time that the reaction mechanism for OTC is EC_iE, and the number of electrons transferred in the rate-limiting step is 1. These results are however subjective to the conditions maintained in this work.

6.1.2 Growth media as a complex matrix for voltammetric analysis

Based on limited information available about the nature of growth media when assessed voltammetrically, this section aimed to probe the possibilities and limitations associated with electrochemistry in complex microbiological growth media. The voltammetric investigation in the presence of microbial growth media revealed several constraints associated with the complex composition of these media. Several of the media examined displayed the presence of redox active components under both acidic and neutral conditions (Figure 4.1 and 4.5 respectively). These components are suspected of being proteinacious, including peptone, malt extract and yeast extract.

Through the use of $Fe(CN)_6^{3-/4-}$ during CV and EIS experiments, it was established that the growth media adsorb to the electrode surface, decreasing the active electrode surface area and hindering electron transport. In light of the data obtained, the author prescribes that voltammetry be limited to minimal salts media (MSM) for its mostly electrochemically inert nature and minimal effect on electrode performance.

However, in the event where voltammetry is required in more complex growth media such as for on-line sensors used during production control, a case study of OTC in malt extract media (MEM) was performed. This study highlighted the complication of interfering redox peaks originating from nitrogenous sources in the growth media. Through the selection of less interfering growth media components and minimising its final concentration in the working solution, an accurate concentration range could be established and OTC was measured at concentrations as low as 500 nM.

6.1.3 Investigation of MWCNT-coated GCEs

In an attempt to improve the anodic current response of OTC, an investigation into the use of acid functionalised MWCNT-modified GCEs was performed. Through the use of an anionic and cationic redox probe, the operational parameters of coated GCEs were probed. It was found that while charge-based interaction occurred between the cation-exchanger Nafion® and the charged probes, such interaction was not observed between the two redox probes and *f*-MWCNTs. Based on current response data for either probe, increases and decreases in I_{pa} appeared closely dependant on the active electrode surface area, a conclusion supported by increases in C_{dl} and Q during EIS, rather than any charge based interactions (Table 5.9). This study into the charge-based interaction between modified electrode surfaces and charged analytes contributes to clearing some of the contentions concerning the application of MWCNTs in electro-analytical chemistry (Ji *et al*., 2006; Maldonado *et al*., 2006; Holloway *et al*., 2008).

When analysing OTC, a similar result was obtained. Based on increased charging current, an increase in active electrode surface area is attributable to the addition of MWCNTs. Adsorption to the Nafion® film was also evident. Through simple optimisation steps, the following electrode surface was found to be most suitable for anodic OTC analysis: 10 hr *f*-MWCNT-Nafion®-GCE with a 4 µl loading volume. Preliminary data has shown this modified electrode can also be used for excluding interfering components such as uric acid (UA) and ascorbic acid (AA) based on their charge.

When using SWV, this complex waveform prevents improvements to OTC detection, brought on by the coated surfaces, to be observed when data was presented in the conventional net current form, I_{net}. A solution is presented by using only the forward current component, I_{for}, though this method warrants caution as background current discrimination is disregarded.

While the use of MWCNTs can indeed improve the anodic detection of OTC, the selection of dispersal agent was found to play a key role and its selection should be carefully considered based on the nature of the analyte of interest.

6.1.4 Closing discussion

To conclude, this work has primarily improved the knowledge related to the voltammetric analysis of OTC, both in defined and undefined matrices. The pioneering study into the voltammetric nature of microbial growth media revealed a range of complications, which must be considered prior to analysis in its presence. While the study was of relevance to OTC, this detailed examination has bearing on any voltammetric studies in growth media.

Lastly, the use of MWCNT-coated GCEs was observed to be beneficial for select analytes, but was a complex interplay between active surface area, length of acid functionalisation and the nature of the dispersal agent used. While charged probes indicated that charge does not play a clear role in facilitating enhanced electrode kinetics, the study indicates that the application and use of MWCNTs should be optimised on an analyte by analyte basis.

6.2 FUTURE RECOMMENDATIONS

While the work presented in this thesis has shown promise for analysis of OTC under defined laboratory conditions in which careful attention was paid to simple techniques for off-site testing, further work into the robustness and versatility of the developed technique would have to be conducted. Specifically, the usability of the technique to detect and quantify OTC in environmental samples, as well as a range of food products needs to be assessed.

With respect to using voltammetry as an on-line sensor during fermentative OTC production, fermentation reactions would have to be conducted to assess the capability of the sensor in the presence of live bacterial cultures and the complexity this would bring to the reaction media.

APPENDIX A

Growth Media Composition

A.1 Clostridium Nutrient Medium (CNM) – Fluka (Sigma-Aldrich)

Composition	g/l
Meat extract	10
Peptone	5
Yeast extract	3
D(+) glucose	5
Starch	1
Sodium chloride	5
Sodium acetate	3
L-Cysteine HCl	0.5
Agar	0.5
Final pH	6.8 (± 0.2) at 25° after autoclaving

Prescribed use: For the cultivation and enumeration of clostridia and other anaerobes as well as facultative microorganisms in food, clinical and other materials.

A.2 Luria Bertani (LB) Broth – Biolab (Merck)

Composition	g/l
Tryptone	12
Sodium chloride	12
Yeast extract	6
Final pH	7.5 (± 0.2) at 25° after autoclaving

Prescribed use: A growth medium used for the cultivation and maintenance of bacteria for generic and molecular studies.

A.3 Nutrient Broth (NB) – Biolab (Merck)

Composition	g/l
Meat extract	1
Yeast extract	2
Peptone	5
Sodium chloride	8
Final pH	7.1 (± 0.2) at 25° after autoclaving

Prescribed use: A general purpose medium suitable for the cultivation of a wide range of non-fastidious microorganisms.

A.4 Minimal Salts Media (MSM) – Custom prepared media

Composition	g/l	Source
Glucose	10	Merck
NH_4Cl	0.1	Saarchem
Na_2HPO_4	1	Merck
NaH_2PO_4	0.6	Merck
$MgSO_4.7H_2O$	0.2	Saarchem
KCl	0.2	Sigma
Yeast extract	0.002	Sigma
Trace element solution	1 (ml)	

Trace element solution	mg/l	Source
H_3BO_3	0.05	Merck
$CaSO_4$	0.2	UniLAB
$CoSO_4$	0.1	Merck
$CuSO_4$	0.2	Merck
$FeSO_4$	3	Merck
$MnCl_2$	0.002	Merck
$ZnSO_4.7H_20$	0.03	Saarchem

Titrated to pH 7 using NaOH before autoclaving. Used do differentiate between heterotrophs and auxotrophs, and when chemically defined media is required.

A.5 Abou-Zeid (1977) OTC production media (AZ) – Custom prepared media

Composition	g/l	Source
Glucose	10	Merck
Glycerol	2.5	Sigma-Aldrich
Peptone	5	Fluka
NaCl	5	Saarchem

Titrated to pH 7 before autoclaving.

Described by Abou-Zeid *et al*. (1977) for the enumeration of *Streptomyces rimosus* and the production of OTC.

A.6 Malt Extract Media (MEM) – Custom prepared media

Composition	g/l	Source
Glucose	10	Merck
Glycerol	2.5	Sigma-Aldrich
Malt extract	5	Fluka
NaCl	5	Saarchem
KNO_3	5	Saarchem

Titrated to pH 7 before autoclaving.

An adaptation to the described media by Abou-Zeid *et al*. (1977) where peptone is replaced with malt extract in addition to an inorganic nitrogen source, KNO_3.

REFERENCE LIST

Abdel-Azize, R.M., Haroun, B.M., Ismail, A.A. and Eslam, A.M. (1982). An automated procedure for the determination of oxytetracycline. *Folia Microbiologica*. 27, 60-64.

Abdel-Hamid, R. (1998). The adsorption behaviour of phenophthalein at a mercury electrode in water-ethanol solutions. *Monatshetfe fur Chemie.* 129, 817-826.

Abou-Zeid, A.A., Eissa, A.I., El-Dewaney, A.I., Abd El-Hamid, M.M., Fouad, M., Fahmi, M. and Yassein, M. (1977). The fermentative production of oxytetracycline on industrial by-products by *Streptomyces rimosus* 12907. *Folia Microbiologica*. 22, 47-54.

Abou-Zeid, A.A., El-Diwany, A.J. and Shaker, H.E. (1980). Utilisation of food industry by-products in the production of oxytetracycline by *Streptomyces rimosus 93060*. *Agricultural Wastes*. 2, 293-301.

Agui, L., Yanez-Sedeno, P. and Pingarron, J.M. (2008). Role of carbon nanotubes in electroanalytical chemistry: A review. *Analytica Chimica Acta*. 622, 11-47.

Ajayan, P.M., Talapatra, S., Vajtai, R., Srivastava, A. and Srivastava, O.N. (2006). Carbon nanotube filters. US patent number: US 2006/0027499 A1. *United States Patent Application Publication.*

Albright, J.L., Tuckey, S.L. and Woods, G.T. (1961). Antibiotics in milk – A review. *Journal of Dairy Science*. 44, 779-807.

Anadon, A. and Martines-Larranaga, M.R. (1999). Current situation and future perspectives of the use of antibiotics as growth promoters. *Cahiers Options Mediterraneennes.* 37, 65-67.

Andrew, H.R. and Norval, R.A.I. (1989). The carrier status of sheep, cattle and African buffalo recovered from heartwater. *Veterinary Parasitology*. 34, 261-266.

Antunes, E.F., Lobo, A.O., Corat, E.J., Trava-Airoldi, V.J., Martin, A.A. and Verissimo, C. (2006). Comparative study of first- and second-order Raman spectra of MWCNT at visible and infrared laser excitation. *Carbon*. 44, 2202-2211.

Bachtold, A., Hadley, P., Nakanishi, T. and Dekker, C. (2001). Logic circuits with carbon nanotube transistors. *Science.* 294, 1317-1320.

Baghlaf, A.O., Abou-Zeid, A.A., El-Diwany, A.I., Eissa, I., Fouad, M. and Yessein, M. (1979). Production of oxytetracycline, by *Streptomyces rimosus* 12907, as an animal feed supplement. *Agricultural Wastes*. 1, 301-310.

Banks, C.E. and Compton, R.G. (2006). New electrodes for old: from carbon nanotubes to edge plane pyrolytic grasphite. *Analyst*. 131, 15-21.

Banks, C.E., Davies, T.J., Wildgoose, G.G. and Compton, R.G. (2005). Electrocatalysis at graphite and carbon nanotube modified electrodes: edge-plane sites and tube ends are the reactive sites. *Chemical Communications*. 829-841. (Viewed online – doi: 10.1039/B413177K).

Bard, A.J. and Faulkner, L.R. (2001). *Electrochemical methods: Fundamentals and applications*. 2nd edition. John Wiley & Sons, Inc. USA. pp. 236, 293-299, 473, 563, 566-571, 589-591.

Beilby, A.L., Sasaki, T.A. and Stern, H.M. (1995). Electrochemical pretreatment of carbon electrodes as a function of potential, pH and time. *Analytical Chemistry*. 67, 976-980.

Bernabeu, P., Tamisier, L., De Cesare, A. and Caprani, A. (1988). Study of the adsorption of albumin on a platinum rotating disk electrode using impedance measurements. *Electrochimica Acta*. 33, 1129-1136.

Bersier, P.M. and Jenny, H. (1988). Quantitative and qualitative analysis of Saframycins. Polarographic and voltammetric behaviour and direct polarographic determination of Saframycin A in fermentation broth and the high-performance liquid chromatographic determination of various Saframycins. *Analyst*. 113, 721-726.

Bobrowski, A., Gawlicki, M., Kaptuski, P., Mirceski, V., Spasovski, F. and Zarebski, J. (2009). The silver amalgam film electrode in adsorptive stripping voltammetric determination of palladium(II) as its dimethyldioxime complex. *Electroanalysis*. 21, 36-40.

Bockris, J.O. and Khan, S.U.M. (1993). *Surface Electrochemistry: A molecular level approach*. Springer Publishing Company. USA. pp. 211-281.

Britto, P.J., Santhanam, K.S.V. and Ajayan, P.M. (1996). Carbon nanotube electrode for oxidation of dopamine. *Bioelectrochemistry and Bioenergetics*. 41, 121-125.

Britton, H.T.S. and Robinson, R.A. (1931). CXCVIII – Universal buffer solutions and the dissociation constant of veronal. *Journal of the Chemical Society*. 1456-1462

Brown, O.R. (1972). Diffusion currents at a cylindrical wire electrode: simultaneous determination of diffusion coefficient and coulometric number. *Journal of Electroanalytical Chemistry*. 34, 419-423.

Castellari, M., Gratacós-Cubarsi, M. and Garcia-Regueiro, J.A. (2009). Detection of tetracycline and oxytetracycline residues in pig and calf hair by ultra-high-performance liquid chromatography tandem mass spectrometry. *Journal of Chromatography A*. 1216, 8096-8100.

Chantaraprateep, P., Prateep, P. and Poomsuwan, P. (1987). Long acting oxytetracycline for control of disease in piglets. *Thai Journal of Health Research*. 1, 1-7.

Char, M.P., Niranjana, E., Swamy, B.E.K., Sherigara, B.S. and Pai, K.V. (2008). Electrochemical studies of the amaranth at surfactant modified carbon paste electrode: A cyclic voltammetry. *International Journal of Electrochemical Science*. 3, 588-596.

Chatten, L.G., Fleischmann, M. and Pletcher, D. (1979). The anodic oxidation of some tetracyclines. *Journal of Electroanalytical Chemistry*. 102, 407-413.

Chen, P. and McCreery, R.L. (1996). Control of electron transfer kinetics at glassy carbon electrodes by specific surface modification. *Analytical Chemistry*. 68, 3958-3965.

Choi, W.B., Chung, D.S., Kang, J.H., Kim, H.Y., Jin, Y.W., Han, I.T., Lee, Y.H., Jung, J.E., Lee, N.S., Park, G.S. and Kim, J.M. (1999). Fully sealed, high-brightness carbon-nanotube field-emission display. *Applied Physics Letters*. 75, 3129-3131.

Chorpa, I and Roberts, M. (2001). Tetracycline antibiotics: Mode of action, applications, molecular biology, and epidemiology of bacterial resistance. *Microbiology and Molecular Biology Reviews*. 65, 232-260.

Clardy, J., Fischbach, M. and Currie, C. (2009). The natural history of antibiotics. *Current Biology*. 19, R437-R441.

Cloete, T.E. (2003). Resistance mechanisms of bacteria to antimicrobial compounds. *International Biodeterioration and Biodegradation*. 51, 277-282.

Coccini, T., Roda, E., Sarigiannis, D.A., Mustarelli, P., Quartarone, E., Profumo, A. and Manzo, L. (2010). Effect of water-soluble functionalized multi-walled carbon nanotubes examined by different cytotoxicity methods in human astrocyte D384 and lung A549 cells. *Toxicology*. 269, 41-53.

Commission Regulations (EC). (1996). No. 281/96. *Official Journal of the European Communities*. No. L37/9.

Compton, R.G., Fisher, A., Lathan, M.H., Brett, C.M.A. and Oliviera Brett, A.M.C.F. (1992). Well-jet electrode linear sweep voltammetry. *Journal of Physical Chemistry*. 96, 8363-8367.

Contu, F., Elsener, B. and Bohni, H. (2002). Characterisation of implant materials in fetal bovine serum and sodium sulfate by electrochemical impedance spectroscopy. I. Mechanical polished samples. *Journal of Biomedical Materials Research.* 62, 412-421 (Published online).

Dai, H. and Shiu, K. (1996). Voltammetric studies of the electrochemical pretreatment of rotating-disc glassy carbon electrodes in phosphate buffer. *Journal of Electroanalytical Chemistry.* 419, 7-14.

Datsyuk, V., Kalyva, M., Papagelis, K., Parthenios, J., Tasis, D., Siokou, A., Kallitsis, I. and Galiotis, C. (2008). Chemical oxidation of multiwalled carbon nanotubes. *Carbon*. 46, 833-840.

De Betono, S.F., Garcia, A.A. and Valentin, J.F.A. (1999). UV-spectrophotometry and square wave voltammetry at nafion-modified carbon-paste electrode for the determination of doxazosin in urine and formulations. *Journal of Pharmaceutical and Biomedical Analysis*. 20, 621-630.

De Ruyck, H. and De Ridder, H. (2007). Determination of tetracycline antibiotics in cow's milk by liquid chromatography/tandem mass spectrometry. *Rapid Communication in Mass Spectrometry*. 21, 1511-1520.

De Waal, D.T. (2000). Anaplasmosis control and diagnosis in South Africa. *Annals of the New York Academy of Science*. 916, 474-483.

Deakin, M.R., Stutts, K.J. and Wightman, R.M. (1985). The effect of pH on some outer-sphere electrode reactions at carbon electrodes. *Journal of Electroanalytical Chemistry.* 182, 113-122.

DeAngelis, T.P. and Heineman, W.R. (1976). An electrochemical experiment using an optically transparent thin layer electrode. *Journal of Chemical Education*. 53, 594-597.

Dewey, C.E., Cox, B.D., Straw, B.E., Bush, E.J. and Hurd, H.S. (1997). Associations between off-label feed additives and farm size, veterinary consultant use, and animal age. *Preventative Veterinary Medicine*. 31, 1333-146.

Doi, A.M. and Stoskopf, M.K. (2000). The kinetics of oxytetracycline degradation in deionized water under varying temperatures, pH, light, substrate, and organic matter. *Journal of Aquatic Animal Health*. 12, 246-253.

Downard, A.J. and Roddick, A.D. (1995). Protein adsorption at glassy carbon electrodes: The effect of covalently bound surface groups. *Electroanalysis*. 7, 376-378.

Emara, K.M., Askal, H.F. and Saleh, G.A. (1991). Spectrophotometric determination of tetracycline and oxytetracycline in pharmaceutical preparations. *Talanta*. 38, 1219-1221.

Engstrom, R.C. and Strasser, V.A. (1984). Characterisation of electrochemically pretreated glassy carbon electrodes. *Analytical Chemistry*. 56, 136-141.

European Commission (EC). (2003). Regulation (EC) No. 1831/2003 of the European Parliament and the Council of 22 September 2003 on Additives for the use in animal nutrition.

Fagan, D.T., Hu, I. and Kuwana, T. (1985). Vacuum heat treatment of activated glassy carbon electrodes. *Analytical Chemistry*. 57, 2759-2763.

Ferloni, P., Mastragostino, M. and Meneghello, L. (1996). Impedance analysis of electronically conducting polymers. *Electrochimica Acta.* 41, 27-33.

Ferraro, J.R. and Nakamoto, K. (2003). *Introductory Raman Spectroscopy*. 2nd Edition. Academic Press. London, UK. pp. 1-17.

Finlay, A.C., Hobby, G.L., P'an, S.Y., Regna, P.P., Routien, J.B., Seeley, D.B., Shull, G.M., Sobin, B.A., Solomons, I.A., Vinson, J.W. and Kane, J.H. (1950). Terramycin, a new antibiotic. *Science*. 111, 85.

Fleming, A. (1929). On the bacterial activity of cultures of a Penicillium with special reference to their use in the isolation of *B. influenza*. *British Journal of Experimental Pahtology*. 10, 226-235.

Fluckinger-Isler, R., Morikofer-Zwez, S., Kahn, J. and Walter, P. (1994). Dietary components of malt extract such as maltodextrins, proteins and inorganic salts have distinct effects on glucose uptake and glycogen concentrations in rats. *The Journal of Nutrition*. 124, 1647-1653.

Forgács, E. and Csethati, T. (1997). Charge-transfer chromatographic study of the interaction of antibiotics with sodium dodecylsulfate. *Journal of Pharmaceutical and Biomedical Analysis*. 15, 1295-1302.

Fowler, D. and Swift, B.L. (1975). Abortion in cows inoculated with *Anaplasma marginale*. *Theriogenology*. 4, 59-67.

Gallinganio, M., Garrigues, S., Martinez-Vado, A. and De la Guardia, M. (1993). Determination of carbaryl in pesticide formulations by Fourier transformation infrared spectrometry with flow analysis. *Analyst*. 118, 1043-1048.

Gardiner, D.J., Graves, P.R. and Bowley, H.J. (1989). *Practical Raman Spectroscopy*. Springer-Verlag. University of Michigan, USA. pp. 3-9

Golabi, S.M. and Irannejad, L. (2005). Preparation and electrochemical study of fisetin modified glassy carbon electrode. Application to the determination of NADH and ascorbic acid. *Electroanalysis*. 17, 985-996.

Gonzalez-Guerrero, A.B., Mendoza, E., Pellicer, E., Alsina, F., Fernandez-Sanchez, C. and Lechuga. (2008). Discriminating the carboxylic groups from the total acidic sites in oxidized multi-wall carbon nanotubes by means of acid-base titration. *Chemical Physics Letters*. 462, 256-259.

Goyal, R.N., Gupta, V.K., Oyama, M. and Bachheti, N. (2006). Differential pulse voltammetry determination of atenolol in pharmaceutical formulation and urine using nanogold modified indium tin oxide electrode. *Electrochemical Communications*. 8, 65-70.

Graham, D.W., Olivares-Rieumont, S., Knapp, C.W., Lima, L., Werner, D. and Bowen, E. (2011). Antibiotic resistance gene abundance with waste discharges to the Almendares river near Havana, Cuba. *Environmental Science and Technology*. 45, 418-424.

Grenfell, T.C., McLaughin, D.J. and Kelly, J.M. (1960). An automated method for the determination of terramycin. *Annals New York Academy of Science*. 87, 857-863

Guo, G., Zhao, F. and Zeng, B. (2009). Voltammetric determination of tetracycline by using multiwall carbon nanotube – ionic liquid film coated glassy carbon electrode. *International Journal of Electrochemical Science.* 4, 1365-1372.

Gupta, V.K., Jain, R., Radhapyari, K., Jadon, N., Agarwal, S. (2011). Voltammetric techniques for the assay of pharmaceuticals – a review. *Analytical Biochemistry*. 408, 179-196.

Gustafson, R.H. and Bowen, R.E.. (1997). Antibiotic use in animal agriculture. *Journal of Applied Microbiology*. 83, 531-541.

Halling-Sørensen, B., Sengeløv, G. and Tjørnelund, J. (2002). Toxicity of tetracyclines and tetracycline degradation products to environmentally relevant bacteria, including selected tetracycline-resistant bacteria. *Archives of Environmental Contamination and Toxicology*. 42, 263-271.

Harrington, D.A. and Van den Driessche, P. (2011). Mechanisms and equivalent circuits in electrochemical impedance spectroscopy. *Electrochimica Acta*. 56, 8005-8013.

Hedge, R.N., Swamy, B.E.K., Sherigara, B.S. and Nandibewoor, S.T. (2008). Electro-oxidation of atenolol at a glassy carbon electrode. *International Journal of Electrochemical Science*. 3, 302-314.

Heiduschka, P. and Dittrich, J. (1992). Impedance spectroscopy and cyclic voltammetry at bare and polymer coated glassy carbon electrodes. *Electrochimica Acta*. 37, 2573-2580.

Höbel, W., Papperger, A. and Polster, J. (1992). Penicillinase optodes: Substrate determinations using batch, continuous flow and flow injection analysis operation conditions. *Biosesor and Bioelectronics*. 7, 549-557.

Holloway, A.F., Wildgoose, G.G., Compton, R.G., Shao, L. and Green, M.L.H. (2008). The influence of edge-plane defects and oxygen-containing surface groups on the voltammetry of acid-treated, annealed and "super-annealed" multiwalled carbon nanotubes. *Journal of Solid State Electrochemistry*. 12, 1337-1348.

Hou, P., Liu, C. and Cheng, H. (2008). Purification of carbon nanotubes. *Carbon*. 46, 2003-2025.

Hou, W. and Wang, E. (1989). Liquid chromatographic determination of tetracycline antibiotics at an electrochemically pre-treated glassy carbon electrode. *Analyst*. 114, 699-702.

Hu, I., Karweik, D.H. and Kuwana, T. (1985). Activation and deactivation of glassy carbon electrodes. *Journal of Electroanalytical Chemistry*. 188, 59-72.

Huang, H., Liu, Z. and Yang, X. (2006). Application of electrochemical impedance spectroscopy for monitoring allergen-antibody reactions using gold nanoparticle-based biomolecular immobilization method. *Analytical Biochemistry*. 356, 208-214.

Huang, K., Luo, D., Xie, W. and Yu, Y. (2008). Sensitive voltammetric determination of tyrosine using multi-walled carbon nanotubes/4-aminobenzeresulfonic acid film-coated glassy carbon electrode. *Colloids and Surfaces B: Biointerfaces*. 61, 176-181.

Huang, W., Yang, C. and Zhang, S. (2003). Simultaneous determination of 2-nitrophenol and 4-nitrophenol based on the multi-wall carbon nanotubes Nafion-modified electrodes. *Analytical and Bioanalytical Chemistry.* 375, 703-707.

Iijima, S. (1991). Helical microtubules of graphitic carbon. *Nature*. 354, 56-58.

Jackson, D.R., Omanovic, S. and Roscoe, S.G. (2000). Electrochemical studies of the adsorption behaviour of serum proteins on titanium. *Langmuir*. 16, 5449-5457.

Jetty, A., Potumarthi, R., Rao, A.G., Rao, B.S. and Ramakrishna, S.V. (2009). Continuous production of oxytetracycline in fluidized bed bioreactor by immobilized cells of *Streptomyces varsoviensis* MTCC-1537: Effect of dilution and glucose loading rates. *Applied Biochemistry and Biotechnology*. 159, 579-588.

Ji, X., Banks, C.E., Crossley, A. and Compton, R.G. (2006). Oxygenated edge plane sites slow the electron transfer of the ferro-/ferricyanide redox couple at graphite electrodes. *ChemPhysChem*. 7, 1337-1344.

Jorio, A., Saito, R., Dresselhaus, G. and Dresselhaus, M.S. (2004). Determination of nanotube properties by Raman spectroscopy. *Physical Transactions of the Royal Society A*. 362, 2311-2336.

Ju, S. and Li, Z.Y. (2006). Theory of thermal conductance in carbon nanotube composites. *Physics Letters A.* 353, 194-197.

Kabasakalian, P., Kalliney, S. and Westcott, A. (1974). Differential pulse polarographic analysis of everninomicin complex in fermentation broth. *Journal of Pharmaceutical Science*. 63, 641-642.

Kalanur, S.S., Seetharamappa, J., Mamatha, G.P., Hadagali, M.D. and Kandagal, P. (2008). Electrochemical behaviour of an anti-cancer drug at glassy carbon electrode and its determination in pharmaceutical formulations. *International Journal of Electrochemical Science*. 3, 756-767.

Karasali, H. and Ioannou, S. (2009). HPLC determination of mepiquat chloride in commercial pesticide formulations. *Bulletin of Environmental Contamination and Toxicology*. 83, 636-639.

Kardo-Sysoeva, L.G., Kardis, R.L., Mikhailova, V.P. and Komarov, E.V. (1981). Polarographic method of determining oleandomycin. *Antibiotiki*. 26, 828-833.

Kazemifard, A.G. and Moore, D.E. (1997). Evaluation of amperometric detection for the liquid-chromatographic determination of tetracycline antibiotics and their common contaminants in pharmaceutical formulations. *Journal of Pharmaceutical and Biomedical Analysis*. 16, 689-696.

Kemper, N. (2008). Veterinary antibiotics in the aquatic and terrestrial environment. *Ecological Indicators.* 8, 1-13.

Khan, S.J., Roser, D.J., Davies, C.M., Peters, G.M., Stuetz, R.M., Tucker, R. And Ashbolt, N.J. (2008). Chemical contamination in feedlot waste: Concentrations, effects and attenuations. *Environmental International*. 34,839-859.

Kim, B. and Sigmund, W.M. (2004). Functionalized multiwall carbon nanotube/gold nanoparticle composites. *Langmuir*. 20, 8239-8242.

Kissinger, P.T. and Heineman, W.R. (1983). Cyclic voltammetry. *Journal of Chemical Education*. 60, 702-706.

Kissinger, P.T. and Heineman, W.R. (1996). *Laboratory Techniques in Electroanalytical Chemistry*. 2nd Edition. Marcel Dekker, Inc. USA. pp 7, 84-94, 168-170, 315-322, 720-726.

Kornmann, H., Rhiel, M., Cannizzaro, C., Marison, I. and Von Stockar, U. (2003). Methodology for real-time, multianalyte monitoring of fermentation using an *in-situ* mid-infrared sensor. *Biotechnology and Bioengineering*. 82, 702-709.

Kreuer, K.M., Ise, M., Fuchs, A. and Maier, J. (2000). Proton and water transport in nano-separated polymer membranes. *Journal de Physique IV.* 10, Pr-279-Pr7-281.

Krishna Priya, B., Subrahmanyam, P., Dakshayani, K. And Chiranjeevi, P. (2007). Spectrophotometric determination of fenpropathrin in its formulations and water samples. *E-Journal of Chemistry*. 4, 480-486.

Krugliak, E.B., Bilushi, S.G., Zaitsev, P.M. and Korshunova, L.G. (1977). Use of polarographic methods for determining trichothecin. *Antibiotiki*. 22, 1088-1093.

Kumar, A.S. and Shanmugam, R. (2011). Simple method for simultaneous detection of uric acid, xanthine and hypoxanthine in fish samples using a glassy carbon electrode modified with as commercially received multiwalled carbon nanotubes. *Analytical Methods*. 3, 2088-2094.

Kurzawa, M. and Kowalczyk-Marzec, A. (2004). Electrochemical determination of oxytetracycline in veterinary drugs. *Journal of Pharmaceutical and Biomedical Analysis.* 34, 95-102.

Lasia, A. (1999). *Electrochemical Impedance Spectroscopy and Its Applications.* Volume 32. Kluwer Academic/Plenum publishers. New York, USA. pp 20.

Lau, C.H., Cervini, R., Clarke, S.R., Markovic, M.G., Matisons, J.G., Hawkins, S.C., Huynh, C.P. and Simon, G.P. (2008). The effect of functionalization on structural and electrical conductivity on multi-walled carbon nanotubes. *Journal of Nanoparticle Research*. 10, 77-88.

Lawrence, N.S. and Wang, J. (2006). Chemical adsorption of phenothiazine dye onto carbon nanotubes: Toward the low potential detection of NADH. *Electrochemistry Communications*. 8, 71-76.

Leddy, J. and Vanderborgh, N.E. (1987). Microstructural enhancement of mass transport through Nafion+nuclepore composite membranes. *Journal of Electroanalytical Chemistry*. 235, 299-315.

Lee, N.S., Chung, D.S., Han, I.T., Kang, J.H., Choi, Y.S., Kim, H.Y., Park, S.H., Jin, Y.W., Yi, W.K., Yun, M.J., Jung, J.E., Lee, C.J., You, J.H., Jo, S.H., Lee, C.G. and Kim, J.M. (2001). Application of carbon nanotubes to field emission displays. *Diamond and Related Materials*. 10, 265-270.

Li, J., Cassell,A., Delzeit, L., Han, J. and Meyyappan, M. (2002). Novel three-dimensional electrodes: Electrochemical properties of carbon nanotube ensembles. *Journal of Physical Chemistry B*. 106, 9299-9305.

Lisdat, F. and Schäfer, D. (2008). The use of electrochemical impedance spectroscopy for biosensing. *Analytical and Bioanalytical Chemistry.* 391, 1555-1567.

Liu, G. and Lin, Y. (2005). Electrochemical sensors for organophosphate pesticides and nerve agents using zirconia nanoparticles as selective sorbents. *Analytical Chemistry*. 77, 5894-5901.

Liu, Y., Yuan, R., Chai, Y., Tang, D., Dai, J. and Zhong, X. (2006). Direct electrochemistry of horseradish peroxidase immobilized on gold colloid/cycteine/nafion-modified platinum disk electrode. *Sensors and Actuators B*. 115, 109-115.

Lovric, M., Komorsky-Lovric, S. and Murray, R.W. (1988). Adsorption effect in square-wave voltammetry of totally irreversible redox reactions. *Electrochimica Acta*. 33, 739-744.

Low, D. (2008). Reducing antibiotic use in influenza: challenges and rewards. *Clinical Microbiology and Infection*. 14, 298-306.

Lunestad, B.T. and Goksøyr, J. (1990). Reduction in the antibacterial effect of oxytetracycline in sea water by complex formation with magnesium and calcium. *Diseases of Aquatic Organisms*. 9, 67-72.

Ly, S.Y., Lee, C.H. and Jung, Y.S. (2007). Measuring oxytetracycline using a simple prepared DNA immobilized on a carbon nanotube paste electrode in fish tissue. *Journal of the Korean Chemical Society.* 51, 412-417.

Macdonald, D.D. (1990). Review of mechanistic analysis by electrochemical impedance spectroscopy. *Electrochimica Acta*. 35, 1509-1525.

Macdonald, D.D., Sikora, E. and Engelhardt, G. (1998). Characterizing electrochemical systems in the frequency domain. *Electrochimica Acta*. 43, 87-107.

Maeda, Y., Fukuda, T., Yamamoto, H. and Kitano, H. (1997). Regio- and sterioselective complexation by a self-assembled monolayer of thiolated cyclodextrin on a gold electrode. *Langmuir*. 13, 4187-4189

Maia, P.P., Rath, S. and Reyes, F.G.R. (2008). Determination of oxytetracycline in tomatoes by HPLC using fluorescence detection. *Food Chemistry*. 109, 212-218.

Maldonado, S., Morin, S. and Stevenson, K.J. (2006). Electrochemical oxidation of catecholamines and catechols at carbon nanotube electrodes. *Analyst*. 131, 262-267.

Malinauskas, A., Ruzgas, T. and Gorton, L. (2000). Electrochemical study of the redox dyes Nile blue and Toluidine blue adsorbed on graphite and zirconium phosphate modified graphite. *Journal of Electroanalytical Chemistry*. 484, 55-63.

Martel, R., Schmidt, T., Shea, H.R., Hertel, T. and Avouris, P. (1998). Single- and multi-wall carbon nanotube field-effect transistors. *Applied Physics Letters*. 73, 2447-2449.

Martínez, J.L. (2008). Antibiotics and antibiotic resistance genes in natural environments. *Science*. 321, 365-367.

Martinez-Huitle, C.A., Carlesi Jara, C., Cerro-Lopez, M. and Quiroz, M.A. (2009). Chitosan-modified glassy carbon electrodes: Electrochemical behaviour as a function of the preparation method and pH. *Canadian Journal of Analytical Sciences and Spectroscopy*. 54, 53-62.

Masawat, P. and Slater, J.M. (2007). The determination of tetracycline residues in food using a disposable screen-printed gold electrode (SPGE). *Sensors and Actuators B*. 124, 127-132.

McMurry, J. (2000). *Organic Chemistry*. 5th Edition. Brooks/Cole. Pacific Grove, USA. pp. 1073-1079.

Miles, A.B. and Compton, R.G. (2000). Simulation of square-wave voltammetry: EC and ECE electrode processes. *The Journal of Physical Chemistry B.* 104, 5331-5342.

Mirceski, V., Komorsky-Lovric, S. and Lovric, M. (2007). *Square-Wave Voltammetry: Theory and Application*. Springer-Verlag. Germany. pp. 79, 93.

Moore, R.R., Banks, C.E. and Compton, R.G. (2004). Basal plane pyrolytic graphite modified electrodes: Comparison of carbon nanotubes and graphite powder as electrocatalysts. *Analytical Chemistry*. 76, 2677-2682.

Moulton, S.E., Barisci, J.N., Bath, A., Stella, R. and Wallace, G.G. (2003). Investigation of protein adsorption and electrochemical behaviour at a gold electrode. *Journal of Colloid and Interface Science.* 261, 312-319.

Moulton, S.E., Barisci, J.N., Bath, A., Stella, R. and Wallace, G.G. (2004). Studies of double layer capacitance and electron transfer at a gold electrode exposed to protein solutions. *Electrochimica Acta*. 49, 4223-4230.

Mukherjee, J.S., Rich, M.L., Socci, A.R., Joseph, J.K., Viru, F.A., Shin, S.S., Furin, J.J., Becerra, M.C., Barry, D.J., Kim, J.Y., Bayona, J., Farmer, P., Smith Fawzi, M.C. and Seung, K.J. (2004). Programmes and principles in the treatment of multidrug-resistant tuberculosis. *Lancet*. 363, 471-481.

Muto, C.A., Jernigan, J.A., Ostrowsky, B.E., Richet, H.M., Jarvis, W.R., Boyce, J.M. and Farr, B.M. (2003). SHEA guidelines for preventing nosocomial transmission of multidrug-resistant strains of *Staphylococcus aureus* and *Enterococcus*. *Infection Control and Hospital Epidemiology.* 24, 362-386.

Nan, C.W., Shi, Z. and Lin, Y. (2003). A simple model for thermal conductivity of carbon nanotube-based composites. *Chemical Physics Letters*. 375, 666-669.

Ni, Y., Li, S. and Kokot, S. (2011). Simultaneous voltammetric analysis of tetracycline antibiotics in foods. *Food Chemistry*, 124, 1157-1163.

Nicholson, R.S. and Shain, I. (1964). Theory of stationary electrode polarography. *Analytical Chemistry*. 36, 706-723.

Niland, M.J., Fogel, R., Flanagan, S.P. and Limson, J.L. (2012). Towards normalising variability in current responses at glassy carbon electrodes using double layer capacitance; a case study of citrinin. *Electroanalysis*. 24, 945-954.

Niranjana, E., Naik, R.R., Swamy, B.E.K, Sherigara, B.S. and Jayadevappa, H. (2007). Studies on adsorption of triton X-100 at carbon paste and ceresin wax carbon paste electrodes on the enhancement effect in dopamine oxidation by cyclic voltammetry. *International Journal of Electrochemical Science*. 2, 923-934.

Nuwer, M.J., O'Dea, J.J. and Osteryoung, J. (1991). Analytical and kinetic investigation of totally irreversible electron transfer reactions by square-wave voltammetry. *Analytica Chimica Acta*. 251, 13-25.

Nwosu, V.C. (2001). Antibiotic resistance with particular reference to soil microorganisms. *Research in Microbiology*. 152, 421-430.

Oka, H., Ito, Y. and Matsumoto, H. (2000). Chromatographic analysis of tetracycline antibiotics in food. *Journal of Chromatography A.* 882, 109-133.

Okumaru, L.L., Saczk, A.A., de Oliviera, M.F., Fulgencio, A.C., Torrezani, L., Gomes, P.N. and Peixoto, R.M. (2011). Electrochemical feasibility study of methyl parathion determination on graphite-modified basal plane pyrolytic graphite electrode. *Journal of the Brazilian Chemical Society*. 22, 652-659.

Olsson, J., Winquist, F. and Lundström, I. (2006). A self polishing electronic tongue. *Sensors and Actuators B*. 118, 461-465.

Osswald, S., Havel, M. and Gogotsi, Y. (2007). Monitoring oxidation of multiwalled carbon nanotubes by Raman spectroscopy. *Journal of Raman Spectroscopy*. 38, 728-736.

Osteryoung, J.G. and Osteryoung, R.A. (1985). Square wave voltammetry. *Analytical Chemistry.* 57, 101-110.

Oungpipat, W., Southwell-Keely, P. and Alexander, P.W. (1995). Flow injection detection of tetracyclines by electrocatalytic oxidation at a nickel-modified glassy carbon electrode. *Analyst*. 120, 1559-1565.

Palaharn, S., Charoenraks, T., Wangfuengkanagul, N., Grudpan, K. and Chailapakul, O. (2003). Flow injection analysis of tetracycline in pharmaceutical formulation with pulsed amperometric detection. *Analytica Chimica Acta*. 499, 191-197.

Park, S. and Yoo, J. (2003). Electrochemical impedance spectroscopy. *Analytical Chemistry*. 75, 455A-461A.

Perez, P., Teijeiro, C. and Marin, D. (2002). Study on the adsorption properties of the drug mitomycin c by stripping voltammetry. *Langmuir*. 18, 1760-1763.

Perlman, D. (1979). *Microbial Technology*. 2nd Edition, Vol.1. Academic Press. New York. pp 252-253, 267-270.

Petry, R., Schmitt, M. and Popp, J. (2003). Raman spectroscopy: A prospective tool in the life sciences. *ChemPhysChem.* 4, 14-30.

Phillips, I., Casewell, M., Cox, T., De Groot, D., Friis, C., Jones, R., Nightingale, C., Preston, R. and Waddell, J. (2004). Does the use of antibiotics in food animals pose a risk to human health? A critical review of published data. *Journal of Antimicrobial Chemotherapy*. 53, 28-52.

Qian, D., Dickey, E.C., Andrews, R. and Rantell, T. (2000). Load transfer and deformation mechanisms in carbon nanotube-polystyrene composites. *Applied Physics Letters*. 76, 2868-2870.

Ratledge, C. and Kristiansen, B. (2001). *Basic Biotechnology*. 2nd Edition. Cambridge University Press. UK. pp. 181-192; 225-227.

Reinke, R. and Simon, J. (2002). The online removal of dissolved oxygen from aqueous solutions used in voltammetric techniques by the chromatomembrane method. *Analytical and Bioanalytical Chemistry.* 374, 1256-1260.

Riaz, M. (1986). The quantitative analysis of tetracyclines. *Journal of the Chemical Society of Pakistan*. 8, 571-583.

Ribeiro, W.F., Selva, T.M.G., Lopes, I.C., Coelho, E.C.S., Lemos, S.G., de Abreu, F.C., do Nascimento, V.B. and de Araujo, M.C.U. (2011). Electroanalytical determination of carbendazim by square wave adsorptive stripping voltammetry with a multiwalled carbon nanotube modified electrode. *Analytical Methods*. 3, 1202 – 1206.

Rosca, I.D., Watari, F., Uo, M. and Akasaka, T. (2005). Oxidation of multiwalled carbon nanotubes by nitric acid. *Carbon*. 43, 3124-3131.

Rosner, B. (2000). *Fundamentals of biostatistics.* 5th Edition. Duxbury: Thomson Learning. Pacific Grove, USA. pp 24-25.

Ross, J.I., Snelling, A.M., Carnegie, E., Coates, P., Cunliffe, W.J., Bettoli, V., Tosti, G., Katsambas, A., Galvan Perez del Pulgar, J.I., Rollman, O., Torok, L., Eady, E.A. and Cove, J.H. (2003). Antibiotic-resistant acne: lessons from Europe. *British Journal of Dermatology*. 148, 467-478.

Roy, P.R., Okajima, T. and Ohsaka, T. (2003). Simultaneous electroanalysis of dopamine and ascorbic acid using poly(*N,N*-dimethyl)-modified electrodes. *Bioelectrochemistry*. 59, 11-19.

Rufino, J.L., Weinert, P.L., Pezza, H.R. and Pezza, L. (2009). Flow-injection spectrophotometric determination of tetracycline and doxycycline in pharmaceutical formulations using chloramine-t as oxidizing agent. *Quinica Nova*. 32, 1764-1769.

Sanli, S., Sanli, N. and Alsancak, G. (2009). Determination of protonation constants of some tetracycline antibiotics by potentiometry and LC methods in water and acetonitrile-water binary mixtures. *Journal of the Brazilian Chemical Society*. 20, 939-946.

Scholz, F. (2002). *Electroanalytical Methods: Guide to Experiments and Applications*. Springer-Verlag. Berlin, Germany. pp. 11, 64, 74-81.

Schügerl, K. (2001). Progress in monitoring, modelling and control of bioprocesses during the last 20 years. *Journal of Biotechnology*. 85, 149-173.

Shaidarova, G., Gedmina, A.V., Chelnokova, I.A. and Budnikov, G.K. (2008). Determination of tetracycline antibiotics using the electrocatalytic response of an electrode modified by a mixed-valence ruthenium oxide – ruthenium cyanide film. *Pharmaceutical Chemistry Journal*. 42, 545-549.

Shao, C., Wei, Y. and Jiang, L. (2008). Study on electrochemical behaviour of tyrosine at multi-wall carbon nanotubes modified glassy carbon electrode. *Journal of New Materials for Electrochemical Systems*. 11, 175-179.

Sharath Shankar, S., Kumara Swamy, B.E., Chandra, U., Manjunatha, J.G. and Sherigara, B.S. (2009). Simultaneous determination of dopamine, uric acid and ascorbic acid with CTAB modified carbon paste electrode. *International Journal of Electrochemical Science.* 4, 592-601.

Smith, E. and Dent, G. (2005). *Modern Raman Spectroscopy: A Practical Approach*. John Wiley Sons Ltd. Chichester, UK. pp. 1-19.

Stokes, J.L., Gunness, M. and Foster, J.W. (1944). Vitamin content of ingredients of microbiological culture media. *Journal of Bacteriology*. 47, 293-299.

Su, S., Chiang, W., Lin, C. and Yokoyama, M. (2008). Multi-wall carbon nanotubes: Purification, morphology and field emission performance. *Physica E*. 40, 2322-2326.

Suni, I.I. (2008). Impedance methods for electrochemical sensors using nanomaterials. *Trends in analytical Chemistry*. 27, 604-611.

Szentirmay, M.N. and Martin, C.R. (1984). Ion-exchange selectivity of Nafion films on electrode surfaces. *Analytical Chemistry*. 56, 1898-1902.

Taskin, M. and Kurbanoglu, E.B. (2011). Evaluation of waste chicken feathers as peptone source for bacterial growth. *Journal of Applied Microbiology*. 111, 826-834.

Teuber, M. (2001). Veterinary use and antibiotic resistance. *Current Opinion in Microbiology*. 4, 493-499.

Thostenson, E.T. and Chou, T. (2002). Aligned multi-walled carbon nanotube-reinforced composites: processing and mechanical characterisation. *Journal of Physics D: Applied Physics.* 35, L77-L80.

Tongaree, S., Flanagan, D.R. and Poust, R.I. (1999). The effect of pH and mixed solvent systems on the solubility of oxytetracycline. *Pharmaceutical Development and Technology*. 4, 571-580.

Tsai, T., Thiagarajan, S. and Chen, S. (2010). Green synthesis of silver nanoparticles using ionic liquid and application for the detection of dissolved oxygen. *Electroanalysis*. 22, 680-687.

Tsai, Y., Chen, J., Li, S. and Marken, F. (2004). Electroanalytical thin film electrodes based on a Nafion^{TM}-multi-walled carbon nanotube composite. *Electrochemsitry Communications*. 6, 917-922.

Tsuji, K. and Goetz, J.F. (1978). HPLC as a rapid means of monitoring erythomycin and tetracycline fermentation processes. *Journal of Antibiotics (Tokyo)*. 4, 302-308.

Tunnemann, R., Mehlmann, M., Sussmuth, R.D., Buhler, B., Pelzer, S., Wohlleben, W., Fiedler, H.P., Wiesmuller, K.H., Gauglitz, G. and Jung, G. (2001). Optical biosensor: Monitoring studies of glycopeptide antibiotic fermentation using white light interference. *Analytical Chemistry*. 73, 4313-4318.

Uslu, B. and Ozkan, S.A. (2007). Solid electrodes in electroanalytical chemistry: Present applications and prospects for high throughput screening of drug compounds. *Combinatorial Chemistry & High Throughput Screening*. 10, 495-513.

Van Benschoten, J.J., Lewis, J.Y., Heineman, W.R., Roston, D.A. and Kissinger, P.T. (1983). Cyclic voltammetry experiment. *Journal of Chemical Education*. 60, 772-776.

Vega, D., Agüí, L., González-Cortés, A., Yáñez-Sedeño, P. and Pingarrón, J.M. (2007). Voltammetry and amperometric detection of tetracyclines at multi-wall carbon nanotube modified electrodes. *Analytical and Bioanalytical Chemistry*. 389, 951-958.

Wang, J. (1994). *Analytical Electrochemistry*. VCH Publishers, Inc. New York. pp 2-3, 138-140, 142, 161-161, 173.

Wang, J. (2001). *Analytical electrochemistry*. 2nd Edition. Wiley-VCH, New York, USA. pp. 3.

Wang, H., Zhao, H. and Quan, X. (2011). Gold modified microelectrode for direct tetracycline detection. *Frontiers of Environmental Science & Engineering in China*. DOI: 10.1007/s11783-011-0323-5

Wangfuengkanagul, N., Siangproh, W. and Chailapakul, O. (2004). A flow injection method for the analysis of tetracycline antibiotics in pharmaceutical formulations using electrochemical detection at anodized boron-doped diamond thin film electrode. *Talanta*. 64, 1183-1188.

Watanabe, N., Bergamaschi, B.A., Loftin, K.A., Meyer, M.T. and Harter, T. (2010). Use and environmental occurrence of antibiotics in freestall dairy farms with manured forage fields. *Environmental Science and Technology*. 44, 6591-6600.

Wickramasuriya, U.G.J.S. (1985). Evaluation of mastitis control programme adopted in small dairies in the district of Colombo. *Journal of the National Science Council of Sri Lanka*. 13, 17-28.

Wildgoose, G.G., Banks, C.E., Leventis, H.C. and Compton, R.G. (2006). Chemically modified carbon nanotubes for the use in electroanalysis. *Microchimica Acta*. 152, 187-214.

Wilson, Jr. E.B., Decius, J.C. and Cross, P.C. (1980). *Molecular Vibrations: The Theory of Infrared and Raman Vibrational Spectra*. Dover Publication. UK. pp. 1-8.

World Bank. (2010). *World Development Indicators*. Ed. Development Data Group. Chapter 4: Economy. Washington, USA. pp 217 – 285.

Wormser, G.P., Nadelman, R.B., Dattwyler, R.J., Dennis, D.T., Shapiro, E.D., Steere, A.C., Rush, T.J., Rahn, D.W., Coyle, P.K., Persing, D.H., Fish, D. and Luft, B.J. (2000). Practice Guidlines for the treatment of Lyme disease. *Clinical Infections Diseases*. 31 (Supp 11), S1-S14.

Xie, X., Gan, T., Sun, D. and Wu, K. (2008). Application of multi-walled carbon nanotubes/Nafion composite film in electrochemical determination of Pb^{2+}. *Fullerenes, Nanotubes, and Carbon Nanostructures*. 16, 103-113.

Yanez-Sedeno, P., Riu, J., Pingarron, J.M. and Rius, F.X. (2010). Electrochemical sensing based on carbon nanotubes. *Trends in Analytical Chemistry*. 29, 939-953.

Yang, C., Zhang, S., Liu, Y. and Huang, W. (2008). Electrochemical behaviours of ofloxacin and its voltammetric determination at carbon nanotubes film modified electrode. *Frontiers of Chemistry in China*. 3, 353-358.

Yang, S.S. and Lee, C.M. (2001). Effect of culture media on protease and oxytetracycline production with mycelium and protoplasts of *Streptomyces rimosus*. *World Journal of Microbiology and Biotechnology*. 17, 403-410.

Yang, S.S. and Ling, M.Y. (1989). Tetracycline production with sweet potato residue by solid state fermentation. *Biotechnology and Bioengineering*. 33, 1021-1028.

Yang, S.S. and Yueh, C.Y. (2001). Oxytetracycline production by immobilized *Streptomyces rimosus*. *Journal of Microbiology, Immunology and Infection*. 34, 235-242.

Yarnitzky, C. and Smyth, W.F. (1991). Square wave polarographic and voltammetric analysis of selected electroreducible drugs. *International Journal of Pharmaceutics*. 75, 161-169.

Yoshimori, A., Kakitani, T. and Mataga, N. (1989). Transfer coefficient in electrochemical reactions. *Journal of Physical Chemistry*. 93, 3694-3702.

Yuan, S., Wang, Q., Yates, S.R. and Peterson, N.G. (2010). Development of an efficient extraction method for oxytetracycline in animal manure for high performance liquid chromatography analysis. *Journal of Environmental Science and Health Part B*. 45, 612-620.

Zachowski, E.J., Wojciechowski, M. and Osteryoung, J. (1986). The analytical application of square wave voltammetry. *Analytica Chimica Acta*. 188, 47-57.

Zare, H.R. and Nasirizadeh, N. (2007). Henatoxylin multi-wall carbon nanotubes modified glassy carbon electrode for electrocatalytic oxidation of hydrazine. *Electrochimica Acta*. 52, 4153-4160.

Zare, H.R. and Nasirizadeh, N. (2011). A comparison of the electrochemical and electroanalytical behaviour of ascorbic acid, dopamine and uric acid at bare, activated and multi-wall carbon nanotubes modified glassy carbon electrodes. *Journal of the Iranian Chemical Society.* 8, S55-S66.

Zen, J. and Hsu, C. (1998). A selective voltammetric method for uric acid detection at Nafion-coated carbon paste electrodes. *Talanta*. 46, 1363-1369.

Zen, J., Jou, J. and Ilangovan, G. (1998). Selective voltammetric method for uric acid detection using pre-anodized Nafion-coated glassy carbon electrodes. *The Analyst*. 123, 1345-1350.

Zhang, Y. and Wang, Y. (2011). Voltammetric determination of vitamin B_6 at glassy carbon electrode modified with gold nanoparticles and multi-walled carbon nanotubes. *American Journal of Analytical Chemistry*. 2, 194-199.

Zhang, Q., Wei, W. and Zhao, G. (2008). Direct electrochemistry of myoglobin on a room temperature ionic liquid modified electrode and its application to nitric oxide biosensing. *Electroanalysis*. 20, 1002-1007.

Zhou, M., Ding, J., Guo, L. and Shang, Q. (2007). Electrochemical behaviour of L-cysteine and its detection at ordered mesoporous carbon-modified glassy carbon electrode. *Analytical Chemistry*. 79, 5328-5335.

Zhou, J., Gerhardt, G.C., Baranski, A. and Cassidy, R. (1999). Capillary electrophoresis of some tetracycline antibiotics coupled with reductive fast cyclic voltammetric detection. *Journal of Chromatography A*. 839, 193-201.

Zidan, M., Tee, T.W., Abdullah, A.H., Zainal, Z. And Kheng, G.J. (2010). Electrochemical oxidation of paracetamol mediated by zinc oxide modified glassy carbon electrode. *Australian Journal of Basic and Applied Science*. 4, 6025-6030.

Zygmunt, W.A. (1961). Oxytetracycline formation by *Streptomyces rimosus* in chemically defined media. *Applied Microbiology*. 9, 502-507.